2016

Process Monitoring and Data Mining with Chemical Process Historical Databases

Michael Carl Thomas
Louisiana State University and Agricultural and Mechanical College

PROCESS MONITORING AND DATA MINING WITH CHEMICAL PROCESS HISTORICAL DATABASES

A Dissertation

Submitted to the Graduate Faculty of the
Louisiana State University and
Agricultural and Mechanical College
in partial fulfillment of the
requirements for the degree of
Doctor of Philosophy

in

The Gordon A. and Mary Cain
Department of Chemical Engineering

by
Michael Carl Thomas
B.E., Vanderbilt University, 2012
M.S., Louisiana State University, 2014
December 2016

To my father,

for teaching me about many things,

from engineering to investing to fantasy football,

and to my mother,

for all her warm love and gumbo.

Acknowledgements

Creating the research in this dissertation would not have been possible without help from many people whose support I greatly appreciate.

I would like to thank my advisor, Dr. José Romagnoli for his guidance and mentorship during my years in graduate school. He helped me explore and develop as a researcher, and I am thankful for the opportunities I have had while working in his lab. I would also like to thank Dr. Jianhua Chen, Dr. John Flake, and Dr. Andreas Giger for serving on my dissertation committee.

More people than I can list here have also enriched my experience in graduate school. In particular I am grateful for the mentorship and help provided by John, Mike, Elaine, and Brian which fostered my growth into a professional engineer. I also appreciated the support of my fellow members of the Romagnoli group: Greg Robertson, Rob Willis, Bing Zhang, Vikram Gowrishankar, Jorge Chebir, Santiago Salas, and Aryan Geraili. I am grateful for their friendship and support while I was flying in and out of the lab and tapping away at code in the corner. I am also grateful to Wenbo Zhu for collaborating with me for some of the work in this dissertation. Finally, I would like to thank my roommate, Navid Ghadipasha, for his support while we commiserated over the challenges of graduate school.

I would also like to gratefully acknowledge Donald W. Clayton for supporting me through his generous Clayton Engineering Award and for giving me ten two-letter words that have encouraged me in graduate school: “If it is to be, it is up to me!”

Finally, thank you to my cat, Carol, and my family for their love and support that has sustained me through graduate school. I am especially grateful for the love and support of my parents.

Table of Contents

Acknowledgements iii

List of Tables vii

List of Figures viii

Abstract xiv

Chapter 1 - Introduction 1
1.1 Background 1
1.2 Dissertation Motivation 5
1.3 Research Aims 8
1.4 Publications and Presentations 9
1.5 Dissertation Contributions 10
1.6 Dissertation Structure 11
1.7 References 12

Chapter 2 - Data Preprocessing 16
2.1 Data Pretreatment 16
2.1.1 Outlier removal 17
2.1.2 Data normalization 17
2.1.3 Missing data approximation 18
2.2 Multiway Unfolding 18
2.3 Dynamic Time Warping (DTW) 20
2.3.1 Synchronization of batch trajectories with DTW 21
2.3.2 Iterative synchronization of multivariate batch process data 26
2.4 Synthetic Minority Over-sampling Technique (SMOTE) 28
2.5 References 31

Chapter 3 - Data Mining Techniques 32
3.1 Data Mining Approach 33
3.2 Dimensionality Reduction (DR) 34
3.2.1 Principal component analysis (PCA) 35
3.2.2 Independent component analysis (ICA) 36
3.2.3 Kernel principal component analysis (KPCA) 39
3.2.4 Isomap 41
3.2.5 Spectral embedding (SE) 42
3.3 Data Clustering 44
3.3.1 K-means clustering 44
3.3.2 DBSCAN 45
3.3.3 Balanced iterative reducing and clustering using hierarchies (BIRCH) 48

3.3.4 Mean shift clustering 50
3.4 Cluster Evaluation 51
3.5 Subspace Clustering Study: Parameters and Analysis 53
3.6 References 56

Chapter 4 - Process Monitoring and Supervision 59
4.1 Introduction to Data-Driven Process Monitoring 60
4.2 Statistical Process Control 63
4.3 PCA-Based Process Monitoring 64
4.3.1 PCA fault detection 65
4.3.2 PCA fault identification 67
4.3.3 PCA Fault diagnosis – discriminant analysis 68
4.3.4 Nonlinear principal component analysis (NLPCA) 68
4.4 Novel Self-Organizing Map (SOM) Monitoring Approach 69
4.4.1 The self-organizing map (SOM) 70
4.4.2 SOM visualization tools for process analysis 72
4.4.3 Clustering of the SOM using k-means 74
4.5 MSOM in Process Monitoring 75
4.5.1 SOM fault detection and diagnosis 75
4.5.2 Variable contribution plots 76
4.6 Multiway Methods for Batch Process Monitoring 78
4.7 Defining Normal Operations: Example on Fisher Iris Data 79
4.7.1 PCA analysis – fault detection 79
4.7.2 Contribution plots – fault identification 80
4.7.3 Discriminant analysis – fault diagnosis 82
4.8 References 85

Chapter 5 - Case Study 1: Tennessee Eastman Process (TEP) 87
5.1 Introduction 87
5.2 Tennessee Eastman Process Description 88
5.3 Tennessee Eastman Process Fault Extraction 91
5.3.1 Normal and fault 1: basic case 92
5.3.2: Reduced TEP data set 92
5.3.3 Full TEP data set 101
5.4 Process Monitoring of the Tennessee Eastman Process 101
5.4.1 Fault detection results 104
5.4.2 Fault identification results 105
5.4.3 Fault diagnosis results 109
5.5 Conclusions 113
5.6 References 114

Chapter 6 - Case Study 2: Industrial Separation Tower 116
6.1 Introduction 116
6.2 Separation Tower Process Description 118
6.3 Separation Tower Dimensionality Reduction (DR) and Clustering 121

6.4 Novel Event Detection 131
6.4.1 Data mining and analysis for monitoring 131
6.4.2 Map training and visualization 133
6.4.3 Determining the quantization error (QE) threshold 137
6.5 Fault Detection and Identification Results 139
6.6 Conclusions 148
6.7 References 151

Chapter 7 - Case 3: Analysis and Monitoring of an Industrial Batch Polymerization Process .. 152
7.1 Introduction 152
7.2 Process Description 153
7.3 Dynamic Time Warping for Batch Synchronization and Unfolding 155
7.4 Fault Detection and Diagnosis on Batch Process 159
7.4.1 Detection of filter clogging 161
7.4.2 Detection of valve sticking 162
7.5 Fault Detection Discussion 162
7.6 Diagnosis of Both Reactor Conditions 165
7.7 Conclusions 165
7.8 References 167

Chapter 8 - FastMan: A Software Tool for Data Mining Chemical Process Data 168
8.1 Introduction 168
8.2 Software Description and Demonstration 169
8.3 Conclusions 171

Chapter 9 - Conclusions 173
9.1 Summary of Results 173
9.2 Future Research Recommendations 174

Appendix A - Complete Clustering Results 176

Vita 190

List of Tables

Table 3.1: Clustering metrics used to compare the quality of clustering results 52

Table 5.1: TEP measured variables 90

Table 5.2: TEP manipulated variables 90

Table 5.3: TEP process faults description 91

Table 5.4: Number of components used by DR projections in clustering TEP data 95

Table 5.5: Clustering results on reduced TEP data set 96

Table 5.6: Data clustering and DR applied to the full TEP data set 104

Table 5.7: Fault detection rate of MPCA and MSOM 106

Table 5.8: Fault detection results for all 20 faults 106

Table 5.9: False alarm rates of the four techniques from the analysis in Table 5.8 107

Table 5.10: Correct diagnosis rates for selected TEP faults 110

Table 5.11: Fault Diagnosis for all 20 TEP faults 111

Table 6.1: Process measurements and derived measurements 122

Table 6.2: Supervised clustering metrics on tower data set 1256

Table 6.3: Sizes of historical data groups and training data 133

Table 7.1: Sizes of reactor fault data sets 159

Table 7.2: Filter clog detection 161

Table 7.3: Valve sticking detection 162

Table 7.4: Diagnosis of batch faults 165

List of Figures

Figure 2.1: Multiway unfolding of batch process data takes the three-dimensional batch process data matrix and unfolds it into a two-dimensional matrix. In the new matrix, each batch's data formed into a single row of entries. 19

Figure 2.2: Batch sensor measurement data (a) before synchronization and (b) after synchronization. In both figures, the average trajectory is indicated by the bolded black line. Two abnormal batches are visible: one occurs before the others (blue) and another dip. 24

Figure 2.3: DTW alignment path of a normal batch from the example batch data trajectories.... 25

Figure 2.4: DTW alignment path of the batch trajectory that dips at the end in Figure 2.2, a. 25

Figure 3.1: Schematic of data mining approach. 34

Figure 3.2: Illustration of the various clustering metrics. 54

Figure 4.1: Industrial process monitoring workflow. 61

Figure 4.2: Shewhart chart. 64

Figure 4.3: Schematic of the overall strategy for fault detection and identification. 71

Figure 4.4: Proposed MSOM process monitoring framework. Data comes from the computerized control system and is first projected onto the SOM of normal operations. 76

Figure 4.5: Illustration of the residual analysis. The SOM based contribution identifies large contributions from both variables relative to the structure of the data. 77

Figure 4.6: Green points were classified as normal and red points were classified as faulty points. The cylinder denotes the normal operating region. PCA was able to clearly separate class 1 from classes 2 and 3. 80

Figure 4.7: Fault detection without using the T2 cylinder. The NOR is represented by the small, dense cluster of points in the lower left corner of the graph. The lower left corner is enlarged in Figure 4.8. 81

Figure 4.8: A detail of the NOR cluster from Figure 4.7. Because the PCA model was created using class 1 data, the error in the model for class 1 is small which yields small T2 and Q statistics. 81

Figure 4.9: Faulty points from each class produce different contribution plots. The petal length and width are most responsible for the "faulty" status..... 82

Figure 4.10: Data scores with respect to the class 1 PCA model. 83

Figure 4.11: Data scores with respect to the class 2 PCA model. 83

Figure 4.12: Data scores with respect to the class 3 PCA model. 84

Figure 4.13: SOM fits to each of the Fisher Iris classes with less overlap compared to the MPCA models..... 84

Figure 5.1: Process schematic with control scheme. 89

Figure 5.2 Data from TEP0 and TEP1 projected to 3 PCs. 93

Figure 5.3 DBSCAN identifies the clusters formed by TEP0 and TEP1. 93

Figure 5.4 Flow of Stream 4 colored by the DBSCAN clusters..... 94

Figure 5.5 A time series plot of each data point's cluster..... 94

Figure 5.6 DBSCAN cluster labels largely correspond to original labels 98

Figure 5.7 DBSCAN cluster labels on data reduced by PCA..... 98

Figure 5.8 K-means cluster labels on data with No DR 99

Figure 5.9 Clusters found using DBSCAN and spectral embedding..... 99

Figure 5.10: Raw mean shift results with ICA reduced data gave rise to a very large number of clusters seen in (a). Combining all clusters with fewer than 10 members into the noise cluster in (b), had only a minor effect on the ARI results. 100

Figure 5.11 PCA projection of the reduced TEP data set colored by true fault group. 102

Figure 5.12 Detail of the data clustered near the TEP's normal operations 102

Figure 5.13 Clustering TEP data with K-means 103

Figure 5.14: DBSCAN with NO DR identified most clusters, though issues with unrelated data and noise data remain challenges. 103

Figure 5.15: Contribution plots of faulty data made my PCA and MSOM. 108

Figure 5.16: Data classification using MPCA, 1-SOM, and MSOM on the testing data set with time colored according to class. Solid lines of color indicate a consistent classification while discontinuous lines indicate an inconsistent classification. 112

Figure 5.17: PCA projections of data from Fault 14+1, the map used in 1-SOM classification (a), and the map fit to Fault 14+1 in MSOM (b). 113

Figure 6.1: Simplified process flow sheet. 119

Figure 6.2: This PCA projection of separation tower data demonstrates the variability of tower data with feed grade. The normal operating region from one grade generally doesn't overlap with other grades. Date are colored according to feed grade. 119

Figure 6.3 Projections of tower data using PCA 123

Figure 6.4 Projections of tower data using ICA 123

Figure 6.5 Projections of tower data using Isomap break up the cluster of normal data 124

Figure 6.6 Projections of tower data using SE separate the data well, but interpretation is less intuitive 124

Figure 6.7 PCA projection of K-means clusters of tower data with k=2 127

Figure 6.8 PCA projection of K-means clustering of tower data with k=3 128

Figure 6.9 PCA projection of DBSCAN clusters 128

Figure 6.10 PCA projection of mean shift clusters 129

Figure 6.11: Adjustments to the eps parameter in DBSCAN finds the smaller clusters in (a). In (b) the data are colored based on time (blue is older, yellow is newer, with dark red being the most recent). 130

Figure 6.12: Graphical tool used to manually classify training data. Selected data is plotted in time series with dense group's circles and added to different fault groups with the controls in the upper left of the window. 132

Figure 6.13: PCA projection of trained map with sampled training data, including synthetic samples from SMOTE. 134

Figure 6.14: Visualizations of the map used in monitoring. (a) the SOM U-matrix visualizes groups in the data. (b) colors are derived from clustering results. (c) is a hit diagram of the training data on the map. (d) labels the map regions. 135

Figure 6.15: Davies-Bouldin index of the clustering given in Figure 6.8, b. Lower values indicate a better clustering. Based on the number of data groups we expect from this set, the five cluster result is accepted as the best. 136

Figure 6.16: SOM component planes for F2, F3, and T7 showing the different normalized measurement values across different regions of the map in Figure 6.8, d. 138

Figure 6.17: Log normal distribution fit to a histogram of the QE calculated over all data from 2012-2013. 139

Figure 6.18: Fault detection using the quantization error of new data vectors on the SOM. The pink line on the top corresponds to the threshold for a detected fault. The bottom graph colors the data based on the region of the map the system is in. 140

Figure 6.19: Close-ups of the QE with time calculated (a) after a regular Tfault and (b) during the Novel Event. 141

Figure 6.20: T2 statistic based MPCA classification. While the PCA model of normal outputs a strong fault signal, classification results are inferior to SOM due to nonlinearity in the data and overlapping fault and normal regions in the data space. 142

Figure 6.21: SOM trajectories of the process state for three separate conditions in the tower: (a) normal startup, (b) regular temperature sensor fault, and (c) Novel Event. Each trajectory plots about one day of data. 143

Figure 6.22: The SOM based fault contribution plot for (a) normal steady state operations, (b) typical temperature sensor fault, and (c) the Novel Event showing which variables could be contributing to an elevated fault detection statistic. 144

Figure 6.23: PCA contribution plots of the sensor fault (a), the temperature fault (b), and the Novel Event (c) with respect to the PCA models for the normal and the sensor fault PCA model (the class much Novel Event data was classified with). 145

Figure 6.24 Time series plot of SG colored by classes found by SOM 146

Figure 6.25 Time series plot of T3_T7 colored by classes found by SOM 147

Figure 6.26 Times series plot of T7 colored by classes found by SOM 147

Figure 6.27 Time series plot of F2 colored by classes found by SOM 148

Figure 6.28: Projection of map vectors to (a) two and (b) three dimensions. The pink data points are data drawn from Novel Event. 149

Figure 7.1: Batch reactor process flow sheet. 154

Figure 7.2: Sticky valve faults can be spotted from patterns in PA flow. 155

Figure 7.3: Clogged filter batches can be seen from a changed pattern in dP1 pressure drop through the filter. 156

Figure 7.4: This synchronized, unfolded batch temperature trajectory matches the raw data well. 157

Figure 7.5: This shows the trajectories of reactor pressure. While this batch's pressure is offset, the general pattern of the batch is preserved. 158

Figure 7.6: The synchronized PA flow from batch with a sticky valve still preserves the characteristic behavior of the fault while still synchronizing the batches relative to the average batch. 158

Figure 7.7: The QE of the training data relative to the map fit to normal operations for MSOM. 160

Figure 7.8: 1-SOM maps fit for fault detection of the clogged filter (a) and sticky valve (b) conditions. 161

Figure 7.9: Hit diagrams of normal data on the maps shown in Figure 7.8. In both cases, a large amount of normal data is being projected on to the faulty side of the map, leading to misdiagnosis by the 1-SOM classifier..... 163

Figure 7.10: T squared statistic generated by MPCA. 164

Figure 7.11: QE results from MSOM. 164

Figure 7.12: (a) From MPCA results, low T2 statistic from the sticky valve PCA model causes consistent misdiagnosis of clogged filter data. MSOM result plotted in (b) is more accurate. The horizontal blue line corresponds to each map's NOR threshold. 166

Figure 8.1: FastMan UI before data has been loaded. Clustering and projection figures are shown adjacent to each other to facilitate comparisons with time series data. 169

Figure 8.2: FastMan UI with data from the industrial separation tower. 171

Figure 8.3: Projected data clustering results are displayed on the left. When the user selects a cluster its constituent data is highlighted in the time series on the right. 172

Abstract

Modern chemical plants have distributed control systems (DCS) that handle normal operations and quality control. However, the DCS cannot compensate for fault events such as fouling or equipment failures. When faults occur, human operators must rapidly assess the situation, determine causes, and take corrective action, a challenging task further complicated by the sheer number of sensors. This information overload as well as measurement noise can hide information critical to diagnosing and fixing faults. Process monitoring algorithms can highlight key trends in data and detect faults faster, reducing or even preventing the damage that faults can cause.

This research improves tools for process monitoring on different chemical processes. Previously successful monitoring methods based on statistics can fail on non-linear processes and processes with multiple operating states. To address these challenges, we develop a process monitoring technique based on multiple self-organizing maps (MSOM) and apply it in industrial case studies including a simulated plant and a batch reactor. We also use standard SOM to detect a novel event in a separation tower and produce contribution plots which help isolate the causes of the event.

Another key challenge to any engineer designing a process monitoring system is that implementing most algorithms requires data organized into “normal” and “faulty”; however, data from faulty operations can be difficult to locate in databases storing months or years of operations. To assist in identifying faulty data, we apply data mining algorithms from computer science and compare how they cluster chemical process data from normal and faulty conditions. We identify several techniques which successfully duplicated normal and faulty labels from expert knowledge and introduce a process data mining software tool to make analysis simpler for practitioners.

The research in this dissertation enhances chemical process monitoring tasks. MSOM-based process monitoring improves upon standard process monitoring algorithms in fault identification and diagnosis tasks. The data mining research reduces a crucial barrier to the implementation of monitoring algorithms. The enhanced monitoring introduced can help engineers develop effective and scalable process monitoring systems to improve plant safety and reduce losses from fault events.

Chapter 1 - Introduction

1.1 Background

The information age has given rise to the generation of huge amounts of data. Each year, the world generates about 1.2 zettabytes (10^{21}) of electronic data (Mervis 2012). The concept of big data and the use of large scale analysis is gaining acceptance in a wide variety of applications including the management of supply chains (Marr 2016), water infrastructure (Grady 2016), as well as cloud based public transport (Daniel 2016). While simply generating and storing such huge amounts of data is its own technical achievement, a large gap exists in our ability to utilize big data for problem solving. Without a means of automatically searching for interesting patterns in data, all of the investments in increasing data storage capacity have created at best an archive of human activity and at worse the creation of forgotten "data graveyards" (Venkatasubramanian 2009).

In response to the accumulation of data, scientists developed data mining and machine learning algorithms to process information and extract knowledge from databases. This loose collection of computing algorithms and analysis techniques arose out of earlier research on statistics and data analysis. The earliest applications of PCA to data analysis problems were by Pearson (1901) and Hotelling (1933) to find projections of multivariate data. One of the earliest methods for the automatic classification of data with multiple measurements was proposed by Fisher (1936). Data clustering can be seen as a descendent of work by another scientist named Fisher (1958) who analyzed the problem of "grouping [arbitrary numbers] so that the variance within groups is minimized." Tukey (1961) described exploratory data analysis as procedures for making the gathering and interpretation of data easier and more accurate, and called for research into novel data analysis. Subsequent increases in computing and data storage capacity have made

data mining, the automatic discovery of useful information in large data bases and machine learning, the automated classification of data objects by computer, dynamic areas of research subject to millions of dollars in research projects by the U.S. government (Mervis 2012).

The two broad categories of tools represented by machine learning and data mining are supervised and unsupervised learning, respectively. Machine learning and artificial intelligence, like neural networks, fall under the umbrella of supervised classification, which uses a set of labeled data objects called a "training set" to fit a model to classify unlabeled data for the user. Data mining or data clustering are classified as unsupervised classification where labels for data objects are generated by the algorithm using only the data itself (Tan 2005). Both categories of algorithms have rapidly developed and become a part of modern life across a variety of disciplines. Clinical medicine (Bellazzi 2008), autonomous vehicles (Urmson et al 2008), fraud detection (Bolton 2002), and gene expression data (Jiang 2004) are only a selection of recent advances in machine learning. Harding et al. (2006) reviewed a wide variety of applications of data mining to manufacturing and engineering applications including studies in fault detection, maintenance, customer relationship management, and other areas.

Chemical engineering has also experienced changes and challenges from the dual computing and data revolution. Chemical systems can generate large amounts of data through chemical manufacturing sensor data, quantum and molecular simulations, as well as from pharmaceutical drug development, taking chemical engineers from a "data poor" to a "data rich" paradigm (Venkatasubramanian 2009). Chemical plants in particular represent fertile ground for data mining and machine learning use to grow due to how much chemical manufacturing is already influenced by computer automation. Modern chemical plants use a distributed control system to maintain a consistent product quality and continuously adjust for disturbances entering the process,

with human operators acting as a supervisor over multiple automatic processes. Physically and mathematically, these processes tend to be highly multivariate and non-linear, making control and modeling of these systems challenging. Engineers designing chemical manufacturing processes place great emphasis on making process systems robust to anticipated disturbances, but continuing challenges arise from how to handle unforeseen faults. A fault is formally defined as an unpermitted deviation of one or more characteristic properties of a system, such as heat exchanger fouling, changes in concentration, or equipment problems like valve sticking (Russell 2000).

Helping operators to sift through the large amounts of process data necessary to manage abnormal fault events is an important and useful application of data mining and machine learning on chemical processes. In a study on fault detection on nuclear submarines, Malkoff (1987) argued that factors that compromise operators' ability to assess and address fault events include not only personnel training, stress, and culture, but also the "Christmas tree effect" where major fault events simultaneously trigger more alarms than the human operator can usefully process. These factors all contributed to the mismanagement of industrial accidents such as 3 Mile Island, Deepwater Horizon, and Piper Alpha. In addition to these isolated large-scale disasters, less serious faults occur much more frequently in industrial process systems, resulting in occupational injuries and economic losses. Techniques for *process monitoring* assist operators in the detection and diagnosis of chemical process faults and are crucial to abnormal event management and maintaining a culture of chemical process safety.

Process monitoring consists of three main tasks: (1) fault detection where operators are initially alerted to a plant's abnormal behavior, (2) fault identification, which draws the operators' attention to a subset of equipment likely responsible for a detected fault, and (3) fault diagnosis which identifies the underlying causes of a fault. When these three steps function properly,

operators can act to fix the faulty status of the plant and return to safe and efficient operations (Russell 2000).

Process monitoring techniques can be divided into three classes: knowledge-based methods, qualitative model-based methods, and process history or data driven approaches (Venkatasubramanian 2003). Analytical- or model-based methods can consist of a mathematical model of the dynamics of a system which requires detailed knowledge and familiarity with a system. Model-based process monitoring methods include parameter estimation, state observers, and signal models. Knowledge-based methods arise from years of accumulated experience of people familiar with the monitored process. Heuristic knowledge of the causes of faults can be translated into IF-THEN rules which reliably and understandably connect symptoms to faulty behavior (Isermann 2005). In large, complex systems like chemical plants, both analytical- and knowledge-based methods can require months to years to construct, validate, and implement. In contrast, data-driven methods are derived directly from process data without assuming any underlying physical laws and can take full advantage of the large repositories of process data. Those advantages enable data-driven monitoring technology to be implemented more rapidly and on larger numbers of systems.

Popular data-based techniques for process monitoring include principal components analysis, partial least squares, and neural networks. Wise (1996) used principal component analysis (PCA) to detect faults on a thermocouple and Kourti (1996) used statistical techniques based on PCA and partial least squares to detect and diagnose faults on a recovery process and a batch polymerization reactor. Himmelblau (2008) has applied neural networks to a wide range of chemical engineering tasks such as process monitoring and polymer product quality prediction. Gardner (2000) used data mining to guide the experimental analysis to diagnose process problems

on a semiconductor manufacturing process, resulting in faster solutions and millions of dollars in cost savings. Comprehensive reviews of the numerous successful applications of process monitoring techniques have been performed by Venkatasubramanian (2003), Qin (2012), and Ge (2013).

1.2 Dissertation Motivation

Much research has been done into adapting PCA to process monitoring; however, PCA makes the assumption that the data are linear and formed from Gaussian distributed data. Further adaptations are required to adjust to multiple operating states and to detect and diagnose truly novel fault events. A valuable tool for addressing these challenges comes in the form of self-organizing maps (SOMs). Also known as Kohonen Networks (Kohonen 2001), SOMs are a type of neural network used in the visualization and analysis of high dimensional data and have been applied to a wide range of engineering problems (Kohonen 1996). SOM's versatility comes from its topology preservation and data representation abilities to isolate the key variables and patterns that emerge from data. Vesanto (1999) demonstrated how to use SOM in conjunction with data clustering and analysis.

Previous research has seen SOM applied to fault detection and diagnosis as well as for novelty detection. Alhoniemi (1999) and Simula and Kangas (1995) demonstrate the basics to using SOM for process monitoring problems on several industrial cases and an anesthesia system. They monitor the quantization error (or distance from the BMU) and track changes in the BMU in response to changes in system state. Ypma (1997) showed how to use SOMs for unsupervised novelty detection in detecting pipeline leaks. Wong (2006) applied a modified SOM to novelty detection to machine vibration signal monitoring and classification on data from a helicopter and a rotating bearing test rig. Ng and Srinivasan (2008a), (2008b) proposed a magnitude-based

resampling strategy to help visualize multistate operations and apply it to case studies on a lab-scale distillation unit, refinery hydrocracker, and the Tennessee Eastman Process simulation. Corona et al. (2010; 2012) used SOM to identify significant operational modes and sensitive process variables before developing a process monitoring and control strategy. Yu et al. (2014) proposed a SOM-based methodology modified for non-Gaussian process behavior and validated their approach on the Tennessee Eastman Process simulation. Recently, Robertson et al. (2015) expanded the SOM capabilities for process monitoring towards an overall SOM strategy for process monitoring by formulating additional tools for fault detection and variable contributions mimicking similar properties of PCA-based approaches. The methodology was validated on the Tennessee Eastman Process using simulated data

This research formulates and validates an SOM-based strategy for characterizing an industrial-scale reactor-separation system, diagnosing its common operating states, and detecting novel events. The challenge was to use data from previous years to train the map to model the expected operating states (startup, normal steady state, and sensor fault) and to test this strategy on data from a subsequent year containing a novel process event occurring simultaneously with a common fault. The novel event considered comes from a recent large process fault with economic costs in the hundreds of thousands. A comparison to a basic implementation of MPCA fault detection and diagnosis is given to demonstrate the need for the additional capabilities offered by SOM in this case study, particularly the robustness to non-linearity and data visualizations. It is shown that the proposed overall SOM strategy successfully detects the unknown event and provides information towards understanding the novel fault's root causes.

The second thrust of research concerns not the algorithms used for fault detection, but how to acquire the data to train them through unsupervised learning. The most effective data-based

models for process monitoring are supervised learning algorithms and require a previously assembled repository of data classified into “normal” and “faulty” by users. However, in practice, data previously labelled as faulty or normal is seldom available. Starting from nothing, expertly labeled data sets require much human effort to build and have characteristics that can change with every maintenance cycle. It is imperative for the scalability and widespread adoption of data-based process monitoring techniques to reduce the difficulty and effort required to build labeled databases used in training. Reducing the difficulty of this initial step could lower the time and money required to create advanced fault detection and diagnosis systems and expand their application in industrial settings.

In this dissertation, we propose the use of unsupervised learning as a tool for helping engineers generate normal and faulty labels to use in training data sets. In contrast with supervised learning where data-based models are fit by checking their accuracy against a training set, unsupervised learning includes the tasks of data clustering and dimensionality reduction. Unsupervised learning is a topic studied widely in computer science, but many clustering techniques beyond k-means have seen relatively limited application in process monitoring situations. Wang and McGreavy (1998) performed an early study in clustering process data from a simulated fluid catalytic cracker simulation with a Bayesian automatic classification method. Harding et al. (2006) reviewed data mining applications in a variety of manufacturing environments, including customer relationship management, decision support, and fault detection. Beaver and Palazoglu (2007) used a moving window clustering algorithm based on PCA to detect process states and transition points disturbed by a periodic signal. Bhushan and Romagnoli (2008) utilized self-organizing maps for unsupervised pattern classification and applied in fault diagnosis for CSTR modelling for a fault diagnosis problem. Zhu et al. (2011) used a k-ICA-PCA modelling

method to capture relevant process patterns applied to monitoring the Tennessee Eastman process. Srinivasan et al. (2004) used DPCA-based similarity factor for clustering transitions between different process states in agile chemical plants. Singhal et al. (2005) developed his methodology to cluster multivariate time-series data from similarity factors based on PCA.

To test the practical applicability of the above research, the studies in this dissertation are performed on not only the benchmark Tennessee Eastman simulation (Downs and Vogel 1993), but also on real industrial-scale process equipment. Moving from simulations to real unit operations in a plant entails challenges in process monitoring, including gradual changes in the parameters of the process with time as well as nonlinear changes due to routine process operations.

1.3 Research Aims

The goal of this dissertation is to improve and add process monitoring tools to simplify model implementation tasks and improve the accuracy of the resulting process monitoring system. Specific contributions are outlined below:

- We develop and validate a new process monitoring technique: multiple self-organizing maps (MSOM) and adapt it to all process monitoring tasks including fault detection, identification, and diagnosis. We demonstrate MSOM's superiority over more traditional process monitoring algorithms through application to the benchmark Tennessee Eastman process simulation.
- MSOM is further modified for batch process monitoring using multiway unfolding to unfold entire batches of data and dynamic time warping (DTW) to synchronize each batch to a uniform time scale. We demonstrate the improved detection and diagnosis abilities of MSOM over a couple of competing batch monitoring methods in detecting process faults on an industrial-scale polymerization reactor.

- Traditional SOM is adapted to the novelty detection and process monitoring of an industrial scale separation tower. We use SOM to create a robust model of three separate operating conditions in the separation tower and demonstrate its ability in diagnosing a known process fault and in detecting a novel fault event. Contribution plots effectively isolate the causes of the novel event to a particular section of the separation tower.
- We confront the difficulty of creating training sets for fault detection and diagnosis algorithms by proposing a data mining framework to separate process data from faulty and undesirable operations from normal data. We analyze data from the Tennessee Eastman benchmark simulation and data from the novel event in the separation tower, and in each case cluster normal and faulty data. We tested and compared combinations of different dimensionality reduction and data clustering techniques in this task using supervised clustering metrics.
- Finally we created a user-friendly process data mining tool (FastMan) to enable plant engineers to discover fault events without advanced knowledge of data mining techniques and combine expert knowledge with data analysis results. The user interface allows the rapid testing of different dimensionality reduction and data clustering techniques at separating data from faulty operations from the larger amount of normal data. Using data labelled by Fastman, an engineer can subsequently train a useful fault detection and diagnosis algorithm.

1.4 Publications and Presentations

This section lists the research contributions arising from the work presented in this dissertation, including conference presentations and research papers:

- Thomas, M. C. and Romagnoli, J. (2014) Topological Preservation Techniques for Nonlinear Process Monitoring. 2014 AIChE Annual Meeting. Atlanta, GA.

- Robertson, G., Thomas, M. C., and Romagnoli, J. (2015) Topological Preservation techniques for Nonlinear process monitoring. *Computers and Chemical Engineering*, 76, 1-16.

- Thomas, M. C. and Romagnoli, J. (2015). Data Mining and Monitoring for Industrial Scale Chemical Processes. 2015 AIChE Annual Meeting. Salt Lake City, UT.

- Thomas, M. C. and Romagnoli, J. (2016). Extracting Knowledge from Historical Databases for Process Monitoring using Feature Extraction and Data Clustering. 26th European Symposium on Computer Aided Process Engineering. Portoroz, Slovenia.

- Thomas, M. C. and Romagnoli, J. (2016) Novel Fault Event Detection in Industrial Systems Using Self-Organizing Maps. (Under review).

- Thomas, M. C., Zhu, W., Romagnoli, J. (2016) Data Mining and Clustering in Chemical Process Databases for Monitoring and Knowledge Discovery. (Under review).

1.5 Dissertation Contributions

This doctoral thesis contains several contributions, which are outlined below.

- Fault detection and diagnosis/novel event detection: Formulated, implemented and tested a generalized approach suitable for nonlinear systems based on self-organizing maps
- Data clustering and dimensionality reduction: Defined an approach to data mining of chemical process data and validated the approach on industrial-scale chemical manufacturing equipment
- Fault detection and diagnosis on a batch process: Formulated a general methodology utilizing DTW to data preprocessing and adapted SOM to fault event detection and diagnosis.
- Pioneered development of a data mining tool to allow non-experts in data mining to use the tools presented in this dissertation.

1.6 Dissertation Structure

- Chapter 2 Introduces the data preprocessing techniques used to prepare data for analysis. First, we briefly discuss the removal of statistical outliners, data normalization, and missing data approximation. Next, additional advanced preprocessing methods are presented. Dynamic time warping (DTW) is presented for synchronizing batch process data and demonstrated on a set of batch temperature trajectories. Multiway unfolding is discussed as a method used to process batch data into a useable form. Next, Synthetic Minority Over-sampling Technique (SMOTE) is presented to adjust training data sets for machine learning algorithms that have data distributed between groups unevenly.
- Chapter 3 presents the methodology used for data mining. First, we present a selection of dimensionality reduction techniques used to remove noise data and amplify signals, followed by several data clustering techniques used in unsupervised classification. Supervised cluster evaluation metrics are presented that will be used to compare results from different clustering methods in addition to an example. The last section describes the techniques used to mine the process data.
- Chapter 4 introduces the pattern recognition techniques used for fault detection and diagnosis. Specifically, standard PCA model tools for fault detection, identification, and diagnosis are described along with the newer methods proposed by this thesis based on MSOM. An example on the Fisher Iris data is presented at the end of the chapter.
- Chapter 5 presents a study of data mining and process monitoring on the benchmark Tennessee Eastman process (TEP) simulation. We survey the performance of the data mining and DR techniques introduced earlier and apply it to the unsupervised classification of fault data from the TEP. Clustering results are evaluated using supervised clustering

metrics. We also compare the performance of four algorithms in the process monitoring of TEP data, including fault detection, identification, and diagnosis.

- Chapter 6 applies the previously discussed techniques for data clustering and process monitoring to an industrial-scale separation tower. The analysis first compares different approaches to data clustering to find data from a process fault from among months of historical data. Next, using the process monitoring methods from Chapter 4, we study how this process fault could be detected and validate a strategy based on self-organizing maps for detecting and identifying the process fault.
- Chapter 7 presents an industrial case in process monitoring on a batch process. We apply a strategy combining multiway unfolding and DTW for batch data synchronization with PCA, SOM, and MSOM for the fault detection and diagnosis of two faults on the industrial-scale polymerization reactor.
- Chapter 8 presents FastMan, a prototype process data mining tool, along with illustrative examples of its use for chemical process problems. The goal of this tool is to make the data mining methods presented in this dissertation more accessible for process engineers at a plant who may not be experts in data mining.
- Chapter 9 discusses the results and conclusions of this work and highlights promising avenues of further research.

1.7 References

Alhoniemi, E., Hollmen, J., Simula, O., Vesanto, J. (1999). Process monitoring and modeling using the self-organizing map. *Integrated Computer-Aided Engineering*, 6, 3-14.

Beaver, S. & Palazoglu, A. (2007). Cluster analysis for autocorrelated and cyclic chemical process data. *Industrial and Engineering Chemistry Research*, 46, 3610-3622.

Bellazzi, R. & Zupan, B. (2008). Predictive data mining in clinical medicine: Current issues and guidelines. *International Journal of Medical Informatics, 77*, 81-97.

Bhushan, B. & Romagnoli, J. A. (2008). Self-organizing self-clustering network: A strategy for unsupervised pattern classification with its application to fault diagnosis. *Industrial and Engineering Chemistry Research*, 47, 4209-4219.

Bolton, R. J., Hand, D. J. (2002). Statistical Fraud Detection: A review. *Statistical Science*, 17(3), 235-249.

Corona, F., Mulas, M., Baratti, R., Romagnoli, J. A. (2010). On the topological modeling and analysis of industrial process data using SOM. *Computers and Chemical Engineering*, 34, 2022-2032.

Corona, F., Mulas, M., Baratti, R., Romagnoli, J. A. (2012). Data-derived analysis and inference for an industrial deethanizer. *Industrial and Engineering Chemistry Research*, 51, 13732-13742.

Daniel, J. (2016, February 15). Big data and the cloud. *Cloud Tweaks*. Retrieved from http://cloudtweaks.com/2016/02/big-data-and-the-cloud-combining-forces/

Downs, J. J. & Vogel, E. F. (1993). A plant-wide industrial process control problem. *Computers and Chemical Engineering*, 17(3), 245-255.

Fisher, R.A. (1936). The use of multiple measurements in taxonomic problems. *Annals of Eugenics*, 7(2), 179-188.

Fisher, W. D. (1958). On grouping for maximum homogeneity. *Journal of the American Statistical Association*, 53(284), 789-798.

Gardner, M. & Bieker, J. (2000). Data mining solves tough semiconductor manufacturing problems. *KDD '00 Proceedings of the sixth ACM SIGKDD international conference on Knowledge discovery and data mining*, 376-383.

Grady, B. (2016, February 19). Can Big Data save our water infrastructure? *GreenBiz*. Retrieved from https://www.greenbiz.com/article/can-big-data-save-our-water-infrastructure

Ge, Z., Song, Z., Gao, F. (2013). Review of recent research on data-based process monitoring. *Industrial and Engineering Chemistry Research*, 52, 3543-3562.

Harding, J. A., Shahbaz, M., Srinivas, S., Kusiak, A. (2006). Data mining in manufacturing: A review. *Journal of Manufacturing Science and Engineering*, 128, 969-976.

Himmelblau, D. M. (2008). Accounts of experiences in the application of artificial neural networks in chemical engineering. *Industrial and Engineering Chemistry Research*, 47, 5782-5796.

Hotelling, H. (1933). Analysis of a complex of statistical variables into principal components. *Journal of Educational Psychology*, 24(6), 417-441.

Iserman, R. (2005). Model-based fault-detection a diagnosis – status and applications. *Annual Reviews in Control*, 29, 71-85.

Jiang, D., Chun, T., & Zhang, A. (2004). Cluster analysis for gene expression data: A survey. *IEEE Transactions on Knowledge and Data Engineering*, 16(11), 1370-1386.

Kohonen, T. (2000). *Self-organizing maps*. Berlin: Springer-Verlag.

Kohonen, T., Oja, E., Simula, O., Visa, A., and Kangas, J. (1996). Engineering Applications of the Self-Organizing Map. *Proceedings of the IEEE*, 84(10), 1358-1384.

Koutri, T. (2002). Process analysis and abnormal situation detection: From theory to practice. *IEEE Control Systems Magazine*, 10-25.

Malkoff, D. B. (1987). A framework for real-time fault detection and diagnosis using temporal data. *Artificial Intelligence in Engineering*, 2(2), 97-111.

Marr, B. (2016, April 22). How big data and analytics are transforming supply chain management. *Forbes*. Retrieved from http://www.forbes.com/sites/bernardmarr/2016/04/22/how-big-data-and-analytics-are-transforming-supply-chain-management/2/#634e1dcc382e

Mervis, J. (2012). U.S. Science Policy: Agencies Rally to Tackle Big Data. *Science*, 335(6077), 22.

Ng, Y. S. & Srinivasan, R. (2008a). Multivariate temporal data analysis using self-organizing maps. 1. Training methodology for effective visualization of multistate operations. *Industrial and Engineering Chemistry Research*, 47, 7744-7757.

Ng, Y. S. & Srinivasan, R. (2008b). Multivariate temporal data analysis using self-organizing maps. 2. Monitoring and diagnosis of multistate operations. *Industrial and Engineering Chemistry Research*, 47, 7758-7771.

Pearson, K. (1901). On lines and planes of closest fit to systems of points in space. *Philosophical Magazine*, 2, 559-572.

Qin, S. J. (2012). Survey on data-driven industrial process monitoring and diagnosis. *Annual Reviews in Control*, 36, 220-234.

Robertson, G., Thomas, M. C., Romagnoli, J. A. (2015). Topological preservation techniques for nonlinear process monitoring. *Computers and Chemical Engineering*, 76, 1-16.

Russell, E. L., Chiang, L. H. , Braatz, R. D. (2000). Data-driven techniques for fault detection and diagnosis in chemical processes. London: Springer.

Simula, O. & Kangas, J. (1995). Process monitoring and visualization using self-organizing maps. *Neural Networks for Chemical Engineers*, 6, 371-384.

Singhal, A. & Seborg, D. E. (2005). Clustering multivariate time-series data. *Journal of Chemometrics*, 19, 427-438.

Srinivasan, R., Wang, C., Ho, W. K., & Lim, K. W. (2004) Dynamic principal component analysis based methodology for clustering process states in agile chemical plants. *Industrial and Engineering Chemistry Research*, 43, 2123-2139.

Tan, P., Steinbach, M., & Kumar, V. (2006) *Introduction to Data Mining*. Boston: Longman.

Tukey, J. W. (1962). The Future of Data Analysis. *The Annals of Mathematical Statistics*, 33(1), 1-67.

Urmson, C., Anhalt, J., Bagnell, D., Baker, C., Bittner, R., Clark, M. N., … Ferguson, D. (2008). Autonomous Driving in Urban Environments: Boss and the Urban Challenge. *Journal of Field Robotics* 25(8), 425-466.

Venkatasubramanian, V., Rengaswamy, R., Kavuir, S. N., & Yin, K. (2003). A review of process fault detection and diagnosis part I: Quantitative model-based methods. *Computers & Chemical Engineering*, 27, 293-311.

Venkatasubramanian, V. (2009). Drowning in Data: Informatics and Modeling Challenges in a Data-Rich Networked World. *AIChE Journal*, 55(1), 2-8.

Wang, X. Z. & McGreavy, C. (1998). Automatic classification for mining process operational data. *Industrial and Engineering Chemistry Research*, 37, 2215-2222.

Wise, B. M. & Gallagher, N. B. (1996). The process chemometrics approach to process monitoring and fault detection. *Journal of Process Control*, 6(6), 329-348.

Wong, M. L. D., Jack, L. B., Nandi, A. K. (2006). Modified self-organising map for automated novelty detection applied to vibration signal monitoring. *Mechanical Systems and Signal Processing*, 20, 593-610.

Ypma, A.& Duin, R. (1997). Novelty detection using self-organizing maps. *Progress in Connectionist-Based Information Systems*, 1322-1325.

Yu, H., Khan, F., Garaniya, V., & Ahmad, A. (2014). Self-organizing map based fault diagnosis technique for non-Gaussian processes. *Industrial and Engineering Chemistry Research*, 53(21), 8831-8843.

Zhu, Z., Song, Z., & Palazoglu, A. (2011) Transition Process Modeling and Monitoring based on dynamic ensemble clustering and multi-class support vector data description. *Industrial and Engineering Chemistry Research*, 50, 13969-13983.

Chapter 2 - Data Preprocessing

Data mining provides methods for analyzing large amount of multivariate data accumulated in modern chemical process databases, however, in many cases these data are not in a form suitable for the desired application. Firstly, data must be normalized to remove the artificial influence of engineering units used in measurements. Errors from sensor instruments and sampling techniques must also be removed as they can give rise to outliers and missing data.

In more advanced case studies, preprocessing can address other crucial issues with the data. In batch process monitoring, methods developed for processes approximately at steady state cannot be applied due to time-dependent variations in the data and the way it occurs in discrete batches in a time-varying trajectory. In applying machine learning and classification to process monitoring and fault diagnosis studies, challenges arise from imbalance in training data sets. Often a large amount of normal, steady state data is available with a relatively small amount of fault data. Data sets with these challenges require specialized algorithms for their proper use.

This chapter reviews basic data preprocessing and also presents two techniques used to preprocess batch data for the adaptation of fault detection and diagnosis algorithms: multiway unfolding and dynamic time warping. Section 2.1 covers basic data cleaning and preprocessing. Section 2.2 introduces the idea behind multiway unfolding. Section 2.3 describes dynamic time warping (DTW) in detail. Section 2.4 presents a technique used to balance and resample training data for machine learning algorithms: Synthetic Minority Over-sampling Technique (SMOTE).

2.1 Data Pretreatment

To ensure accurate and effective process monitoring, data must be cleaned and pretreated. Three standard pretreatment operations are outlier removal, data normalization, and missing data interpolation.

2.1.1 Outlier removal

An outlier is a statistical anomaly that does not follow the statistical distribution of the bulk of the data. Outliers represent extreme values far outside the statistical distribution of practical measurements. Outliers can be influential observations and cleaning the data of outliers can dramatically affect the estimates, confidence region, and other tests performed on the data. Because of the effects outliers can have on the integrity of a data set, their detection and removal is crucial before further analysis. (Romagnoli 2012). Chen and Romagnoli (1998) used a mean minimum distance-based clustering method for outlier removal. Russell et al. (2000) proposed a method for outlier removal using the T^2 statistic. Other techniques for outlier removal are reviewed in Rousseeuw (1987).

2.1.2 Data normalization

In monitoring, data must be autoscaled or normalized to remove the effects of engineering units on the statistics of a process. For example, a change in a flow measurement from 0.1 kg/hr to 1 kg/hr is much more significant than a change in a temperature measurement from 400°C to 410°C. In this dissertation, to ensure that each measurement is given equal weight in the modeling process, all data used for monitoring are scaled to zero mean and unit variance. For each sensor, a sample mean is calculated from the process historical data along with the sample standard deviation. To normalize the data set as well as new sensor measurements, we subtract the mean from each measurement and divide by the standard deviation

$$x_n = \frac{x - \hat{\mu}}{\hat{\sigma}}$$

When x is a measurement, x_n is the normalized measurement and the feature sample mean and standard deviation are $\hat{\mu}$ and $\hat{\sigma}$ respectively. Another common normalization is range

normalization, which scales each feature of the data set to have the range 0 to 1 by subtracting the minimum value and dividing by the range:

$$x_n = \frac{x - x_{min}}{x_{max} - x_{min}}$$

where x_{min} and x_{max} is the minimum and maximums of the data set (Tan 2005).

2.1.3 Missing data approximation

Missing data may arise in process databases from instrument or software errors. They can often be removed without affecting data analysis, but in smaller data sets they can have a larger impact. In these cases, data must be filled in using interpolation techniques to facilitate further analysis. In this dissertation, missing data are filled in using linear interpolation.

2.2 Multiway Unfolding

Most process monitoring systems are designed for steady state operations where the normality of the system is often evaluated based on the statistical significance data from a single unit of time. The ideal steady state system normally experiences measurement noise or small perturbations but generally remains in a well-defined region of normal operations. In contrast to steady state systems, batch processes experience large amounts of non-linear, time-varying changes over the course of each batch. Data-based models of batch processes for fault detection and diagnosis must take into consideration these fluctuations in order to adequately characterize the region of normal operations.

Multiway unfolding introduced by Nomikos and McGregor (1994) allows an entire batch's data to be considered as an individual data object. In a typical batch run, $j = 1,2, \dots, J$ variables are measured at $k = 1,2, \dots, K$ time intervals throughout the batch. Similar data exists on several ($i = 1,2, \dots, I$) similar process batch runs. This vast amount of data can be organized into a three-way array $\underline{X}(I \times J \times K)$ (Nomikos and MacGregor 1995). In the time-wise unfolding approach

depicted in Figure 2.1, the three-way array is reorganized into a two-way array. The method combines the measured variables dimension with time. The first J columns of the unfolded matrix contain the first measurement recorded for each sensor for the first timestamp. Columns J through 2J contain measurements from the J sensors taken during the second time point and so forth. Complete rows of the unfolded matrix correspond to individual batches. Each vertical slice is a $(I \times J)$ matrix representing the values of all sensors for all batches at the common time interval k (Nomikos and MacGregor 1994).

Once the three-way array is decomposed into two-way form, the data can be modeled using PCA or another approach in similar fashion with steady state data. However, in contrast to steady state process monitoring systems where new data is evaluated at each new time point, the multiway monitoring approach creates a new row at the end of each batch. This approach has been adapted so that statistical process control can use data from each time point of the batch (Nomikos and MacGregor 1995).

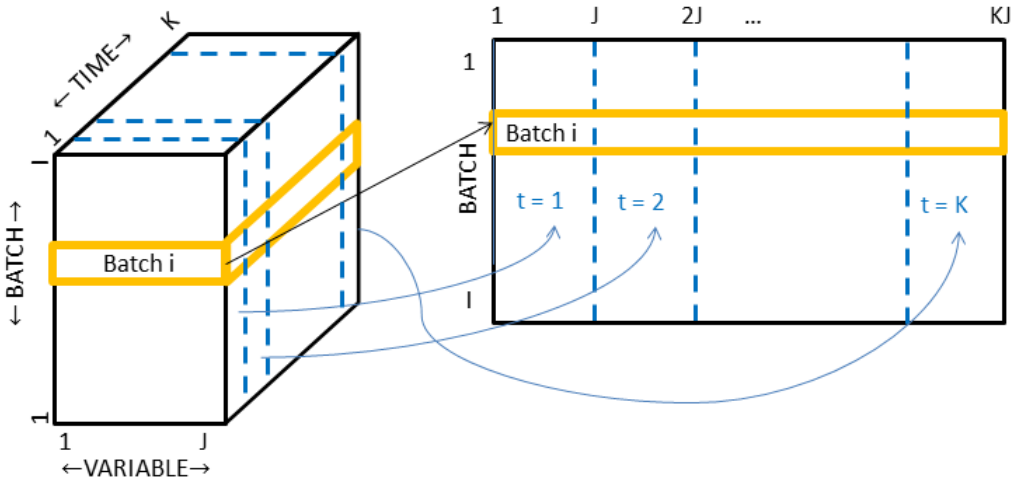

Figure 2.1: Multiway unfolding of batch process data takes the three-dimensional batch process data matrix and unfolds it into a two-dimensional matrix. In the new matrix, each batch's data formed into a single row of entries.

2.3 Dynamic Time Warping (DTW)

In the previous section, multiway unfolding is presented as a way to adapt steady state process monitoring strategies to batch processes. While multiway unfolding is crucial for making batch process monitoring a tractable problem, an additional challenge posed by batch processes is that often each batch has a different length of time. As a result, the three-dimensional matrix in Figure 2.1 contains a large amount of variation in the time dimension. Decomposition to the two-dimensional matrix required for the monitoring techniques studied requires each batch to use the same amount of time.

The simplest way to synchronize batch trajectories of different length is to simply use the minimum time length of each batch (Rothwell et al 1998), but this approach clearly ignores large amounts of data and the variations in the batch durations. Nomikos and MacGregor (1995) executed their monitoring strategy based on a "trigger variable" which synchronizes each batch at time 0 using set criteria. Yao and Gao (2009) present a comprehensive review of different approaches to the batch monitoring problem, particularly phase division methods which use the multiphase characteristics of batch processes. The selection of the correct phase division is crucial, and phase division methods based on expert knowledge, process data analysis, or data-based methods.

The approach used in this dissertation uses the method proposed by Kassidas et al. (1998) which synchronizes each batch to the same timeframe using dynamic time warping (DTW), a technique drawn from speech recognition (Itakura 1974) and modified for multivariate process monitoring. DTW was originally developed by Sakoe and Chiba (1978) as a pattern-matching algorithm for spoken word recognition with a nonlinear time-normalization effect. DTW minimizes the distance between two time trajectories by aligning similar data observations. Series

of data may be expanded, compressed, or shifted in time and some data points may be duplicated, but these operations are done in a way that minimizes the distance between the two trajectories of data. The key advantage of the DTW strategy discussed below is that it synchronizes all batch data trajectories to be the same length in time, which allows the use of the entire trajectory of a batch of data instead of only a smaller amount of points selected artificially.

2.3.1 Synchronization of batch trajectories with DTW

The DTW algorithm proposed by Kassidas et al. (1998) uses a combination of symmetric and asymmetric synchronization. In a symmetric DTW algorithm, the synchronized trajectories are given a newer, longer length that arises out of the calculations and cannot be fixed at the beginning, meaning that synchronizing each trajectory to $\boldsymbol{B}_{REF}$will yield a trajectory with a different length. Each $\boldsymbol{B}_i$ will be synchronized with $\boldsymbol{B}_{REF}$, but not with any other batch in the data set, which does not meet the need of uniform duration required for training a process monitoring model. Therefore, asymmetric synchronization is desirable because it favors $\boldsymbol{B}_{REF}$ and outputs trajectories with the same length as the reference trajectory. The disadvantage of using only asymmetric synchronization is that it may miss data points that do not precisely match the reference trajectory. Training a process monitoring data with these inconsistent data filtered out would yield a fault detection algorithm biased towards false alarms, since anything inconsistent in a new batch trajectory would look like a fault. Therefore, the DTW algorithm used first synchronizes with symmetric DTW before using asymmetric DTW (Kassidas et al. 1998). The result is still a symmetric algorithm, meaning that the optimal path found passes through all data points in both patterns.

The DTW algorithm used to synchronize the batch data studied in this dissertation is given below (Kassidas et al. 1998). Let $\boldsymbol{B}_i, i = 1, \dots, I$ be a set of I batch trajectories. Each $\boldsymbol{B}$ is a b x N

matrix where b is the number of measured variables. In our application, the data have been normalized to zero mean and unit variance. Before beginning synchronization, a $\boldsymbol{B}_{REF}$ baseline reference batch is selected at the beginning of the process. $\boldsymbol{B}_{REF}$ affects how long the synchronized batch data trajectory will be and for the first few iterations of the algorithm, $\boldsymbol{B}_{REF}$ functions as an average batch.

- Step 1: Symmetric DTW Algorithm
    - For each $\boldsymbol{B}_i$, apply DTW between $\boldsymbol{B}_i$ and $\boldsymbol{B}_{REF}$ using the following constraints
        - Fixed endpoint constraints
        - Band global constraint
        - Local constraint

$$\boldsymbol{D}_A(i,j) = min\begin{Bmatrix} \boldsymbol{D}_A(i-1,j) + d(i,j) \\ \boldsymbol{D}_A(i-1,j-1) + d(i,j) \\ \boldsymbol{D}_A(i,j-1) + d(i,j) \end{Bmatrix}, \boldsymbol{D}_A(1,1) = d(1,1)$$

After the trajectory is synchronized symmetrically, the result is compressed via an asymmetric synchronization step:

- Step 2: Asymmetric synchronization
    - When multiple points from $\boldsymbol{B}_i$ are aligned with a single point of $\boldsymbol{B}_{REF}$:
        - Average of the points from $\boldsymbol{B}_i$.
        - Align the average point with the point from $\boldsymbol{B}_{REF}$
    - After synchronization, $\boldsymbol{B}_i$ contains the same number of data points as $\boldsymbol{B}_{REF}$.

As an illustration of asymmetric synchronization, assume that $\boldsymbol{B}_i$ is placed on the horizontal and $\boldsymbol{B}_{REF}$on the vertical axis. This arrangement does not affect the DTW algorithm in Step 1 since it is symmetric. Also, assume that after DTW, the following three points are included in the optimal

path: $(i-1,j),(i,j)$, and $(i+1,j)$. According to them, the $(i-1)$th and $(i+1)$th points of $\boldsymbol{B}_i$ are all aligned with the jth point of $\boldsymbol{B}_{REF}$. The proposed method takes the average of the three:

$$\frac{\boldsymbol{B}_i(i-1,:)+\boldsymbol{B}_i(i,:)+\boldsymbol{B}_i(i+1,:)}{3}$$

And synchronizes this average with $\boldsymbol{B}_{REF}(j,:)$

Figure 2.2, a. and Figure 2.2, b. show the utility of DTW in synchronizing a measurement over a set of batch data trajectories. Each colored line in Figure 2.2 corresponds to the evolution of a measured variable over the course of the batch and the black bolded line represents the baseline average batch $\boldsymbol{B}_{REF}$ which all the other batches are compared. Therefore, each batch $\boldsymbol{B}_i$ is of dimension $1 \times N$, where N is the time length of each batch that varies from batch to batch. Each batch ranges in length from 29 minutes to 43 minutes. While the normal batches generally remain close to the bolded line representing the average batch, two trajectories are noticeably abnormal. The blue trajectory that begins low also ends early, and may be out of sync due to abnormal factors in other parts of the process. The magenta trajectory that dips towards the end may also be experiencing abnormal conditions. Figure 2.2, b. shows the batch trajectories after they have been synchronized with the average batch. DTW brings each batch's behavior closer to the average line, making small adjustments in the timing of observations to minimize distance between each $\boldsymbol{B}_i$ and $\boldsymbol{B}_{REF}$.

The DTW alignment plots in Figures 2.3 and 2.4 display the distances considered by DTW in synchronizing two sample trajectories and plots the path of minimum distance chosen by DTW. Figure 2.3 shows the alignment path of a normal batch. Perfect alignment would be a straight diagonal line, but the low distances along the alignment path point to good matching between $\boldsymbol{B}_i$ and $\boldsymbol{B}_{REF}$. Figure 2.4 shows the alignment path of an abnormal batch. The abnormality of this batch is visible by the higher distances (dark reds) towards the bottom right corner, where the

optimum end point should be located. Though the data poorly matches $\boldsymbol{B}_{REF}$, the abnormal characteristics are largely preserved in the synchronized trajectory.

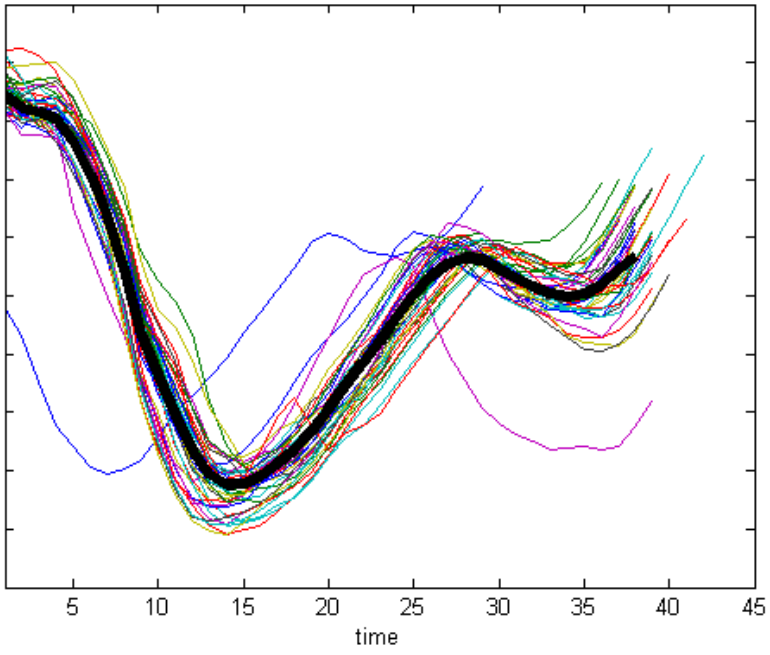

(a)

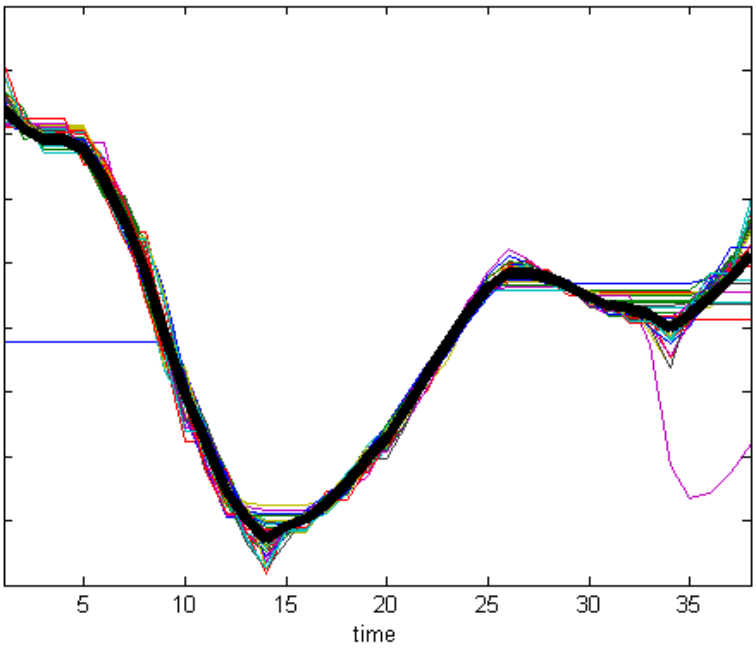

(b)

Figure 2.2: Batch sensor measurement data (a) before synchronization and (b) after synchronization. In both figures, the average trajectory is indicated by the bolded black line. Two abnormal batches are visible: one occurs before the others (blue) and another dip.

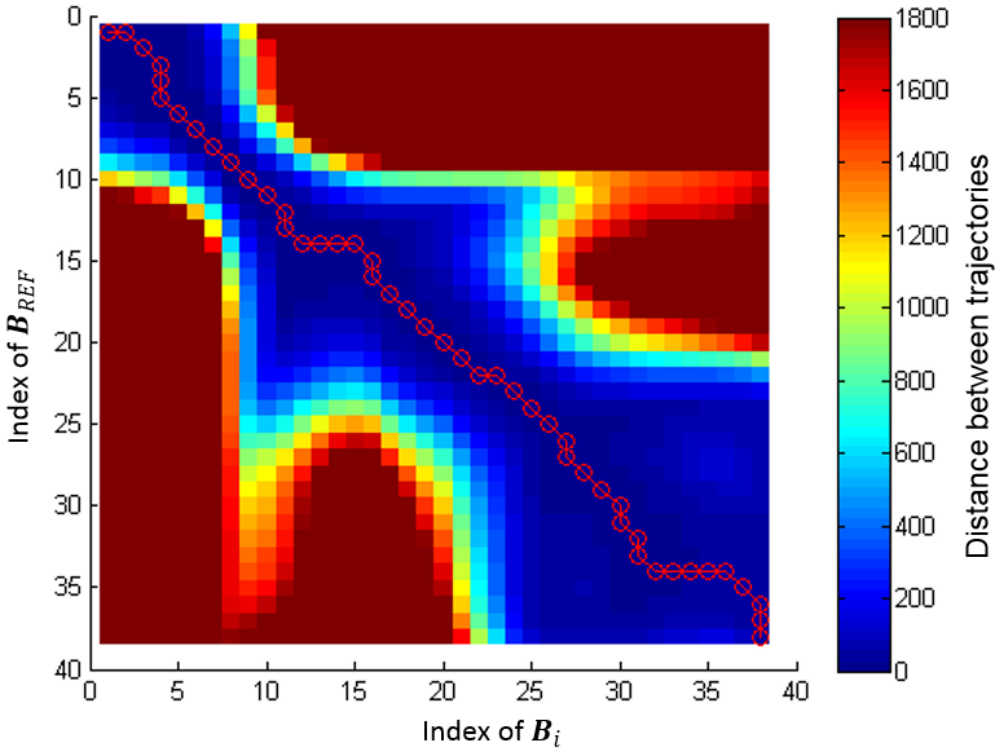

Figure 2.3: DTW alignment path of a normal batch from the example batch data trajectories.

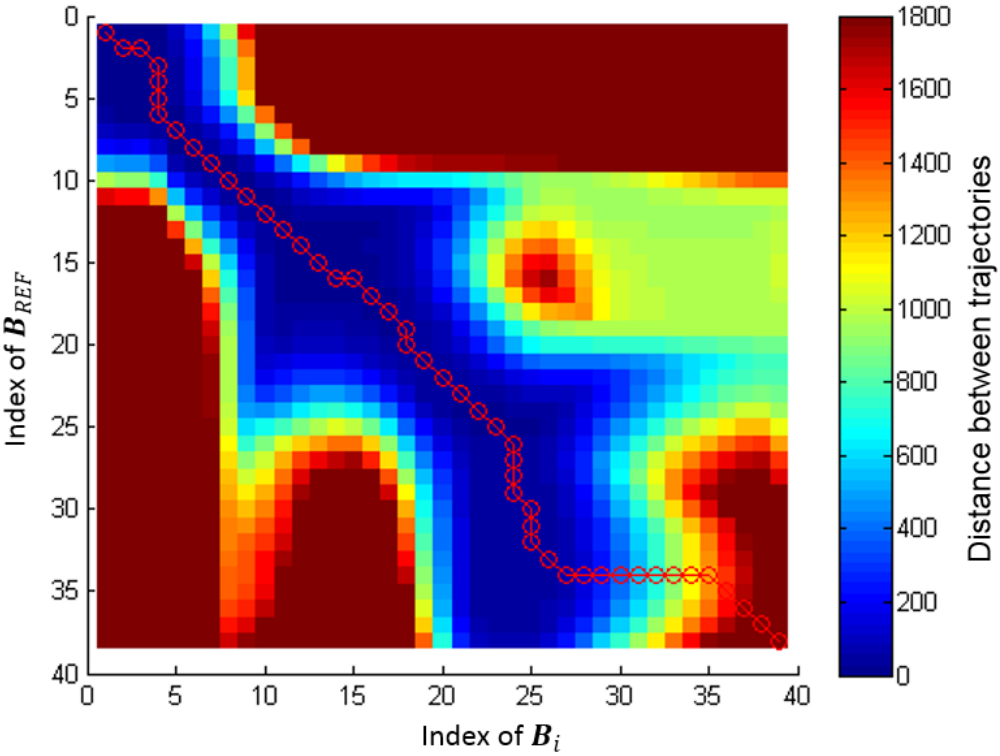

Figure 2.4: DTW alignment path of the batch trajectory that dips at the end in Figure 2.2, a.

2.3.2 Iterative synchronization of multivariate batch process data

The algorithm presented in the last section symmetrically synchronizes two trajectories of batch process data. When synchronizing an entire set of batch process data, initial steps must be taken to ensure that the relative importance of different measurements are considered in the synchronization process and to remove any bias that might arise from the selection of the reference trajectory.

Scaling the data set is important for emphasizing the variables that are very consistent from batch to batch. Subjective weights could be assigned to each variable, but that approach requires process knowledge. Instead a procedure to weight the variables is built into the synchronization algorithm. For each variable, the sum of squared error from the reference trajectory over every batch considered is used as an indicator of its consistency. The relative importance of variables is encoded in the weight matrix $\boldsymbol{W}$ that is used in the distance computation in DTW, given by:

$$d(i,j) = [\boldsymbol{B}_i(i,:) - \boldsymbol{B}_{REF}(j,:)] \cdot \boldsymbol{W} \cdot [\boldsymbol{B}_i(i,:) - \boldsymbol{B}_{REF}(j,:)]^T$$

First the data must be scaled according to the procedure below.

- Let $\boldsymbol{B}_{RAW}, i = 1, \dots, I$ be a set of unsynchronized trajectories which contain raw measurements from *I* good quality batches.
- For each variable, calculate its average range by averaging the range from each batch; store these values because they will be used in the offline and online monitoring of a new batch.
- Divide each variable in all batches with its average range.
- Let$\boldsymbol{B}_i, i = 1, \dots, I$ be the resulting set of scaled batch trajectories.

Below is the DTW synchronization procedure:

- Step 0: Initialization:

- Select the reference trajectory from the training set of batch trajectories $\boldsymbol{B}_k$, i.e. $\boldsymbol{B}_{REF} = \boldsymbol{B}_k$. Consequently: $b_{REF} = b_k$
- Set W (the weight matrix in the DTW algorithm) equal to the identity matrix.
- Execute the following steps for a specified maximum number of iterations.

- Step 1, synchronize all $\boldsymbol{B}_i, i = 1, \dots, I$ with $\boldsymbol{B}_{REF}$ according to the procedure described in the previous section. Now $\widehat{\boldsymbol{B}}_i, i = 1, \dots, I$ are synchronized trajectories, each with the same duration as b_{REF}.
- Step 2. Calculate the average trajectory $\overline{\boldsymbol{B}}$, by $\overline{\boldsymbol{B}} = \sum_{i=1}^{i} \widehat{\boldsymbol{B}}_i / I$
- Step 3. For every variable, calculate the sum of squared error (SSE) from $\overline{\boldsymbol{B}}$
  - The inverse of the SSE will be the weight of variable in the following iteration. More specifically, $\boldsymbol{W}$ will be the diagonal matrix with:

$$\boldsymbol{W}(i,j) = \left[\sum_{i=1}^{I}\sum_{k=1}^{b_{REF}}\left[\widehat{\boldsymbol{B}}(k,j) - \overline{\boldsymbol{B}}(k,j)\right]^2\right]^{-1}$$

  - Normalize $\boldsymbol{W}$ such that the sum of the weights is equal to the number of variables. To accomplish this, $\boldsymbol{W}$ is multiplied by the number of variables N divided by the sum of the diagonals in :

$$\boldsymbol{W} = \boldsymbol{W} * \left(N / \left[\sum_{j=1}^{N} \boldsymbol{W}(j,j)\right]\right)$$

- Step 4. For the first three iterations, use the same $\boldsymbol{B}_{REF}$ selected initially.
- For subsequent iterations, use the average trajectory: $\boldsymbol{B}_{REF} = \overline{\boldsymbol{B}}$

At the end of this procedure, the length of the synchronized trajectories will match the length of the reference trajectory $\boldsymbol{B}_{REF}$ selected initially. The duration of the synchronized batch

could be adjusted by calculating the average duration of the initial batches and choosing a good trajectory close to the average duration to act as the $\boldsymbol{B}_{REF}$. With this approach, the duration of the synchronized trajectories will be the average duration of all batches. The maximum number of iterations is a parameter that must be selected by the user. Changes in $\boldsymbol{W}$ could be monitored every iteration and used to evaluate the convergence of the algorithm.

2.4 Synthetic Minority Over-sampling Technique (SMOTE)

In practice, fault detection and diagnosis and other data-driven classification applications often have a problem with data set imbalance. Normal data by definition will be more numerous than fault data, often by a sizable margin. In a data set with 99% normal data, a default guess of normal would achieve 99% accuracy. In these cases, there is a higher cost of missing fault cases than missing normal cases. Data set imbalance is an important issue with discriminant analysis and in training fault diagnosis algorithms where imbalance in the data can cause one fault class to dominate the others. To balance the representation of normal and faulty data in a data-based model for fault diagnosis, it is vital to make maximum use of the information in faulty data by oversampling fault data and undersampling data from normal operations.

Ling and Li (1998) performed a comprehensive study of the interaction of oversampling and undersampling and how it affects classification performance using a data set from product marketing. Different undersamplings of the majority class were tested and measured using lift analysis and the study determined that the best lift index is obtained when the classes are equally represented. Oversampling with replacement itself was found not to significantly improve minority class recognition. As the minority class is over-sampled by increasing amounts, the effect is to identify similar but more specific regions in the feature space as the decision region for the minority class. In the fault diagnosis case, for example, where fault regions of space must be

distinguished from the normal operating region, sampling with replacement can actually make the minority decision region smaller and more specific as minority samples in the region are duplicated. SMOTEd data has larger decision regions and leads to larger decision regions with improved characterization of the shape and size of the fault regions.

SMOTE is an over-sampling approach in which the minority class is over-sampled by creating "synthetic" examples rather than by over-sampling with replacement. SMOTE creates new data along line segments between randomly chosen *k* nearest neighbors among the minority class of data. The user specifies *k*, the number of nearest neighbors to generate. For each minority data point, SMOTE finds its *k* nearest neighbors in the minority data set, selects a number of them based on the percent over-sampling specified (for example, when $N = 200\%$, two neighbors are selected), and randomly generates a synthetic data point along the line between the data point and its nearest neighbor. This process generalizes and "fleshes out" the decision region of the minority class to a larger and less specific region (Chawla 2002).

The SMOTE algorithm in full is:

Algorithm $SMOTE(T, N, k)$
Input: Number of minority class samples *T*; Amount of SMOTE *N*%; Number of nearest neighbors *k*
Output: $(N/100) * T$ synthetic minority class samples

1. */* If N is less than 100% randomize the minority class samples as only a random percent of them will be SMOTEd */*
2. ***if*** $N < 100$
3. Then randomize the T minority class samples
4. $T = \left(\frac{N}{100}\right) * T$
5. $\mathrm{N} = 100$
6. ***endif***
7. $N = (int)(N/100)$ */* The amount of SMOTE is assumed to be integral multiples of 100.*/*
8. k = number of nearest neighbors found for synthetic data generation
9. $Numattrs$ = number of attributes
10. $Sample[\,][\,]$: array storing original samples drawn from the minority class
11. $newindex$: counts the number of synthetic samples generated, initialized at 0

12. $Synthetic[\,][\,]$: array for synthetic samples /* Compute k nearest neighbors for each minority sample only. */
13. $\boldsymbol{for}\ i \leftarrow 1\ to\ T$
14. Compute *k* nearest neighbors for i, and save the indices in the $nnarray$
15. $Populate(N, i, nnarray)$
16. $\boldsymbol{endfor}$

$Populate\ (N, i, nnarray)$ /* Function to generate the synthetic samples. */

17. $\boldsymbol{while}\ N \neq 0$
18. Pick one of the *k* nearest neighbors of i with a random number between 1 and *k*
19. $\boldsymbol{for}\ attr \leftarrow 1\ to\ numattrs$
20. Compute: $diff = Sample[nnarray[nn]][attr] - Sample[i][attr]$
21. Compute: $gap =$ random number between 0 and 1
22. $Synthetic[newindex][attr] = Sample[i][attr] + gap * dif$
23. $\boldsymbol{endfor}$
24. $newindex++$
25. $N = N - 1$
26. $\boldsymbol{endwhile}$
27. $\boldsymbol{return}$ /* End of Populate */

End of Pseudo-Code (Chawla 2002)

To undersample data from the majority class, samples are randomly removed from the population until the size of the majority class becomes some specified percentage of the minority class. In SMOTE terminology, stating that "the majority class is under sampled at 200%," means that in the modified, "SMOTEd" data set, the number of data points from the minority class will be double the number of data points from the majority class. For example, if the minority class had 50 samples and the majority class had 200 samples and we under sample the majority at 200%, the majority class would end up having 25 samples. Equal representation between minority and majority classes occurs when the majority class is under sampled at 100% (i.e. the number of majority samples is 100% of the number of minority samples). To create a balanced dataset, generally both oversampling of the minority class and undersampling of the majority class are required.

2.5 References

Chawla, N. V., Bowyer, K. W., Hall, L. O., & Kegelmeyer, W. P. (2002). SMOTE: Synthetic minority over-sampling technique. Journal of Artificial Intelligence Research, 16, 321-357.

Chen, J., & Romagnoli, J. A. (1998). Strategy for simultaneous dynamic data reconciliation and outlier detection. Computers and Chemical Engineering, 22, 559-562.

Itakura, F. (1975). Minimum prediction residual principle applied to speech recognition. IEEE Transactions on Acoustics, Speech, and Signal Processing, 23(1), 67-72.

Kassidas, A., MacGregor, J. F., & Taylor, P. A. (1998). Synchronization of batch trajectories using dynamic time warping. American Institute of Chemical Engineers Journal, 44(4), 864-875.

Ling, C. X., & Li, C. (1998). Data mining for direct marketing: Problems and solutions. Proceedings of the Fourth International Conference on Knowledge Discovery and Data Mining, 73-79.

Nomikos, P., & Macgregor, J. F. (1994). Monitoring batch processes using multiway principal component analysis. American Institute of Chemical Engineers Journal, 40(8), 1361-1375.

Nomikos, P., & Macgregor, J. F. (1995). Multivariate SPC charts for monitoring batch processes. Technometrics, 37(1), 41-59.

Romagnoli, J. A., & Palazoglu, A. (2012). Introduction to process control. Boca Raton: Taylor and Francis Group.

Rothwell, S. G., Martin, E. B., & Morris, A. J. (1998). Comparison of methods for dealing with uneven length batches. Proceedings of the 7th International Conference on Computer Application in Biotechnology (CAB7), 387–392

Rousseeuw, P.J., & Leroy, A. M. (1987). Robust regression and outlier detection. New York: Wiley.

Russell, E. L., Chiang, L. H., & Braatz, R. D. (2000). Data-driven techniques for fault detection and diagnosis in chemical processes. London: Springer.

Sakoe, H., & Chiba, S. (1978). Dynamic programming algorithm optimization for spoken word recognition. IEEE Transactions on Acoustics, Speech, and Signal Processing, 26(1), 43-49.

Tan, P., Steinbach, M., & Kumar, V. (2006) Introduction to data mining. Boston: Longman.

Yao, Y., & Gao, F. (2009). A survey of multistage/multiphase statistical modeling methods for batch processes. Annual Reviews in Control, 33, 172-183.

Chapter 3 - Data Mining Techniques

Each year, the world generates 1.2 zettabytes (10^{21}) of data composed of everything from social media posts, pictures, videos to scientific sensor measurements (Mervis 2012). As impressive as society's ability to generate data may be, extracting useful information from large data sets remains a challenge. While traditional statistics remain vital tools for the design and analysis of experiments, they are poorly suited to the challenges of extremely large data sets. Data mining techniques are algorithms for computationally discovering meaningful patterns and relationships among large data sets that would be difficult to find through traditional analysis methods. For example, Gardner and Bieker (2000) demonstrated several case studies in which hypotheses generated through data mining solved complex manufacturing problems on semiconductor processes that conventional experimental and statistical approaches consistently missed.

This dissertation will evaluate the applicability of dimensionality reduction (DR) and data clustering techniques drawn from computer science literature to extract fault knowledge from chemical process databases. Previous approaches to data clustering in the chemical engineering literature often involve elaborate modifications and combinations of PCA or other statistical concepts, but few have utilized the potential of standard clustering strategies from the computer science literature. Innovative and proven clustering techniques such as DBSCAN, BIRCH, Meanshift, and others can offer improved and efficient methods for finding clusters in chemical process data. The role of dimensionality reduction, also known as feature extraction, is also considered because of the prominent role it plays in knowledge discovery as well as process monitoring. As an example, Ding (2004) explores the close relationship between unsupervised

learning and dimensionality reduction and provides a theoretical basis for the use of PCA dimensionality reduction in K-means clustering.

This chapter presents the algorithms we use to study chemical process data. Section 3.1 discusses the general workflow used in analysis. Section 3.2 covers dimensionality reduction algorithms used to project data to a reduced subspace for clustering. Section 3.3 introduces the clustering algorithms considered. Section 3.4 presents several ways to evaluate clustering results including homogeneity, completeness, and adjusted Rand index (ARI).

3.1 Data Mining Approach

Figure 3.1 outlines the data mining approach used. First, DR techniques project the raw process data, removing redundant, correlated sensor measurements and combining them into lower dimensional scores. DR may project data in two or three dimensions to enable visualization, or the technique may simply function to remove redundant information from raw process data. In some cases DR may not be necessary for feature extraction if the data are of good quality.

After projection by a DR technique, data clustering algorithms partition the data using any number of clustering techniques. Xu (2005) presents a thorough survey of data clustering techniques, but clustering is a subjective process and there is no universal definition of a cluster except that it consists of groups with members more similar to each other than data from different groups. Depending on the data and the parameters used to calculate the clustering, clusters found may or may not correspond to significant process trends, therefore, cluster evaluation metrics are important to help the user judge the quality of the clusters extracted before more detailed analysis.

Finally, in the Cluster Assignment step, the user analyses the data in the clusters to relate them to meaningful process events such as faults or operating procedures. When labelled according to process events, the data can be used by machine learning or other supervised fault detection or

diagnosis algorithms for training and fitting. Extracting information in this way from databases is called knowledge discovery. The advanced data mining algorithms used in this study were drawn from the Python Scikit-learn module (Pedregosa 2011), which provides a rich environment of well-known supervised and unsupervised machine learning algorithms.

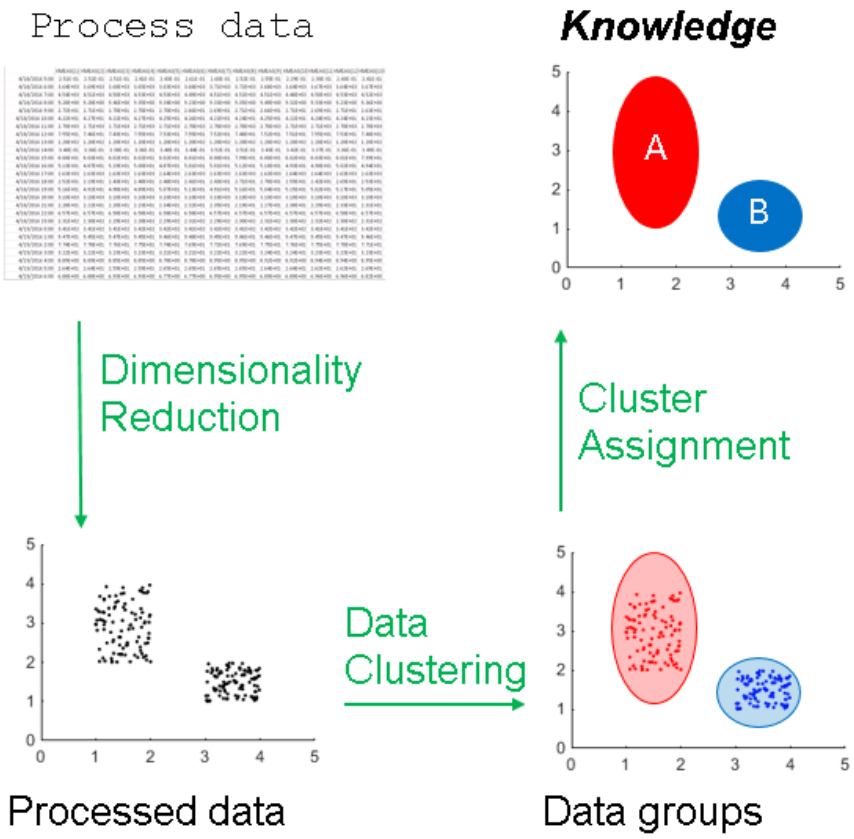

Figure 3.1: Schematic of data mining approach.

3.2 Dimensionality Reduction (DR)

The dimensionality reduction (DR) methods considered here were chosen based on their characteristics and computational costs. Principal component analysis (PCA) is the most commonly used dimensionality reduction technique and has numerous successful applications in process data (Russell 2000). ICA and KPCA have been successfully adapted to process monitoring (Lee et al. 2004, Lee et al. 2006), so it is natural to also evaluate them in data mining tasks. Isomap

and spectral embedding are more recently developed non-linear manifold learning DR techniques that can be more sensitive to non-linear structures in the data than PCA, ICA, or KPCA which are based on matrix decompositions. As a benchmark, clustering results where the data has undergone little preprocessing apart from normalization are also considered. A comparative study by van der Maaten et al. (2008) revealed that while advanced nonlinear dimensionality reduction outperformed PCA and others at reducing data sets with artificial structure, on other "natural" data sets not artificially generated by computers all dimensionality reduction techniques considered failed to provide any advantage at all! A brief discussion of each DR technique considered in this dissertation follows.

3.2.1 Principal component analysis (PCA)

Principal component analysis (PCA) is a linear distance preservation technique which determines a set of orthogonal vectors which optimally capture the variability of the data. The orthogonal vectors are determined through an eigenvalue decomposition of the covariance matrix and arranged in order of the variance explained in the loading vector directions (Russell 2000).

PCA reduces the data as follows. For a given training set of *n* observations and *m* sensor measurements stored in $X^{n\times m}$, its sample covariance matrix *S* can be calculated:

$$S = \frac{1}{n-1} X^T X = P \Lambda P^T$$

By finding the eigenvalues (Λ) of covariance matrix *S*, the projections of the observation in *X* into the lower-dimensional space are calculated in the score matrix:

$$T = XP$$

In our dimensionality reduction studies we determine the number of principal components, a, using the percent variance test. The percent variance test calculates the smallest number of loading vectors needed to explain a minimum percentage of the total variance, judged by the sum

of the a largest eigenvalues (Russell 2000). Our models include enough principal components needed to model 95% of the variance of the original data.

3.2.2 Independent component analysis (ICA)

Independent component analysis (ICA) is used in multivariate signal separation for extracting hidden and statistically independent components (ICs) from the observed data and has been adapted for process monitoring tasks similar to PCA by Lee (2004). Signal source separation recovers the independent signals after linear mixing. In other words, for mixed signals represented by x, independent signal sources s are linearly mixed in the matrix A by:

$$\boldsymbol{x} = \sum_{k=1}^{n} s_k a_k = As$$

The goal of ICA is to find the source signals s using information stored in x. After matrix A is estimated, the matrix inverse W ($W = \boldsymbol{A}^{-1}$) can be used to calculate the original independent source signals by:

$$s = Wx$$

The matrix W can be found using the FastICA algorithm of Hyvarinen and Oja (2000). In separating signals, the two key assumptions that ICA makes is that the source signals are independent of each other and the values in each source signals have non-Gaussian distributions. W is calculated through fixed point iteration to find components with the maximum non-gaussianity, measured using negentropy (Hyvarinen and Oja 2000). Negentropy comes from the information theory concept of entropy. Entropy measures the heterogeneity of data (Mitchell 1997); therefore, the more unpredictable and unstructured a variable is, the higher its entropy. Negentropy functions as a measure of non-gaussianity that is zero for a Gaussian variable, always nonnegative, and defined by the difference:

$$J(y) = H(y_{gauss}) - H(y)$$

Where H is the continuous entropy function, y is a random vector, and y_{gauss} is a Gaussian random variable with the same covariance matrix as y (Hyvarinen and Oja 2000). Negentropty is the most direct way to measure non-gaussianity, but estimating negentropy requires knowledge of the probability distribution function (PDF). Due to the complexity of finding the PDF, negentropy is usually approximated as

$$J(y) \approx [E\{G(y)\} - E\{G(v)\}]^2$$

Where y is a random variable with zero mean and unit variance, v is a Gaussian variable with zero mean and unit variance, and G is any non-quadratic function (Lee 2004). Choosing the correct G can greatly improve the quality of negentropy estimations. The following functions were suggested by Hyvarinen and Oja (2000) as being suitable for G:

$$G_1(u) = \frac{1}{a_1}\log\cosh(a_1 u)$$

$$G_2(u) = exp(-a_2 u^2/2)$$

$$G_3(u) = u^4$$

Where $1 \leq a_1 \leq 2$ and $a_2 \approx 1$ (Hyvarinen and Oja 2000). This study uses G_1 to estimate negentropy.

FastICA requires two simple preprocessing to simplify calculations: data must be mean centered (by subtracting the mean from all data records) and whitened. Whitening is the process of finding a linear transform such that the "white" data set has components that are uncorrelated with variances of 1, meaning that the covariance matrix is equal to the identity matrix. A simple way to whiten the data is to perform an eigenvalue decomposition on the covariance matrix $\boldsymbol{x}\boldsymbol{x}^T =$

$\boldsymbol{EDE^T}$ where $\boldsymbol{D}$ is a diagonal matrix holding the eigenvalues and $\boldsymbol{E}$ holds the eigenvectors of $\boldsymbol{xx^T}$. The whitened data can be calculated by:

$$\tilde{\boldsymbol{x}} = \boldsymbol{ED}^{-1/2}\boldsymbol{E}^T\boldsymbol{x}$$

$\boldsymbol{D}^{-1/2}$ can be calculated quickly by taking the square root of diagonal components. The whitening operation changes the mixing transform operation to the following form:

$$\tilde{x} = ED^{-1/2}E^TAs = \tilde{A}s$$

In this form, $\tilde{A}$ can be shown to be orthogonal, which reduces the number of parameters that must be found by half because A has n^2 degrees of freedom while $\tilde{A}$ has $(n-1)/2$ degrees of freedom (Oja and Hyvarinen 2000).

To calculate a number of ICs *m* selected by the user, the following algorithm has been proposed:

1. Choose a random initial weight vector $\boldsymbol{w}_i$.
2. Let $\boldsymbol{w}_i = E\{\boldsymbol{x}G'(\boldsymbol{w}_i{}^T\boldsymbol{x})\} - E\{G''(\boldsymbol{w}_i{}^T\boldsymbol{x})\}\boldsymbol{w}_i$
3. Decorrelate components using: $\boldsymbol{w}_i = \boldsymbol{w}_i - \sum_{j=1}^{i-1}(\boldsymbol{w}_i)^T\boldsymbol{w}_j\boldsymbol{w}_j$
4. Normalize $\boldsymbol{w}_i$: $\boldsymbol{w}_i = \boldsymbol{w}_i/\|\boldsymbol{w}_i\|$
5. If *w* has not converged, return to step 2

The algorithm converges when the old and new values of *w* in the algorithm point in the same direction (i.e. $\boldsymbol{w}_{i-1} \cdot \boldsymbol{w}_i = 1$) (Hyvarinen and Oja 2000). To select the number of ICs to include in the data model, Lee (2006) suggest several methods. The subspace clustering study performed in this dissertation simply uses the same number of ICs as PCs in our PCA model, since the selected PCs can give a good approximation for the number of ICs needed.

3.2.3 Kernel principal component analysis (KPCA)

Kernel principal component analysis extends traditional principal component analysis to nonlinear data spaces. Instead of directly taking eigenvalue decomposition of the covariance matrix as in PCA, KPCA takes a data set with non-linear features that that PCA fails to preserve and projects them to a higher dimensional space where they vary linearly. The high dimensional space is called the *feature space* (*F*). KPCA first assumes that the data have been transformed non-linearly using a non-linear mapping function $\Phi(x)$. Conventional PCA is then performed in the feature space to perform the transformations for dimensionality reduction (Scholkopf 1997).

After the data have been mapped into the feature space, the covariance matrix in the feature space is calculated by:

$$\bar{C} = \frac{1}{L}\sum_{j=1}^{L} \Phi(x_j)\Phi(x_j)^T.$$

To diagonalize the covariance matrix, the following eigenvalue problem must be solved:

$$\lambda V = \bar{C}V.$$

After substituting for $\bar{C}$ and simplifying, the eigenvalue problem becomes:

$$\lambda(\Phi(x_k) \cdot V) = (\Phi(x_k) \cdot \bar{C}V) \text{ for all } k = 1, \dots, L$$

We also assume that there exist coefficients $\alpha_i (i = 1, \dots, N)$ such that:

$$V = \sum_{i=1}^{L} \alpha_i \Phi(x_i).$$

Finally we define a $L \times L$ matrix K:

$$K_{ij} \coloneqq \left(\Phi(x_i) \cdot \Phi(x_j)\right)$$

Which allows us to substitute kernel function $k(x, y)$ for all occurrences of $(\Phi(\mathrm{x}), \Phi(\mathrm{y}))$. After substituting in for $\bar{C}$, V, and finally K and simplifying, the eigenvalue problem reduces to:

$$L\lambda\alpha = K\alpha$$

for non-zero eigenvalues (Scholkopf 1997). K is important because it allows us to calculate dot products using the non-linear mapping function Φ without knowing its form. It can be shown through functional analysis that for certain Φ, $K(x, y)$ can compute the dot product in the feature space F. Some possible kernel functions are:

$$Polynomial\ kernel\text{:}\ \ k(x, y) = \langle x, y\rangle^d$$

$$Sigmoid\ kernel\text{:}\ \ k(x, y) = \tanh(\beta_0\langle x, y\rangle + \beta_1)$$

$$Radial\ basis\ kernel\text{:}\ \ k(x, y) = \exp\left(-\frac{\|x - y\|^2}{c}\right)$$

In this work, we use the radial basis kernel $k(x, y) = \exp(-\|x - y\|^2/c)$. The following algorithm for KPCA arises from the previous derivations:

1. Compute dot product matrix $K_{ij} = \left(k\left(x_i, x_j\right)\right)_{ij}$
2. Solve $L\lambda\alpha = K\alpha$ by diagonalizing K
3. Normalize the eigenvector expansion coefficients α^n by requiring that $(\alpha^k \cdot K\alpha^k) = 1$
4. Extract PCs for each new data vector x by computing its projection onto eigenvectors using $t_k = k\alpha^k\Lambda^{-1/2}$

As with other non-linear dimensionality reduction methods (i.e. Isomap), the major weakness of KPCA is the high computational cost of calculating a feature matrix (or kernel matrix for KPCA). To determine the number of PCs, in accordance with Lee (2004) we applied the cut-off method using the average eigenvalue which only includes PCs with eigenvalues above the average.

3.2.4 Isomap

Isomap performs non-linear dimensionality reduction by learning the data's non-linear topology using a fitted graph structure and then projecting the data with non-metric multidimensional scaling (MDS) based on the ordering. Isomap overcomes some of the limitations of other approaches by representing the data set within a single coordinate system, all using a noniterative procedure with a polynomial computational complexity and guaranteed global optimality (Tenenbaum et al. 2000).

Isomap only begins learning a mapping after the topological structure of the data has been learned. The graph fit by the Isomap algorithm contrasts with that of self-organizing maps, which attempt to fit a model based on a predefined structure. In Isomap, Euclidian distances are used to find the geodesic distances defined as the shortest line between two points on the topological surface formed by the data, and this distance along the surface of the data's topological structure is used in the dimensionality reduction of the input data. The full Isomap algorithm proceeds as follows (Tenenbaum 1998):

1. Build the neighborhood graph by randomly selecting r points to be nodes in the graph and use their nearest neighbors to form connections between all points within radius ϵ. Graph G is created by connecting two nodes g_i and g_j if there exists at least one data point whose two nearest nodes are g_i and g_j.
2. Calculate the manifold distance between nodes. First, assign weights between nodes in the graph using the Euclidean distance: $w_{ij} = d_X^{ij} = \|x_i - x_j\|$. The geodesic distance d_G^{ij} between two nodes on G is defined as the sum of link weights along the shortest path between the nodes. After calculating the geodesic distance between all pairs of nodes in G,

the shortest path between all pairs of points is found using Floyd's all pairs shortest-path $O(r^3)$ algorithm (Foster 1995).

3. Create d-dimensional embedding between all points using non-metric or "ordinal" MDS from Cox and Cox (1994) which finds a Euclidean embedding that preserves the graph distances. The use of MDS is important because MDS works for any monotonically decreasing function of distance. In contrast to metric MDS, which preserves distances between points, non-metric MDS preserves only the rank ordering of distances, independent of the metric used to calculate the ordering. MDS will find a projection which minimizes the stress function:

$$S = \min_{\hat{d}_G^{ij}} \sqrt{\frac{\sum_{i<j}\left(d_Y^{ij} - \hat{d}_G^{ij}\right)^2}{\sum_{i<j}\left(d_Y^{ij}\right)^2}}$$

Where d_Y^{ij} is the Euclidean distance between feature vectors i and j and the $\hat{d}_G^{ij}$ is the primary monotone least-squares regression of the data's pairwise Euclidean distances and the graph distances (Cox and Cox 1994).

3.2.5 Spectral embedding (SE)

Spectral embedding, also known as LaPlacian Eigenmaps, is a manifold non-linear dimensionality reduction technique using the LaPlacian of a graph based on the topology of the data set to non-linearly project data in a way that optimally preserves local neighborhood information and emphasizes clustering structures in the data (Belkin and Niyogi 2003).

The adjacency graph used by SE is created using pairwise distances between points in the data set. Belkin and Niyogi (2003) presents two variations:

- ϵ-neighborhood graph: connect all points whose distances are smaller than a threshold ϵ.
- k-nearest neighbor graph: connect data vectors v_i and v_j if v_j is among the k-nearest neighbors of v_i or if v_i is among the k-nearest neighbors of v_j. The edges of the resulting graph are weighted by the similarity between their endpoints, i.e. the distance between v_i and v_j (von Luxburg 2007).

Once the graph is defined, we must calculate the LaPlacian to generate the embedding of the data. Two matrices are needed to do this. The weighted adjacency matrix weights edges between the vertices of the graph based on their distance and is defined as $\boldsymbol{W} = w_{ij}$ for $i, j = 1, \dots, n$. From the weight matrix, the degree of a vertex v_i in the connected graph is defined as:

$$\boldsymbol{D}_{ii} = \sum_j \boldsymbol{W}_{ji}$$

The normalized LaPlacian implemented in the Scikit-learn package is calculated from:

$$\boldsymbol{L} = \boldsymbol{D}^{-1/2}(\boldsymbol{D} - \boldsymbol{W})\boldsymbol{D}^{-1/2}$$

Where $\boldsymbol{L}$ is a symmetric, positive semidefinite matrix.

Finally, we can calculate the non-linear embedding of the data using eigenvectors found by solving the generalized eigenvector problem:

$$\boldsymbol{L}\boldsymbol{f} = \lambda \boldsymbol{D}\boldsymbol{f}$$

$\boldsymbol{L}$ will have n non-negative, real-valued eigenvalues:

$$0 = \lambda_0 \leq \lambda_1 \leq \cdots \leq \lambda_n$$

Leaving out the corresponding eigenvector of eigenvalue 0, the embedding in m-dimensional Euclidean space comes from the next m eigenvectors:

$$\boldsymbol{x}_i \rightarrow (\boldsymbol{f}_1(i), \dots, \boldsymbol{f}_m(i))$$

The eigendecomposition of the graph LaPlacian has been previously used for clustering in spectral clustering algorithms. The clustering methods developed by Shi and Malik (2000) and Ng et al. (2002) among others begin by performing an eigenvalue decomposition on the graph LaPlacian to embed the data, followed by K-means clustering to find clusters. Within the subspace clustering framework studied here, spectral embedding is used for dimensionality reduction while several different techniques for data clustering are tested for the clustering step.

3.3 Data Clustering

The goal of data clustering is the unsupervised classification of data into groups or clusters that are useful and meaningful. Using data clustering, the key groups within a database can be isolated and connected to meaningful operating conditions in a plant. The techniques K-means, DBSCAN, Meanshift, and BIRCH were selected for their scalability and ability to find clusters corresponding to regions of high density in data. The latter three techniques locate clusters based on density, and therefore have the ability to find clusters of any arbitrary shape. Additionally, all techniques applied here consider each data measurement to be independent of time. Fu (2011) reviews data mining techniques for time series data. Partitional algorithms which separate all data into different clusters are preferred in our approach over hiearchical techniques, our study focuses on these algorithms.

3.3.1 K-means clustering

The fundamental concept of K-means clustering was developed independently by several researchers studying “optimal partitioning”. MacQueen (1967) coined the term “K-means” and provided the one of the earliest formal introduction of the K-means clustering process. In spite of its age, K-means is still one of the most widely used algorithms for clustering due to its simplicity

and efficiency (Jain 2010) and was recognized as one of the top 10 data mining algorithms by IEEE (Wu 2008).

For a d-dimensional spatial data set $X = \{x_i\}, i = 1, \dots, n$, where n is the number of data points, K-means partitions the data into K clusters $C = \{c_k, k = 1, \dots, K\}$ specified by the user. The K-means algorithm seeks to minimize the sum of squared error (SSE) between each mean μ_k of each cluster c_k given by:

$$SSE(C) = \sum_{k=1}^{K} \sum_{x_i \in c_k} \|x_i - \mu_k\|^2$$

Minimizing the SSE objective function is an NP-hard problem, thus K-means will converge to a local minimum. The mains steps of K-means are (Jain 2010):

1. Select an initial partition of K clusters
2. Assign each point to its nearest cluster center
3. Compute new cluster centers by averaging cluster data
4. Repeat steps 2 and 3 until cluster membership stabilizes

The K-means implementation used here randomly chooses k points from the data set and sets these points as the initial centroids of the specified number of clusters the algorithm must find.

3.3.2 DBSCAN

Density-based clustering locates regions of high density of any shape that are separated from one another by regions of low density. DBSCAN, an acronym of Density-Based Spatial Clustering of Applications with Noise, divides all the data in a set into three categories based on their neighborhood: Core points making up the body of a cluster, border points in more diffuse regions of the data but near a few core points, and noise points far from concentrated groups of data. DBSCAN is ideally suited to clustering chemical process data, since clusters in real data sets

are rarely spherical and often clouded by noise (Tan 2005). Removing this noise can focus attention on the densest clusters in the data set.

For each core point within a cluster, the neighborhood of a given radius (Eqs) must contain a minimum number of points ($MinPts$ parameter), i.e. the density of the point's neighborhood must exceed a threshold. The shape of the clusters found can depend on the distance metric selected. Unlike K-means, the clusters found by DBSCAN arise from a series of specific definitions. Each definition assumes the specification of a particular value of Eps and MinPts.

Definition 1, Eps-neighborhood of a point: The Eps neighborhood of a point p ($N_{Eps}(p)$) is defined as: $N_{Eps}(p) = \{q \in D | \, dist(p, q) \leq Eps\}$.

The shape of this neighborhood is determined by the distance criterion used. Euclidian distance was used in our studies, but in practice any appropriate distance metric may be used. A simple approach could require every point in the cluster to have at least $MinPts$ in its neighborhood, but this would miss the border points on the outside of the cluster. Border points are within the Eps neighborhood of at least one core point, but a border point's neighborhood contains fewer points than $MinPts$.

Definition 2, directly density-reachable: Point p is directly density-reachable (DDR) from point q if:

1. p is in $N_{Eps}(q)$
2. $N_{Eps}(q) \geq MinPts$ (i.e. q is a core point)

In other words, if q is a core point, other data points in its Epsilon neighborhood are said to be directly density-reachable. Core points are directly density-reachable with each other.

Border points are directly density-reachable from core points, but core points are not directly density-reachable from border points due to condition 2. Arising from the directly density-reachable definition is the concept of density reachability for groups of core points:

Definition 3, density reachable: a point p is density reachable from a point q if there is a chain of points $p_1, \dots, p_n$, where $p_n = q$ such that p_{i+1} is directly density reachable from p_i.

Two points are DR if there is a chain of core points DDR from each other connecting the two points. A border point can be density reachable from a core point, but because of the definition of DDR, no core points are DR from a border point. What finally defines clusters in DBSCAN is the concept of density connectivity:

Definition 4, Density connected: A point p is density connected to a point q if there is a point o such that both p and q are density reachable from o.

In other words, if both p and q are density reachable from a point o, they are said to be density connected. Therefore, clusters in DBSCAN are groups of density connected points.

Definition 5: Cluster definition: For database D, a cluster C is a non-empty set such that:

1. $\forall p, q$ if $p \in C$ and q is density reachable from p, then $q \in C$
2. $\forall p, q \in C$, p is density connected to q

Noise points are simply defined as data that are not associated with any cluster (Ester 1996).

To find clusters, the user must specify parameters Eps and $MinPts$. There is no simple way to determine the correct value of Eps and $MinPts$, but Ester (1996) suggests a heuristic which

uses the *sorted k-dist graph*, which is created by finding the distance to each point's k-th nearest neighbor, sorting the distances found in descending order, and plotting. Eps is determined by the distance value of the first "valley" of the sorted k-dist graph. In essence, the user is estimating the percentage of noise in the data. Further details of the DBSCAN algorithm are presented by Ester et al. (1996).

3.3.3 Balanced iterative reducing and clustering using hierarchies (BIRCH)

Different from previously discussed clustering methods, BIRCH finds subclusters of data and condenses them into a three element data vector. The Clustering Feature (CF) vectors of the subclusters are combined using a specialized tree structure to generate the output clusters. This approach affords BIRCH advantages over other clustering techniques, particularly in a computing environment with limited memory resources. The combined CF tree and vector approach treats dense areas of data as a single vector, and can allow BIRCH to obtain a clustering of data with one scan of the input data. In other words, the decisions to combine and split clusters are made locally, without the need to calculate the pairwise distances over the entire data set. Sparse regions of data can be removed with additions to the algorithm.

The CF vector representing individual subclusters is represented as $CF = (N, \overrightarrow{LS}, \overrightarrow{SS})$ where N is the number of data points in the cluster, $\overrightarrow{LS}$ is the linear sum of the N data points calculated by $\sum_{i=1}^{N} \vec{X}_i$ and $\overrightarrow{SS}$ is the square sum calculated from $\sum_{i=1}^{N} \vec{X}_i^2$. CF vectors allow BIRCH to accurately and incrementally combine subclusters of data within the CF tree structure (Zhang et al. 1996).

A CF tree is a height balanced tree with two parameters: branching factor B and threshold T. The tree is composed of split nodes (non-leaf nodes) which branch and ultimately terminate in leaf nodes. Each split node contains at most B entries of the form $[CF_i, child_i]$, where $i =$

$1,2,\ldots,B$, and $child_i$ is a pointer to its ith child node, and CF_i is the CF of the subcluster represented by this child. Leaf nodes have at most L entries and represent a cluster made up of all the subclusters of its entries of the form $[CF_i]$, where $i = 1,2,\ldots,L$. To be part of a leaf node, a subcluster must have a diameter or radius less than the defined threshold T. The radius and diameter are defined relative to the cluster centroid $\vec{X}_0$ defined as:

$$\vec{X}_0 = \frac{\sum_{i=1}^{N} \vec{X}_i}{N}$$

The cluster radius R and diameter D are defined as:

$$R = \left(\frac{\sum_{i=1}^{N} \left(\vec{X}_i - \vec{X}_o\right)^2}{N} \right)^{1/2}$$

$$D = \left(\frac{\sum_{i=1}^{N} \sum_{j=1}^{N} \left(\vec{X}_i - \vec{X}_j\right)}{N(N-1)} \right)$$

Where R is the average distance from member points to the centroid, D is the average pairwise distance within a cluster, and N is the number of data points. The value of T limits the size of the tree. Larger T values will yield smaller trees as the subclusters under consideration absorb larger amounts of data by spreading through the data space.

A new data point or subcluster X_i is added to the tree by starting at the root and descending the CF tree by choosing the closest branch based on a chosen distance metric, such as Euclidian. At a leaf node, BIRCH first tests whether X_i can be incorporated into one of the other subclusters present on the leaf. If the leaf node can absorb X_i, the leaf nodes CF vector is updated with the data from X_i, but if not a new split node is created at the leaf using the farthest pair of entries as seeds. Additional operations refine the clusters that arise from this approach as described in Zhang et al. (1996).

3.3.4 Mean shift clustering

Mean shift clustering is a probability density formulation of the clustering problem. In two dimensions for example, probability density functions (PDF) form structures like mountains around clusters, with slopes and a peak at the point of highest density in the cluster as the cluster density increases to a peak. Mean shift clustering uses the theory of probability density estimation to create clusters using the mean shift procedure first introduced by Fukunaga and Hostetler (1975).

The most widely used nonparametric technique for finding an estimation of the PDF for a set of data is kernel density estimation. For data $X_i \; i = 1, \dots, n$, the multivariate kernel estimator with kernel K is defined as:

$$\hat{f}(x) = \frac{1}{nh^d} \sum_{i=1}^{n} K\left(\frac{x - X_i}{h}\right)$$

Where K is a kernel function, h is the bandwidth or window width, and d is the number of dimensions in the data (Silverman 1986). Selection of the bandwidth is a crucial parameter for mean shift clustering. In our application we calculated acceptable results using a heuristic based on the median of pairwise distances. The selection of the kernel also affects results, but the common normal or Gaussian kernel K_N is usually most effective:

$$K_N(\boldsymbol{x}) = (2\pi)^{-d/2} exp\left(-\frac{1}{2}\|\boldsymbol{x}\|^2\right)$$

Mean shift clustering first finds the zeros of $\widehat{\nabla} f(x)$, which correspond to local maxima and minima of the PDF. The mean shift procedure itself is important for finding zeros in $\widehat{\nabla} f(x)$ without estimating the density (Comaniciu 2002). Arising from this approach is the mean shift vector:

$$m(x) = \frac{\sum_{i=1}^{n} x_i g\left(\left\|\frac{x - x_i}{h}\right\|^2\right)}{\sum_{i=1}^{n} g\left(\left\|\frac{x - x_i}{h}\right\|^2\right)} - x_i$$

Where g is defined as

$$g(x) = -k'(x)$$

Which arises from the "shadow" of the kernel K, a concept introduced by Cheng (1995). Derivations and additional details about the mean shift procedure can be found in Fukunaga and Hostetler (1975) and Cheng (1995). The resulting mean shift vector always points towards the direction of maximum increase in probability density, and following the mean shift vector through the PDF leads us to a zero of $\widehat{\nabla} f(x)$.

In the mean shift clustering approach presented by Comaniciu (2002), clusters arise from this mode seeking process. All the points visited by each execution of the mean shift procedure are associated in the cluster corresponding to the local maximum the procedure converges upon.

3.4 Cluster Evaluation

Almost every clustering algorithm will find clusters in a data set, even if that data set has no natural cluster structure. Cluster evaluation metrics are important to give an idea of the validity of a given clustering generated by an algorithm. This study uses four cluster evaluation metrics: homogeneity, completeness, V-measure (Rosenburg 2007), and Adjusted Rand Index (ARI) (Hubert and Arabie 1985). Each metric gives the output of a clustering algorithm a score from 0 (corresponding to a poor or random clustering) to 1. A brief summary of these clustering metrics is given in Table 3.1.

Homogeneity determines whether data points defined in the same cluster are from the same single class. The score is between 0 to 1, where 1 represents for perfectly homogeneous labelling. Completeness determines whether data from the same single group is defined in the same cluster.

Table 3.1: Clustering metrics used to compare the quality of clustering results

	1 when…
Homogeneity	All clusters contain data from a single class
Completeness	Members of a class are elements of the same cluster
V-measure	Harmonic mean of homogeneity and completeness
ARI (-1 to 1)	Cluster labels match true labels (0 for random labelling)

The score is between 0 to 1, where 1 represents for perfectly complete labelling. V-measure is the harmonic mean between homogeneity and completeness. Formulas for homogeneity, completeness and V-measure are:

$$h = 1 - \frac{H(C|K)}{H(C)}$$

$$c = 1 - \frac{H(K|C)}{H(K)}$$

$$v = 2 \cdot \frac{h \cdot C}{h + C}$$

Where $H(C|K)$ is the conditional entropy of the classes given the cluster assignments, and $H(C)$ is the entropy of the classes:

$$H(C|K) = -\sum_{c=1}^{|C|}\sum_{k=1}^{|K|}\left[\frac{n_{c,k}}{n} \cdot \log\left(\frac{n_{c,k}}{n_k}\right)\right]$$

$$H(C) = -\sum_{c=1}^{|C|}\frac{n_c}{n} \cdot \log\left(\frac{n_c}{n}\right)$$

Finally, we judge the similarity of a given clustering result to the true clusters of data using the Adjusted Rand Index (ARI) of Hubert and Arabie (1985). ARI is derived from the Rand Index and compares classes resulting from data clustering to a "null" model of random clusters based on probabilities of agreement and disagreement between clusters and truth classes. In this dissertation we calculate the ARI by the equation:

$$ARI = \frac{\sum_{i,j}\binom{n_{ij}}{2} - \sum_i \binom{n_i}{2}\sum_j \binom{n_j}{2}/\binom{n}{2}}{\frac{1}{2}\left(\sum_i \binom{n_{i.}}{2} + \sum_j \binom{n_{.j}}{2}\right) - \sum_i \binom{n_{i.}}{2}\sum_j \binom{n_{.j}}{2}/\binom{n}{2}}$$

where two clusterings of the data, U and V, are compared. The indices i and j refer to groups within U and V respectively: $n_{i.}$ and $n_{.j}$ refer to the number of objects in class u_i in U and class v_j in V. The contingency table in Hubert and Arabie (1985) fully illustrates this notation.

Figure 3.2 illustrates the meaning of the various clustering metrics using the Fischer Iris data set (Fisher 1936). The Iris data is composed of 3 species of flowers, and Figure 3.2 gives several possible clustering results found by K-means similar to good and bad clustering results: 1. all data in one cluster, 2. Data is separated into many clusters, and 3. Data is separated into 3 clusters (which closely match the true clusters). The sample cases in Figure 3.2 illustrate how homogeneity and completeness give us insight into how the clusters separate the data, particularly their relative size to each other, whether they might be too general or too specific. ARI gives an evaluation of how accurately the clustering results capture the true grouping of the data (assuming the true clusters are known).

3.5 Subspace Clustering Study: Parameters and Analysis

Each DR and clustering technique had one or more parameters which needed to be specified, and the determination of these parameters has a substantial effect on clustering performance and the validity of the analysis. Finding appropriate values can be a trial and error process; therefore, in order to simulate the trial and error process an engineer might use to find a useful clustering of the process data, we tested a range of different values for each clustering technique, usually based on heuristics. As an example, our use of the 95th percentile nearest neighbors distance for DBSCAN comes from the convention of using the 95% significance to accept or reject a null hypothesis. In some cases we did not attempt to avoid using our knowledge

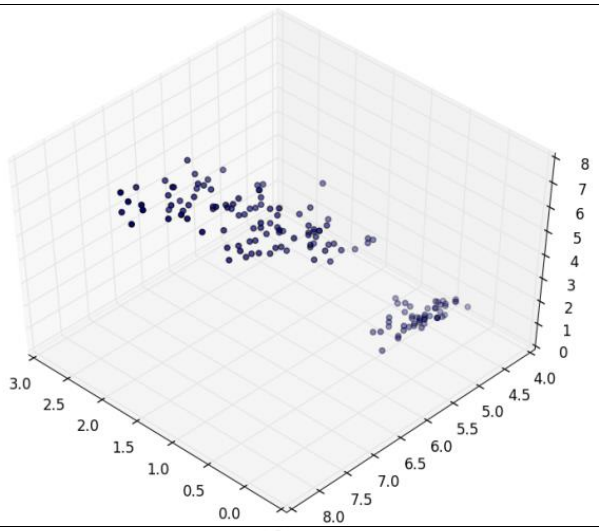	1. All data in one cluster Homogeneity: -0.000 Completeness: 1.000 V-measure: -0.000 Adjusted Rand Index: 0.000 When all the data is put into a single cluster, completeness is high, at the expense of all other metrics.
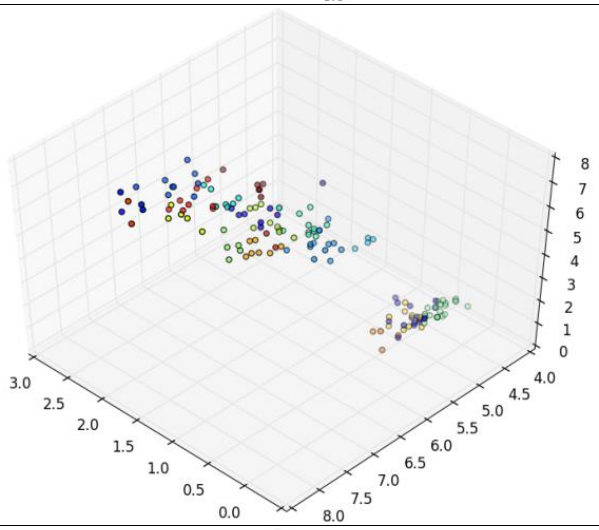	2. K-means, k = 20 Homogeneity: 0.934 Completeness: 0.363 V-measure: 0.522 Adjusted Rand Index: 0.226 Dividing all the different classes of data into multiple smaller clusters yields a clustering that is high in homogeneity, but relatively low in completeness and AMI.
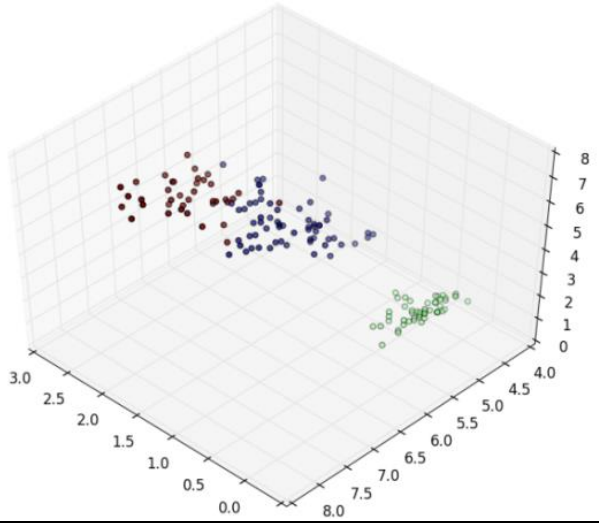	3. K-means, k = 3 Homogeneity: 0.828 Completeness: 0.521 V-measure: 0.640 Adjusted Rand Index: 0.451 The best clustering of the three examples (kmeans, k = 3), produces good values for all metrics calculated. If it perfectly matched the true clusters, each would equal 1.

Figure 3.2: Illustration of the various clustering metrics.

of the sets, as in tests with K-means where we based a central estimate of the number of clusters on the number of groups known to be in the data and varying *k* around this estimate.

- DBSCAN: minPts was fixed at 10, while eps was determined using the k-nearest neighbors (kNN) graph as suggested by Ester et al. (1996). We varied the range of the percentile of the kNN graph used between the values 0.99, 0.95, 0.9, 0.8, and 0.7.
- K-means: *k* was varied around the number of groups that were known to be in the data. For example, in the reduced fault data set from the Tennessee Eastman process, the values of *k* considered were 6, 7, 8, 9, and 10.
- The base estimate for the bin width parameter of mean shift was determined by finding the average median nearest neighbor distance over the entire data set. This estimate was varied by multiplying by five sets of factors: 1.8, 1.5, 1 (no modification of initial estimate), 0.5, and 0.2.
- The threshold parameter of BIRCH has conceptual similarity to the bin width parameter of mean shift, and was varied in the same fashion. The branching factor had a limited effect on clustering results and was fixed at 50.

The dimensionality reduction techniques used also required some parameters to be specified. In this case we assumed some simple benchmarks to specify the dimensionality of the projections:

- PCA: Cross validation was used such that 95% of the variance was preserved in the projection.
- KPCA: we used the average eigenvalue approach utilized by Lee et al. (2006) which accepts all components with eigenvalues above the average eigenvalue.

- ICA, Isomap, and SE each required an estimate of the intrinsic dimensionality for the projection. In practice, this can be difficult to estimate, so as a benchmark we used the same number of components as PCA.

In the clustering results in Chapters 5 and 6, we present the best ARI result out of the five parameter guesses for each clustering/DR combination. Full results are provided in Appendix A and can be informative in judging the reproducibility of the maximum ARI clustering results highlighted in the chapters. It should be noted that in a clustering study without any *a priori* knowledge of the true data groups, ARI cannot be calculated. Without true cluster labels, only unsupervised clustering metrics like the Davies-Bouldin Index (Davies and Bouldin 1979) provide a benchmark for the accuracy of a clustering of the data.

3.6 References

Belkin, M., & Niyogi, P. (2002). Laplacian eigenmaps for dimensionality reduction and data representation. *Neural Computation, 15*(6), 1373-1396.

Cheng, Y. (1995). Mean shift, mode seeking, and clustering. *IEEE Transactions on Pattern Analysis and Machine Intelligence, 17*(8), 790-799.

Comaniciu, D., & Meer, P. (2002). Mean shift: A robust approach toward feature space analysis. *IEEE Transactions on Pattern Analysis and Machine Intelligence, 24*(5), 603-619.

Cox, M. A. A., & Cox, T. F. (1994). Multidimensional scaling. In *Handbook of Data Visualization* (315-347). Heidelberg: Springer.

Davies, D. L., & Bouldin, D. W. (1979). A cluster separation measure. *IEEE Transactions on Pattern Analysis and Machine Intelligence, 1*(2), 224-227.

Ding, C., & He, X. (2004). K-means clustering via principal component analysis. *Proceedings of the 21st International Conference on Machine Learning*, 29-38.

Ester, M., Kriegel, H.P., Sander, J., & Xu, X. (1996). A density based algorithm for discovering clusters in large spatial databases with noise. *Proceedings of 2nd International Conference on Knowledge Discovery and Data Mining*, 226-231.

Fisher, R. A. (1936). The use of multiple measurements in taxonomic problems. *Annals of Eugenics, 7*(2), 179-188.

Foster, I. (1995). *Designing and building parallel programs*. Retrieved from http://www-unix.mcs.anl.gov/dbpp/text/book.html

Fu, T. (2011). A review on time series data mining. *Engineering Applications of Artificial Intelligence, 24*, 164-181.

Fukunaga, K., & Hostetler, L. D. (1975). The estimation of the gradient of a density function, with applications in pattern recognition. *IEEE Transactions on Information Theory, 21*(1), 32-40.

Gardner, M., & Bieker, J. (2000). Data mining solves tough semiconductor manufacturing problems. *KDD '00 Proceedings of the Sixth ACM SIGKDD International Conference on Knowledge Discovery and Data Mining*, 376-383.

Hubert, L., & Arabie, P. (1985). Comparing patterns. *Journal of Classification, 2*, 193-218.

Hyvarinen, A., & Oja, E. (2000). Independent component analysis: Algorithms and applications. *Neural Networks, 13*(4-5), 411-430.

Jain, A. K. (2010). Data clustering: 50 years beyond K-means. *Pattern Recognition Letters, 31*, 651-666.

Lee, J., Qin, S. J., & Lee, I. (2006). Fault detection and diagnosis based on modified independent component analysis. *American Institute of Chemical Engineers Journal, 52*(10), 3501-3514.

Lee, J., Yoo, C. K., Choi, S. W., Vanrolleghem, P. A., & Lee, I. (2004). Nonlinear process monitoring using kernel principal component analysis. *Chemical Engineering Science, 59*, 223-234.

MacQueen, J. (1967). Some methods for classification and analysis of multivariate observations. *Fifth Berkeley Symposium on Mathematics, Statistics, and Probability*, 281-297.

Mervis, J. (2012). U.S. science policy: Agencies rally to tackle big data. *Science, 335*(6077), 22.

Mitchell, T. M. (1997). *Machine learning*. Singapore: McGraw-Hill.

Ng, A., Jordan, M., & Weiss, Y. (2002). On spectral clustering: Analysis and an algorithm. In T. Dietterich, S. Becker, & Z. Ghahramani (Eds.), *Advances in Neural Information Processing Systems*, (849-856). Cambridge: MIT Press.

Pedregosa, F., Varoquaux, G., Gramfort, A., Michel, V., Thirion, B., Grisel, O., … Duchesnay, E. (2011). Scikit-learn: Machine learning in Python. *Journal of Machine Learning Research, 12*, 2825-2830.

Rosenberg, A., & Hirschberg, J. (2007). V-Measure: A conditional entropy-based external cluster evaluation measure. *Proceedings of the 2007 Joint Conference on Empirical Methods in Natural Language Processing and Computational Natural Language Learning*, 410-420.

Russell, E. L., Chiang, L. H., & Braatz, R. D. (2000). *Data-driven techniques for fault detection and diagnosis in chemical processes*. London: Springer.

Scholkopf, B., Smola, A., & Muller, K. R. (1999). Kernel principal component analysis. In *Advances in kernel methods – Support vector learning* (327-352). Cambridge: MIT Press.

Shi, J., & Malik, J. (2000). Normalized cuts and image segmentation. *IEEE Transactions on Pattern Analysis and Machine Intelligence, 22*(8), 888 – 905.

Silverman, B. W. (1986). *Density estimation for statistics and data analysis*. London: Chapman and Hall.

Tan, P., Steinbach, M., & Kumar, V. (2006). *Introduction to data mining*. Boston: Longman.

Tenenbaum, J. B. (1998). Mapping a manifold of perceptual observations. *Advances in Neural Information Processing Systems, 10*, 682-688.

Tenenbaum, J. B., De Silva, V., & Langford, J. C. (2000). A global geometric framework for nonlinear dimensionality reduction. *Science, 290*(5500), 2319-2323.

Van der Maaten, L., Postma, J., & van den Herik, J. (2008). Dimensionality reduction: A comparative review. Retrived from https://lvdmaaten.github.io/publications/papers/TR_ Dimensionality _ Reduction_Review_2009.pdf

Von Luxburg, U. (2007). A tutorial on spectral clustering. *Statistics and Computing, 17*, 395-416.

Xu, R., & Wunsch, D. (2005). Survey of clustering algorithms. *IEEE Transactions on Neural Networks, 16*(3), 645-678.

Zhang, T., Ramakrishnan, R., & Livny, M. (1996). BIRCH: An efficient data clustering method for very large databases. *SIGMOD '96*, 103-114.

Chapter 4 - Process Monitoring and Supervision

Modern chemical plants have advanced distributed control systems (DCS) that handle normal, day-to-day operations of quality control. However, some events, such as heat exchanger fouling or equipment breakdowns, cannot be compensated for by the DCS. These events are called faults. When process faults occur, the burden falls on the human operator to rapidly assess the situation, determine the causes, and take corrective action. This is a challenging task further complicated by information overload. The average DCS measures hundreds of variables every second and important trends for the correct diagnosis can be hidden beneath sensor noise. Mistakes in managing major process faults cost the U.S. chemical industry billions of dollars in occupational injuries, damages, and lost products (Venkatasubramanian 2003). Detecting faults early is crucial to prevent the progression of the incident and reduce losses.

This research is focused on process monitoring algorithms: mathematical computer programs designed to assist plant operators in the detection and diagnosis of chemical process faults. A wide array of statistical methods, such as principal component analysis (PCA), have been adapted to fault detection with success, but too often PCA performs poorly on non-linear processes. Here, our work develops an advanced process monitoring algorithm based on self-organizing maps (SOM) that is robust to the challenges posed by non-linear processes and uses ideas from data mining and artificial intelligence.

This chapter introduces data-based methods for process monitoring tasks. A key issue associated with multivariate statistical monitoring schemes is the construction or definition of process normal operating region, which can be thought of as the acceptable level of variation around target values. Statistics are generated from new observations to quantify the degree of

belongingness in the normal region and are employed as an indicator of the process performance and product quality.

In univariate process monitoring, the normal operating region is constructed based upon the assumption of normality and independence. Although a similar approach has been extended to multivariate case using Principal Components Analysis (PCA), the underlying assumptions such as linearity can be restrictive and inappropriate for complex processes. Still, one of the main advantages of PCA is its simplicity and the range of tools it provides which covers all fault detection, identification, and diagnosis tasks discussed above. In this dissertation we will develop a nonlinear approach that will mimic PCA by defining similar measures for process monitoring and fault detection.

Section 4.1 introduces the basic concepts and goals of process monitoring technology. Section 4.2 introduces a basic univariate process monitoring technique. Section 4.3 briefly overviews PCA tools for multivariate process monitoring. Section 4.4 introduces the fundamentals of self-organizing maps and Section 4.5 introduces our new method for process monitoring using multiple SOMs. Section 4.6 explains how SOM methods can be adapted to batch processes using multiway unfolding. Section 4.7 presents an illustrative demonstration of PCA and MSOM monitoring on the Fisher Iris data.

4.1 Introduction to Data-Driven Process Monitoring

Chemical process monitoring can be separated into several tasks outlined in the flowchart in Figure 4.1. The four main tasks that compose process monitoring are fault detection (also known as abnormal event detection or AED), fault identification, fault diagnosis, and process recovery. This dissertation studies every task but process recovery which is the process through which the human operators act to address fault events and close the “control loop” illustrated in Figure 4.1.

Each process monitoring task uses data initially drawn from plant sensor measurements stored in the process's DCS. Fault detection, diagnosis, and identification all involve some amount of mathematical calculation using this digitized sensor measurement data. The data are first processed by a fault detection algorithm which often functions similar to a statistical test. Similar to the way that a *z*-test or Student's *t*-test might generate a test statistic and compare it to some threshold value, the fault detection task usually involves the generation of a test statistic against a bound representing the boundary between normal and faulty operations.

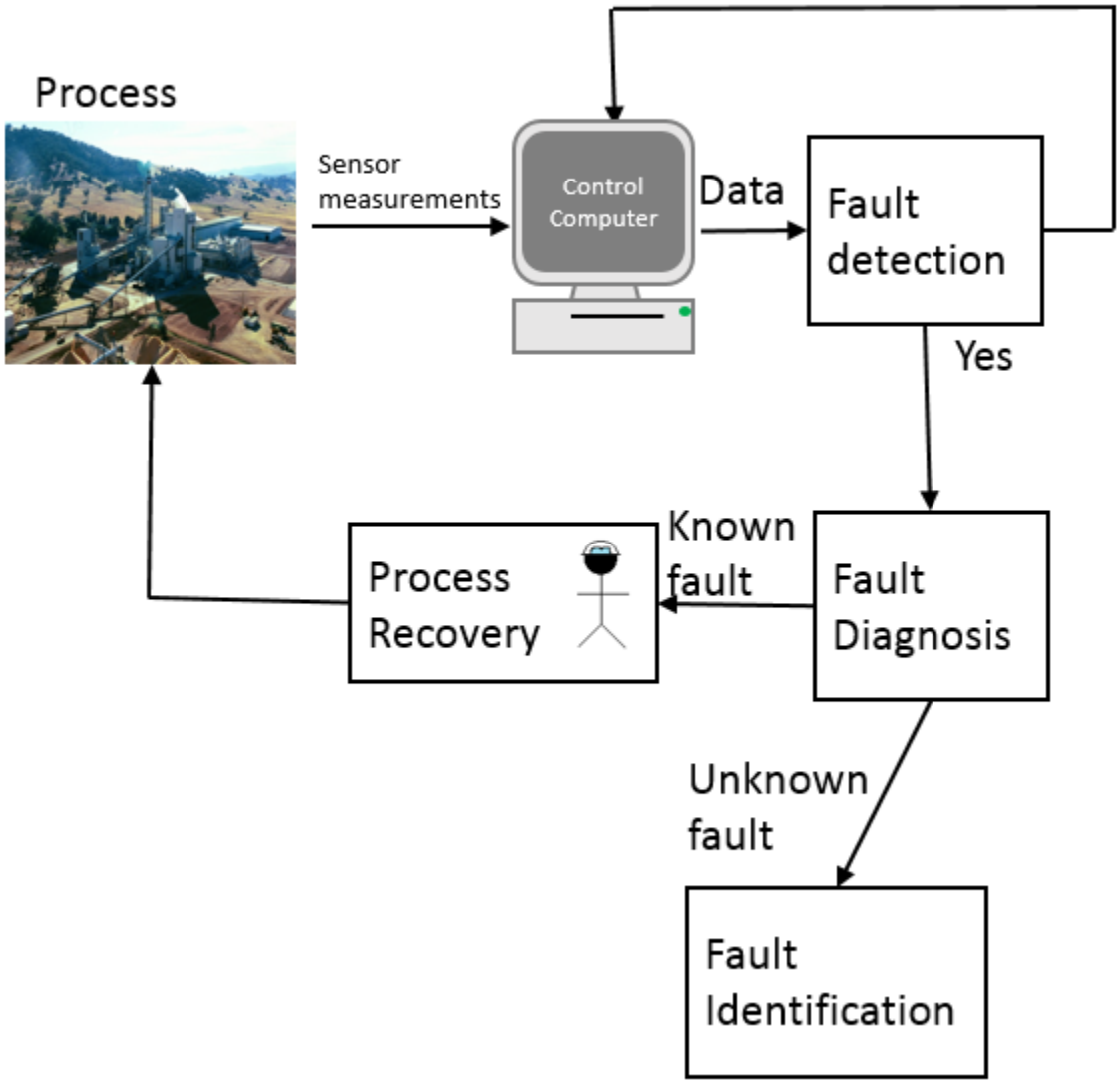

Figure 4.1: Industrial process monitoring workflow.

When our test statistic exceeds this bound, we say a fault has occurred, and while the statistic is below the bound we say operations are normal. When the statistic above the bounds for normal is observed, the next step is the fault diagnosis step. If data from previously experienced or expected faults is available, pattern recognition fault diagnosis algorithm can be trained to associate the data to the known fault and enable operators to proceed immediately to the process recovery step to address the conditions creating the fault status. If there is no data from previously available faults or the observed abnormal data does not fit into any known fault models, the workflow proceeds to fault identification. Fault identification uses the model of normal operations to assist operators in isolating the sensor measurements responsible for faulty observations. Without fault identification, operators may see a faulty plant status but not take action if the sensors producing the faulty statistic are not obvious. Fault identification can guide operators' investigation into the root causes of the fault event by focusing attention to a certain area of the plant more relevant to the diagnosis of the fault.

The purpose of implementing a process monitoring AED system is not to automate the management of abnormal events, but to assist in incorporating operators into the loop. Process monitoring must provide useful insight in quickly assessing an abnormal situation and offer a user friendly way for operators to view and process large amounts of information. Additionally, they must accomplish all these tasks in a scalable, user-friendly manner without requiring expensive, time-consuming maintenance from application engineers or experts in data mining.

Process monitoring falls into three broad categories: data-driven, analytical, and knowledge-based. Analytical models are built from first principles chemistry and physics models of the system which fully model all possible behavior of the system. However, in practice, constructing and validating non-linear analytical models of processes from scratch can take months

to years in analysis and experimentation. Knowledge based approaches are based on cause-effect descriptions and IF-THEN rules to describe the behavior of faults. Often knowledge-based methods are built on past experiences of operators following fault events with clearly isolated causes. In contrast, data driven models are built from only accumulated process data. Data driven models are based on machine learning or statistics, but have the disadvantage that they behave unpredictably when encountering situations not covered in the training data set. Therefore training data for data-based process monitoring methods must be as diverse as possible to ensure the model that arises is robust to multiple unusual (but not faulty) events that a process experiences such as weather variations or irregularities arising from normal maintenance procedures (Chiang et al. 2000). The following sections discuss various strategies for the process monitoring tasks.

4.2 Statistical Process Control

Process industries are under constant pressure to produce high quality products, reduce product rejection rates, and to satisfy strict safety and environmental regulations (Romagnoli and Palazoglu 2012). These requirements led to the extensive use of statistical process control (SPC), here referred to as process monitoring. SPC assumes that a process experiencing natural variations will remain in a state of statistical control under which certain process or product variables will remain close to their desired values (Venkatasubramanian 2003). The simplest and most common technique for process monitoring and quality control is a Shewhart control chart, where a single variable is plotted against time (Shewhart 1931). The target is the centerline, and upper and lower limits define a normal region for acceptable variation from the target, as shown in Figure 4.2. The upper and lower limits represent three-sigma (sample standard deviation) from the sample, defined as:

$$\sigma = \sqrt{\frac{\sum_{i=1}^{n}(x_i - \bar{x})^2}{n-1}}$$

Here x_i is an individual sample, $\bar{x}$ is the mean (arithmetic average) of the data, and n is the total number of measurements. The three-sigma control limit can also be called 99.73% confidence level, meaning that 99.73% of the training data falls within the normal operation region. When the measurement is above or below the three sigma control limits, the process is said to be in a faulty state. It is important to note that this method assumes that data follow a normal distribution.

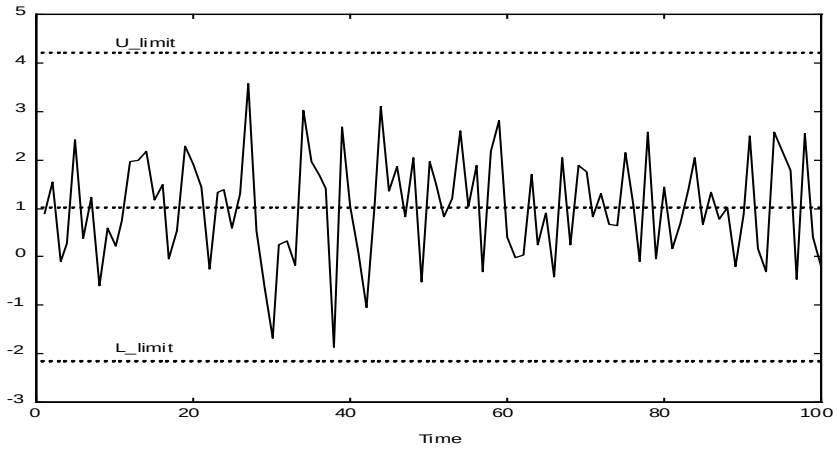

Figure 4.2: Shewhart chart.

If the monitored process variables are not independent, univariate controls charts could mislead or fail to indicate a faulty status due to correlations between variables. Multivariate statistical techniques were developed to compress data and to emphasize the most important behavior in the data.

4.3 PCA-Based Process Monitoring

Given the large number of variables monitored in a large plant, it is important to develop techniques that monitor more than one variable at a time in order to execute effective process monitoring. This section explains how the PCA decomposition from Section 3.2.1 can be applied

to the three process monitoring tasks of fault detection, identification, and diagnosis. Besides its statistical ability to detect large deviations from normal operations, PCA is also useful for feature extraction and dimensionality reduction (DR). Some monitored variables can generate highly noisy data with few significant variations, and PCA is adept at ignoring the noise and capturing a signal in data.

PCA is a widely used benchmark in process monitoring research. Raich and Cinar (1996) demonstrated the use of standard PCA for fault detection and diagnosis on the Tennessee Eastman process. A thorough treatment of PCA and other statistical techniques to the Tennessee Eastman process is presented in Chiang et al. (2000). In addition to the techniques presented here, PCA has been applied to process monitoring in other forms which more specifically take into account dynamics and non-linearity. NLPCA developed by Kramer (1994) uses non-linear feedforward neural networks employing a "bottleneck" layer to uncover linear and non-linear correlations. Ku (1995) developed an important adaptation of PCA process monitoring strategies called DPCA which uses "time lag shifts" to include dynamic behavior in PCA models.

The following sections explain how to use PCA models for process monitoring.

4.3.1 PCA fault detection

Faulty data can be detected with PCA in two ways: either the scores can move outside the normal operating region or the residuals generated by the PCA model could become large. Using the projections of multivariate process data described in Section 3.2.1, deviations from the normal operating region are measured using Hotelling's T^2 statistic. A high T^2 indicates a fault is occurring, and a low T^2 indicates a normal status. In similar fashion, the residuals generated by the PCA model in response to a new data point are used to calculate the squared prediction error (SPE) also known as the Q statistic. The calculations for both statistics are described below.

Given the $1 \times a$ projection of a $1 \times m$ observation row vector into the score space *t*, the T^2 statistic can be calculated:

$$T^2 = t^T \Lambda_a^{-1} t$$

Where Λ_a is the diagonal matrix containing the first *a* largest eigenvalues in order of decreasing magnitude. The T^2 statistic threshold for normal operation can be represented as an ellipsoid with a $1 - \alpha$ statistical significance using the T_α^2 threshold and a level:

$$t^T \Lambda_a^{-1} t \leq T_\alpha^2$$

When the actual covariance matrix is estimated from the sample covariance matrix, the T_α^2 threshold is found from the *F* distribution by the equation:

$$T_\alpha^2 = \frac{a(n-1)(n+1)}{n(n-a)} F_\alpha(a, n-a)$$

Where *n* is the number of data points and a is the number of principal components. The T^2 statistic is highly sensitive to inaccuracies in the PCA space corresponding to the smaller eigenvalues (Chiang 2000) because it directly measures scores corresponding to the smaller singular values.

The $m - a$ smallest principal components can be monitored using a supplement to fault detection based on the T^2 statistic, or the Q statistic. Also known as the squared prediction error (SPE), the Q statistic can be computed to measure how well each sample conforms to the PCA model and the amount of variation not captured by the principal components retained in the model (Wise 1996). The part of the observation space corresponding to the *m* – *a* smallest singular values, which correspond to the *m* – *a* ignored by the reduction in dimension, can be monitored using the Q statistic:

$$r = (I - PP^T)x \qquad\qquad Q = r^T r$$

Where, *r* is the residual vector, a projection of observation *x* into the residual space. The threshold for the Q statistic is given by the following equations from Wise and Gallagher (1996).

$$Q_\alpha = \Theta_1 \left[\frac{c_\alpha \sqrt{2\Theta_2 h_0^2}}{\Theta_1} + \frac{\Theta_2 h_0 (h_0 - 1)}{\Theta_1^2} + 1 \right]^{\frac{1}{h_0}}$$

where c_α is the standard normal deviate corresponding to the upper $1 - \alpha$ percentile and

$$h_0 = 1 - \frac{2\Theta_1 \Theta_3}{3\Theta_2^2}$$

and

$$\Theta_i = \sum_{j=a+1}^{N} \lambda_j^i \qquad \text{for } i = 1 - 3$$

where the λ_i are the eigenvalues of the covariance matrix of X and N is the total number of principal components, which is either the number of variables or samples in X, whichever is smaller. The thresholds defined for the T^2 and Q statistics set the boundaries for normal variations and random noise, and a violation of the threshold indicates that the random noise has changed (Chiang et al. 2000) and a statistically separate operating status reached.

4.3.2 PCA fault identification

Contribution plots are a PCA approach to fault identification based on determining the process variable responsible for the faulty condition. For a T^2 violation, follow the approach in Chiang et al. (2000) in which the contribution of each variable is calculated according to:

$$cont_{i,j} = \frac{t_i}{\lambda_i} p_{i,j} (x_j - \mu_j)$$

Where $p_{i,j}$ is the i^{th} element of the loading matrix P. The total contribution of the j^{th} process variable is determined from:

$$CONT_j = \sum_{i=1}^{r} (cont_{i,j})$$

The $CONT_j$ for all process variables are then plotted on a single graph in order to decide which variables are responsible for the faulty condition.

4.3.3 PCA Fault diagnosis – discriminant analysis

To determine the root cause of a given fault, data previously collected from out of control or faulty operations can be grouped and used by a pattern classification scheme to diagnose future faults. Pattern classification proceeds via three steps: feature extraction, discriminant analysis, and maximum selection. Feature extraction is the process of isolating the important trends in the data and removing noise which could disrupt classification. PCA performs feature extraction in the projection into the score space using P in the fault detection step. The pattern classification system assigns an observation x to class i if

$$g(x)_i > g(x)_j \quad \forall j \neq i$$

Where, g_j is the discriminant function for class j. $g(x)_i$ can be approximated using the $-T^2$ statistic assuming the probability of each class is the same and the total amount of variability in each class is the same.

PCA, and similar techniques that use matrix decomposition, assume linearity and preserve distances. Preserving topologies with non-linear techniques maintains the order of data, which may aid our classification goals. In the next section, SOM as a topological preservation method is discussed.

4.3.4 Nonlinear principal component analysis (NLPCA)

Nonlinear PCA (NLPCA) is an extension of PCA proposed by Kramer (1991) and Dong and McAvoy (1996). A critical result for NLPCA is the proof by Cybenko (1989) that arbitrary decision regions can be well approximated by continuous feedforward neural networks with only one hidden layer and continuous sigmoidal nonlinearity. Like linear PCA, NLPCA seeks to remove

noise variables and weight statistically important variables in the detection and diagnosis of faults. While PCA uses multivariate statistics, NLPCA performs the reduction in dimensionality using a feedforward neural network. The neural network consists of a mapping or "bottleneck" layer, which reduces the input data to the intrinsic dimension, and a de-mapping layer that can reconstruct the original signals input into the neural network. In this work, we use the NLPCA implementation presented in Dong and McAvoy (1996) for fault detection. We use the SPE of reconstructed data was used as the fault detection statistic. For fault diagnosis, an equivalent to MPCA with individual models for each fault class was used for NLPCA fault diagnosis, a technique referred to here as MNLPCA (Multiple NLPCA). We use MNLPCA as a benchmark nonlinear process monitoring technique. The SPE of a competing set of NLPCA neural networks was calculated, and the class assigned to the group with the minimum SPE.

4.4 Novel Self-Organizing Map (SOM) Monitoring Approach

A valuable tool for addressing these challenges of high dimensional data sets, novelty detection, and multiple operating states comes in the form of self-organizing maps (SOMs). Also known as Kohonen networks (Kohonen 2000), SOMs are a type of neural network used in the visualization and analysis of high dimensional data and have been applied to a wide range of engineering problems (Kohonen 1996). SOM's versatility comes from its topology preservation and data representation abilities which help isolate the key variables and patterns that emerge from data. Vesanto (1999) demonstrated how to use SOM in conjunction with data clustering and analysis.

Figure 4.3 illustrates the overall approach followed. Using the groups of training data created, an SOM is fitted to the data. Next the map is analyzed using SOM visualization tools and K-means clustering. Different groups of data are projected onto the SOM to explain the meaning

of the clusters and determine which events or operating regimes that area of the map represents. After that, training data is projected to the map, and the quantization error (QE) is calculated for each point. A distribution is also fit to the QE results, which is used to create a reference value for detecting novel events. After the projection and analysis steps are complete, the map is prepared for process monitoring: detection through QE scores, identification using contribution plots, and diagnosis using the map structure. Some detection, diagnosis, and identification results are duplicated using the PCA monitoring strategies presented by Russell et al. (2000) which use PCA with parallel analysis to model data, Hotelling's T^2 and Q statistic for classification, and minimum T^2 statistic for discriminant analysis.

4.4.1 The self-organizing map (SOM)

The self-organizing map (SOM) is a type of neural network that can be used to non-linearly project high dimensional data onto a lower dimensional array of neurons. Mapping with an SOM preserves topological relationships as the SOM conforms to the multidimensional shape of the data and allows the neurons organization to preserve whatever clustering might arise from the data. (Kohonen 1996) This study used the MATLAB implementation of SOM developed by Vesanto et al. (2000).

An SOM is a connected array of nodes forming a regular rectangular or hexagonal grid structure. The prototype vectors making up each map model vectors within the training data. The number of map nodes is determined by a heuristic algorithm related to the number of data points in the training data. The prototype vectors can be represented in both the data space and in the dimensionality reduced space within the map structure. A data point's representation on the map is found by locating its best matching unit (BMU). In short, the BMU of a given data vector is the

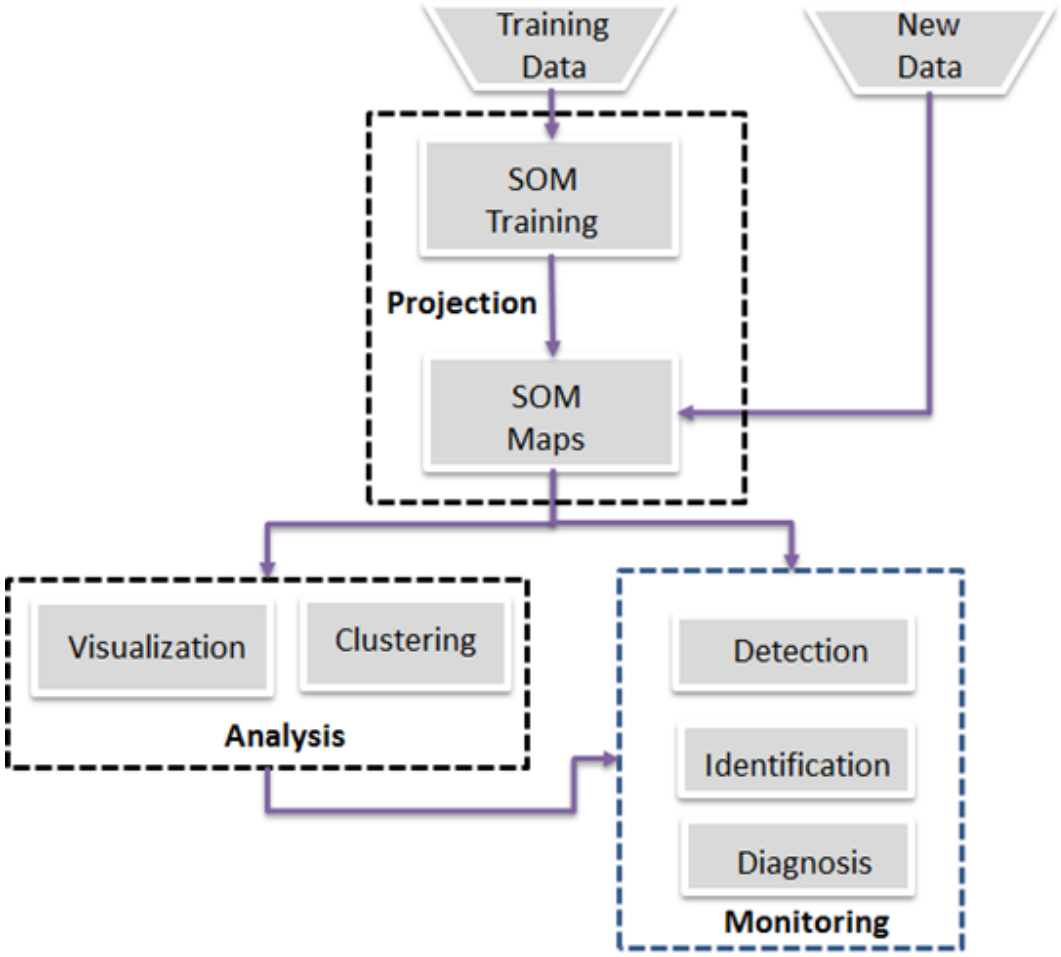

Figure 4.3: Schematic of the overall strategy for fault detection and identification.

map unit nearest to it or with minimum Euclidian distance, $\partial(m_k, v_i)$), according to:

$$BMU_i = \arg\min\left(\partial(v_i, m_k)\right), \forall k$$

The Euclidean distance between a data point and its BMU is also called the *quantization error* (QE) and will be used later in the novelty detection step.

During training, map vector m_k's position is updated using each data point from a training set according to the formula:

$$m_k(t+i) = m_k(t) + \alpha(t)h_{k,BMU_i}\left(v_i(t) - m_k(t)\right)$$

where t is the mapping time step and α is the monotonically decreasing learning rate, h_{k,BMU_i} denoting a neighborhood kernel function centered at the BMU. The training algorithm matches data vectors to prototype vectors using Euclidean distance. The neighborhood kernel h_{k,BMU_i} centered at $m_k(t)$ is usually chosen in the Gaussian form:

$$h_{m_k,BMU_i} = exp\left(\frac{\|m_k - BMU_i\|^2}{2\sigma^2}\right)$$

$\sigma(t)$ denotes the monotonically decreasing width of the kernel that allows for a regular smoothing of the prototypes (Kohonen 2000).

A common alternative to the update rule outlined above is the SOM batch training algorithm. During the batch training algorithm, the training data is passed through once to determine which data vectors lie in each prototype's neighborhood. Then each map unit is replaced by the weighted average of the data vectors in its neighborhood, where the weighting factors are the neighborhood kernel values. In the notation used previously:

$$m_i(t+1) = \frac{\sum_{j=1}^{n} h_{i,c(j)}(t)\boldsymbol{x}_j}{\sum_{j=1}^{n} h_{i,c(j)}(t)}$$

where $c(j)$ is the BMU of the sample vector $\boldsymbol{x}_j$, $h_{i,c(j)}$ is the neighborhood kernel defined above, and *n* is the number of data vectors used for training. This variant of the training algorithm is often used because it is much faster to calculate and the results are typically as good as or better than the sequential training algorithm (Kohonen 2000).

4.4.2 SOM visualization tools for process analysis

A key advantage to using SOM in process monitoring comes from the insights it provides into high dimensional structures within the data on the two dimensional map. The visualizations discussed below allow us to see the shape of the data distribution, cluster borders, projection directions, and possible dependencies between the variables. Common visualizations discussed

here include component planes, distance matrices, and projections as proposed by Kaski (1997), Vesanto (1999), (Vesanto 2002), and Himberg, (2001).

- Component Planes: A component plane displays the value of individual variables at each prototype vector in the map. Each component plane is associated to one variable in the observation space. The value of the variable at all map nodes is visualized using different colors which allows the user to visually identify possible dependencies between variables (Vesanto 1999, Lampinen 2000). The dependencies between variables can be seen as similar patterns in identical locations on the component planes. In that sense, the SOM reduces the effect of noise and outliers in the observations and, therefore, may actually make any existing dependency clearer than in the original data.
- Distance Matrices: Distance matrices show the pairwise distances between nodes within the map structure. Using the lower dimensional structure of the SOM, colors are used to show high or low distances, which provides insight into the dominant clustering patterns present in the data. The most common visualization of the distance matrix is the U-matrix (Ultsch 1993), which visualizes all pairwise distances between nodes in the map. In a U-matrix, the dominant clustering structure can be seen as areas with small distances separated by large distances. As in the basic U-matrix, visualization of the clusters can be greatly improved by augmenting the distance matrix with an additional entry between each prototype vector and each of its neighbors.
- Projections: Finally, projections onto the map are very important visualization tools. Highlighting the BMU of data illustrates the location of the observations on the map relative to other observed data. Two important figures derived from projections are hit diagrams and trajectories. Hit diagrams project a collection of data points to show a region

belonging to a group of data. Trajectories take a series of time and project them on to the map, connecting them with lines. The trajectory makes it possible to visually indicate the current state of the process and observe how that state has been reached.

4.4.3 Clustering of the SOM using k-means

The final goal of our analysis of an SOM is to identify meaningful regions of the map and groups of SOM vectors with similar characteristics to help us understand structure in data. It is useful to perform clustering on the SOM itself as a way to add more information about the associations that emerge within groups of map vectors that might be difficult to identify from a U-matrix or component plane alone. Separating map vectors into different clusters can, in combination with the visualizations mentioned previously, give an engineer more insight about the SOM results by showing which variables differentiate the clusters and revealing sub clusters, among other uses (Vesanto 2000).

In this work, we used K-means to cluster the SOM. K-means is a popular and fairly simple method to implement for unsupervised data clustering. First, K initial centroids are chosen, corresponding to the number of clusters desired. Each point in the dataset is then assigned to the closest centroid, and each collection of points assigned to a centroid is a cluster. The centroid of each cluster is then updated based on the points assigned to the cluster. The assignment and update steps are repeated until no point changes clusters or until the centroids remain the same (Tan 2005).

In a k-means analysis on a data set, several groups of clusters are found and evaluated for quality based on the Davies-Bouldin index (DBI). DBI, $\bar{R}$, is based on the ratio of within cluster scatter to between cluster scatter:

$$R_{ij} = \frac{S_i + S_j}{M_{ij}}$$

$$\bar{R} = \frac{1}{N}\sum_{i=1}^{N} R_i$$

For clusters i and j. M_{ij} holds the distances between cluster centroids and R_i is the maximum of $R_{ij}, i \neq j$. S is the dispersion of the cluster which is usually measured by the standard deviation of data in the cluster relative to the cluster centroids (Davies and Bouldin 1979).

4.5 MSOM in Process Monitoring

4.5.1 SOM fault detection and diagnosis

Figure 4.4 outlines the MSOM approach to process monitoring. Fault detection and diagnosis is performed by using the Euclidian distance, also called the quantization error (QE), between a new data point produced by the DCS as a measure of novelty and its BMU on the SOM. Once the quantization error rises above a previously determined threshold (i.e. the process data at a given time point move a certain distance away from its BMU), a novel event is said to have occurred. Here, the threshold that defines the boundary between a normality and novelty was determined by fitting a statistical distribution to the QE's performance on the training data. Since in this case known, faults are modeled and we want to detect novel events with a very low probability, we will use the 99.99% confidence interval. A confidence interval like 99% on one-minute data could give rise to large number of false alarms. The QE calculated from the training data in these case studies followed a lognormal distribution, which was used to generate the QE threshold for monitoring.

Incoming data is sorted by simply giving new data the same class as its BMU. When the BMU is known, the new data can be projected onto a two-dimensional representation of the map to locate where the new data falls on the map relative to other data of the same type.

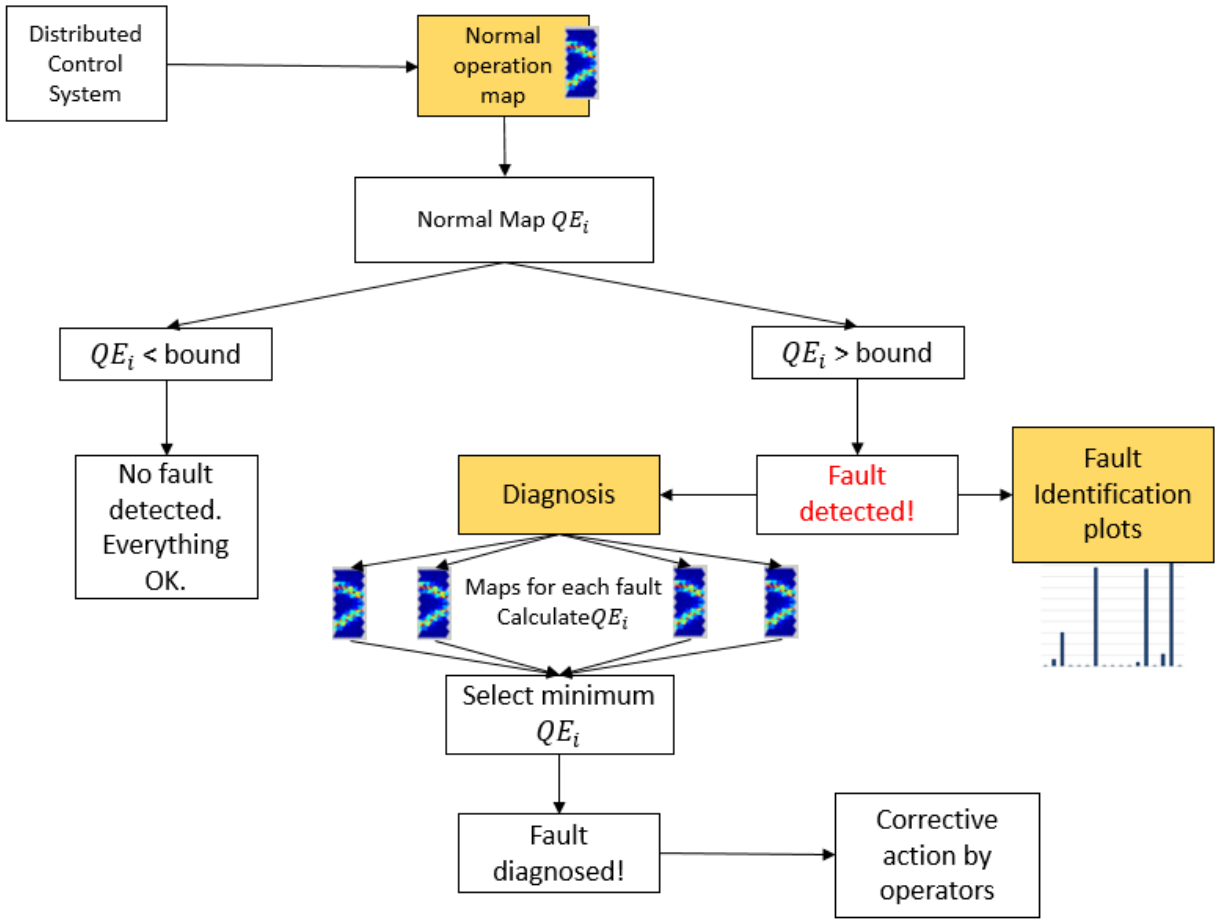

Figure 4.4: Proposed MSOM process monitoring framework. Data comes from the computerized control system and is first projected onto the SOM of normal operations.

4.5.2 Variable contribution plots

SOM contribution plots can identify the variables most responsible for the fault by analyzing the residual of the faulty point and the SOM model of normal or other faults. The approach applied exploits the capabilities of the SOM and mimics the PCA approach to create a variable contribution plot that can be used to isolate where in the unit the fault is occurring.

In the proposed approach, analysis of the residual between a faulty point and its BMU in the SOM used for monitoring highlights the variables most responsible for the fault. First, we

identify the BMU through the method discussed in Section 4.4.1 and then we project the given data point onto the map. For variable j, the residual is calculated by:

$$r_j(t) = \left(x_j(t) - m_{c_j}\right)^2$$

Where $x_j(t)$ denotes the value of measurement j at time t, and m_{c_j} is the value of the jth variable of the BMU. Since QE, or the Euclidian distance, is used for fault detection, this approach isolates which variables contribute the most to the observed Euclidian distance.

Figure 4.5 demonstrates the advantage to analyzing the residuals for the SOM model for fault identification compared to a simple parabola-shaped normal region. In this example, a data

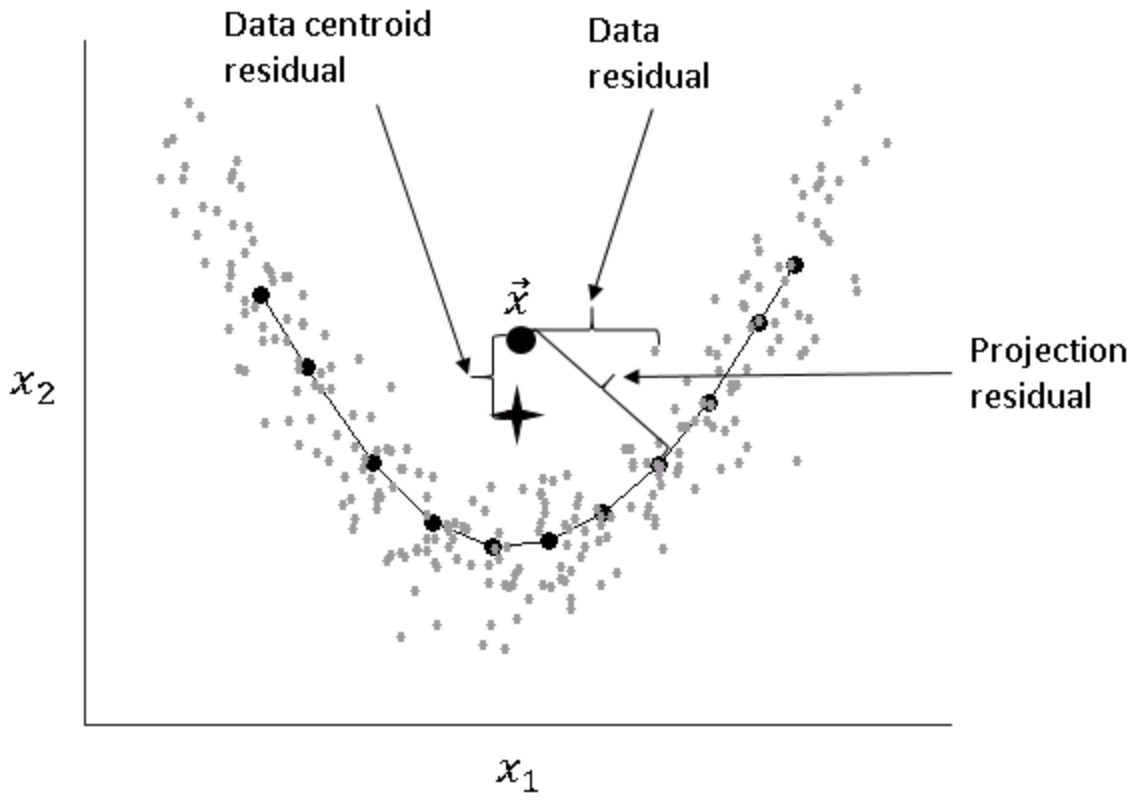

Figure 4.5: Illustration of the residual analysis. The SOM based contribution identifies large contributions from both variables relative to the structure of the data.

set exists with related dimensions x_1 and x_2 and other independent variables. A "fault" gives rise to deviations in both the x_1 and x_2 directions through the alteration of an unmeasured variable, and takes the point out of the general trend of the data.

Figure 4.5 plots three residuals from the faulty point using the black brackets: the centroid, the nearest data point, and the BMU in the SOM. In this case, the centerline of the nonlinearly related data does not lie within the data cloud itself. Therefore, the deviations from the data point are negligible and do not represent the point's deviation from the data. The residual vector is small and would erroneously capture only x_1 as the deviated variable, which ignores the deviation in x_2.Using raw uncompressed data causes the faulty point to be matched with a noisy outlier. The SOM residual approximates an orthogonal projection onto the topological structure of the data cloud. The SOM residual accurately captures both x_1 and x_2's contribution (Robertson et al. 2015).

4.6 Multiway Methods for Batch Process Monitoring

Batch processes experience many changes in dynamics and time variations, in contrast to continuous processes which typically operate around a fixed target region represented by PCA process monitoring as a bound on the T^2 or Q statistic. As discussed in Section 2.2, multiway unfolding can be used to adapt techniques developed for continuous processes to batch processes. This section will discuss two techniques for batch process monitoring: multiway-PCA and a batch adaptation of MSOM.

Both multiway PCA and MSOM techniques perform fault detection at the end of batches using batch data processed through multiway unfolding. In addition to performing automated process monitoring tasks, projecting data processed by multiway unfolding can lead to insights about operating procedures and pinpoint sources of batch-to-batch variations. In creating training

data sets for batch process monitoring, the modeler must identify historical batches that operators would expect to be marked as abnormal and remove them to enhance the characterization of normal operations. Data must be analyzed batch-to-batch. For the modeling step itself, both batch adaptations of PCA and MSOM monitoring operate similarly to the continuous case except that they use multiway data. The data model (PCA or SOM) is fit as described in Sections 4.3 and 4.4 to data unfolded as in Figure 2.1, where individual rows of the data matrix correspond to all the measurements taken during a batch. For multiway unfolding to function as desired, each batch needs to have an identical length in time. A batch process dataset with variable lengths can be synchronized through DTW technique discussed in Section 2.3. Yao and Gao (2009) review alternatives.

In contrast to Nomikos and MacGregor (1994), we perform detection and diagnosis at the end of the batch, though there are adaptations allowing online diagnosis. In the case of MSOM, MSOM could be adapted to the online batch process monitoring by adjusting how the BMU is found. If only half of the time period is known, half of the measured data could be used still be used to find the BMU without any other changes to the SOM model of data.

4.7 Defining Normal Operations: Example on Fisher Iris Data

4.7.1 PCA analysis – fault detection

The results of applying PCA fault detection, using Class 1, or Setosa data, as the normal operating region (NOR), is given in Figure 4.6. Fault points are points that lie outside of the T^2 and Q statistical thresholds (represented by the cylinder drawn in black lines), and are colored red. Only four points in Class 1 were misclassified giving a misclassification rate for the entire data set of 2.67% and a misclassification rate within Class 1 of 8%.

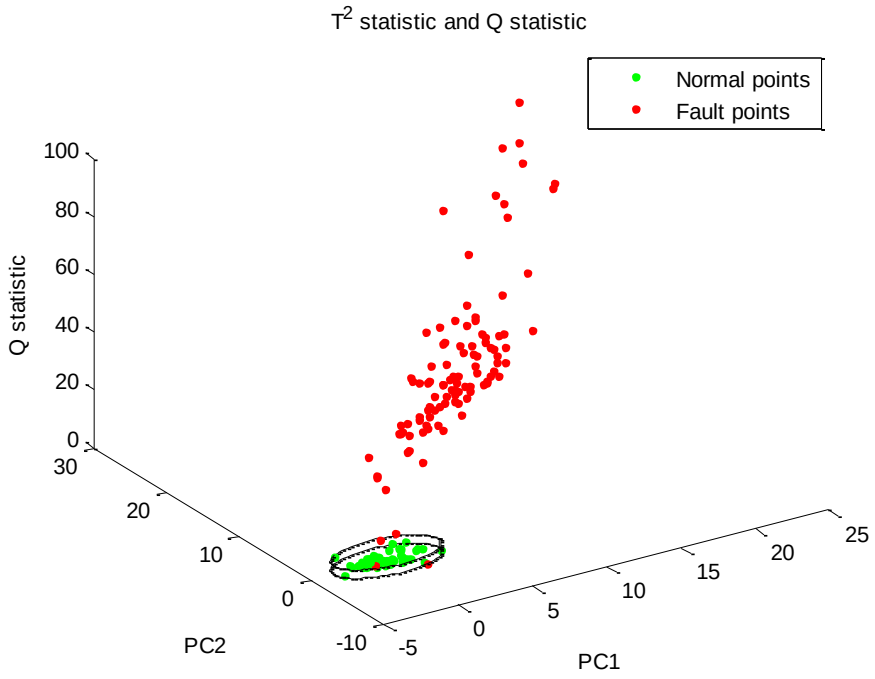

Figure 4.6: Green points were classified as normal and red points were classified as faulty points. The cylinder denotes the normal operating region. PCA was able to clearly separate class 1 from classes 2 and 3.

Figures 4.7 and 4.8 show the T^2 and Q statistics of each data point in the iris data set. Green data points are "normal" and red points are "faulty". Figure 4.6 shows the T^2-Q fault detection cylinder defined by Chiang (2000), while Figure 4.7 simply shows the two statistics plotted together, which is a simpler way to display the T^2 and Q statistic boundaries if more than two dimensions of the score space are used to calculate the T^2 statistic. Figure 4.8 shows an enlargement of the NOR shown in Figure 4.7, which clearly shows the small number of misclassified Class 1 points.

4.7.2 Contribution plots – fault identification

Figure 4.9 shows the contribution statistics calculated by the PCA model of Class 1 over selected fault points from classes 1, 2, and 3. The Class 1 faulty point was misclassified and registered as a fault because it was above the Q statistic boundary and therefore registers low

contributions from all variables. For both fault points from Classes 2 and 3, petal length and petal width contributed the most to the faulty state of the data point. They strongly registered as faults and therefore have large contributions in their key variables.

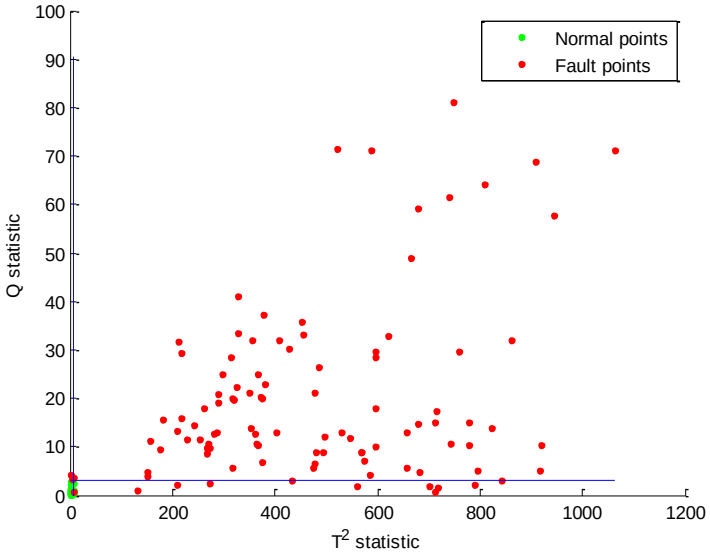

Figure 4.7: Fault detection without using the T2 cylinder. The NOR is represented by the small, dense cluster of points in the lower left corner of the graph. The lower left corner is enlarged in Figure 4.8.

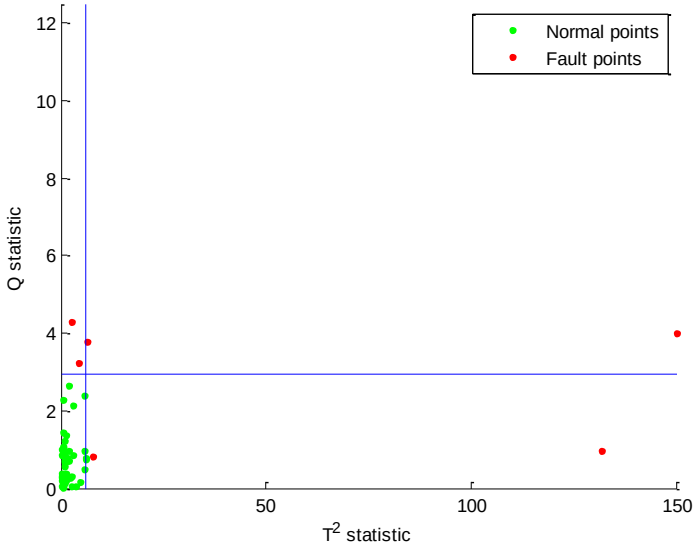

Figure 4.8: A detail of the NOR cluster from Figure 4.7. Because the PCA model was created using class 1 data, the error in the model for class 1 is small which yields small T2 and Q statistics.

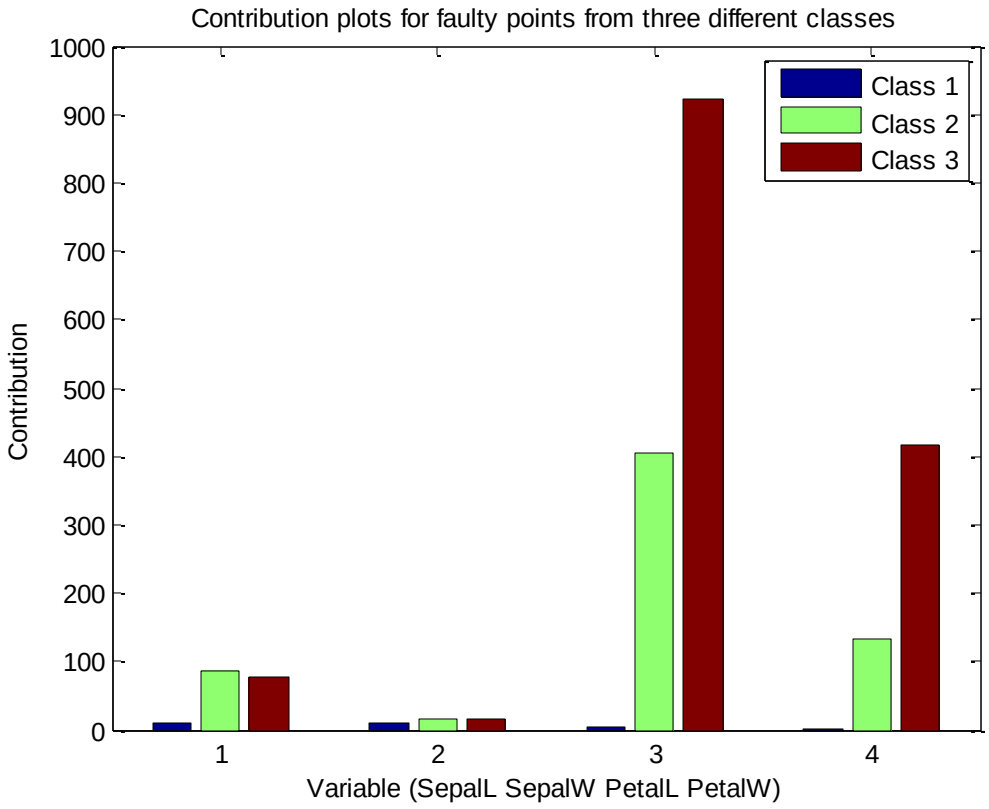

Figure 4.9: Faulty points from each class produce different contribution plots. The petal length and width are most responsible for the "faulty" status.

4.7.3 Discriminant analysis – fault diagnosis

Fault diagnosis was done using the multiple PCA procedure for discriminant analysis described above, which assigns classes based on the value of the T^2 statistic. The data were classified with a 90.6% correct classification rate. Most of the classification errors were in discriminating between Classes 2 and 3 due to the overlap between the two classes, but points within well-defined Class 1 were correctly identified 100% of the time.

The graphs in Figures 4.10 through 4.12 illustrate the T^2 boundaries used to classify each point into the three classes, however, a given point's class is determined based only on its T^2 statistic, not its position on the graph. Therefore, a point far away from every class would still be

classified into one of the three classes given. Additionally, the spread of the different classes has a direct effect on the size of the regions in the data space defined by each class. Class 1 has a small, well separated region separating it from the other two classes while Class 2 and 3 have more spread and a correspondingly larger area that also overlaps for the two classes.

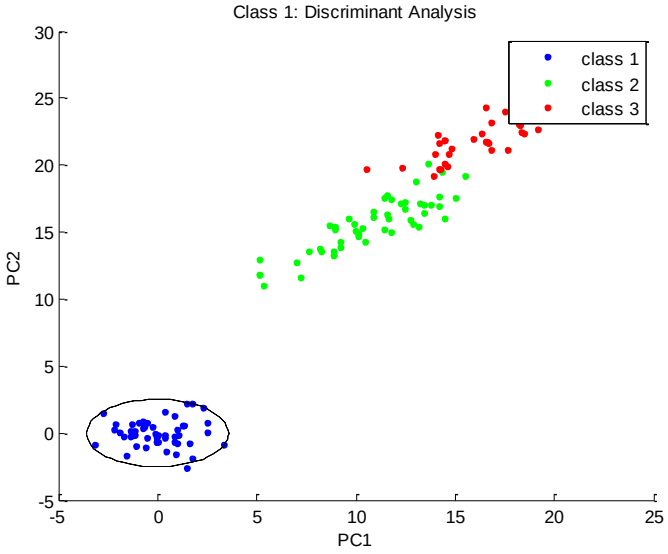

Figure 4.10: Data scores with respect to the class 1 PCA model.

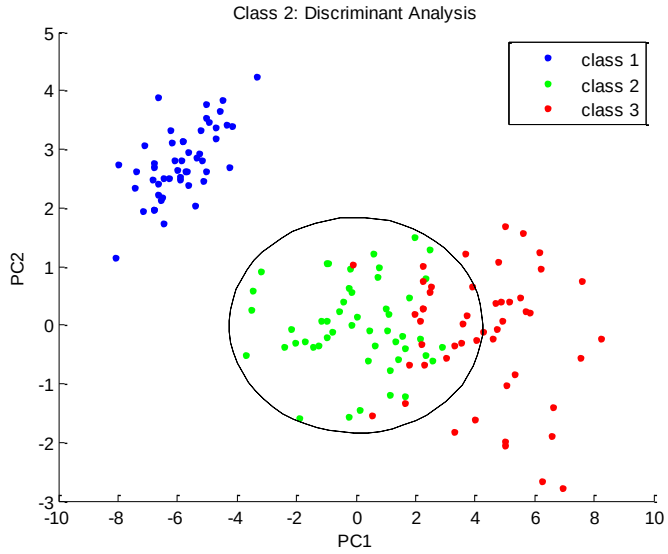

Figure 4.11: Data scores with respect to the class 2 PCA model.

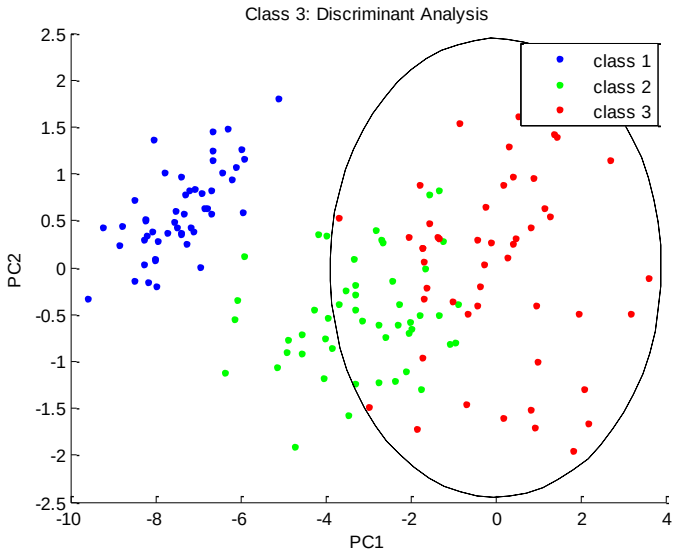

Figure 4.12: Data scores with respect to the class 3 PCA model.

Finally, Figure 4.13 shows MSOM maps fit to each region of the data. The SOM maps are more flexible and can model normal operating regions in shapes other than spherical. This approach achieves 3% correct classification rate, since the maps can more accurately model the region where the two classes nearly overlap.

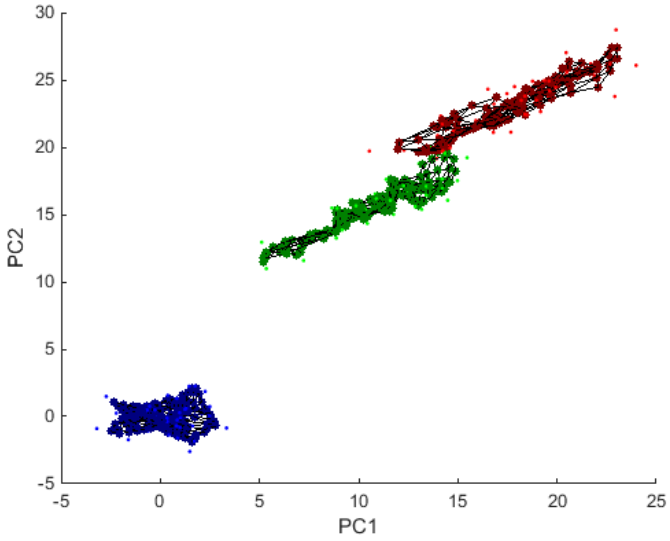

Figure 4.13: SOM fits to each of the Fisher Iris classes with less overlap compared to the MPCA models.

4.8 References

Chiang L. H., Russell E. L., & Braatz, R. D. (2000). Fault detection in chemical processes using Fischer discriminant analysis, discriminant partial least squares, and principal component analysis. *Chemometrics and Intelligent Laboratory Systems, 50,* 243-252.

Davies, D. L., & Bouldin, D. W. (1979). A cluster separation measure. *IEEE Transactions on Pattern Analysis and Machine Intelligence, 1*(2), 224-227.

Himberg, J. (2001). *From insights to innovations: Data mining, visualization, and user interfaces.* (Doctoral dissertation). Retrieved from http://lib.tkk.fi/Diss/2004/ isbn9512273373/

Kaski, S. (1997). *Data exploration using self-organizing maps*. (Doctoral dissertation). Retrieved from http://users.ics.aalto.fi/sami/thesis/

Kohonen, T., Oja, E., Simula, O., Visa, A., & Kangas, J. (1996). Engineering applications of the self-organizing map. *Proceedings of the IEEE, 84*(10), 1358-1384.

Kohonen, T. (2000). *Self-organizing maps*. Berlin: Springer-Verlag.

Kramer, M. A. (1991). Nonlinear principal component analysis using autoassociative neural networks. *American Institute of Chemical Engineers Journal, 37*(2), 233-243.

Ku, W., Storer, R. H., & Georgakis, C. (1995). Disturbance detection and isolation by dynamic principal component analysis. *Chemometrics and Intelligent Laboratory Systems,* 30, 179-196.

Lampinen, J., & Kostiainen, T. (2000). Self-organizing maps in data analysis – Notes on overfitting and overinterpretation. *Proceedings of the European Symposium on Artificial Neural Networks,* 239-244.

Nomikos, P., & Macgregor, J. F. (1994). Monitoring batch processes using multiway principal component analysis. *American Institute of Chemical Engineers Journal, 40*(8), 1361-1375.

Raich, A., & Cinar, A. (1996). Statistical process monitoring and disturbance diagnosis in multivariable continuous processes. *American Institute of Chemical Engineers Journal, 42*(4), 995-1009.

Robertson, G., Thomas, M. C., & Romagnoli, J. A. (2015). Topological preservation techniques for nonlinear process monitoring. *Computers and Chemical Engineering, 76,* 1-16.

Romagnoli, J. A., & Palazoglu, A. (2012). *Introduction to process control*. Boca Raton: Taylor and Francis Group.

Russell, E. L., Chiang, L. H., & Braatz, R. D. (2000). *Data-driven techniques for fault detection and diagnosis in chemical processes*. London: Springer.

Shewhart, W. A. (1931). *Economic control of quality of manufactured product*. New York: Van Nostrand.

Tan, P., Steinbach, M., & Kumar, V. (2006). *Introduction to Data Mining*. Boston: Longman.

Ultsch, A. (1993). Self-organizing neural networks for visualization and classification. In Opitz, O., Lausen, B., & Klar, R. (Eds), *Information and Classification* (307-313). Berlin: Springer.

Venkatasubramanian, V., Rengaswamy, R., Kavuir, S. N., & Yin, K. (2003). A review of process fault detection and diagnosis part I: Quantitative model-based methods. *Computers & Chemical Engineering, 27*, 293-311.

Vesanto, J., & Ahola, J. (1999). Hunting for correlations in data using the self-organizing map. *Proceedings of the International ICSC Congress on Computational Intelligence Methods and Applications*, 279-285.

Vesanto, J., & Alhoniemi, E. (2000). Clustering of the self-organizing map. *IEEE Transactions on Neural Networks, 11*(3), 586-600.

Vesanto,L., Himberg, J., Alhoniemi, E., & Parhankangas, J. (2000). SOM toolbox for Matlab 5 [Computer software]. Helsinki University of Technology: Helsinki, Finland.

Vesanto, J. (2002). *Data exploration process based on the self-organizing map*. (Doctoral dissertation). Retrieved from http://lib.tkk.fi/Diss/2002/isbn9512258978/

Wise, B. M., & Gallagher, N. B. (1996). The process chemometrics approach to process monitoring and fault detection. *Journal of Process Control, 6*(6), 329-348.

Yao, Y., & Gao, F. (2009). A survey of multistage/multiphase statistical modeling methods for batch processes. *Annual Reviews in Control, 33*, 172-183.

Chapter 5 - Case Study 1: Tennessee Eastman Process (TEP)

5.1 Introduction

Modern process monitoring is marked by the extensive use of advanced computer systems and large numbers of sensors to determine if a plant is operating in a safe state and to detect when a problem occurs. Identifying these states can be difficult due to the large number of variables measured, but data driven methods offer ways to quickly and efficiently extract useful information from the large data sets common in process industries. The goal of process monitoring systems is to detect and manage faults in order to minimize downtime, increase safety, reduce manufacturing costs, and improve performance.

Creating process monitoring systems for chemical manufacturing units from scratch is a challenging task. The most effective process monitoring and data classification methods are supervised, meaning that the data must be supplied with labels for model fitting. In practice, data are seldom labelled, and creating labelled process data is a time-consuming process that requires a large amount of process knowledge. Further, the definition of "normal" data can change with each turnaround and maintenance cycle of process equipment. Implementing and maintaining process monitoring and fault detection algorithms could be greatly simplified with unsupervised learning techniques like data clustering and dimensionality reduction.

In this chapter, we demonstrate how data clustering and dimensionality reduction can be used to discover fault classes in historical databases, and we apply the process monitoring methodologies described in Chapter 4 to detecting process fault events. The data studied is drawn from the benchmark Tennessee Eastman process (TEP). We test the ability of different combinations of data clustering and dimensionality reduction at effectively recreating the faults of the TEP using supervised cluster evaluation metrics. Next, we train process monitoring algorithms

using PCA, NLPCA, SOM, and MSOM for the detection, identification, and diagnosis of TEP faults. Both studies first consider a reduced data set of TEP faults for a simpler illustration and analysis of the effectiveness of the methods tested, followed by studying performance on the complete data set of 20 TEP faults.

Section 5.2 describes the TEP and its set of pre-programmed faults. Section 5.3 presents the results of the data clustering and DR study. Section 5.4 contains the process monitoring study of the fault detection, identification, and diagnosis of the TEP faults. Section 5.5 summarizes the results and offers conclusions.

5.2 Tennessee Eastman Process Description

First introduced as a process control challenge problem by Downs and Vogel (1993), the TEP is a simulation based on a real chemical process and has become an important benchmark in the evaluation of process control and process monitoring techniques (Yin 2012). The process uses four gaseous reactants (A, C, D, and E) to produce two liquid products (G and H) in competition with an unwanted by-product (F) and in the presence of an inert (B). There are four competing reactions related to temperature through Arrhenius laws, two producing desired products and the others producing the by-product. The entire simulation includes five unit operations: a reactor, condenser, separator, compressor, and a stripper. There are 41 measured variables, but many are delayed composition measurements. Our approach ignored delayed composition measurements and instead uses only the 22 measured variables defined in Table 5.1 along with 9 of the 12 original manipulated variables (Ricker (1996) holds three manipulated variables constant) defined in Table 5.2. Downs and Vogel (1993) also defined 20 disturbances or faults for the challenge process (see Table 5.3).

The data were generated using the control scheme and Simulink code from Ricker (1996), who applied a decentralized control strategy to the process that partitioned the plant into subunits and created a controller for each. The process flow sheet and controller scheme is given in Figure 5.1.

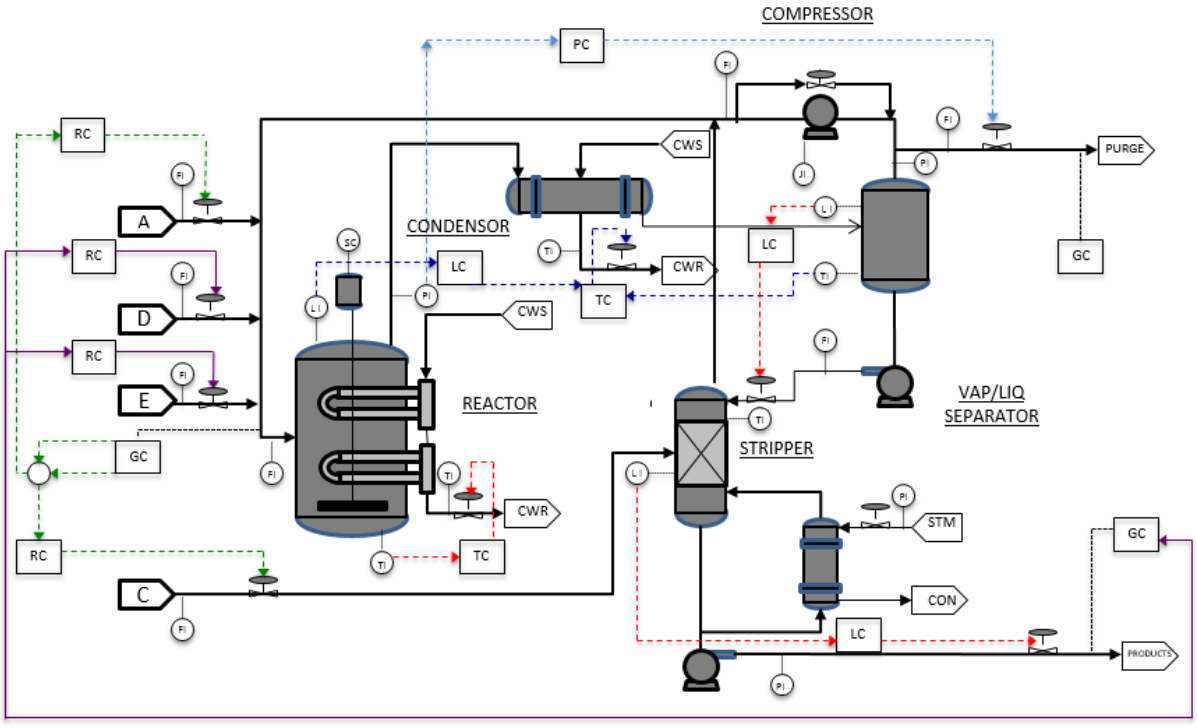

Figure 5.1: Process schematic with control scheme.

Initial clustering and process monitoring studies which included faults with random variations, such as Fault 13 (slow drift in reaction kinetics), showed that dynamic faults contributed noise without forming the dense groups that can be found by data clustering. Therefore, in addition to the full data set with all of its challenges, we studied a reduced data set in more detail. The reduced data set primarily contained step change faults with fewer faults with time-varying dynamics that could obfuscate our analysis. The reduced data set consists of data from faults 0, 1,

2, 4, 6, 7, 8, and 14, with 8 and 14 possessing time-varying dynamics that might be more challenging to learn than the step faults.

Table 5.1: TEP measured variables

Number	Variable Name	Units
1	A feed (stream 1)	kscmh
2	D feed (stream 2)	kg/hr
3	E feed (stream 3)	kg/hr
4	A and C feed (stream 4)	kscmh
5	Recycle Flow (stream 8)	kscmh
6	Reactor feed rate (stream 6)	kscmh
7	Reactor Pressure	kPa gauge
8	Reactor Level	%
9	Reactor Temperature	Deg. C
10	Purge Rate (stream 9)	kscmh
11	Product Separator Temperature	Deg. C
12	Product Separator Level	%
13	Product Separator Pressure	kPa gauge
14	Product Separator Underflow (stream 10)	m^3/s
15	Stripper Level	%
16	Stripper Pressure	kPa gauge
17	Stripper Underflow (stream 11)	m^3/s
18	Stripper Temperature	Deg. C
19	Stripper Steam Flow	kg/hr
20	Compressor Work	kW
21	Reactor Cooling Water Outlet Temperature	Deg. C
22	Separator Cooling Water Outlet Temperature	Deg. C

Table 5.2: TEP manipulated variables

Number	Variable Name	Units
23	D Feed Flow (stream 2)	%
24	E Feed Flow (stream 3)	%
25	A Feed Flow (stream 1)	%
26	A and C Feed Flow (stream 4)	%
27	Purge Valve (stream 9)	%
28	Separator Pot Liquid Flow (stream 10)	%
29	Stripper Liquid Product Flow (stream 11)	%
30	Reactor Cooling Water Flow	%
31	Agitator Speed	%

Table 5.3: TEP process faults description

Fault No.	Description	Type
1	A/C Feed Ratio, B Composition Constant (Stream 4)	Step
2	B Composition, A/C Ratio Constant (Stream 4)	Step
3	D Feed Temperature (Stream 2)	Step
4	Reactor Cooling Water Inlet Temperature	Step
5	Condenser Cooling Water Inlet Temperature	Step
6	A Feed Loss (Stream 1)	Step
7	C Header Pressure Loss - Reduced Availability (Stream 4)	Step
8	A, B, C Feed Composition (Stream 4)	Random Variation
9	D Feed Temperature (Stream 2)	Random Variation
10	C Feed Temperature (Stream 2)	Random Variation
11	Reactor Cooling Water Inlet Temperature	Random Variation
12	Condenser Cooling Water Inlet Temperature	Random Variation
13	Reaction Kinetics	Slow Drift
14	Reactor Cooling Water Valve	Sticking
15	Condenser Cooling Water Valve	Sticking
16	Unknown	
17	Unknown	
18	Unknown	
19	Unknown	
20	Unknown	

5.3 Tennessee Eastman Process Fault Extraction

The goal in our study of clustering and dimensionality reduction on the Tennessee Eastman process is to examine how effectively various approaches to clustering extract different process operating regimes from the data. In contrast to the separation tower study in Chapter 6 where the data contain one large normal cluster and a much smaller fault cluster, the TEP simulates a variety of behaviors including step changes, random variations, and other plant trends. An additional advantage to using the simulation is that the ground truth classes are known with certainty which allows the use of supervised cluster evaluation metrics.

5.3.1 Normal and fault 1: basic case

To demonstrate in a simple case our proposed approach to clustering, we first study two simple operating regimes: normal operations and Fault 1, which is a step change in one of the feeds to the process. Here, we would expect the clustering algorithm to reproduce the groups in the data that might be difficult to find without projection and clustering. We project the data using PCA and DBSCAN for this example, but any technique in this paper could accomplish this task.

Figure 5.2 projects the data to 3 principal components, showing the dense cluster corresponding to normal operations as well as the transition to Fault 1's steady state. Figure 5.3 shows the result of DBSCAN applied to the data set. Blue corresponds to the faulty data, green is the normal cluster, and the black data is identified by the DBSCAN algorithm as noise. Figure 5.4 and 5.5 point to how to use clustering results to reveal knowledge from data sets. Coloring a time series plot of the evolution of the Stream 4 flow with the clusters found by DBSCAN, green, blue, and noise groups can be clearly connected to changes in Stream 4 and studied as separate process states. This result can reveal the dominant behavior of each cluster and, if the ultimate goal is the creation of a process monitoring algorithm, it can be used to separate normal and faulty groups for training.

5.3.2: Reduced TEP data set

We consider a reduced data set consisting of TEP faults 0, 1, 2, 4, 6, 7, 8, and 14 because the results are simpler to analyze and visualize than a data set including all 20 TEP faults studied later. Most of these faults are step changes that are simpler to detect, but faults 8 and 14 express dynamic, non-linear variations that do not form into a dense group, and might disrupt the clustering of other data. All data studied were first normalized to zero mean and unit variance with respect

to normal operations, which is common with plant data due to the overabundance of data from normal operations. The numbers of components used by each technique is given in Table 5.4.

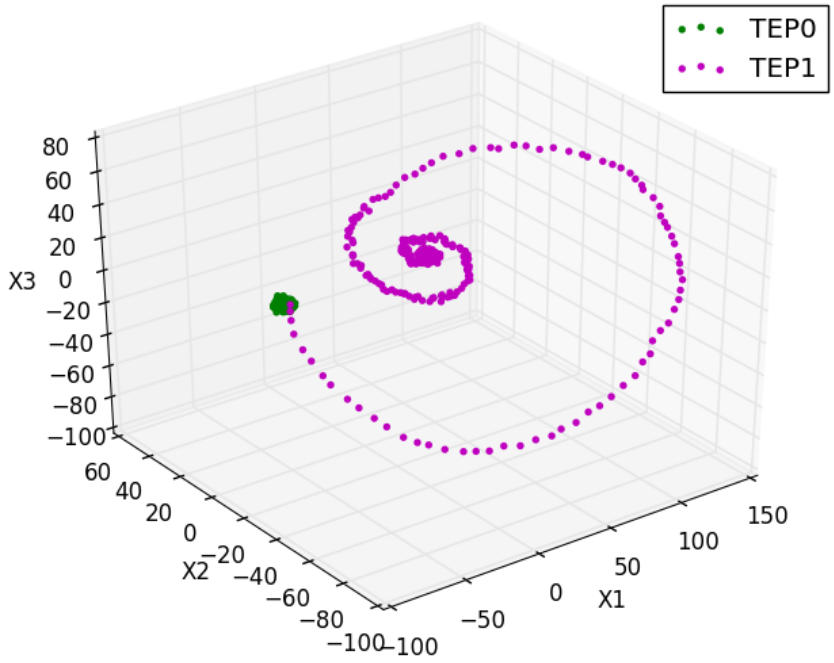

Figure 5.2 Data from TEP0 and TEP1 projected to 3 PCs.

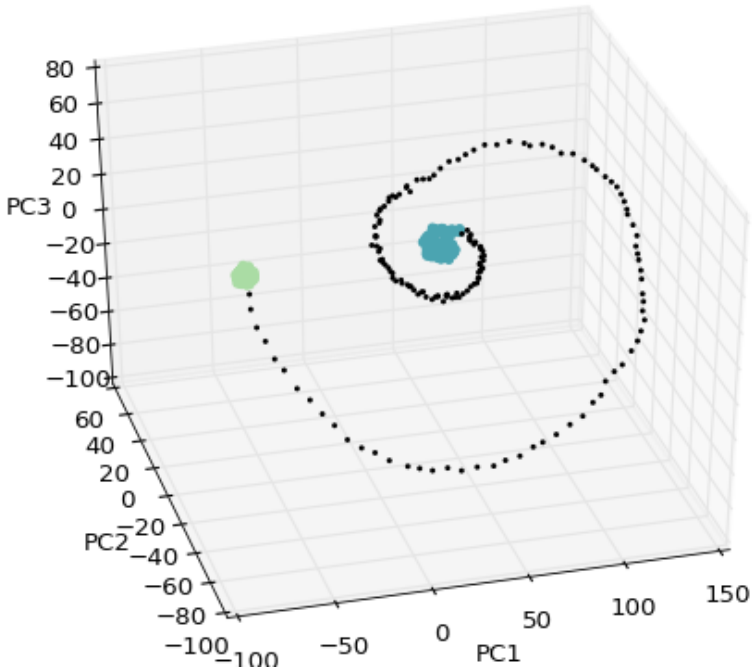

Figure 5.3 DBSCAN identifies the clusters formed by TEP0 and TEP1.

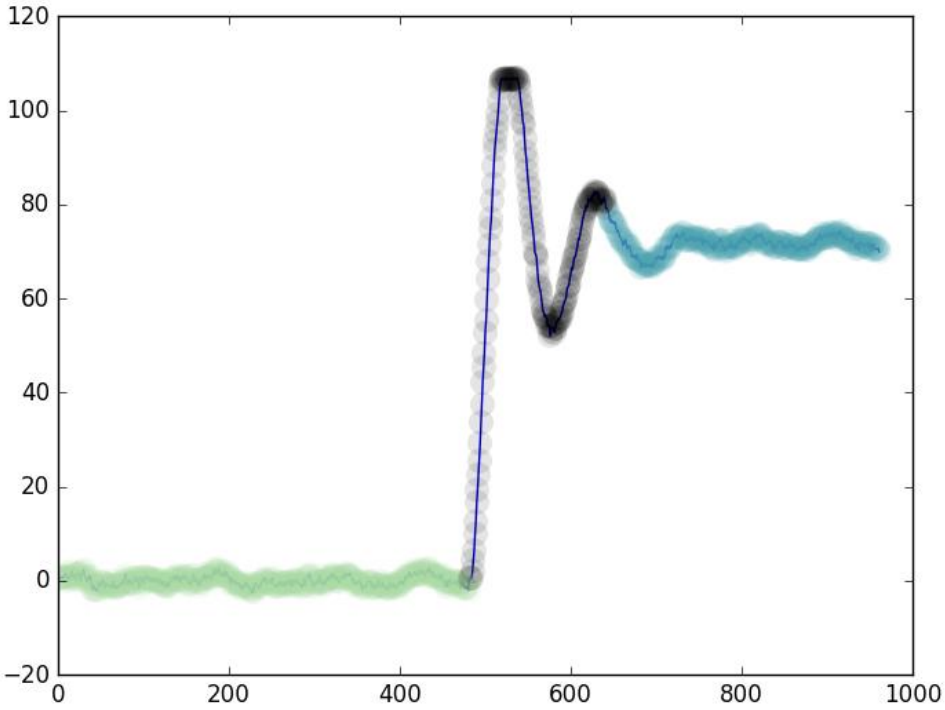

Figure 5.4 Flow of Stream 4 colored by the DBSCAN clusters

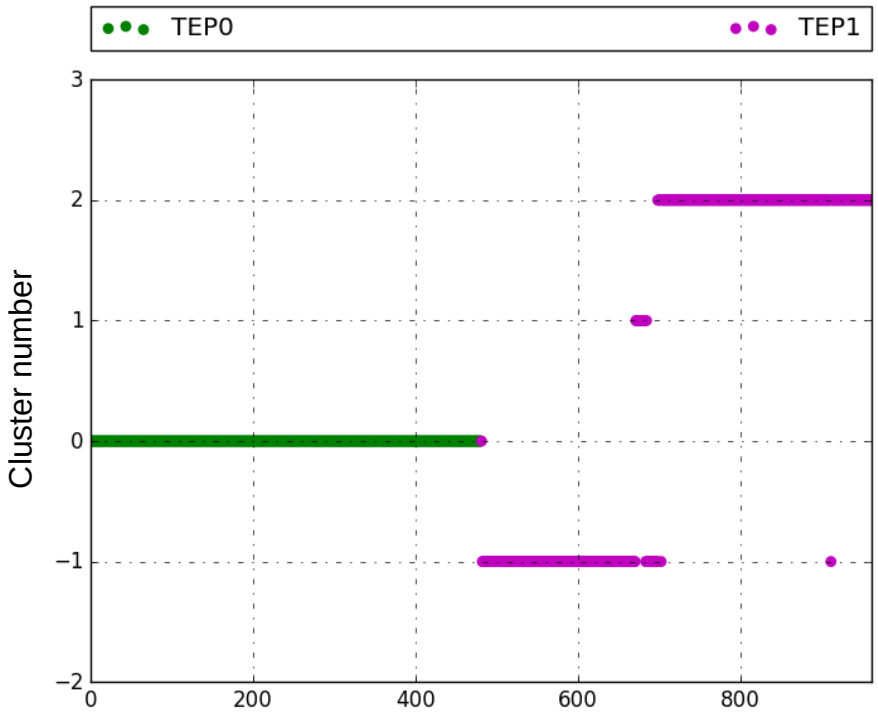

Figure 5.5 A time series plot of each data point's cluster.

Table 5.4: Number of components used by DR projections in clustering TEP data

	PCA	ICA	KPCA	Isomap	SE
Reduced	7	7	8	7	7
Full	9	9	11	9	9

Table 5.5 gives the cluster evaluation results of four data clustering techniques and dimensionality reduction techniques applied in the manner described in Section 3.5. Each clustering in Table 5.5 had the best ARI among the five clustering parameters tested according to the method described in Section 3.5. The complete set of clustering results can be found in Appendix A. The best homogeneity, completeness, and ARI observed on each data set is shaded, but the most accurate reconstruction of the original TEP classes will have the highest ARI. The number of clusters is also important as the most desirable number of clusters matches the number of true clusters in the database. In practice, a perfect result is rare, but a large number of clusters can obfuscate useful groupings in the data and makes an engineer's job of interpreting clustering results more difficult.

Judging by ARI, DBSCAN without any DR produced the most accurate duplication of the true data clusters closely followed by SE reduced k-means results. Many techniques were successful due to the data set's bias towards step change faults which often give rise to well-defined spherical clusters. As can be seen in Figure 5.6, the clusters found by DBSCAN without dimensionality reduction most closely match the true groups of TEP data. DBSCAN successfully found groups of all step faults except Fault 6, and even grouped data from valve sticking in Fault 14. Data from Fault 6 (A feed loss) and 8 (random feed composition variations) were all classified into the "noise".

Table 5.5: Clustering results on reduced TEP data set

DR	Clustering	Homogeneity	Completeness	No. clusters	ARI
NO DR	DBSCAN	0.86	0.86	10	0.81
NO DR	K-means	0.73	0.79	10	0.59
NO DR	Mean Shift	0.71	0.76	15	0.53
NO DR	BIRCH	0.97	0.63	112	0.72
PCA	DBSCAN	0.66	0.88	8	0.53
PCA	K-means	0.72	0.79	9	0.59
PCA	Mean Shift	0.80	0.59	148	0.61
PCA	BIRCH	0.86	0.64	83	0.65
ICA	DBSCAN	0.67	0.85	10	0.52
ICA	K-means	0.71	0.79	10	0.58
ICA	Mean Shift	0.87	0.59	184	0.66
ICA	BIRCH	0.92	0.62	116	0.70
KPCA	DBSCAN	0.65	0.79	7	0.48
KPCA	K-means	0.68	0.82	7	0.52
KPCA	Mean Shift	0.66	0.75	8	0.47
KPCA	BIRCH	0.58	0.78	6	0.37
Isomap	DBSCAN	0.81	0.88	11	0.74
Isomap	K-means	0.75	0.79	10	0.60
Isomap	Mean Shift	0.81	0.67	56	0.62
Isomap	BIRCH	0.88	0.71	35	0.70
SE	DBSCAN	0.78	0.78	15	0.67
SE	K-means	0.87	0.83	10	0.79
SE	Mean Shift	0.81	0.58	62	0.48
SE	BIRCH	0.84	0.83	16	0.71

Dimensionality reduction had mixed effects on clustering results. Projecting data with KPCA lead to significantly lower quality results than the No DR case. BIRCH produced results of comparable accuracy regardless of the DR technique used (except for KPCA) while mean shift benefited from DR by PCA, ICA, and Isomap, DBSCAN saw performance decrease with DR by PCA and ICA. Interestingly, k-means performed the best on SE reduced data, a case where it is the clustering technique of choice in the spectral clustering techniques of Shi and Malik (2000) and Ng et al. (2002).

In addition to evaluations of the overall clustering, we can use a time series plot of cluster membership where vertical position indicates cluster membership to evaluate how well the individual faults were learned. Figure 5.6 through 5.9 gives a sampling of cluster series plots. Clusters found by DBSCAN with no DR largely correspond to the original sets from the TEP simulation, though transitions between steady states as well as all of Fault 8 and Fault 14 were designated as "noise". In Figure 5.7, DBSCAN with PCA finds many of the same clusters but incorrectly combined data from faults 4, 6, and 14. In the simulation, Fault 4 and 14 both affect the cooling water of the reactor, so the PCA clustering results suggest that PCA removed the information in the cooling water temperature sensor's data. Figure 5.8 shows K-means incorrectly associating large amounts of data with normal operations, which can result when K-means seeks to impose spherical clusters on groups of data that are not spherical. Figure 5.9 shows a case where a high ARI was calculated, but the data from some classes are inconveniently divided into multiple clusters.

In several cases where mean shift and BIRCH produced a large number of clusters, a good homogeneity and completeness is still observed because many of these clusters have less than 10 members. Unlike DBSCAN, mean shift and BIRCH do not define clusters with one member as noise, which leads to the large cluster count of these techniques. Figure 5.10, a. shows the clustering results of mean shift data reduced by ICA, where the algorithm found many clusters containing one or two members. Enforcing the same requirement from DBSCAN that each cluster has a minimum of 10 points leads to the plot in Figure 5.10, b. with 20 clusters and a slightly improved ARI of 0.71. For the cases studied here, enforcing a minimum number of points had only minor effects on ARI in cases where mean shift or BRICH output large numbers of clusters, and therefore we use only the basic clustering algorithm for simplicity.

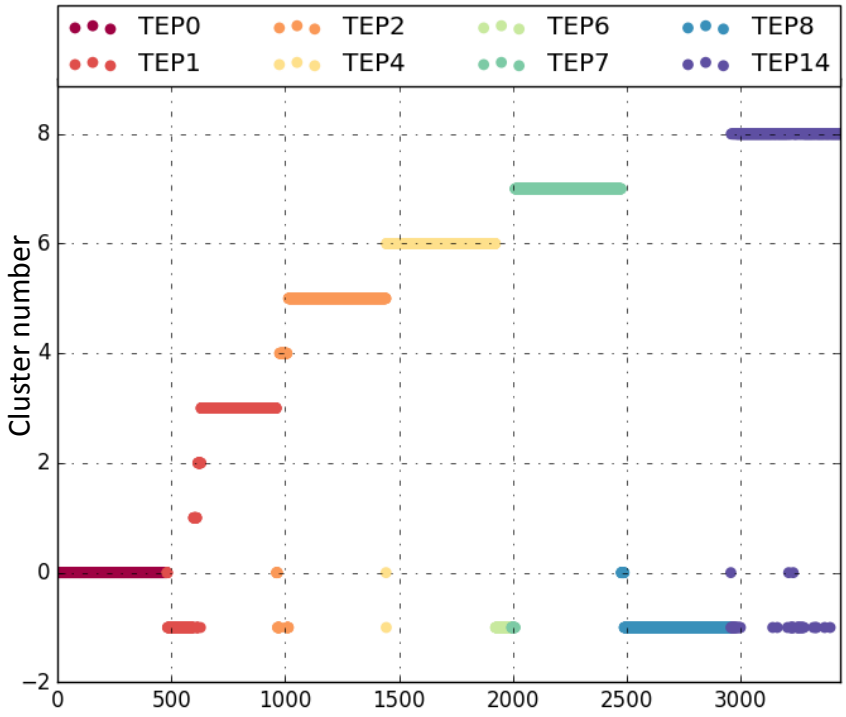

Figure 5.6 DBSCAN cluster labels largely correspond to original labels

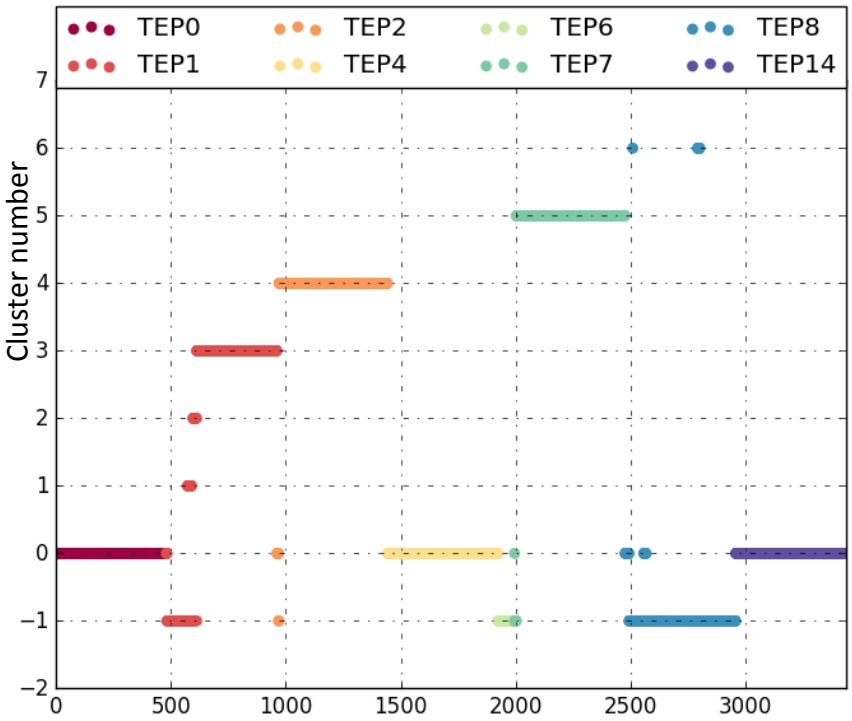

Figure 5.7 DBSCAN cluster labels on data reduced by PCA

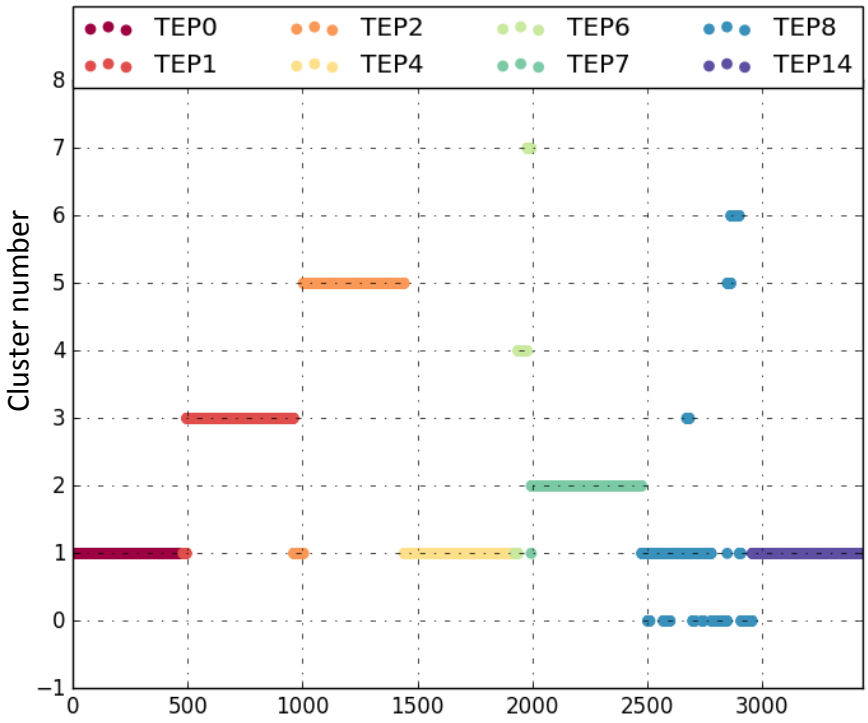

Figure 5.8 K-means cluster labels on data with No DR

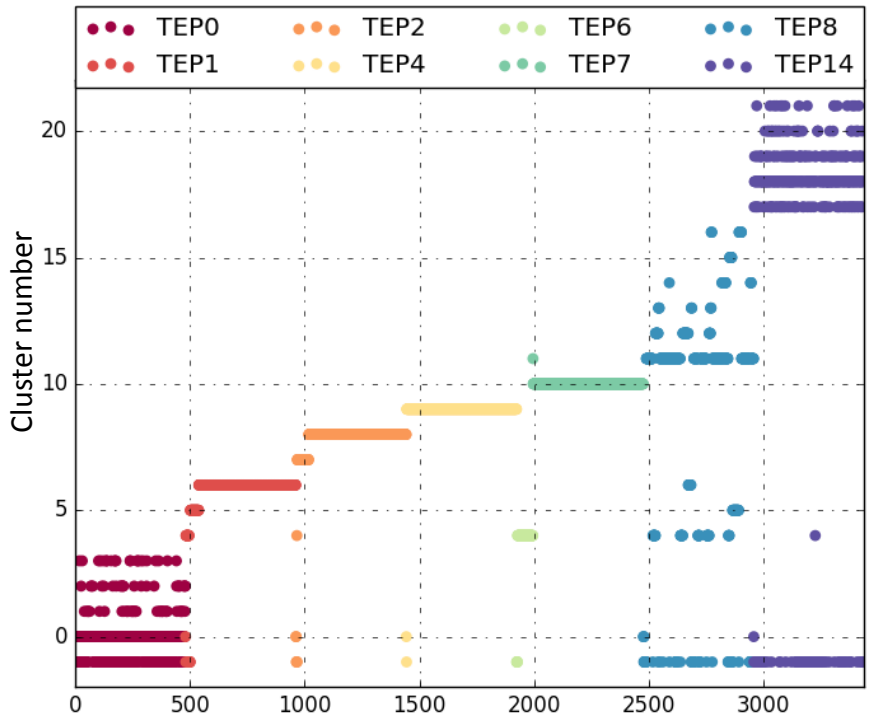

Figure 5.9 Clusters found using DBSCAN and spectral embedding

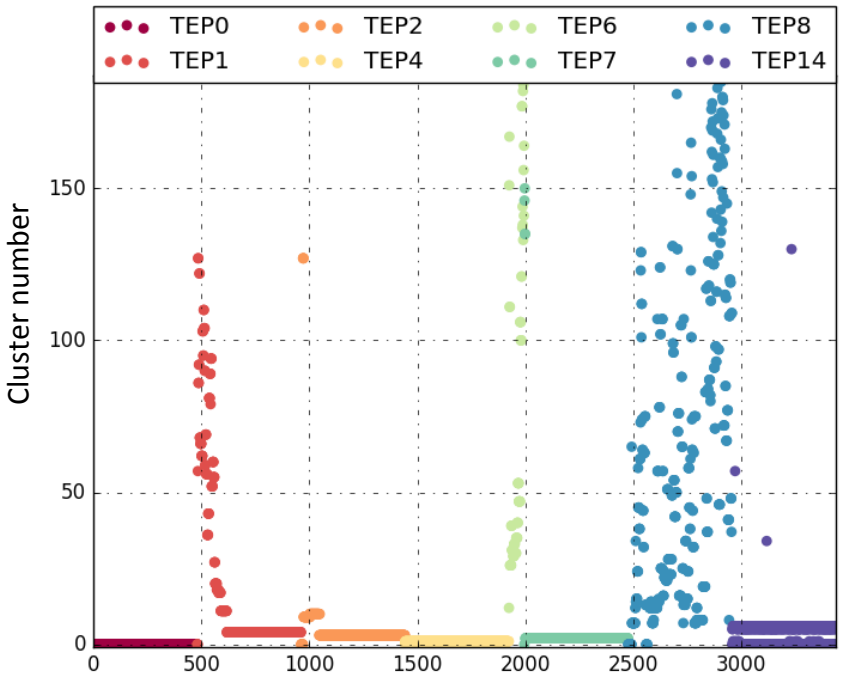

(a)

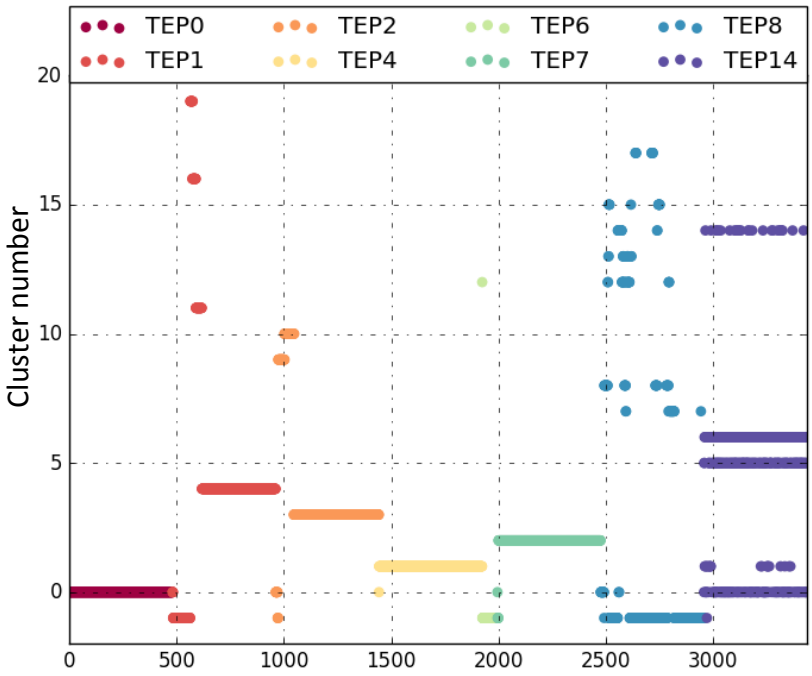

(b)

Figure 5.10: Raw mean shift results with ICA reduced data gave rise to a very large number of clusters seen in (a). Combining all clusters with fewer than 10 members into the noise cluster in (b), had only a minor effect on the ARI results.

Figures 5.11 through 5.14 provide a view of how dimensionality reduction affects the data being clustered using a PCA projection to the first 3 components. Recall however, that in the practical case where data labels are not known, the comparison between clustering results and true labels typically is not possible without more knowledge of the data set. Coloring the data by cluster, as in Figure 5.11, gives us further insight into the results in Table 5.5. Figure 5.12 shows a detail of the cluster from normal operations where we can see closeness of normal data and data from Faults 2, 4, 14. Figure 5.13 shows how K-means attempts to fit the data into hyperspherical clusters, which causes long, narrow transitions between steady states to be grouped into different clusters. Figure 5.14 shows how DBSCAN effectively identifies dense groups of related data but unfortunately removes most data from transitions as noise.

5.3.3 Full TEP data set

Finally, Table 5.6 shows DR/clustering results over the full TEP data set consisting of behavior from all 20 faults. As might be expected, the results as measured by ARI are poorer owing to the greatly increased complexity of the data. All ARI are low and closer to 0 (corresponding to random cluster labels) than in the reduced data set, and no particular dimensionality reduction technique consistently improved over the No DR case. In this case, DBSCAN consistently yielded the lowest metrics while BIRCH and mean shift performed slightly better, though still poorly.

5.4 Process Monitoring of the Tennessee Eastman Process

Once an engineer has labeled historical data from each fault, process monitoring can begin. The next sections study fault detection, identification, and diagnosis on data from the TEP simulation. Here, we assume that perfectly labeled TEP data is available to train process monitoring models. For an additional diagnosis challenge, we add an additional fault to the reduced data set with data from fault 1 and 14 in combination (Fault 14+1).

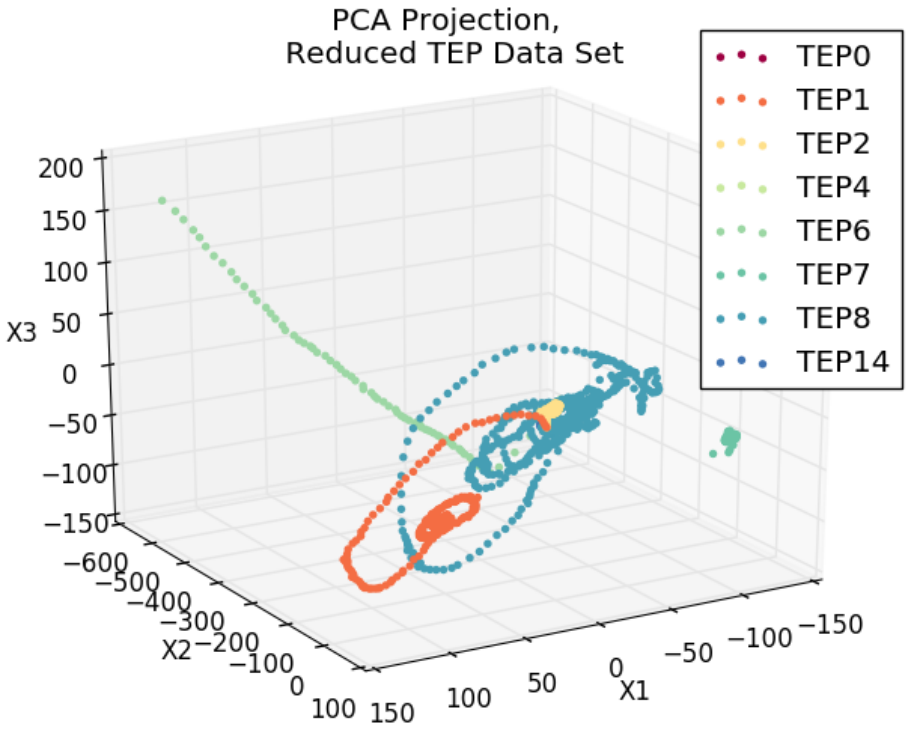

Figure 5.11 PCA projection of the reduced TEP data set colored by true fault group.

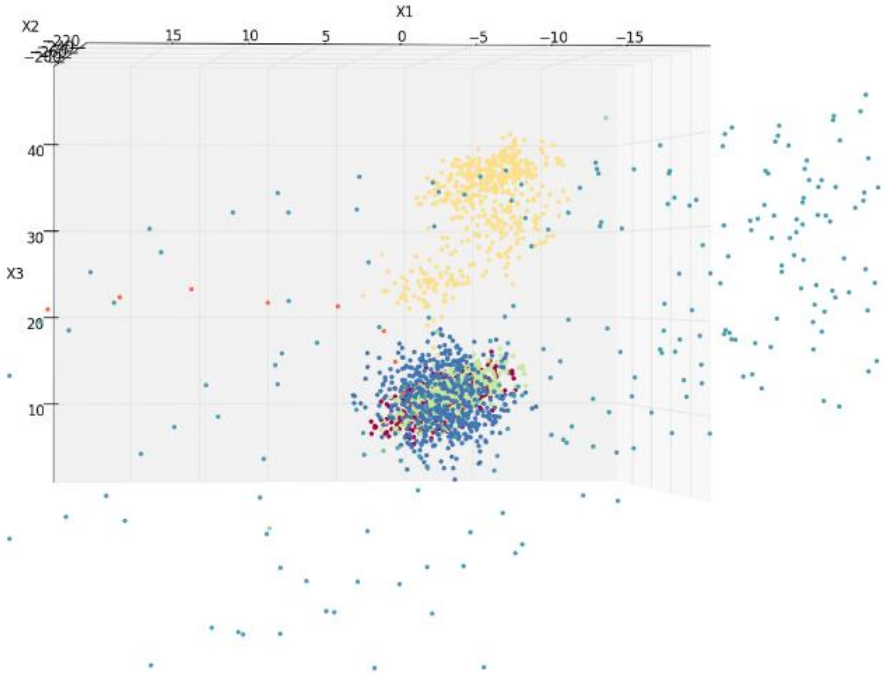

Figure 5.12 Detail of the data clustered near the TEP's normal operations

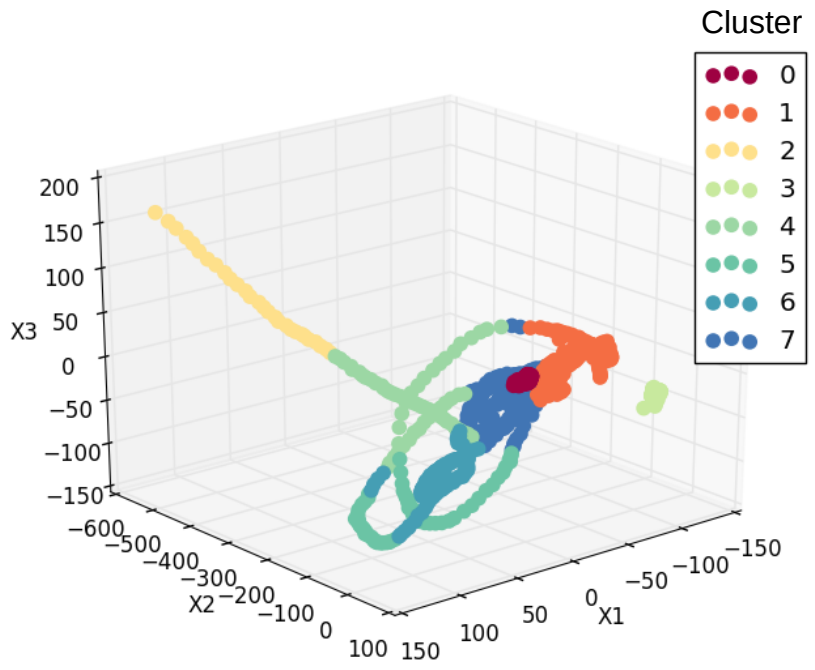

Figure 5.13 Clustering TEP data with K-means

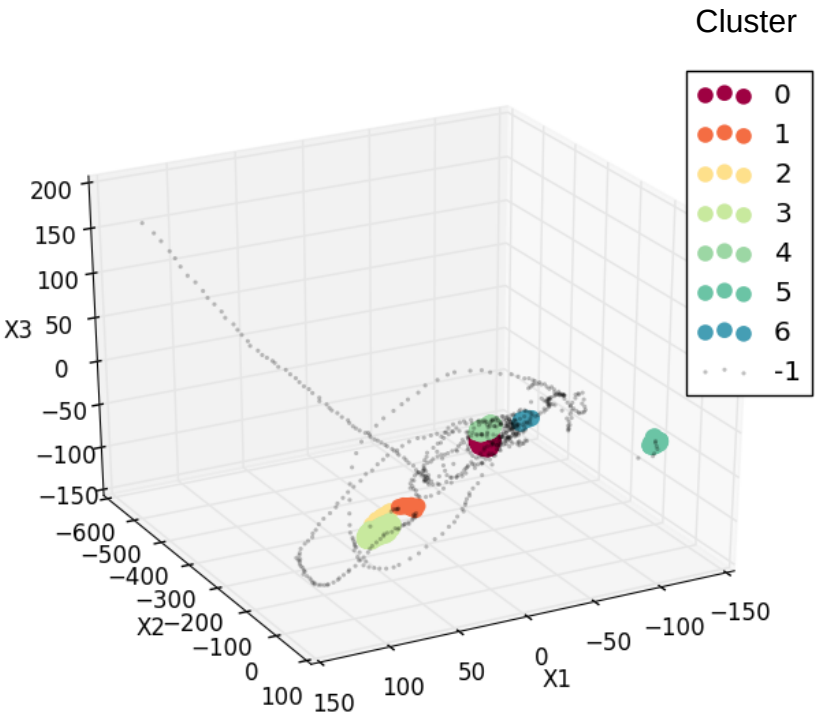

Figure 5.14: DBSCAN with NO DR identified most clusters, though issues with unrelated data and noise data remain challenges.

Table 5.6: Data clustering and DR applied to the full TEP data set

DR	Clustering	Homogeneity	Completeness	No. clusters	ARI
NO DR	DBSCAN	0.37	0.80	19	0.13
NO DR	K-means	0.46	0.71	21	0.12
NO DR	Mean Shift	0.46	0.63	227	0.16
NO DR	BIRCH	0.71	0.55	633	0.20
PCA	DBSCAN	0.30	0.79	13	0.09
PCA	K-means	0.46	0.71	23	0.13
PCA	Mean Shift	0.57	0.54	654	0.16
PCA	BIRCH	0.63	0.54	459	0.18
ICA	DBSCAN	0.28	0.79	11	0.09
ICA	K-means	0.46	0.68	22	0.13
ICA	Mean Shift	0.56	0.53	789	0.16
ICA	BIRCH	0.54	0.61	150	0.14
KPCA	DBSCAN	0.11	0.30	59	0.03
KPCA	K-means	0.36	0.47	22	0.12
KPCA	Mean Shift	0.34	0.69	9	0.13
KPCA	BIRCH	0.42	0.36	493	0.12
Isomap	DBSCAN	0.39	0.73	38	0.13
Isomap	K-means	0.48	0.71	23	0.15
Isomap	Mean Shift	0.51	0.59	302	0.14
Isomap	BIRCH	0.55	0.61	201	0.13
SE	DBSCAN	0.35	0.58	60	0.08
SE	K-means	0.54	0.69	23	0.20
SE	Mean Shift	0.48	0.51	279	0.11
SE	BIRCH	0.62	0.54	236	0.17

5.4.1 Fault detection results

Fault detection was tested by comparing PCA- and NLPCA-based fault detection methods with SOM and MSOM. Data were collected for the six faulty operating regimes and run through each fault detection algorithm. All variables without a time delay were used except the compressor recycle valve, stripper steam valve, and agitator speed as these numbers were held constant by Ricker's control system. For fault detection, 480 data points were collected from normal operations, corresponding to 48 hours of operation. This data was then used as a training set for a

SOM, PCA and NLPCA models of normal operations. An SOM map of normal operations was fit for the MSOM strategy and the QE bound for normal operation was found using the optimization described in section 3.2. For PCA, an alpha significance level of 0.01 was used to determine the T^2-Q boundaries for normality. Principal components (PCs) were included in the model so 99% of the variance of the original data set was included – or 26 PCs. The number of mapping nodes used by NLPCA was the same as the number of components retained by PCA. The threshold SPE value representing a faulty condition was calculated similar to the MSOM probably bound calculation.

The correct detection rates of the two methods over the data sets of interest are given in Tables 5.7 and 5.8. Table 5.9 illustrates the false alarm rates found by each method on the 20 fault data set. Overall, for this application, MSOM performs as well as MPCA in detecting the simulated data and both of them outperform 1-SOM. For NLPCA, the results vary between runs of the algorithm based on the random initialization of the neurons, and the results given here represent a typical result of the algorithm.

5.4.2 Fault identification results

Fault identification was performed on data sets from the TEP according to the PCA method and the MSOM method proposed in Section 3.2. Contribution plots of faulty data points from each fault were analyzed and compared with contribution plots calculated by a PCA method and our process knowledge to evaluate the proposed method's ability to isolate the causes of the faulty condition. Sometimes, the root causes of the problem are not in variables we have data for, so the goals of fault identification are to isolate a subsection of the plant where the root causes of the issue are likely located and to give engineers useful clues on how to identify them. In Figure 5.15, we used a data vector roughly 10 hours after the imposition of the faulty condition to create

Table 5.7: Fault detection rate of MPCA and MSOM

	Detection Rate (%)			
TEP fault	MPCA	NLPCA	1-SOM*	MSOM
1	99.9%	99.9%	97.8%	99.9%
8	99.4%	99.4%	82.7%	99.3%
11	99.3%	99.3%	79.1%	99.0%
13	99.5%	99.5%	88.3%	99.5%
14	99.9%	99.9%	94.8%	99.9%
14+1	99.9%	99.9%	90.3%	99.9%

***** The results for SOM given here are the same as those in Table 5.10 from the diagnosis results since diagnosis and detection are the same step when 1-SOM is used. They are included in this table in order to facilitate a comparison with the other techniques.

Table 5.8: Fault detection results for all 20 faults

	% Detected			
TEP Fault	MPCA	NLPCA	1-SOM*	MSOM
1	99.9%	99.9%	98.0%	99.9%
2	97.8%	97.7%	90.5%	97.8%
3	9.8%	3.1%	34.5%	9.9%
4	99.9%	99.9%	97.4%	99.9%
5	4.0%	2.1%	21.7%	6.5%
6	100.0%	100.0%	94.4%	100.0%
7	100.0%	100.0%	99.7%	100.0%
8	99.4%	99.4%	74.4%	99.4%
9	13.6%	5.6%	20.5%	16.0%
10	97.1%	91.3%	73.9%	93.0%
11	99.3%	99.0%	58.3%	99.5%
12	55.9%	40.9%	51.2%	59.9%
13	99.5%	99.5%	77.8%	99.5%
14	99.9%	99.9%	79.6%	99.9%
15	4.5%	1.8%	15.9%	7.2%
16	3.3%	1.8%	0.0%	5.7%
17	99.7%	99.6%	87.8%	99.7%
18	87.8%	79.7%	71.0%	87.4%
19	99.7%	99.5%	93.1%	99.6%
20	99.6%	99.5%	98.0%	99.5%

***** The results for SOM given here are the same as those in Table 5.11, since diagnosis and detection are the same step when 1-SOM is used. They are included in this table in order to facilitate a comparison with the other techniques.

Table 5.9: False alarm rates of the four techniques from the analysis in Table 5.8

MPCA	NLPCA*	1-SOM	MSOM
3.3%	1.8-25%	81.9%	5.0%

***** Results vary between runs of the algorithm based on the random initialization of the neurons.

contribution plots as illustrative examples of the proposed method. A table of the variable numbers and names can be found in Tables 5.1 and 5.2.

In Figure 5.15, contribution plots generated from Fault 1 data are compared. In response to the changes in the composition of the feed, the composition controller on the reactor feed creates changes in streams 1 and 4 in response to the disturbance. Both PCA and MSOM point to a disturbance in the composition of the feeds to the process since the plots indicate that variables associated with the feeds (stream 1 through 4) have significant contributions. In both cases, the variable with the largest contribution is the controller output to stream 1, and based on the knowledge that stream 1 and 4 are in the same control loop, this points to a feed composition issue.

Applying a similar analysis to Fault 13, MSOM successfully reproduces the results of PCA in isolating the fault to changes in the pressure of the reactor and in the separation units following the reactor. Dramatic changes in all of these variables at the same time could point to a change in the reactor outlet's composition. In fact, Fault 13 creates a "slow drift" in the kinetics of the reactor. The result is wild variations spread over many process variables, but both methods successfully isolate the signal to a subset of variables related to the reactor and its composition.

Faults 11 and 14 are illustrative of the value of using MSOM. Both faults relate to the cooling water of the reactor, which may not be very important to the PCA model, as under normal operations reactor cooling water flow remains relatively constant. The result for Fault 11 and 14 is that when a fault related to the cooling water occurs, cooling water variables have low weights in favor of more variable flow variables. For fault identification, MSOM uses all online measured

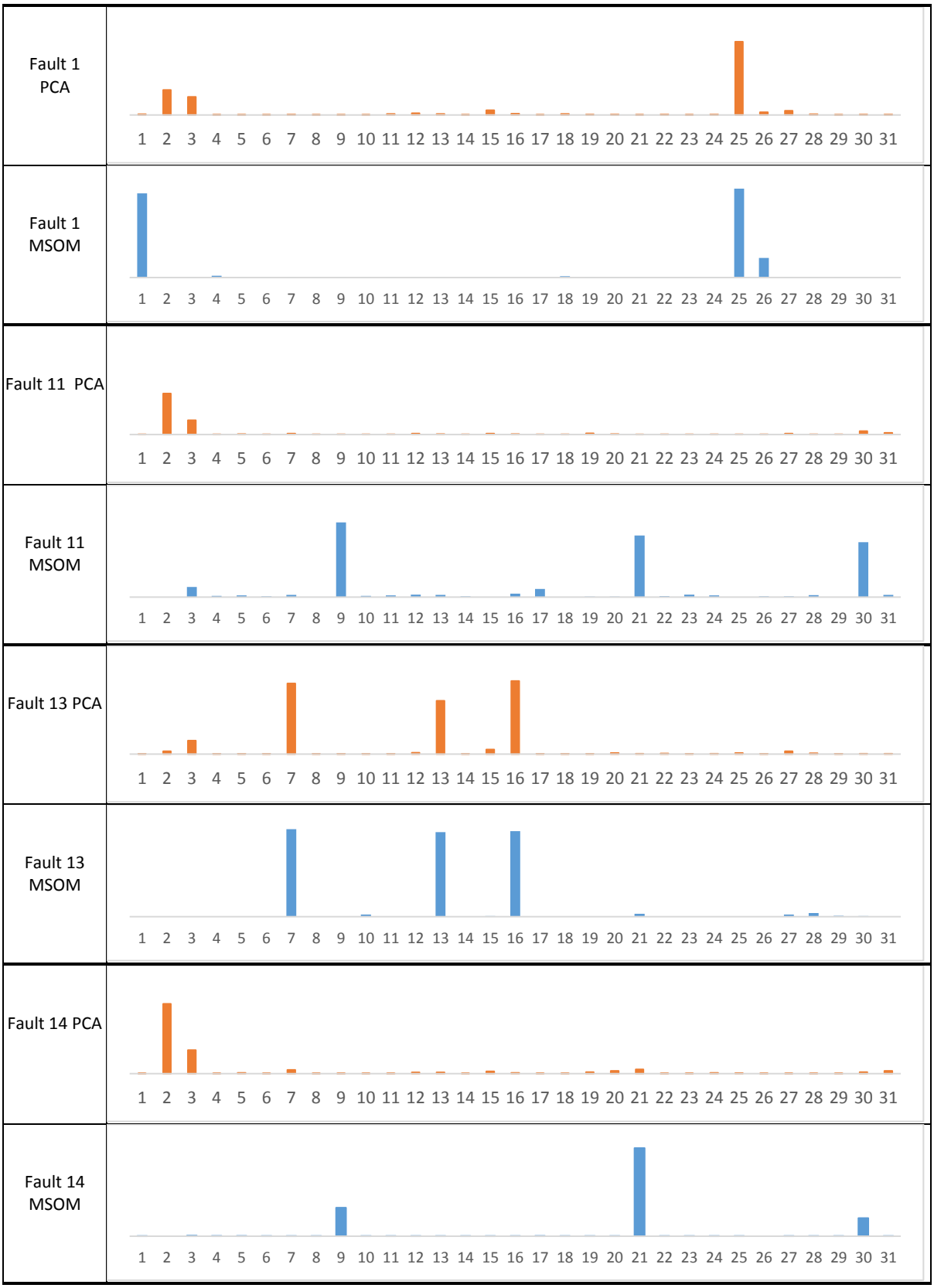

Figure 5.15: Contribution plots of faulty data made by PCA and MSOM.

variables and weighs them equally. The result is that while PCA appears to point to more changes in feed streams, MSOM's largest contribution variables clearly point to the specific problem with the reactor and its cooling water.

The plots in Figure 5.15 illustrate MSOM's superior ability in identifying variables responsible for a deviation from normal operation. The data compression abilities of SOM help identification by reducing the noise in individual data without the loss of information that comes with performing a dimensionality reduction using PCA. The next section will illustrate the effectiveness of MSOM in diagnosing the faulty condition of the process.

5.4.3 Fault diagnosis results

In this section, the MSOM method proposed is used to classify data sets from the faults of interest and compared to some standard techniques: MPCA, MNLPCA (NLPCA using fault-specific neural networks trained to each fault as described in Section 4.3.4), and the standard form of SOM which uses a single map for classification. In each case, a series of data from an operating regime of the Tennessee Eastman process is given to each set of models, and every data point is classified into the different fault categories using each technique's discriminant function. PCA uses Hotelling's T^2 statistic, 1-SOM uses a given data point's BMU on the map of the process, and MSOM uses the QE calculated relative to each fault's SOM map.

From the results in Table 5.10, both 1-SOM and MSOM techniques represent a dramatic improvement over conventional MPCA and MNLPCA fault diagnosis. 1-SOM gave fewer false fault classifications, but MSOM had a better correct classification rate, particularly for the random variation faults. As a benchmark, the performance of each method over all TEP faults is given in Table 5.11. MSOM outperforms the other techniques with the exception of a few special cases. In

addition, improved diagnosis ability relative to MNLPCA, MSOM maps train in a fraction of the time required to fit the neural networks composing the NLPCA diagnosis strategy.

Figure 5.16 shows how each method classified different portions of the process data. MNLPCA is not included because the results will vary based on the random initialization of the neurons. Visualizing the results in this way allows us to analyze possible reasons for low classification rates in the results. For example, MPCA's successful diagnosis of Fault 13 suggests that this fault has been characterized well by its PCA model, while Figure 5.16 shows that this high detection rate for Fault 13 came at the expense of a large number of points from Faults 8, 11, and 14 being incorrectly classified into Fault 13 due to its large T^2 bounds.

Table 5.10: Correct diagnosis rates for selected TEP faults

	Correct Diagnosis Rate (%)			
TEP fault	MPCA	MNLPCA*	1-SOM	MSOM
1	5.7%	92.1%	97.8%	97.81%
8	79.5%	61.8%	82.7%	90.84%
11	76.3%	96.6%	79.1%	96.05%
13	97.6%	97.9%	88.3%	93.44%
14	38.1%	89.4%	94.8%	99.79%
14+1	99.3%	91.5%	90.3%	93.44%

* These results were taken from a particular initialization of MNLPCA. Results vary between runs of the algorithm based on the random initialization of the neurons.

Another challenge comes from regions where multiple fault operating regimes overlap. For example, Fault 14's classification has been spread by MPCA between Fault 8, 11, 13, and 14 due to overlap of the four models. A similar case is the high detection rate for the combination Fault 14+1 where a high correct diagnosis rate for Fault 14+1 was achieved at the cost of many points from Fault 1 being incorrectly diagnosed due to overlapping regions for Faults 1 and 14+1. In the diagnosis of the combination fault, a challenge is that classifications algorithms can mistake the constituent faults (here, 14 and 1) for the combination of faults. For example, if a T^2-Q boundary

is created for Fault 1 and Fault 14+1, the latter will have a larger diagnosis region encompassing nearly all the data from Fault 1 due to the random variations in Fault 14+1. Consequently, as can be seen from the plot of the PCA classification results in Figure 5.16, many points from Fault 1 were incorrectly classified into the combination 14+1 category.

Table 5.11: Fault Diagnosis for all 20 TEP faults

	Correct Diagnosis Rate (%)			
TEP fault	MPCA	MNLPCA*	1-SOM	MSOM
1	96.9%	96.6%	98.0%	99.3%
2	1.6%	23.1%	90.5%	96.6%
3	0.0%	0.0%	34.5%	3.5%
4	1.7%	50.9%	97.4%	95.3%
5	0.0%	0.0%	21.7%	2.3%
6	94.4%	98.6%	94.4%	98.6%
7	99.0%	99.9%	99.7%	99.9%
8	79.5%	61.8%	74.4%	87.5%
9	0.0%	0.2%	20.5%	6.7%
10	0.1%	61.7%	73.9%	87.2%
11	66.7%	89.4%	58.3%	92.4%
12	0.0%	13.2%	51.2%	50.0%
13	97.6%	97.4%	77.8%	89.5%
14	30.0%	73.5%	79.6%	99.3%
15	0.0%	0.0%	15.9%	1.6%
16	0.0%	0.0%	0.0%	0.0%
17	59.8%	88.0%	87.8%	95.5%
18	1.7%	60.2%	71.0%	80.3%
19	13.8%	80.6%	93.1%	97.9%
20	49.8%	57.2%	98.0%	99.4%

* These results were taken from a particular initialization of MNLPCA. Results vary between runs of the algorithm based on the random initialization of the neurons.

Some of the improvement in diagnosis by MSOM can be attributed to the specialization of the maps. With a single SOM map, each group of training data affects all nearby map vectors, giving some regions of the map a mixture of characteristics from several classes. Multiple maps

are an advantage in that each map vector is trained only with data from its particular fault and contain fewer characteristics from other faults. In 1-SOM, these regions with mixed characteristics are more likely to be classified by one node, which would give many of them a false classification. MSOM would have different map nodes trained by the different data sets, so map nodes in a mixed characteristic region are moved closer to their faulty trajectory, giving a more probable correct classification of the transition regions.

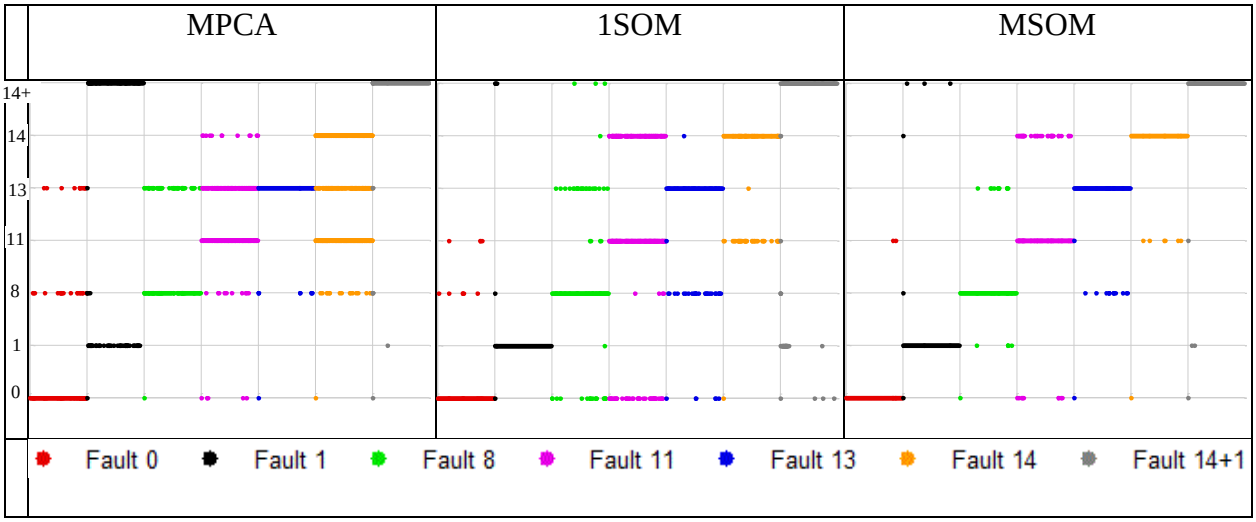

Figure 5.16: Data classification using MPCA, 1-SOM, and MSOM on the testing data set with time colored according to class. Solid lines of color indicate a consistent classification while discontinuous lines indicate an inconsistent classification.

To illustrate this idea, Figure 5.17 gives PCA projections of the SOMs used in the classification of Fault 14+1 for both 1-SOM and MSOM. The map nodes are colored based on the class they are associated with. Data from Fault 14+1 are colored based on whether each algorithm classified given points correctly (green dots) or incorrectly (red stars). In Figure 5.17, a., the trajectory of Fault 14+1 can be seen passing through regions of the 1-SOM map belonging to other classes on its way to its steady state area. In Figure 5.17, b., the additional specialization of the maps used for MSOM meant more maps nodes were assigned to Fault 14+1 and they were close enough to the faulty data to make a difference in the classification process. This allowed MSOM

to correctly classify the early trajectory of Fault 14+1 better than 1-SOM. For faults with dynamics like Fault 8, 11, and 13, the process state is constantly experiencing similar dynamics, and the diagnosis results show the advantage MSOM provides in the classification of data from these cases. Further, when the amount of faulty data is large compared to the amount of normal data used in training, the region assigned to normal becomes small enough that false alarms become a problem, as shown in the false alarm rate for SOM on the set of 20 faults given in Table 5.9.

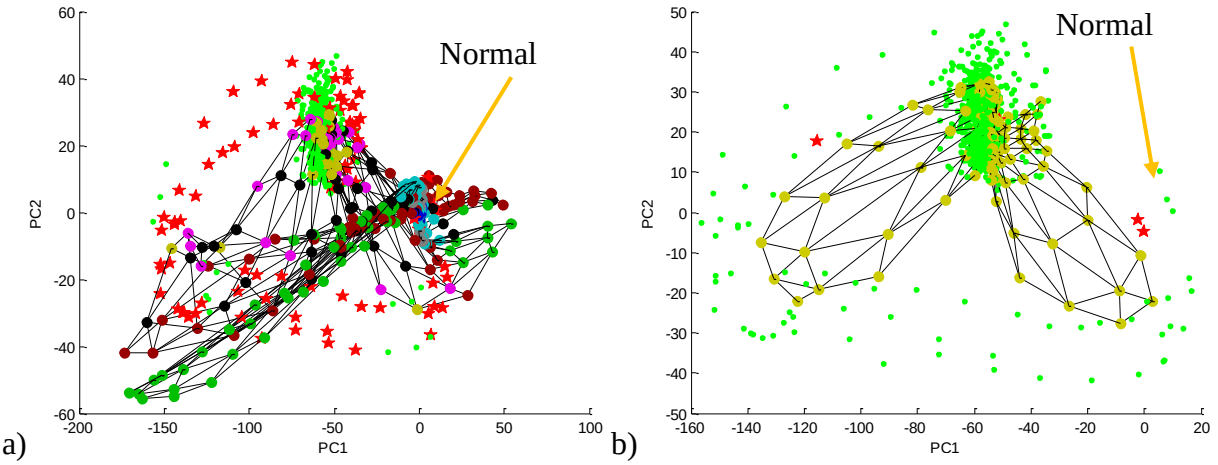

Figure 5.17: PCA projections of data from Fault 14+1, the map used in 1-SOM classification (a), and the map fit to Fault 14+1 in MSOM (b).

5.5 Conclusions

This research studied the complete process monitoring workflow proposed in Chapter 5 on the Tennessee Eastman process simulation and applied all the steps from DR and clustering to fault detection. Data clustering and DR functioned in tandem to isolate data from the different faults in the process, information which is vital for training a supervised classification technique for fault detection. We studied the performance of four different clustering techniques and six

different dimensionality reduction strategies. Performance varied greatly between different combinations of clustering techniques and DR, and no one technique clearly outperformed the others. On a reduced set containing many step faults, nearly all techniques effectively duplicated the original labels; however, no technique performed satisfactorily on the data set containing all TEP faults.

We introduce an SOM-based strategy for nonlinear process monitoring. In the proposed approach, SOMs were extended to cover all aspects of process monitoring to develop a nonlinear topological preservation approach. The aim was to mimic PCA by defining similar measures for process monitoring and fault detection and diagnosis. In particular, fault diagnosis was performed using multiple SOMs to characterize different fault classes, which enables the calculation of contribution plots with respect to normal and improves the quality of the diagnosis. In this regard, a number of contributions were proposed for detection, identification, and diagnosis of process faults.

We compared the proposed MSOM process monitoring architecture to PCA, NLPCA, and a more conventional SOM monitoring with data generated from the Tennessee Eastman process, with a focus on faulty conditions containing non-linear variations with time that have not been previously analyzed with SOM. The results indicate that MSOM outperforms MPCA and NLPCA and also improves upon conventional SOM for fault diagnosis and identification steps. The fault identification technique presented was extremely accurate at identifying the highest contributors to faults in places where PCA was inaccurate.

5.6 References

Downs, J. J., & Vogel, E. F. (1993). A plant-wide industrial process control problem. *Computers and Chemical Engineering, 17*(3), 245-255.

Ng, A., Jordan, M., & Weiss, Y. (2002). On spectral clustering: analysis and an algorithm. In T. Dietterich, S. Becker, & Z. Ghahramani (Eds.), *Advances in Neural Information Processing Systems*,(849 – 856). Cambridge: MIT Press.

Ricker, N. L. (1996). Decentralized control of the Tennessee Eastman challenge process. *Journal of Process Control*, *6*(4), 205-221.

Shi, J., & Malik, J. (2000). Normalized cuts and image segmentation. *IEEE Transactions on Pattern Analysis and Machine Intelligence, 22*(8), 888 – 905.

Yin, S., Ding, S. X., Haghani, A., Hao, H., & Zhang, P. (2012). A comparison study of basic data-driven fault diagnosis and process monitoring methods on the benchmark Tennessee Eastman process. *Journal of Process Control*, *22*, 1567-1581.

Chapter 6 - Case Study 2: Industrial Separation Tower

6.1 Introduction

The global trend in chemical process control towards increased automation, integration, and computerization has led to the generation, use, and management of massive amounts of data. Sifting through overwhelming amounts of information, plant engineers seek knowledge of what events are occurring in a plant. Data-based algorithms for process monitoring and fault diagnosis can give access to this event knowledge without the challenge of creating the detailed process models required by alternative approaches.

Challenges to data-based process monitoring are many. First, the average control system measures hundreds of variables every second and often important trends for the correct diagnosis are hidden from plant operators beneath sensor noise. Second, the most effective process monitoring algorithms require labeled data to fit fault classification models and often this information is unavailable. Third, data-driven fault detection and diagnosis schemes are trained to classify a subdivision of previously analyzed faults, but such a system can behave unpredictably when a combination of faults occurs or the system encounters an unexpected novel fault. An effective monitoring scheme must detect novel events and present information to plant operators to help diagnose a new and unknown fault's root causes.

In this chapter, we apply supervised and unsupervised classification techniques to the analysis and monitoring of data from an industrial-scale separation tower. This research validates the proposed approach to process monitoring on a manufacturing-scale unit, which presents different challenges from the monitoring and mining data from the TEP simulation. The data contains a novel event from a large process fault in a separation tower with economic costs in the hundreds of thousands.

We study the monitoring of this unit from two perspectives. First, we consider the case where we attempt use data clustering to isolate this process fault from within the historical database months after it has occurred. We test different data clustering and dimensionality reduction techniques on the task of extracting the fault data from six months of tower operations using the dimensionality reduction and data clustering strategy used in Chapter 5 to separate data from different TEP faults. The different methods are compared using supervised clustering metrics and data labels created from expert knowledge of the process.

Second, we study how we could create a process monitoring regime which could have detected and prevented the fault in the first place by fitting a model using data from before the fault and validating process monitoring performance on six months of data containing the fault. To study this separation tower and fault event from a process monitoring perspective, we use data from previous years to train the map to model the expected operating states (startup, normal steady state, and sensor fault) and test this strategy on data from a subsequent year containing a novel process event occurring simultaneously with a common fault. SOM was compared to PCA in the task of characterizing the operations of the separation tower, diagnosing its common operating states, and detecting novel events.

An initial problem with training data-based models to represent the difference states of the process arose from asymmetry in the size of data sets. To prevent normal operations from dominating the map representation of the data and to create a more balanced representation on the SOM, the data were balanced using SMOTE (Chawla 2002) for minority oversampling. The SOM strategy was used in conjunction with K-means clustering to characterize the operating regimes considered and assign model prototypes to each group in the training data. We demonstrate that

the proposed overall SOM strategy successfully detects the unknown event better than PCA and provides information towards understanding the novel fault's "hidden" root causes.

Section 6.2 provides a description of the industrial separation tower studied and further information about the problem examined. Section 6.3 details the results of analyzing the data from this tower using dimensionality reduction and data clustering. Section 6.4 details the process of training the SOM model used for monitoring and novelty detection. Section 6.5 presents the results of the process monitoring study on this tower including the isolation of data from a common fault and fault detection and identification. Finally, Section 6.6 provides conclusions and summarizes the results.

6.2 Separation Tower Process Description

An industrial separation tower was used to study fault detection and diagnosis as well as data clustering to extract fault event information from historical data. Figure 6.1 presents a flow sheet of the sensors and equipment considered with the measurements indicated in Table 6.1. The feed to the system is produced by a reactor upstream and varies depending on the petroleum grade fed into the system. The reactor and separation system is fed a number of different grades, including two "standby" grades thus leading to a number of start-up conditions during the grade changes. Different grades can result in large differences between many process variables as visualized in Figure 6.2. The differences between operations based on grade can form a significant separating factor in the data, therefore, in this case study it is important to consider each grade independently.

Before entering the tower outlined in Figure 6.1, the feed is passed through Tank 1 to remove water. Feed then enters the tower at a high temperature and pressure, and a mixture of

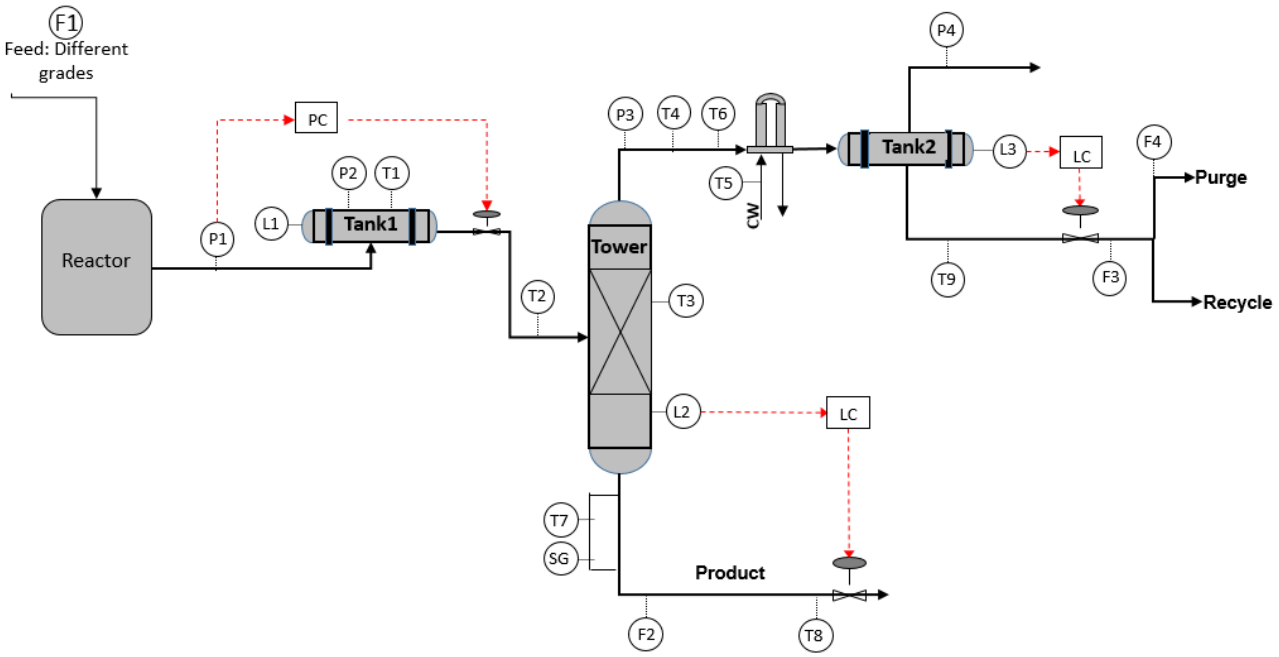

Figure 6.1: Simplified process flow sheet.

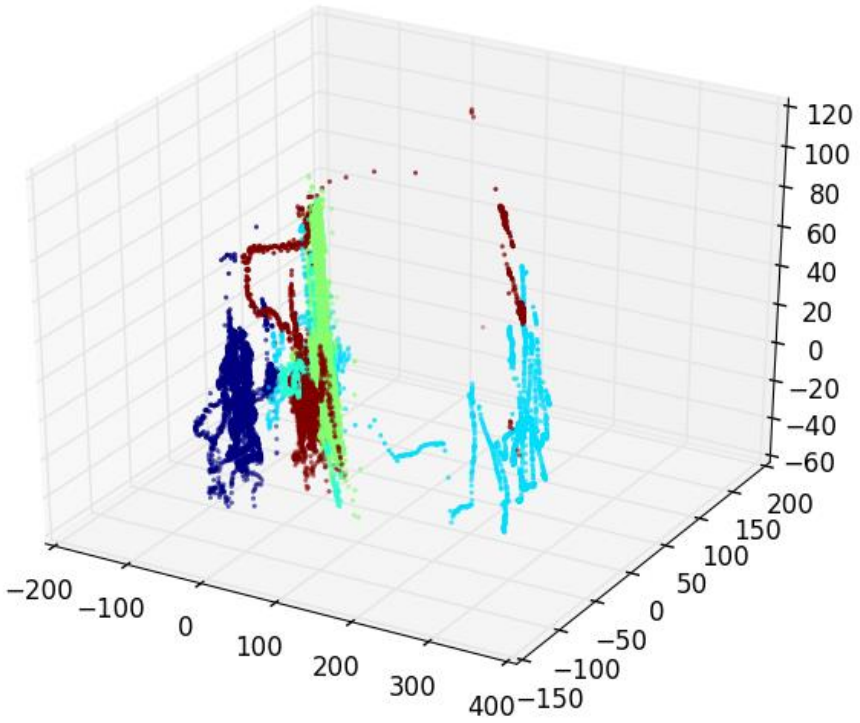

Figure 6.2: This PCA projection of separation tower data demonstrates the variability of tower data with feed grade. The normal operating region from one grade generally doesn't overlap with other grades. Date are colored according to feed grade.

solvent and product leaves out the bottoms with extra solvent and any water leaving out of the top of the column. Tank 2 removes any remaining water before recycling the solvent. To give a sense of scale, the tower is approximately two stories tall. The specific gravity sensor at the bottom of the column is used to evaluate the quality of the separation and to manually control the feed to the tower by manipulating the flow of steam to Tank 2. The product quality specification is loosely based on the composition of the polymer product in the bottoms of the tower evaluated by the specific gravity analyzer (SG). The specific gravity is controlled by manipulating the amount of steam fed to Tank 1.

In the fault detection and diagnosis section, a common fault (referred to as the "Tfault") lies in the SG and T7 sensors in the flash tower. These sensors work through the use of a small side stream that occasionally gets clogged with polymer. Detection of this sensor fault is fairly straightforward; however, it can "mask" other problems that may occur during operation. That is, when the SG and T7 sensors report odd measurements, operators might believe that a typical clog in the small side stream occurred when a different fault actually occurred.

Recently, a larger fault (the Novel Event) that created changes in many disparate process variables occurred at the same time the sensor fault occurred, and the timely detection of this fault could prevented losses in the hundreds of thousands dollars from off-spec product. This Novel Event occurred at the same time as a more common sensor fault, which masked the existence of the Novel Event. In this dissertation, we will consider two different aspects of this problem: the isolation of the faulty data among months of data from normal operations data and creating an algorithm to detect the Novel Event while diagnosing the state of the process.

To study how to diagnose this situation, we first constructed a data set to train the algorithm. We drew from operations data from one particular grade from 2012 and 2013 that had

been stored in the process historian database (PHD). Measurements were taken every minute, resulting in about 165,000 data points from 20 sensors as well as 9 derived variables to improve the signature of the commonly expected sensor fault as well as to directly incorporate the process relationships of other variables into the model. Validation data came from early 2014 when a major fault occurred. Without knowing the time of the major fault, researchers were tasked with creating a fault detection model from the 2012 and 2013 data only and to use the trained model to detect the 2014 event. This is a similar situation to what a process engineer might experience when designing a fault or novelty detection scheme: a system needed to be designed using historical data that would be able to classify known process states as well as detect and identify novel process events.

The data mining study considered a smaller data set. Additionally, the derived variables used in the process monitoring study defined above were not considered in data clustering to minimize the *a priori* knowledge used in mining the data. We studied about seven months of measurements from the tower taken at 10 minute intervals from one particular grade of operation. The total data set consisted of about 4,500 data points. Using a smaller data set, instead of sampling from every second or minute, did not disadvantage the analysis. A higher sampling frequency adds to noise in the measurements and considerably increases the computational load on analysis with few benefits. The truth labels used to evaluate the labels generated by clustering algorithms were added through expert knowledge.

6.3 Separation Tower Dimensionality Reduction (DR) and Clustering

The goal of data mining on the tower is to identify the faulty series of data from the fault event among the larger amount of data from normal operations. Working within the workflow

Table 6.1: Process measurements and derived measurements

Variable Name	Description	Derived Var. Name	Derived Var. Description
F1	Feed to upstream reactor	P1_P2	Tank 1 Feed pressure change
T1	Tank 1 Temperature	T1_T2	Tank 1 to Feed temperature change
P1	Tank 1 feed pressure	T3_T4	Mid-tower to top tower temperature change
P2	Tank 1 pressure	T3_T7	Tower to sensor temperature change
L1	Tank 1 level	T3_T6	Tower to overhead temperature change
T2	Tower feed temperature	P3_P4	Tower overhead to Tank 2 temperature change
T3	Middle Tower temperature	T6_T5	Exchanger temperature gradient
L2	Tower level	T9_T6	Overhead to product temperature change
T4	Tower overhead temperature	T8_T6	Overhead and product temperature change
T5	Cooling water temperature		
T6	Tower overhead temperature		
P3	Overhead Pressure 3		
F2	Bottoms flow		
T7	Bottoms temperature		
T8	Bottoms Product temperature		
SG	Specific gravity sensor		
F3	Total Overhead product flow		
F4	Non-recycle overhead product flow		
T9	Overhead Product temperature		
P4	Vapor Purge		
L3	Tank 2 Level		

described in Figure 3.1, the data will be projected using dimensionality reduction techniques, clustered using a sampling of data clustering algorithms, and evaluated using clustering metrics. Here, because expert analysis already determined which data are faulty and which are normal, we can use supervised cluster evaluation methods.

Figures 6.3, 6.4, .6.5, and 6.6 show 4 different dimensional projections of data from the tower made by four different dimensionality reduction techniques for visualization of the data.

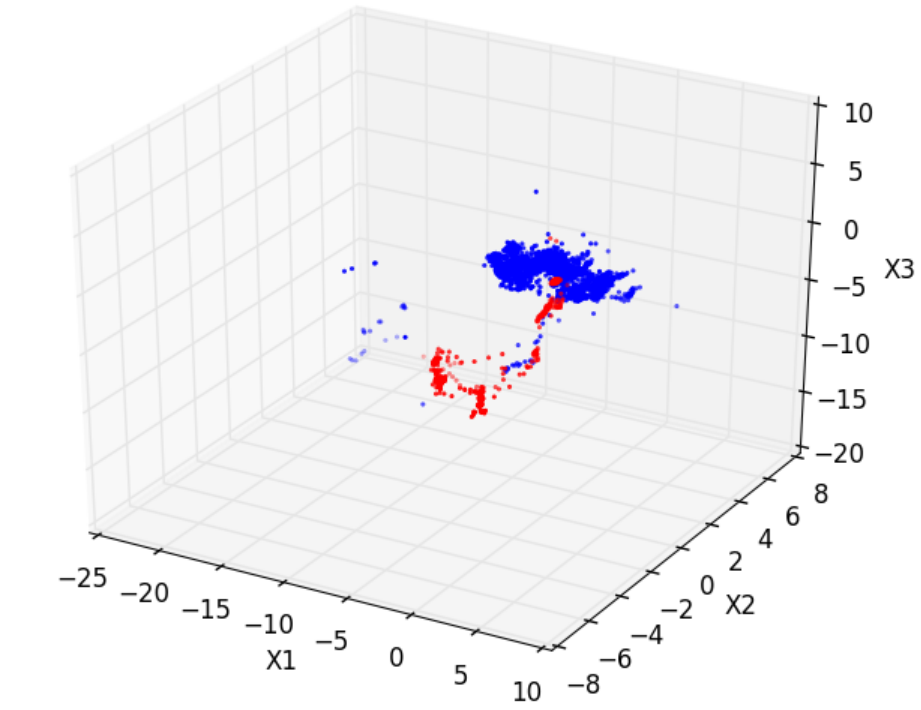

Figure 6.3 Projections of tower data using PCA

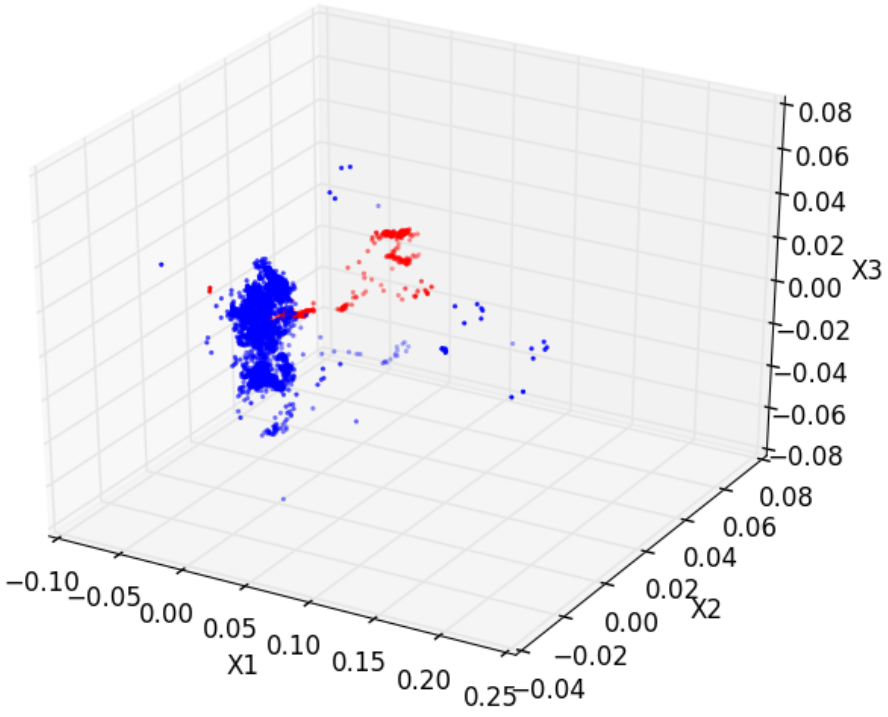

Figure 6.4 Projections of tower data using ICA

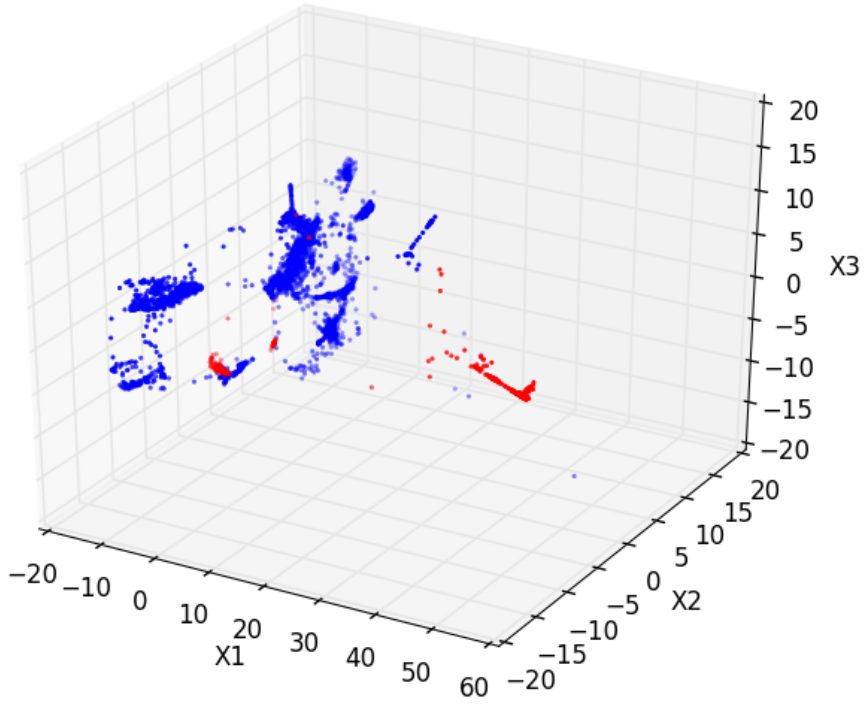

Figure 6.5 Projections of tower data using Isomap break up the cluster of normal data

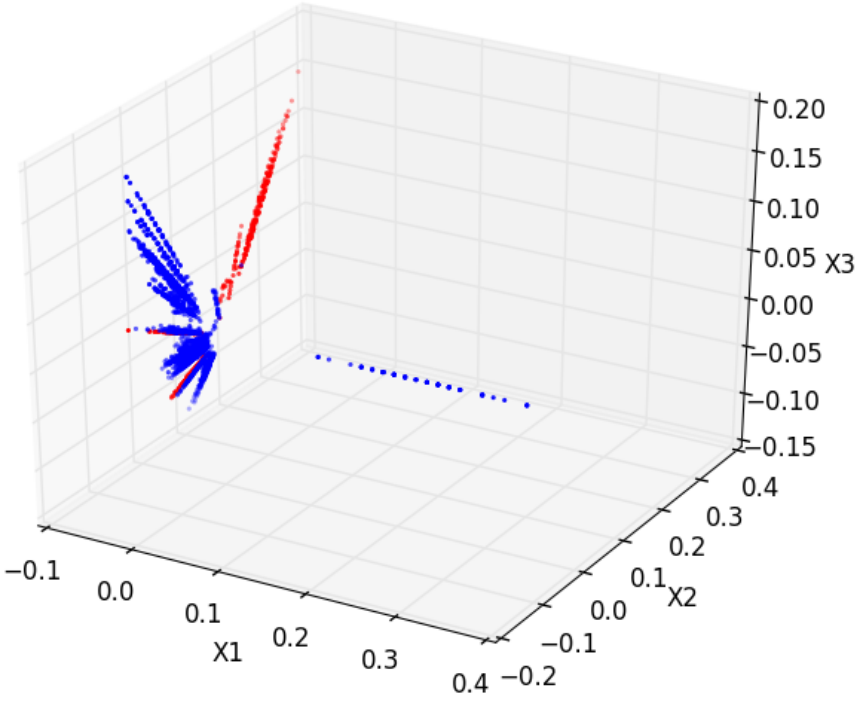

Figure 6.6 Projections of tower data using SE separate the data well, but interpretation is less intuitive

PCA in Figure 6.3 and ICA in Figure 6.4 yield qualitatively similar projection results preserve the density of normal operations. Both have large, dense normal regions in blue and a smaller cluster for the fault event in red. In contrast, Isomap in Figure 6.5 and SE in Figure 6.6 break apart the dense normal cluster into smaller clusters (which from Figure 6.11, we can see are related to the time). The data in the faulty group could be straightforwardly linked to a fault event using latent variable methods and time series plots of the original sensor.

For data clustering, we consider the case where the faulty period of data was not known beforehand to analyze how effectively data clustering techniques isolate the faulty data series and check the results against the known groups in the data. Table 6.2 shows the quality of the clusterings obtained by combinations of DR and clustering techniques applied to the data set. Each clustering in Table 6.2 had the best ARI among the five clustering parameters tested according to the method described in Section 3.5. The complete set of clustering results can be found in Appendix A.

As might be expected for a "natural" data set not generated by a simulation, results in this study are more varied in contrast to the Tennessee Eastman process, where most techniques produced clustering corresponding fairly closely to the base classes. BIRCH and SE produced the highest ARI of the cases considered, although both performed poorly with the other DR and clustering techniques. Mean shift and K-means also produced good quality results in several cases.

Here, some techniques produced random clusters (i.e., ARIs close to zero), as was the case for all tests on KPCA-reduced data. Also different from the simulation study, many of the DR techniques improved clustering results over the No DR case. ICA and Isomap dramatically improved the results of DBSCAN and k-means, even compared to PCA which had poor results for

Table 6.2: Supervised clustering metrics on tower data set

DR	Clustering	Homogeneity	Completeness	No. clusters	ARI
NO DR	DBSCAN	0.67	0.32	8	0.48
NO DR	K-means	0.57	0.21	4	0.19
NO DR	Mean Shift	0.47	0.44	10	0.58
NO DR	BIRCH	0.10	0.04	8	0.07
PCA	DBSCAN	0.68	0.25	9	0.29
PCA	K-means	0.56	0.21	3	0.19
PCA	Mean Shift	0.47	0.42	14	0.57
PCA	BIRCH	0.67	0.22	10	0.22
ICA	DBSCAN	0.46	0.44	8	0.59
ICA	K-means	0.44	0.48	3	0.57
ICA	Mean Shift	0.46	0.37	28	0.54
ICA	BIRCH	0.35	0.07	25	0.09
KPCA	DBSCAN	0.89	0.15	25	0.08
KPCA	K-means	0.25	0.12	2	0.07
KPCA	Mean Shift	0.61	0.11	8	0.05
KPCA	BIRCH	0.59	0.09	9	0.04
Isomap	DBSCAN	0.47	0.46	4	0.58
Isomap	K-means	0.39	0.52	2	0.62
Isomap	Mean Shift	0.39	0.47	3	0.61
Isomap	BIRCH	0.42	0.15	9	0.20
SE	DBSCAN	0.25	0.08	11	0.09
SE	K-means	0.64	0.19	6	0.20
SE	Mean Shift	0.15	0.28	3	0.23
SE	BIRCH	0.78	0.43	5	0.71

all techniques except the mean shift. SE also produced poor results for all techniques besides BIRCH.

It is important to consider these results in the context of the complete results in Appendix A Table 1. All techniques were very sensitive to the clustering parameter specified. For example, in the case of the very good BIRCH and SE result in Table 6.2, every other clustering BIRCH obtained from that data set in Appendix Table 1 had an ARI at or near zero. This pattern holds true for most other cases considered in the tower data set: the highest ARI represents one good result

among five other very poor results. Only mean shift working with Isomap produced clusters similar to the truth classes in 3 out of 5 cases.

Different clustering results from Table 6.2 are projected using PCA in Figures 6.7 through Figure 6.10. It must be noted that higher dimensional data was used for clustering, not just the three PCs given in this figure. In the K-means results in Figure 6.7 and Figure 6.8 both split the normal cluster, but in the in the k = 2 case it erroneously grouped faulty and normal data together. K-means with k = 3 in Figure 6.8, DBSCAN in Figure 6.9, and mean shift in Figure 6.10 each successfully assigned the faulty data its own cluster.

If the time of the fault was not known beforehand, data clustering, dimensionality reduction, as well as time series plots of the original data could be used in tandem to analyze the significance of clusters found, as in the basic approach illustrated in the previous chapter. DR projections to two or three dimensions can display the general clustering structure of the data. The clusters found can be used to isolate sections of a time series plot of raw sensor data to locate and guide analysis of the data isolated by the cluster algorithm.

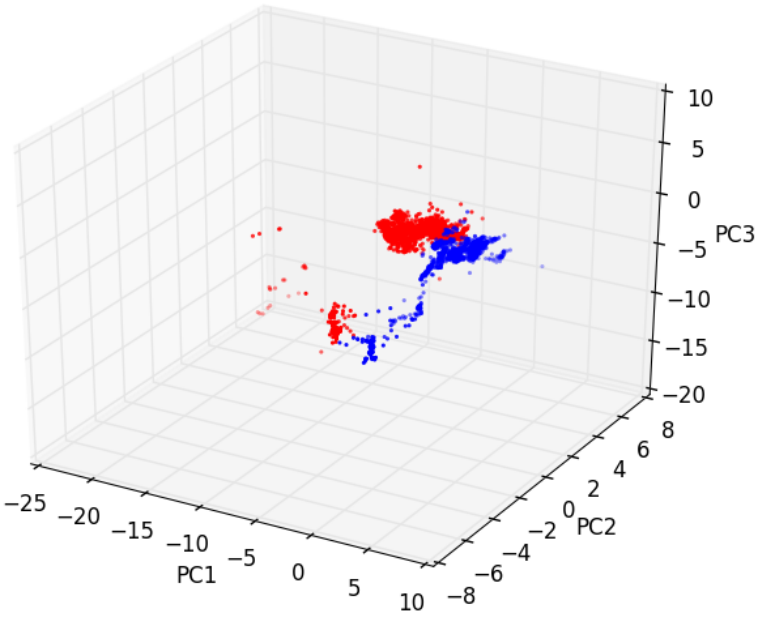

Figure 6.7 PCA projection of K-means clusters of tower data with k=2

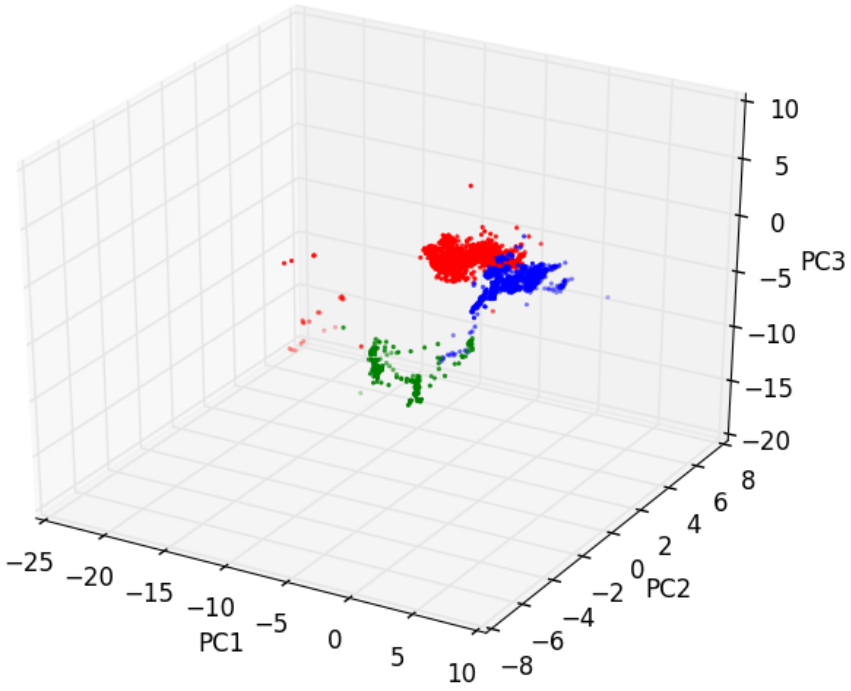

Figure 6.8 PCA projection of K-means clustering of tower data with k=3

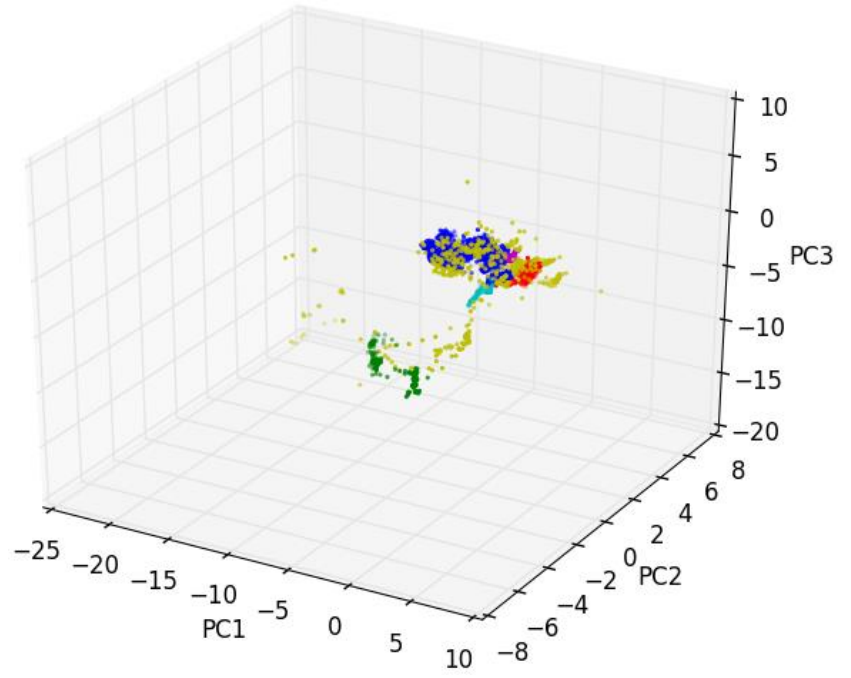

Figure 6.9 PCA projection of DBSCAN clusters

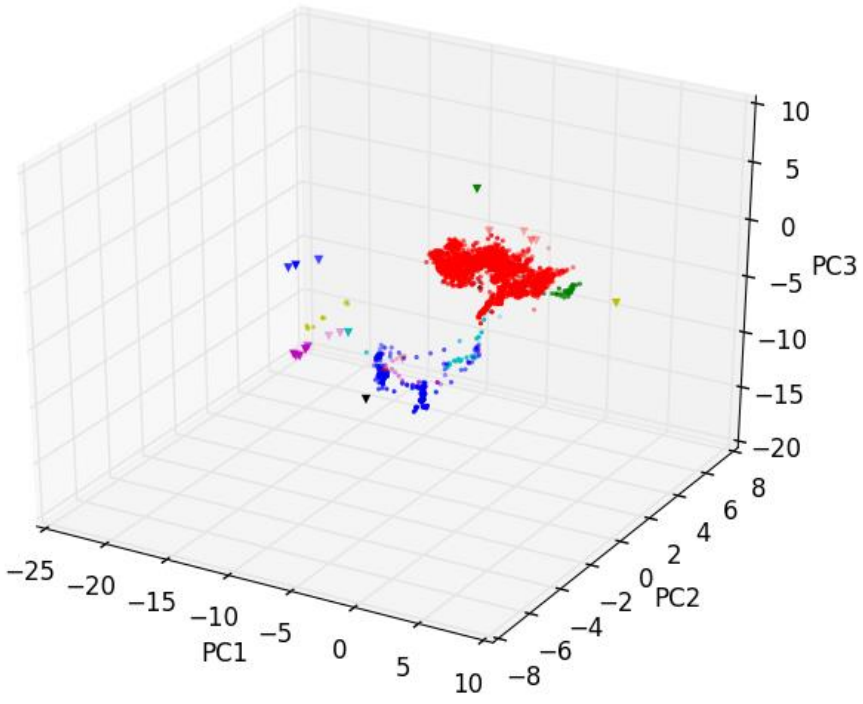

Figure 6.10 PCA projection of mean shift clusters

Manually adjusting and visualizing this data set produced an interesting finding among the normal data. Applying DBSCAN to this data with the eps parameter set to 1 and removing data classified as “noise” yields the clustering shown in Figure 6.11, a., which separates the normal cluster into several smaller clusters. While nothing in particular distinguishes these clusters from each other, Figure 6.11, b. shows the clusters colored based on the time of observation. Each cluster has a consistent color, meaning that the dense normal cluster is composed of multiple smaller, time-dependent clusters. The clusters could be distinguished by factors not immediately obvious from the sensors such as maintenance operations or the ambient temperature. A new cluster may be formed during each new run of the tower. This behavior poses a significant challenge to all modeling of this process because the parameters of the system are gradually and subtly changing with time, requiring models and controls to be constantly adjusted

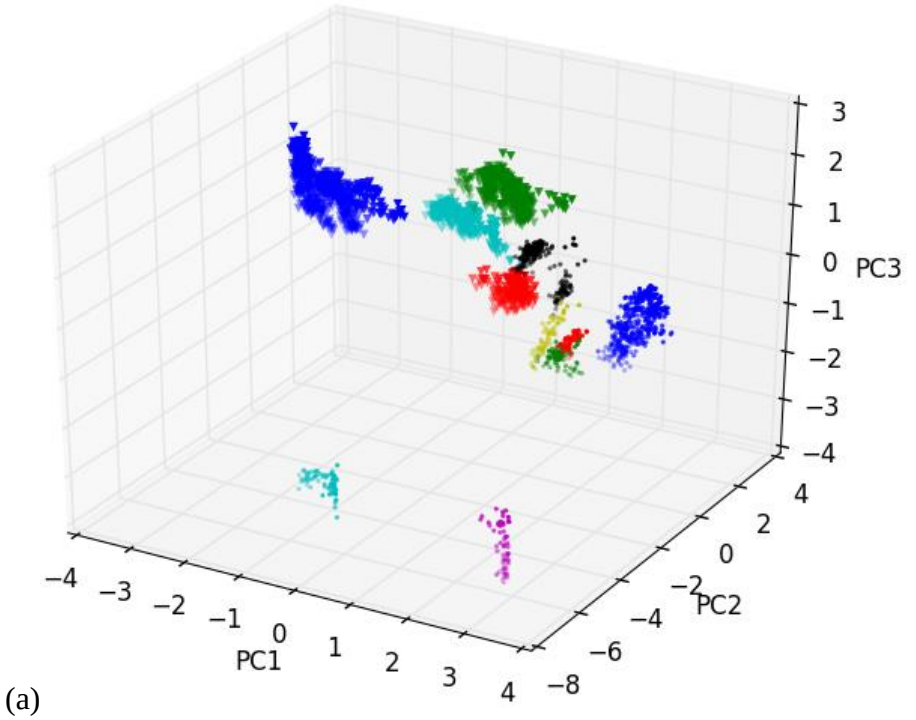

(a)

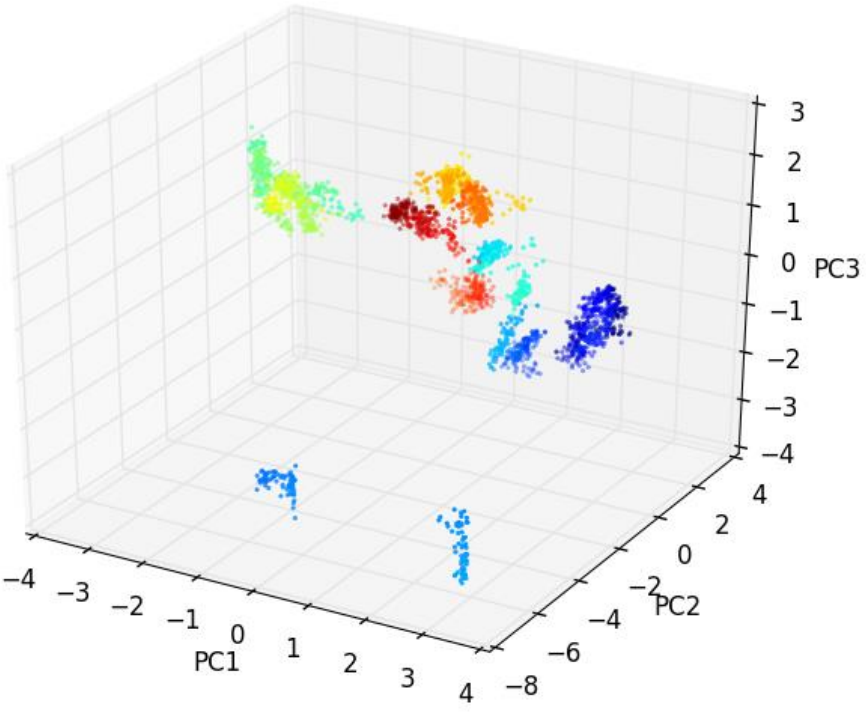

(b)

Figure 6.11: Adjustments to the eps parameter in DBSCAN finds the smaller clusters in (a). In (b) the data are colored based on time (blue is older, yellow is newer, with dark red being the most recent).

6.4 Novel Event Detection

6.4.1 Data mining and analysis for monitoring

The following research attempts to use historical data to detect the previously considered novel fault event. A historical data set spanning 2012 to 2013 was used as a training set while data from 2014 was used to validate the effectiveness of the models created. In order to make a more broadly useful characterization of the process (i.e. not only for detecting the sensor fault described in Section 6.2, but also good for general fault detection), nearly all measurements around the unit were selected for the mining task, excluding only variables associated with equipment that is seldom used.

Additionally, new variables were created by taking the difference between related measurements in different parts of the process, such as the temperature difference between the middle of the column and the top of the column, or the pressure difference between the feed pressure and the pressure in the first tank. This included taking the difference between T3 (middle tower temperature) and T7 (bottom tower temperature), which allowed the easy separation of the known sensor fault from normal operations. This allows the user to add a small amount of process knowledge by giving the data some of the structure of the process and created a potentially useful new set of variables from the process. Combining the temperature difference with the qualitative knowledge about the appearance of startup and temperature faults, the simple graphical tool shown in Figure 6.12 was created to quickly select data and organize it into different groups.

To effectively diagnose the state of the process, three pools of data were created:

- a larger data set containing all normal data for a particular grade,
- a smaller set containing data from startup conditions

- an even smaller data set holding measurements from operations with the temperature sensor fault.

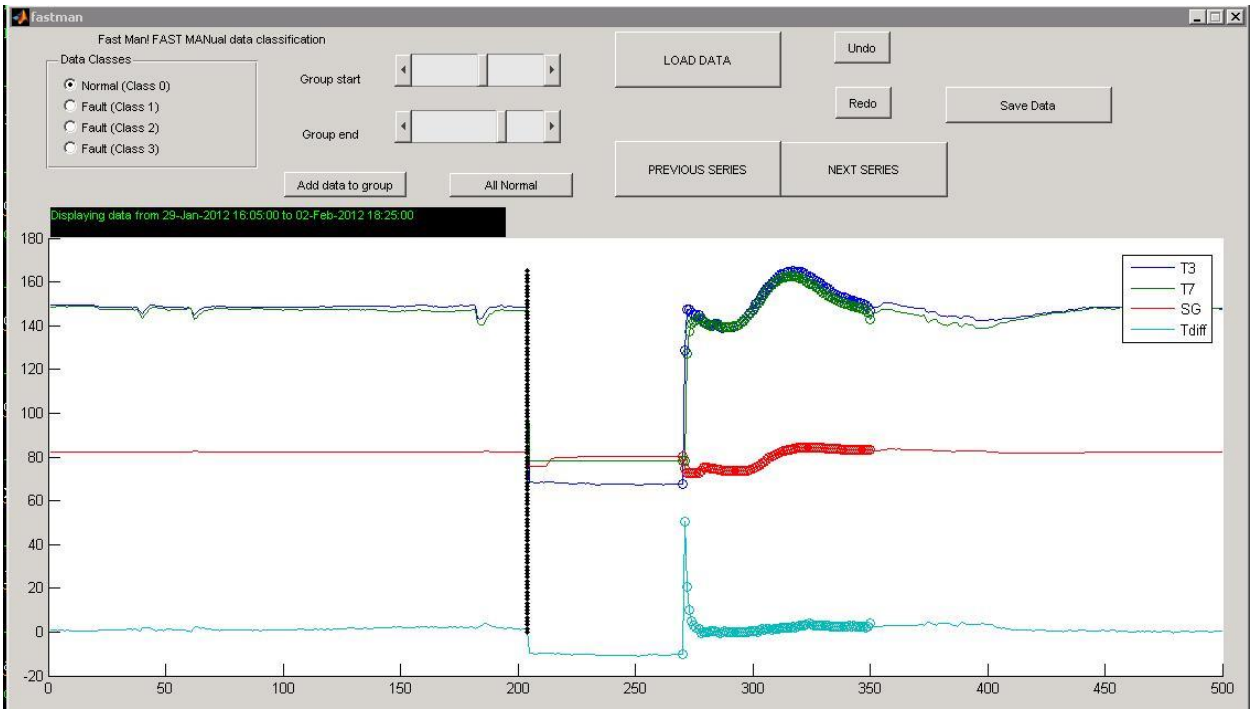

Figure 6.12: Graphical tool used to manually classify training data. Selected data is plotted in time series with dense group's circles and added to different fault groups with the controls in the upper left of the window.

The asymmetry in the data presented a challenge to fitting data-based models to represent the different states of the process. The relative size of each data set considered is in Table 6.3. Data at normal operations is available in abundance while faulty data is relatively rare: normal data are over 100 times as numerous as sensor fault data. SMOTE, an over-sampling technique from Chawla (2002) was used to balance the data set to achieve training data for classification. In short, SMOTE generates synthetic data in classes with fewer records by interpolating between data points based on their nearest neighbors in the smaller class. The larger normal and startup classes were reduced by randomly removing data from the larger class until a specified proportion defined with

respect to the smaller class remained. For comparison, the size of each original pool of data is given in Table 6.3.

Table 6.3: Sizes of historical data groups and training data

Pool of data used in training	Size of historical data set	Size of training data set
Normal operations	162,000	3,280
Startup	2,180	1,640
Temperature sensor fault (Tfault)	820	1,640

6.4.2 Map training and visualization

Map training and data projection occur in seconds due to the relatively small size of the training data (thousands of points), but the SOM batch algorithm discussed earlier allows similarly short training times even with larger data sets. The plant computer for this research used had limited memory, which compelled us to favor smaller training sets, though previous analysis of larger data sets showed only limited advantages in using additional data.

Figure 6.13 gives a PCA projection of the map formed after training an SOM to data from the separation tower. The two components used in this projection represent about 18% of the variance of the data. Various SOM visualizations of the map are given in parts a. through d. of Figure 6.14. The goal is to find regions of the map which explain the various operating regimes within the data so that new data can be projected and diagnosed based on where they occur on the map. In our approach, k-means clustering is used to isolate distinct portions of the map we can explain using SOM tools.

Figure 6.14, a. visualizes the distances in the different map nodes in a U-matrix where large regions of dark blue correspond to distinct and contiguous groups in the data and yellows and reds correspond to distances between those groups. From the U-matrix, we see several well-defined groups in the data at the top corners of the map and, to a lesser extent, between the left and right bottom portions of the map.

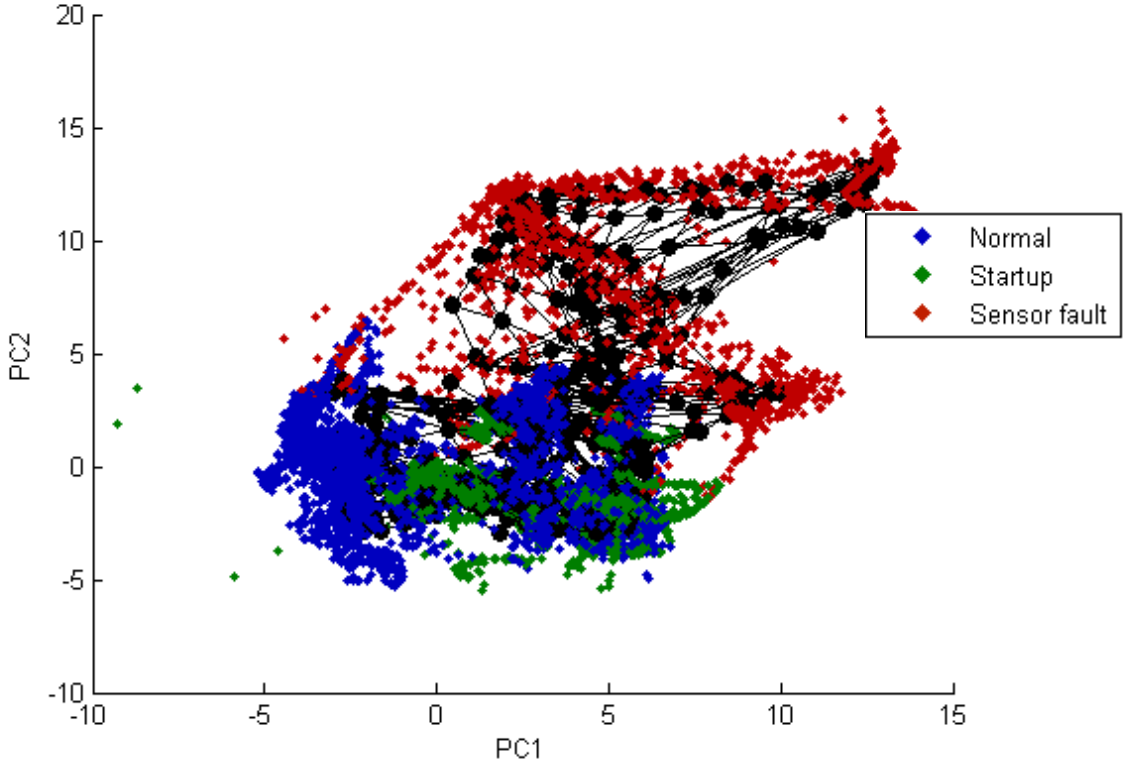

Figure 6.13: PCA projection of trained map with sampled training data, including synthetic samples from SMOTE.

K-means clustering is used to find the specific boundaries between clusters seen in the U-matrix and to function as a check on map training. For example, if clustering is unable to separate startup and sensor fault data, it could point to problems in the data. From our knowledge of the data, we expect to find at least three groups based on how the data was initially grouped. According to the Davies-Bouldin index (DBI) calculations for several trial numbers of clusters in Figure 6.15,

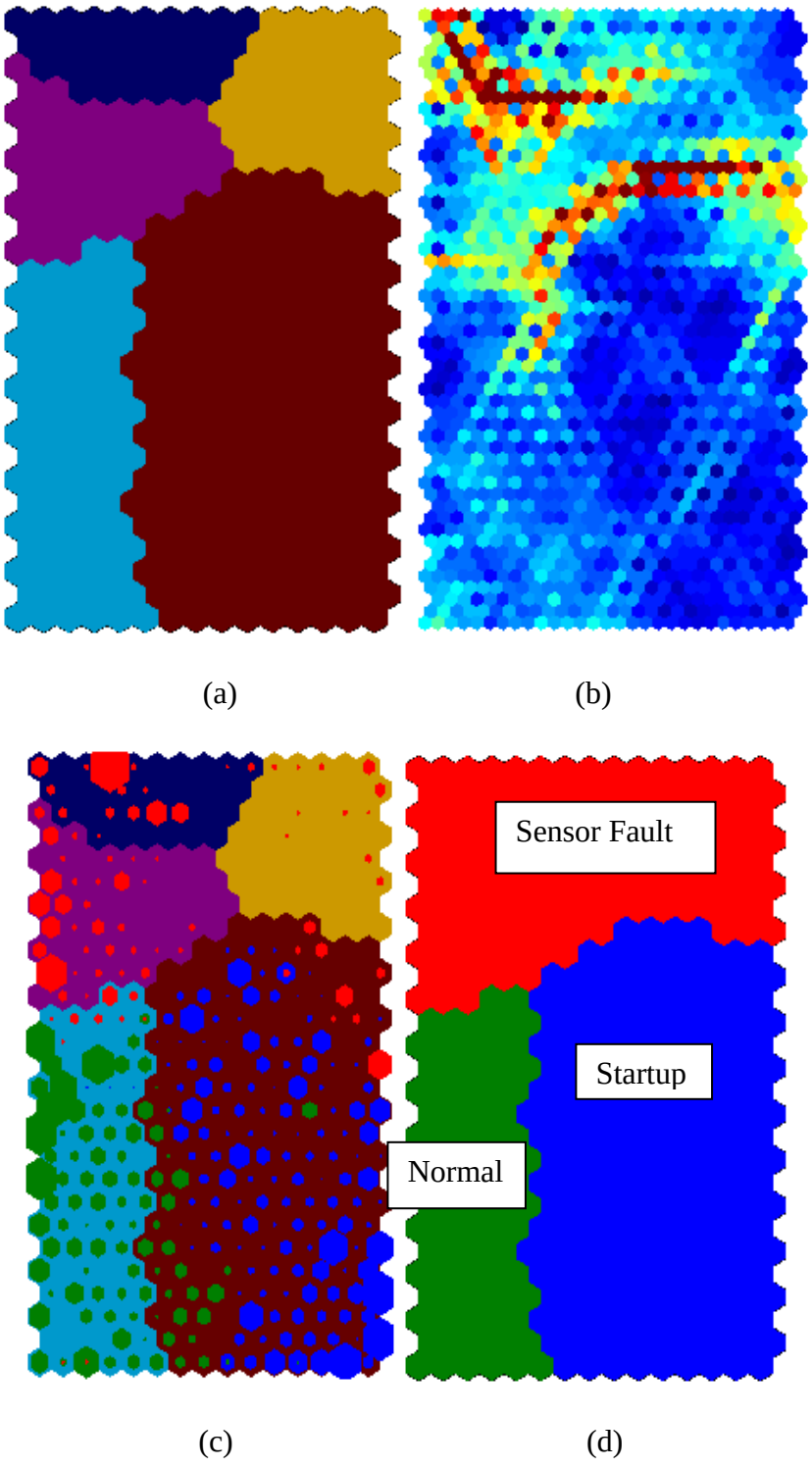

Figure 6.14: Visualizations of the map used in monitoring. (a) the SOM U-matrix visualizes groups in the data. (b) colors are derived from clustering results. (c) is a hit diagram of the training data on the map. (d) labels the map regions.

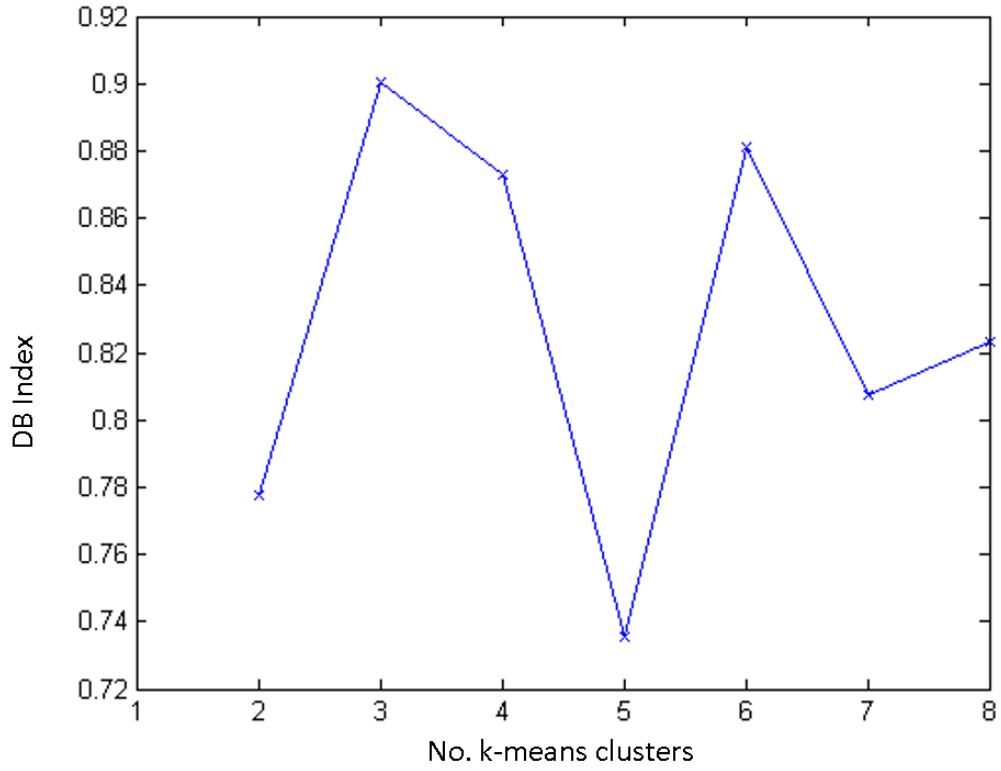

Figure 6.15: Davies-Bouldin index of the clustering given in Figure 6.8, b. Lower values indicate a better clustering. Based on the number of data groups we expect from this set, the five cluster result is accepted as the best.

the best clustering of the data occurs at five clusters. The SOMs in Figure 6.14, b. and 6.14, c. show the map colored according to these five clusters found from K-means clustering, and each belongs to one of the predefined classes of our training data. These clusters can be taken to form the definite boundaries of the clusters observed from inspection of the U-matrix earlier and helps ensure that all data is grouped with similar observations.

Next, to explain the meaning of clusters found from the K-means analysis, the data are projected to the map to find the dominant patterns expressed in each cluster. From the hit diagram in Figure 6.14, c., we can see that three of the five clusters are subdivisions of the sensor fault group (red data). Note that larger hexagons correspond to a relatively large amount of data being

projected to that area of the map. The cluster identified as the normal region of the map contains some points classified as faulty or startup but more similar to normal operations (representing noise in the training set or transitional measurements while moving between states in the map).

Finally, we can name the regions of the map so that when new data can be projected to the map and classified online. Naming each cluster based on its dominant data group results in the SOM in Figure 6.14, d. with one well defined region for each operating condition of interest. While the SOM was able to organize a good separation between the representations of the different classes, the K-means results removed the effects of some of the noise in the training data and, more importantly, helped explain the regions of the map for analysis of the process state.

Component planes can be used to show the multidimensional characteristics of the state space of the tower operations and different variables are correlated with the operating states in the structure of the map. in a. through c. of Figure 6.16 shows component planes for variables F2, F3, and T7. The value of each variable at different parts of the map is color-coded. How each variable changes over the map gives us insight as to the meaning of different regions of the map. Figures 6.16, a. and 6.16, b. show that the sensor fault often corresponds to low bottoms flow (F2) and lower temperature measurements where in Figure 6.16, c. the sensor fault is correlated with high flows through the product stream (F3).

6.4.3 Determining the quantization error (QE) threshold

In order to create a useful reference to quantify how well new data fit to the SOM, a probability distribution was fit to the QE calculated from the training data. Using the fit distribution, the bound of the 99.99% one-sided confidence limit was chosen to avoid a large number of false alarms. The histogram of the QE calculated over the training data is given in Figure

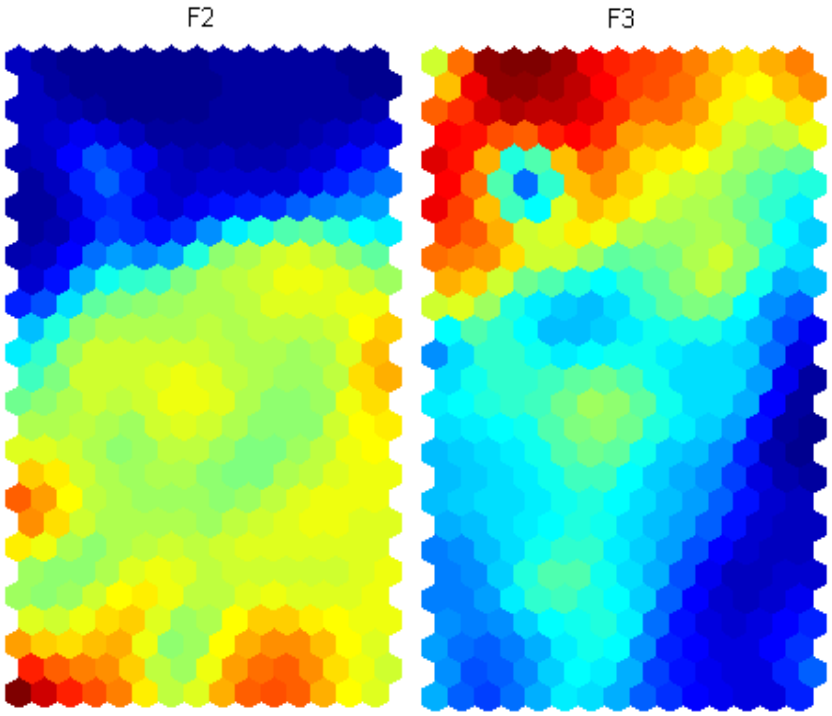

(a) (b)

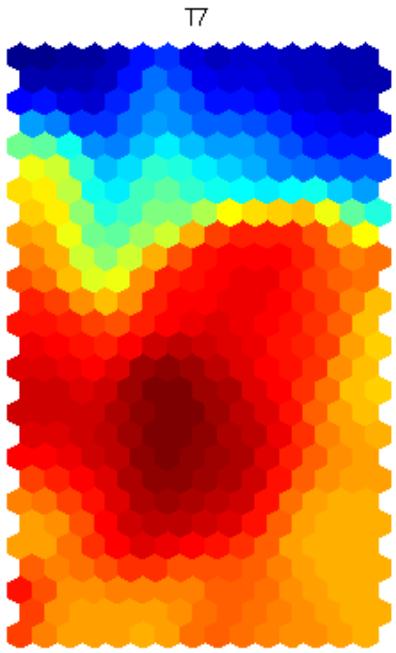

(c)

Figure 6.16: SOM component planes for F2, F3, and T7 showing the different normalized measurement values across different regions of the map in Figure 6.8, d.

6.17. A lognormal was fit to this histogram with parameters 0.9037 and 0.3370. From the distribution, the threshold for a faulty status with 99.99% confidence occurred at a QE of 8.64.

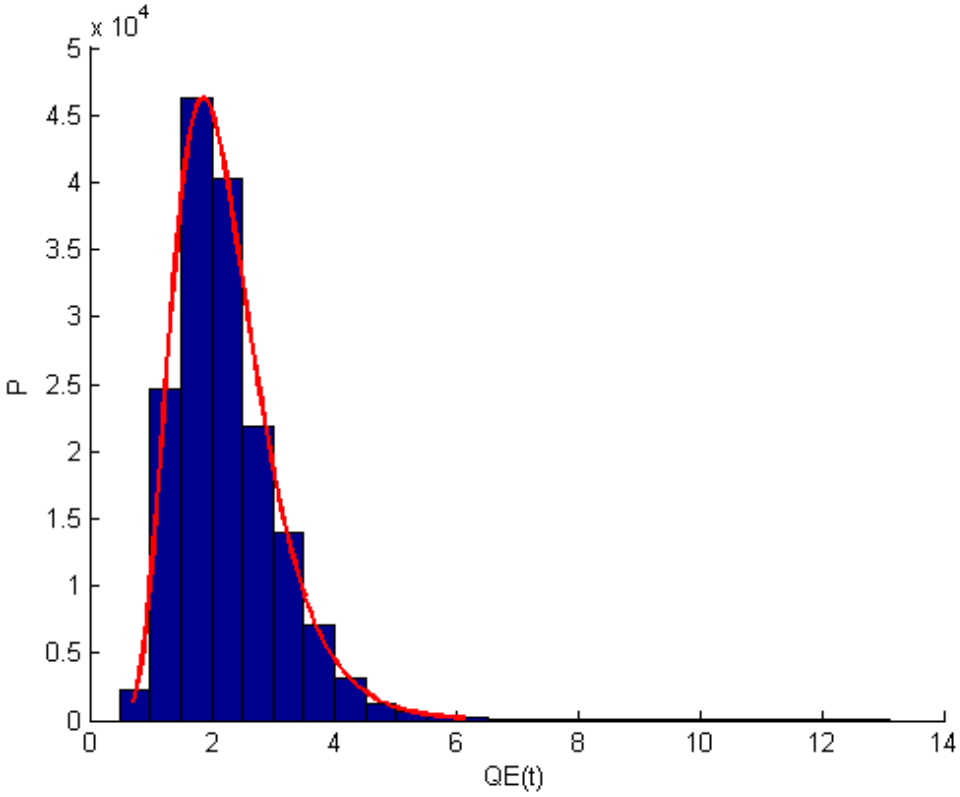

Figure 6.17: Log normal distribution fit to a histogram of the QE calculated over all data from 2012-2013.

6.5 Fault Detection and Identification Results

To quantitatively test the ability of the fault detection scheme to detect a novel event occurring, we projected data from 2014 to the map and calculated the quantization error (QE). A low QE indicates close proximity to a map vector, whether that map vector means normal, startup, or faulty. A time series of this fault detection statistic is given in the upper plot of Figure 6.18. The QE E is colored according to the predicted class of the process in the lower plot of Figure 6.18. The QE calculations contain many uninteresting peaks from startups or feed grade switches, but the faulty condition can be easily identified by an extended period lasting several days in which

the fault detection statistic was high (QE > 8) around the time indicated by the red circle. This indicates that the process is in a condition not included in the SOM model of the process. Figure 6.19 shows details of SOM QE plots of observations from a well-diagnosed sensor fault (Figure 6.19, a.) and the Novel Event (Figure 6.19, b.), we will study further using contribution plots. SOM successfully identified the ongoing sensor fault occurring in the process as well as clearly indicating that an abnormal event was occurring.

Similar to the SOM results, the PCA results in Figure 6.20 have a very strong signal indicating that an abnormal event was occurring, however the fault diagnosis results contain many

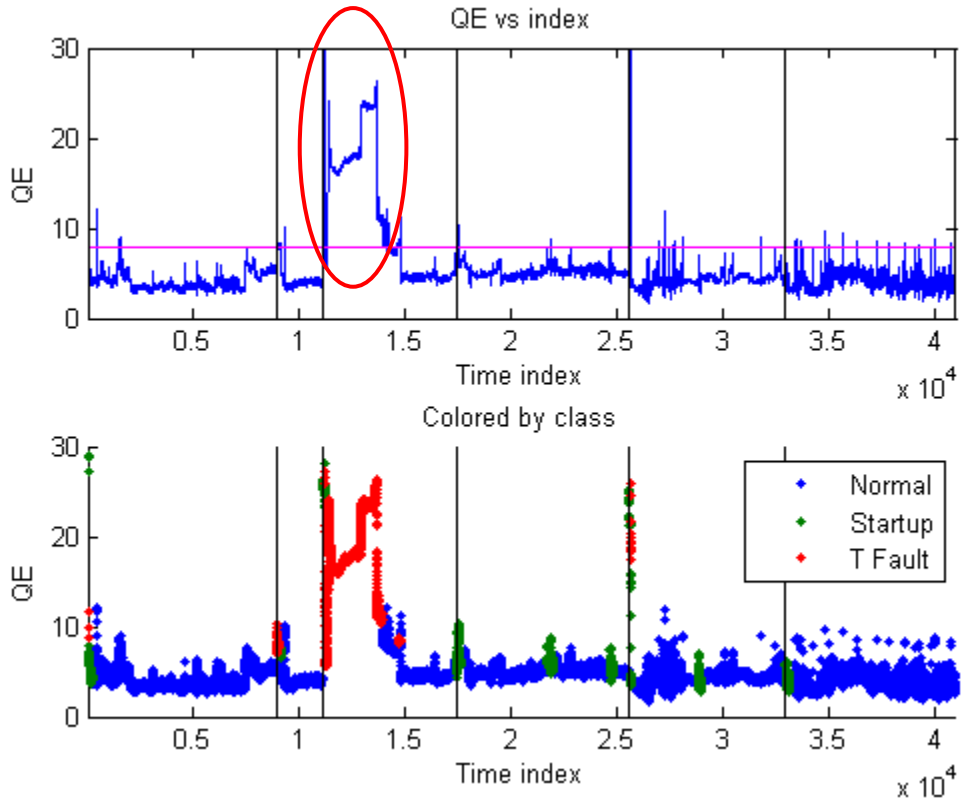

(Vertical black lines correspond to start ups and grade switches,
and may represent weeks of operations not plotted.)

Figure 6.18: Fault detection using the quantization error of new data vectors on the SOM. The pink line on the top corresponds to the threshold for a detected fault. The bottom graph colors the data based on the region of the map the system is in.

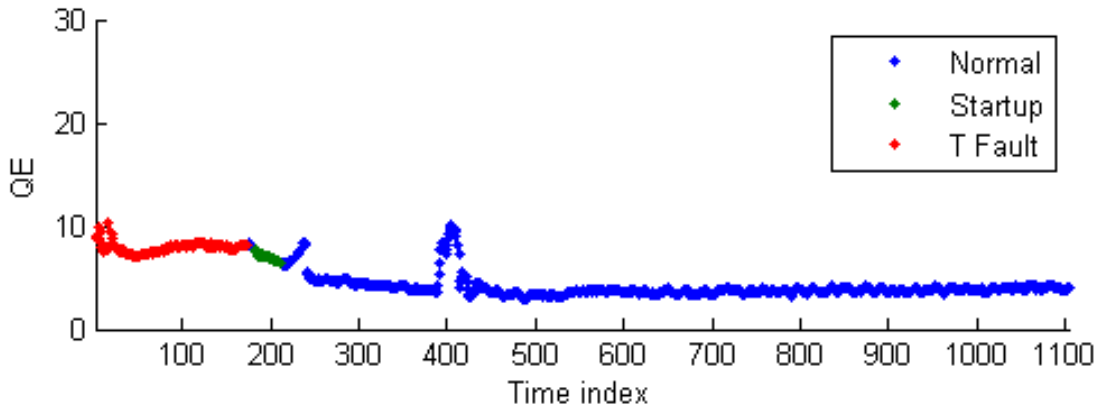

(a)

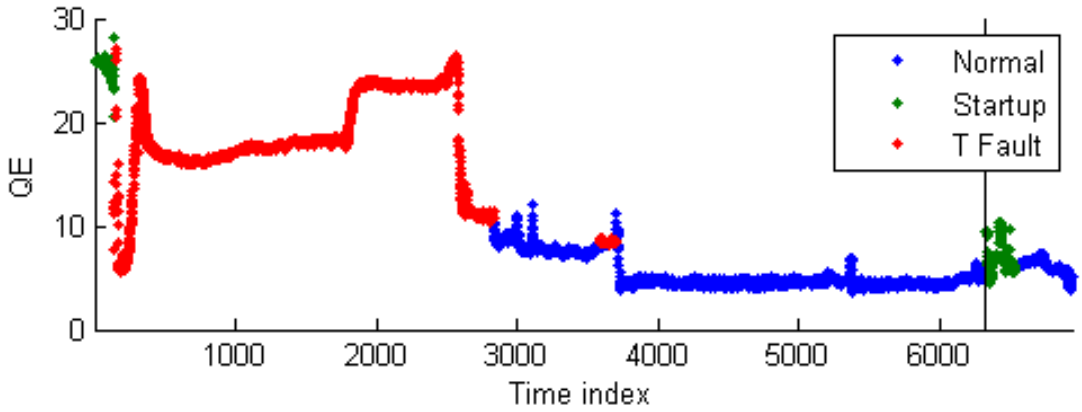

(b)

Figure 6.19: Close-ups of the QE with time calculated (a) after a regular Tfault and (b) during the Novel Event.

false fault events diagnosed incorrectly. Non-linearity in the sensor fault training data inflated the size of the sensor fault's diagnosis region, causing it to overlap with normal and startup data and leading to many of the misdiagnosed sensor faults and unremarkable fault detection statistic calculations during the Novel Event. The failure of MPCA to yield a T^2 statistic that very strongly

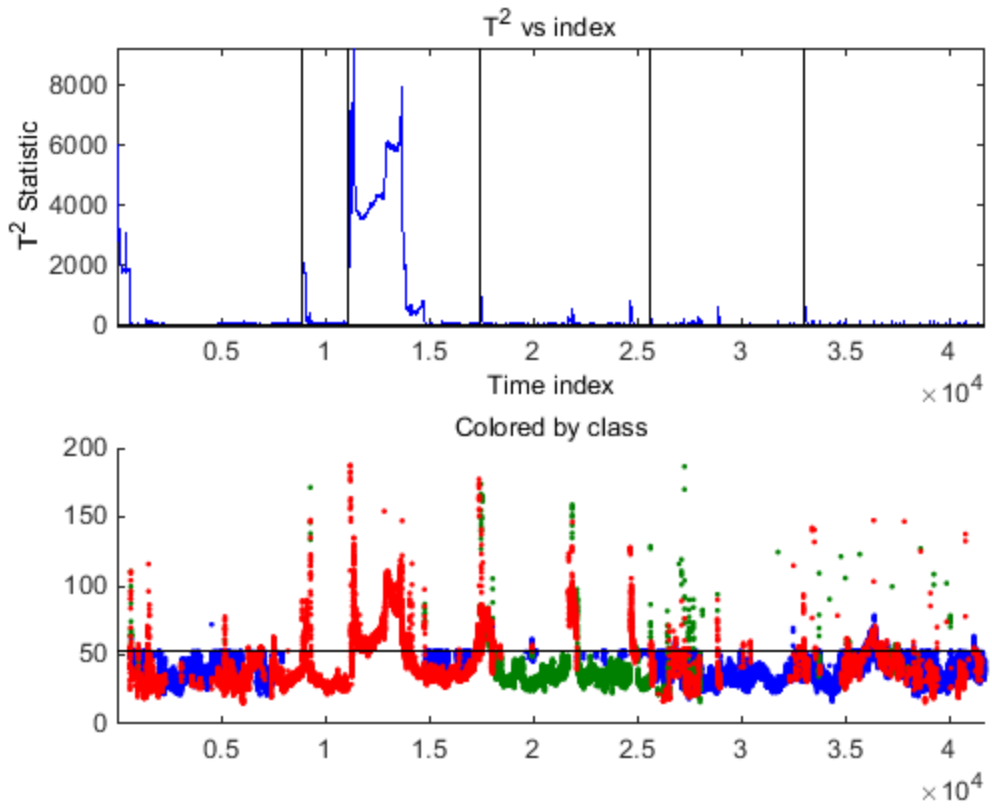

Figure 6.20: T2 statistic based MPCA classification. While the PCA model of normal outputs a strong fault signal, classification results are inferior to SOM due to nonlinearity in the data and overlapping fault and normal regions in the data space.

indicated that something besides a normal sensor fault was occurring could have led to the incorrect diagnosis of the abnormal event as a common sensor fault.

The classification map created from the K-means clustering analysis can be used to track the state of the process visually using an SOM trajectory plot. This visualizes the map units touched by the process state. Larger circles indicate more time was spent on those particular nodes and thicker lines correspond to more switching between two particular nodes. The projection can be seen switching between regions of the map previously identified as normal or faulty by the K-means clustering or hit diagram. Figure 6.21 gives three examples of tracking the state of the process through historical data with SOM trajectory plots.

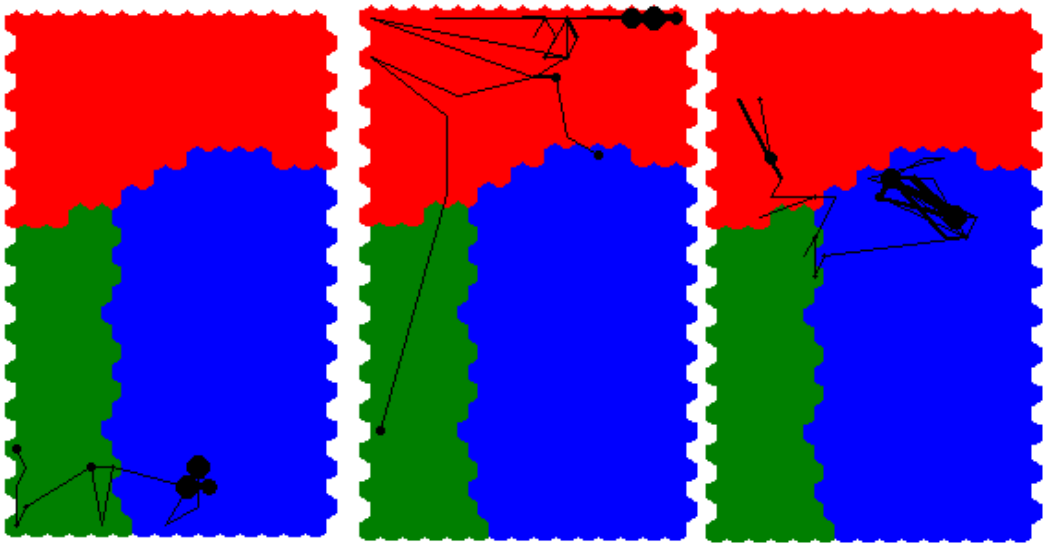

(a) (b) (c)

Figure 6.21: SOM trajectories of the process state for three separate conditions in the tower: (a) normal startup, (b) regular temperature sensor fault, and (c) Novel Event. Each trajectory plots about one day of data.

First, Figure 6.21, a. is taken from a typical startup sequence: the trajectory begins in the startup region and moves into the normal steady state region where it remains until operators choose to halt production. Figure 6.21, b. plots sensor fault in a startup sequence a few days before the Novel Event occurred, and it follows a well-characterized path from fault through normal startup (after it was fixed) to normal steady state operations. Figure 6.21, c. shows what the trajectory looks like during the Novel Event. In this case, operations began normally and moved into the sensor fault region shortly after starting. When the Novel Event begins, the trajectory makes a dramatic jump to the edge of the map and remains there while the fault detection statistic remains consistently elevated above the reference line in the plot of the quantization error in Figure 6.19, b. This behavior where the process state switched from the map interior with relatively low QE to the edge of the map with elevated QE would be further indication of a dramatic, abnormal

change in process dynamics, more than a slightly elevated PCA statistic indicating a common sensor fault.

To give operators valuable feedback from the tower to diagnose the root causes of the fault, a fault contribution plot was calculated using the faulty data point's BMU. Figure 6.22 shows SOM contribution plots calculated for several test points. The contribution of a data point from the Novel

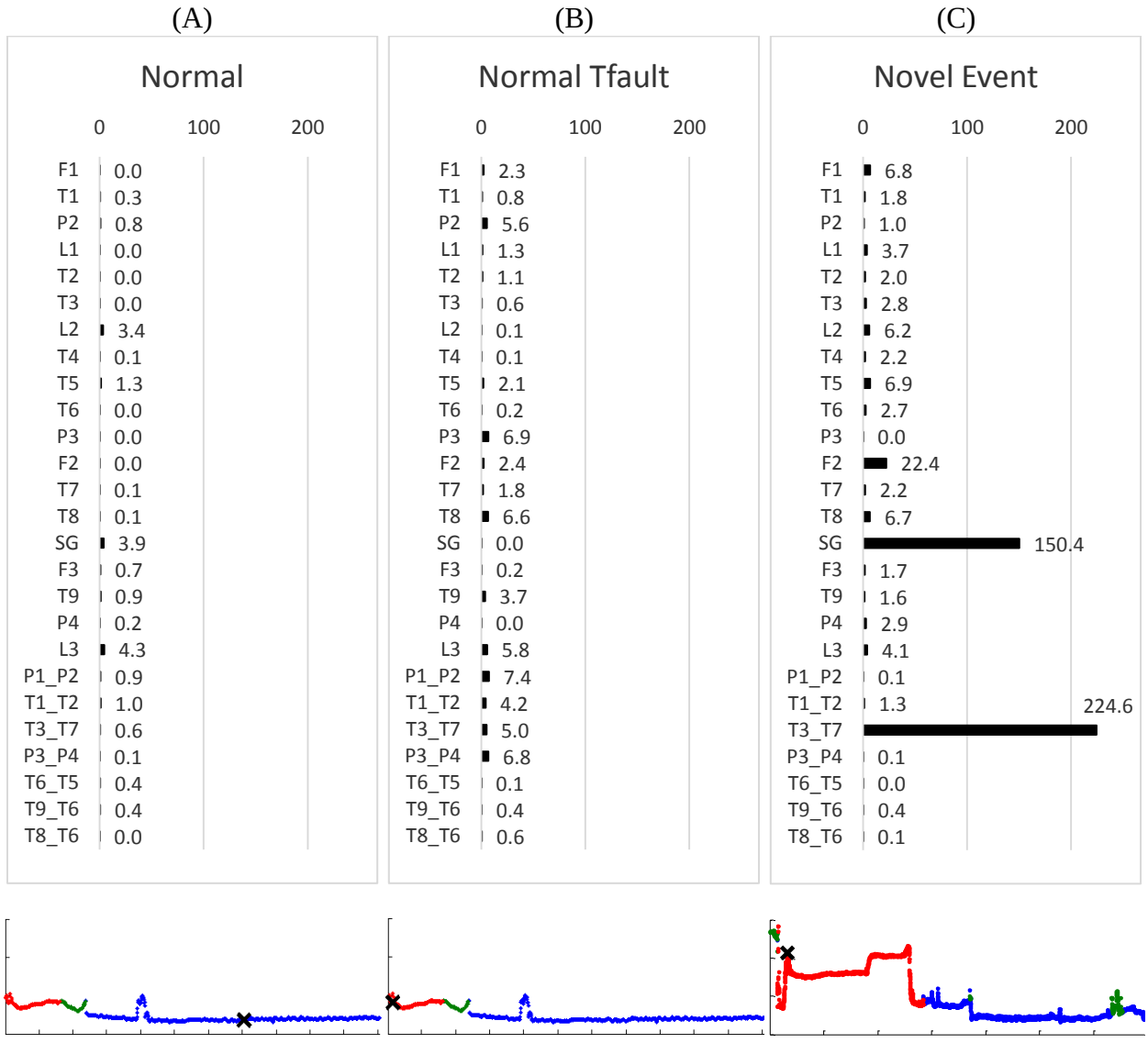

Figure 6.22: The SOM based fault contribution plot for (a) normal steady state operations, (b) typical temperature sensor fault, and (c) the Novel Event showing which variables could be contributing to an elevated fault detection statistic.

Event is given in Figure 6.22, c., along with a contribution plot of a data point from steady state normal operations before the Novel Event (Figure 6.22, a.) and a typical temperature sensor fault (Figure 6.22, b.) for reference. In the time series of the fault detection statistic below, a black "×" indicates the time point analyzed in relation to the time series of the fault detection statistic. To compare, contribution plots from the PCA model are given in Figure 6.23. Figure 6.23, a. shows the contribution plot created by the PCA model of normal during the sensor fault. The PCA model

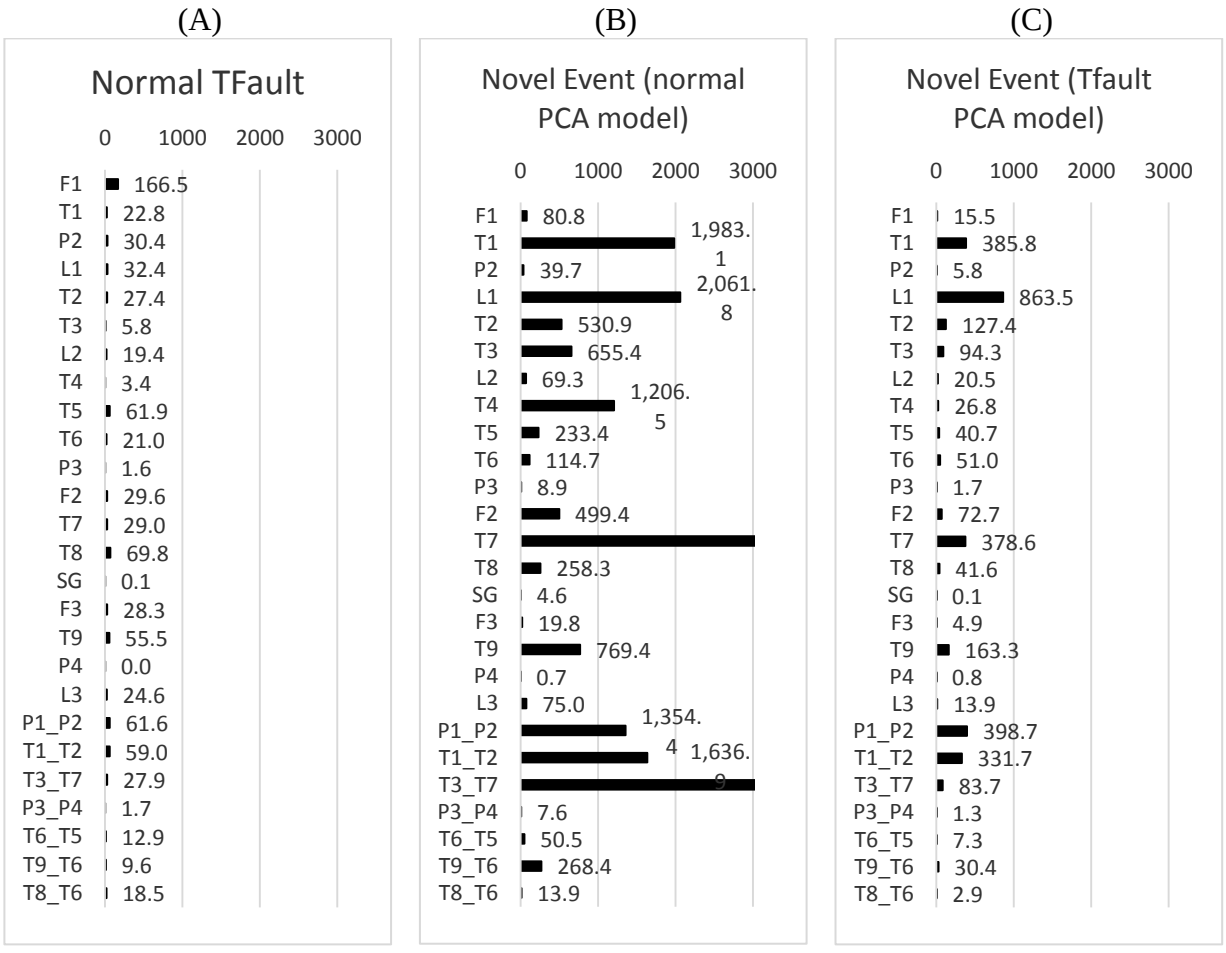

Figure 6.23: PCA contribution plots of the sensor fault (a), the temperature fault (b), and the Novel Event (c) with respect to the PCA models for the normal and the sensor fault PCA model (the class much Novel Event data was classified with).

of normal fails to identify which sensor is generating faulty measurements even with the derived variable created to specifically indicate this fault. In the Novel Event contribution plots in Figure 6.23, a. and Figure 6.23, b., key trends in the F2 and SG sensors are ignored, and there is little to guide a user to a specific part of the unit, except potentially to Tank 1, where the root cause was not located.

Figures 6.24, 6.25, 6.26, and 6.27 show plots of the time progression of some notable variables during the Novel Event colored according to the different regions in the SOM map. Each variable with an elevated contribution undergoes an enormous change during the period of interest (indicated by the corresponding red color) and this behavior indicates important changes in the process have been extracted by the contribution plots.

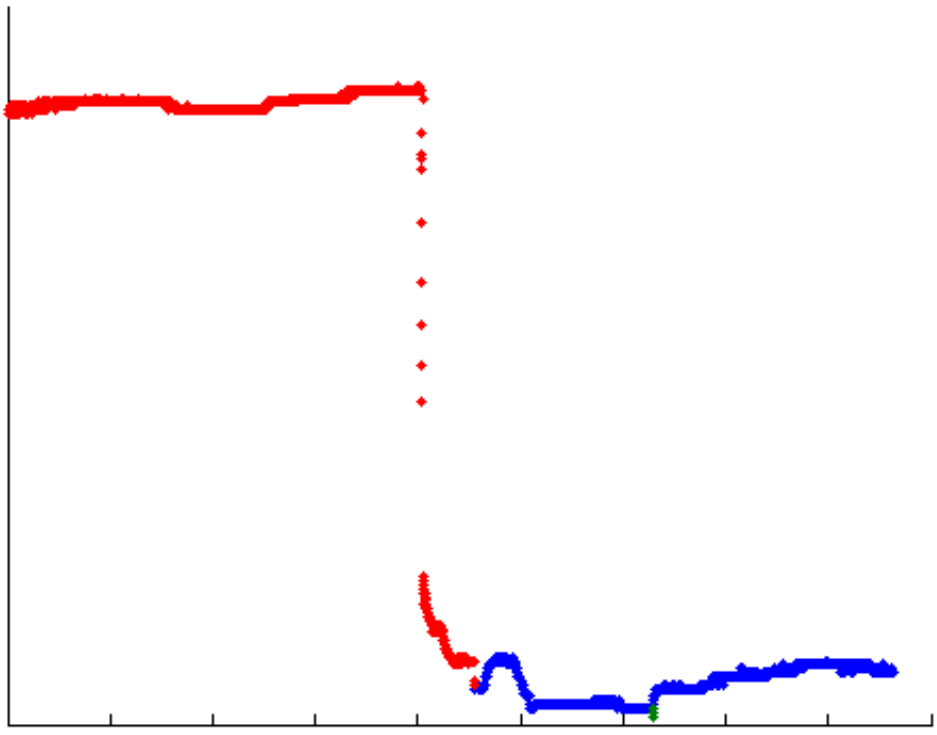

Figure 6.24 Time series plot of SG colored by classes found by SOM

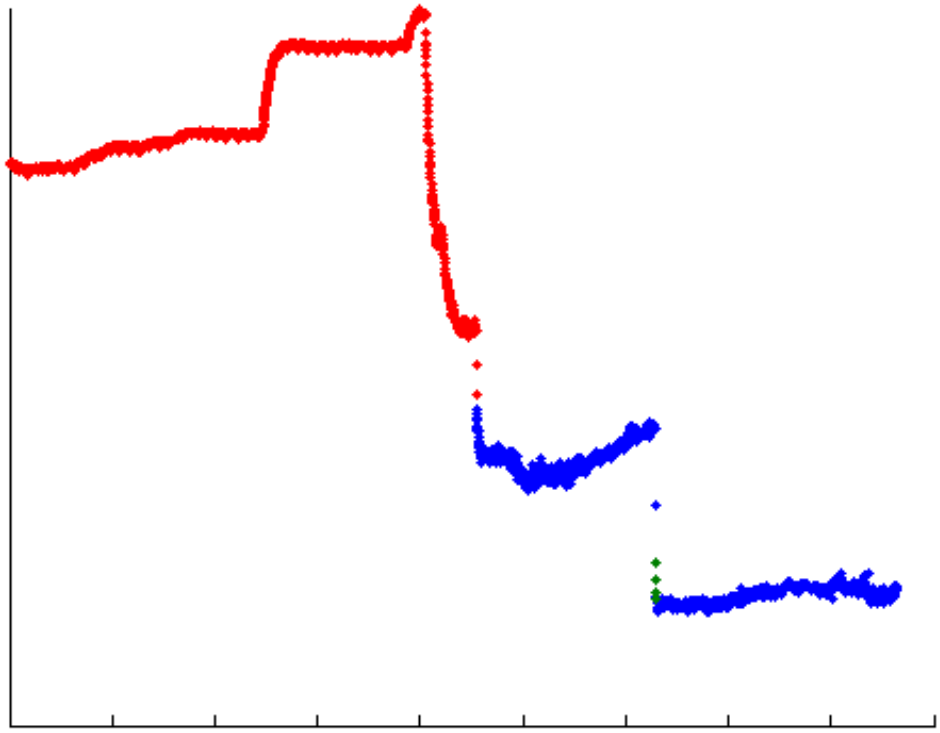

Figure 6.25 Time series plot of T3_T7 colored by classes found by SOM

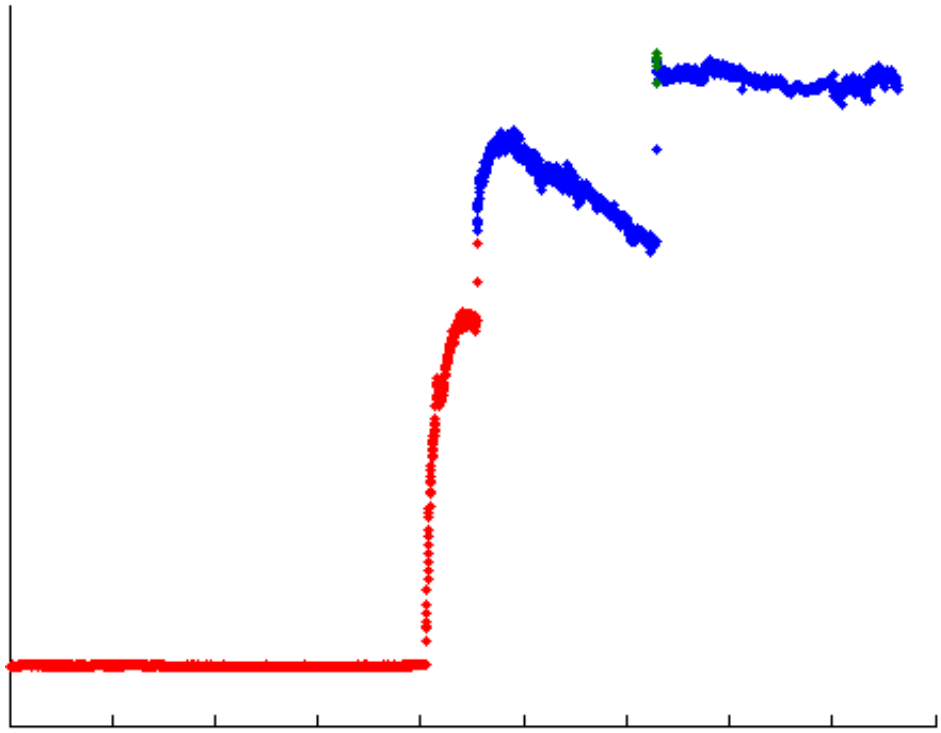

Figure 6.26 Times series plot of T7 colored by classes found by SOM

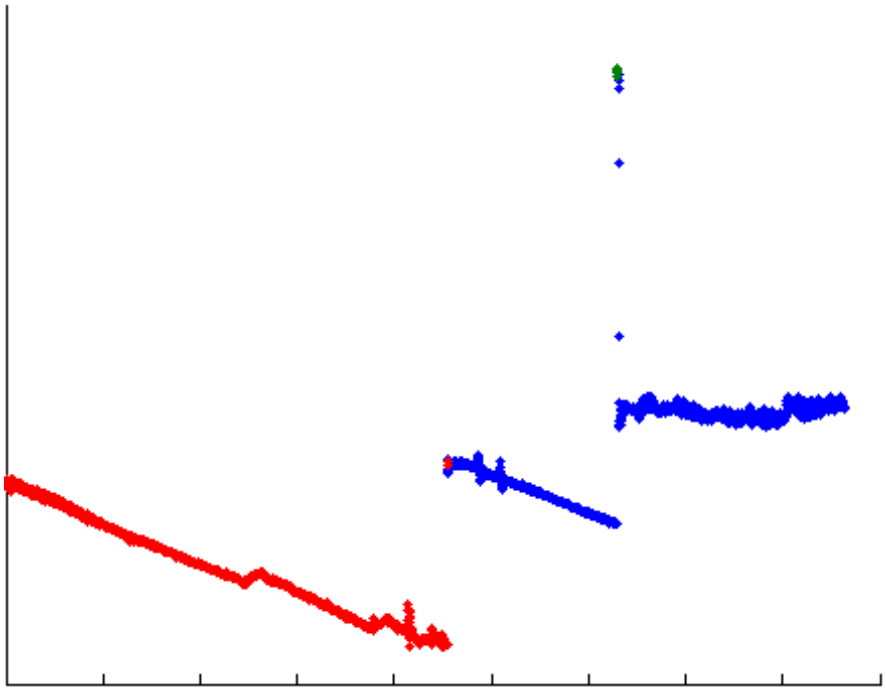

Figure 6.27 Time series plot of F2 colored by classes found by SOM

Some idea as to the position of the faulty data in multidimensional space can be seen in the projections of the map to 2 and 3 PCs in Figure 6.28, a. and 6.28, b. The major fault moves beneath the outer borders of the area modeled by the map and drifts into empty areas not covered. Based on the elevated QE observed during the Novel Event, the real multidimensional characteristics of the fault event probably has a larger deviation from normal conditions that is not fully captured by the linear 2-PC projection.

6.6 Conclusions

This research considered two important aspects of process monitoring in the analysis of an industrial separation tower. The first study sought to fill the gap between the need for labelled data for training supervised monitoring algorithms and the raw, unclassified data that have accumulated in all process historical databases. We demonstrated how unsupervised learning techniques drawn

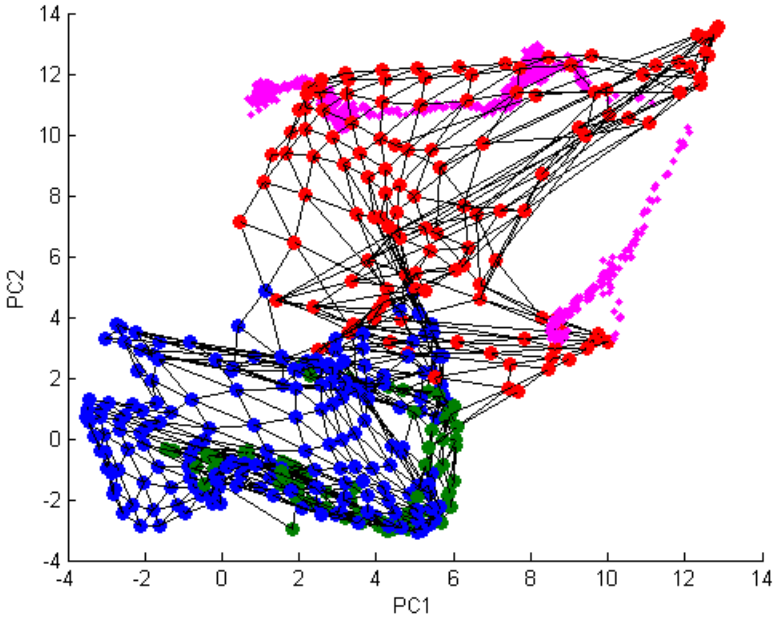

(a)

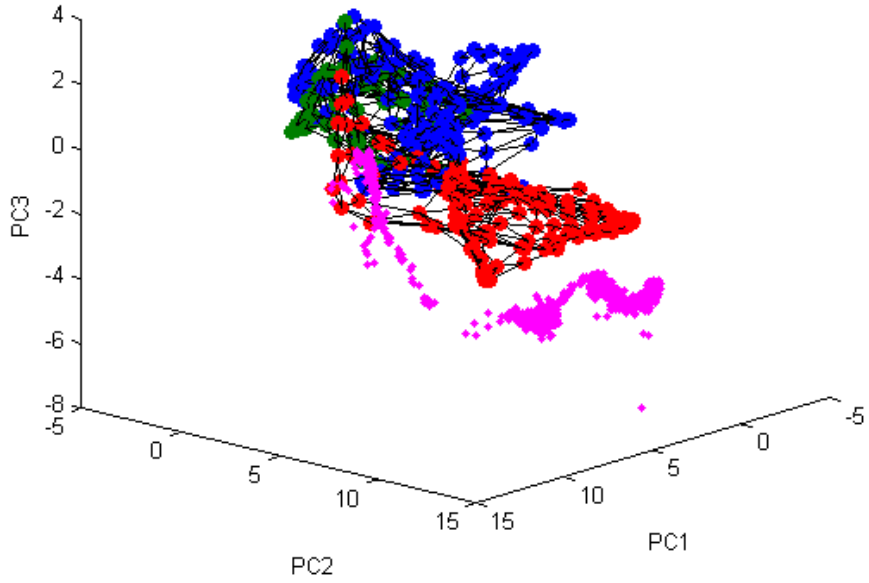

(b)

Figure 6.28: Projection of map vectors to (a) two and (b) three dimensions. The pink data points are data drawn from Novel Event.

from the computer science literature can extract knowledge from chemical process databases. Dimensionality reduction and data clustering identified a major process fault that had occurred during the months of data considered and distinguished it from a large, dense normal region corresponding to normal process operations. Additional analysis revealed that at the grade studied, each start-up of the column formed a new cluster in the dimensionally-reduced space, as visualized by a PCA projection of the clusters found by DBSCAN.

Next, we demonstrated the implementation and testing of an SOM-based strategy for process monitoring on an industrial-scale separation tower system. The study shows SOM and data clustering can be used together to explore large process data sets, simultaneously diagnose a known fault, and detect a novel fault. The proposed approach uses SOM in tandem with k-means clustering to find and explain contiguous regions of an SOM trained with two years of historical data and to also extract the key data patterns they represent. The process state was diagnosed in a historical data set and showed that the quantization error calculated from the map can effectively detect a novel process event that occurred simultaneously with a more common process fault. Additionally, SOM trajectory plots provide a qualitative visualization of the process state changing over time. Finally, SOM-based contribution plots indicated the variables with the biggest deviation from the expected process conditions early in the progression of the fault, thus helping to isolate the root causes of the novel fault faster. A standard MPCA approach was shown to produce less informative results compared to SOM and could have led to operators ignoring the fault event.

Altogether, the study from data clustering to process monitoring shows the complete workflow proposed in Section 3.1. Data clustering and projections generated by dimensionality reductions are key tools in the isolation of fault data for training process monitoring algorithms and aid in reducing model development time of data-based fault detection algorithms.

Additionally, we demonstrate how SOM can effectively model the operations of an industrial-scale separations tower and detect a novel event without detailed knowledge of the process.

6.7 References

Chawla, N. V., Bowyer, K. W., Hall, L. O., & Kegelmeyer, W. P. (2002). SMOTE: Synthetic minority over-sampling technique. *Journal of Artificial Intelligence Research, 16,* 321-357.

Chapter 7 - Case 3: Analysis and Monitoring of an Industrial Batch Polymerization Process

7.1 Introduction

Batches and semi-batch processes encompass most processes in the chemical industry, particularly for specialty chemicals, polymers, pharmaceuticals, and biochemicals. Batch processes are distinguished by their limited duration and the discrete steps that make up their operations including charging, processing (or the reacting stage), and discharging (Nomikos and MacGregor 1994). The conventional steady state approaches to process monitoring used in previous chapters fail on batch processes due to the dynamics of multiphase batch operations. Special adaptations taking into account the dynamics of individual batches are necessary for effective monitoring.

Direct composition and product quality measures often require offline laboratory tests on a product sample. Multivariate statistical process control, while more complex on batch processes due to the need for preprocessing like dynamic time warping (DTW) to consider the full progression of each batch, has been widely studied nonetheless because of the desire for faster and more frequent product quality measurements. Nomikos and MacGregor (1994) introduced some of the earliest applications of multiway principal component analysis (multiway PCA) to batch processes which enabled monitoring. Yao and Gao (2009) provide a comprehensive review of batch process monitoring methods.

This chapter considers fault detection and diagnosis of a batch polymerization reactor system, which presents particular challenges due to time-varying batch dynamics. Most standard process monitoring algorithms assume steady state operations, and adapting to dynamic batch operations is no trivial task. We apply several adaptations of steady state process monitoring algorithms based on PCA, SOM, and the MSOM technique presented earlier using DTW and

multiway unfolding strategies discussed in Chapter 2 and compare their performance in diagnosing two process faults on the reactor system.

Section 7.2 briefly describes the batch polymerization reactor studied. Section 7.3 demonstrates the synchronization of the batch trajectories. Section 7.4 studies the fault detection of individual process faults and Section 7.5 discusses the results of this study. The work in Section 7.6 attempts the diagnosis of both fault conditions considered. Section 7.7 offers additional discussion and conclusions.

7.2 Process Description

The polymerization reactor in Figure 7.1 converts monomer mixtures to a product with certain qualities. The different batches are distinguished according to the specific feed blends and the feed is preheated with a pump around stream from the reactor and heated by hot oil in a heat exchanger. Reactor operations proceeds through five phases in which reactants are fed, heated inside the batch to a specific temperature, left inside the vessel to react for a predetermined amount of time, transferred to downstream separation units and a finishing plant, and a stand-by phase where the reactor is prepared for the next batch. The quality of the product is evaluated based on its softening point, or the point at which the polymer interacts with water, measured via an offline laboratory experiment with a considerable time delay. Each particular grade has a target softening point, and the feeds to the reactor are controlled manually by operators to hit the target.

Occasionally, the valve controlling F1 experiences value sticking, which affects process performance and can lead to off-spec products. Personnel can correct this occurrence by opening and closing the valve, also called “stroking” the valve. The characteristic behavior of a sticky valve is shown in Figure 7.2. The pump-around flow rate is operating abnormally for six batches, corresponding with abnormalities in the behavior of the flow valve. Another common fault is

caused by the clogging of the filter beneath the reactor. The filter will periodically become saturated with product and interfere with pump around flow from the bottom of the reactor. This fault can be identified by the behavior of the dP1 variable plotted in Figure 7.3.

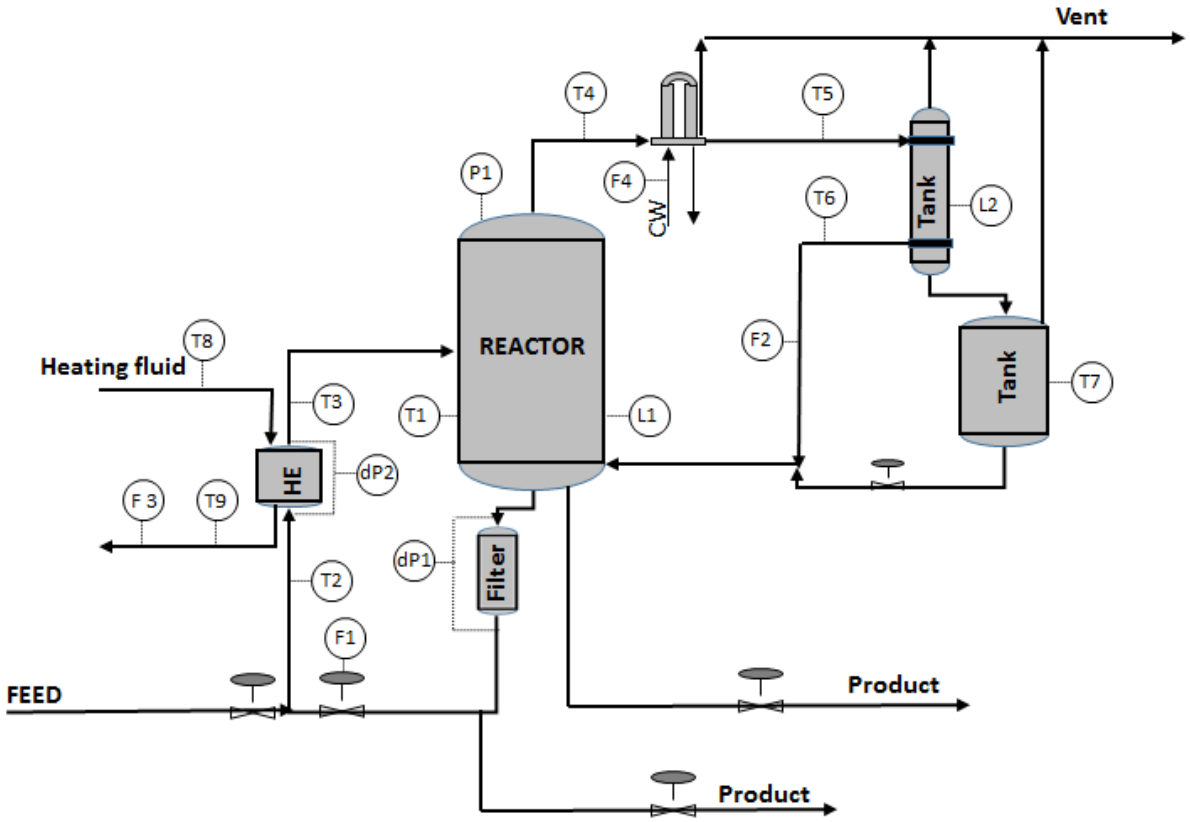

Figure 7.1: Batch reactor process flow sheet.

Currently, these problems can persist for many batches before personnel identify the problem by trial and error and take corrective action. Delays in diagnosing problems lead to abnormal batches and off-spec product. Each batch that underperforms causes reduced mixing during the batch and an extended heat-up period. Sub-optimal operations can affect the product quality and reduce the yield of the desired product. The reduced yield not only has the associated opportunity costs of lost product, but when the composition of the product changes, additional unreacted components must be stripped at a finishing plant downstream, raising the energy costs

needed to meet the final product specifications. Furthermore, because the product quality is judged based on an offline lab test, several batches can elapse before a problem is diagnosed and fixed. Fixing these issues can result in substantial financial savings.

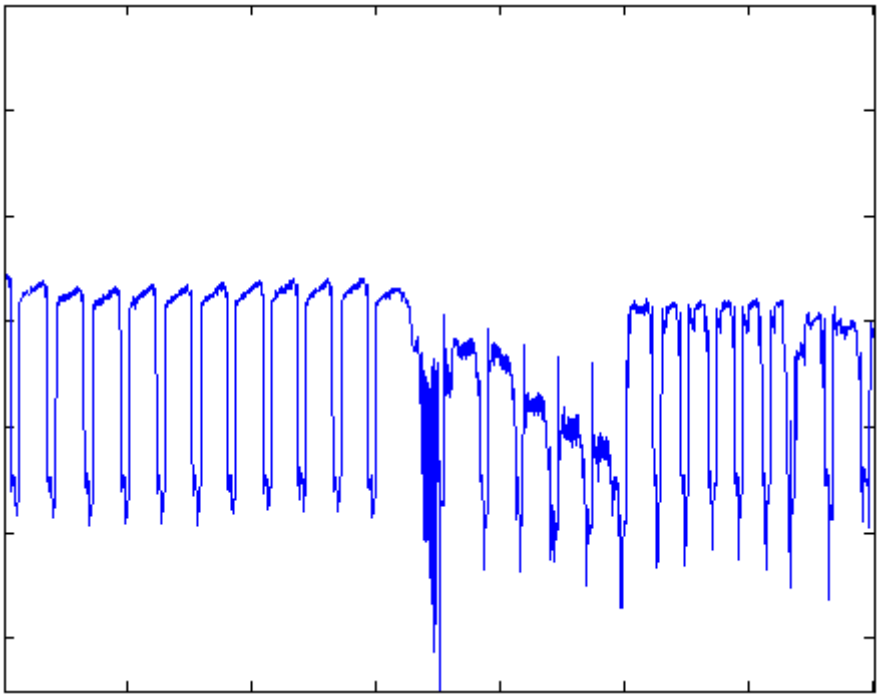

Figure 7.2: Sticky valve faults can be spotted from patterns in PA flow.

Using data from the reactor described above presents a new set of challenges from previous work on the Tennessee Eastman process simulation and the separation tower. The most important of these is defining the region of normal operations in spite of constantly changing batch dynamics. The goal of this research is to create a suitable model for detecting and diagnosing the process faults on the pump around stream: filter clogging and sticky valves.

7.3 Dynamic Time Warping for Batch Synchronization and Unfolding

The batches used in this analysis take place over a variety of time spans. The shortest runs use about an hour and a half minutes while the longest batches in the set ranged over 6 hours where two or three runs were mistakenly combined together. These time variations needed to be removed

by synchronization and multiway unfolding to design a data-based batch monitoring algorithm and allow the holistic consideration of each batch's data.

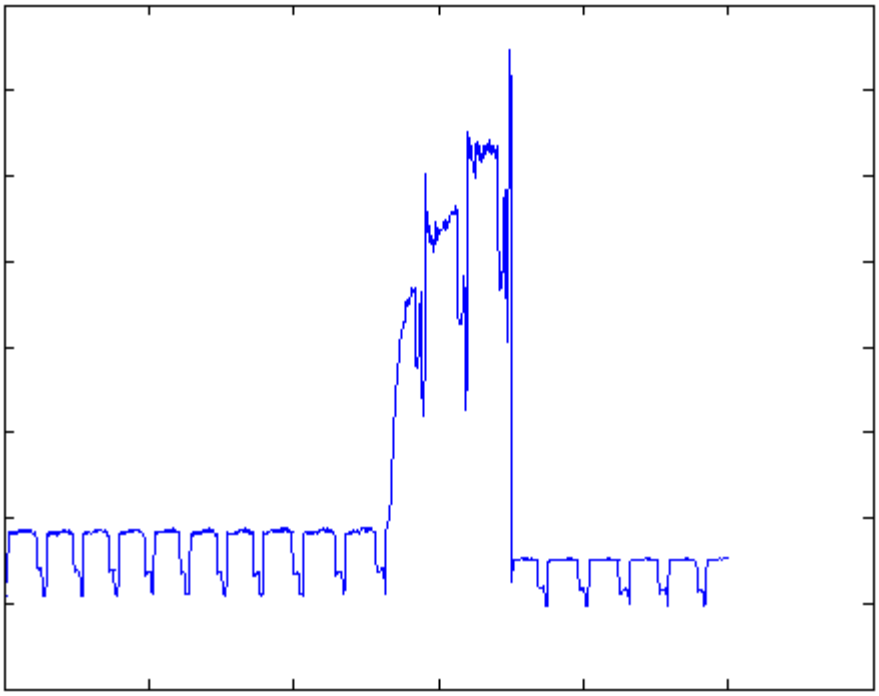

Figure 7.3: Clogged filter batches can be seen from a changed pattern in dP1 pressure drop through the filter.

Figures 7.4 through 7.6 illustrate a few cases crucial to our fault detection problem of how DTW-synchronized data from several batches while preserving the key behavior of each batch. In each figure the bold black line is the behavior recorded in the raw historical data from the database. The average batch trajectory of each variable used by DTW in the synchronization is noted by the green line. Data in red comes from the DTW synchronization, where starred data points note data that is included in the multiway unfolding. Because 31 data points are included from each batch, this means that when multiplied by the 18 sensors monitored, the synchronized, unfolded data set has a dimensionality of 558.

Figures 7.4 and 7.5 show synchronized batch data from the reactor temperature and pressure trajectories. Synchronized data is the raw data after synchronization with DTW while unfolded data refers to the multiway unfolding of the synchronized data. Figure 7.5 shows that normal batches can have a big offset, affecting the fault detection statistics without any difference in performance. Compared to the offset created by variations in the normal batches with those arising from the sticky valve fault in Figure 7.6, we can see that monitoring a batch for changes in one variable will be difficult – large variations can arise from normal operations that can sometimes overlap the variations caused by faults in operations.

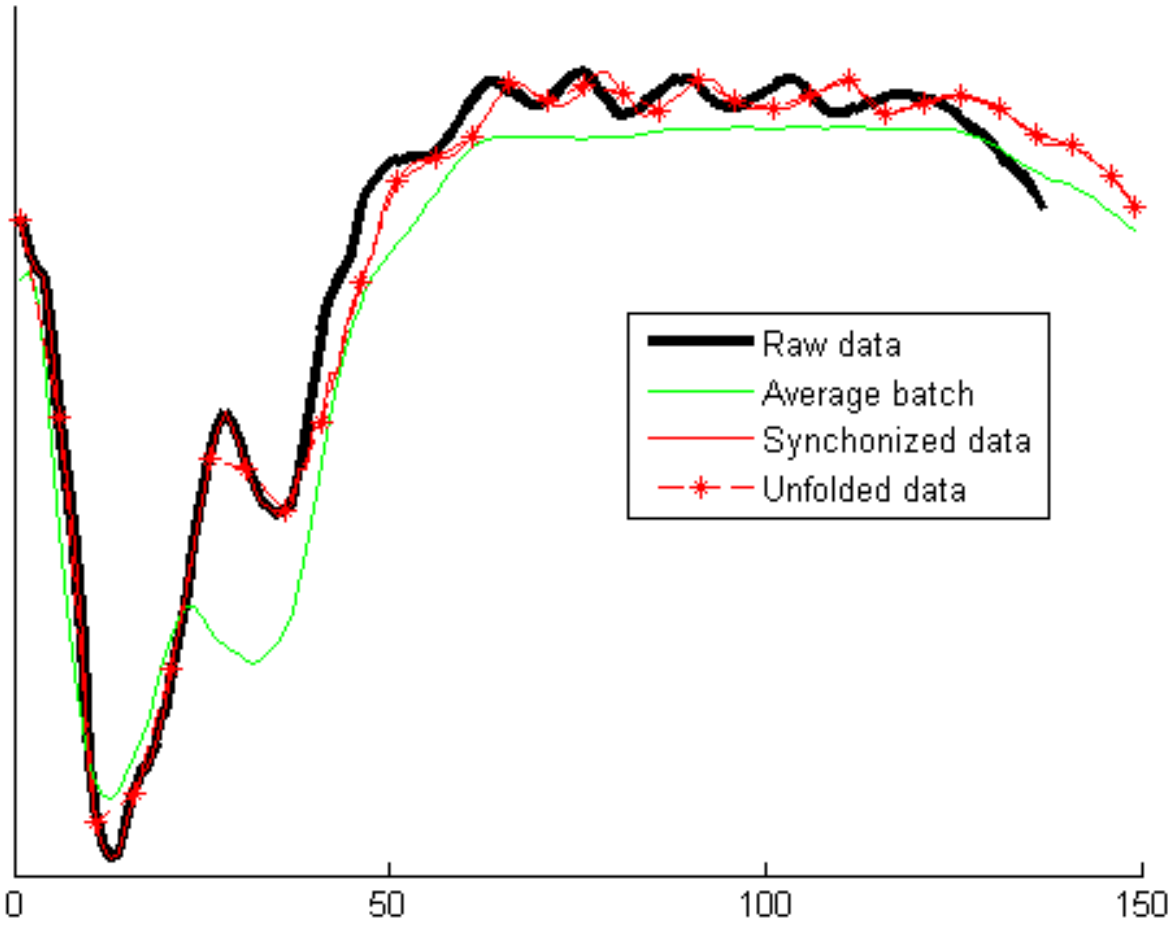

Figure 7.4: This synchronized, unfolded batch temperature trajectory matches the raw data well.

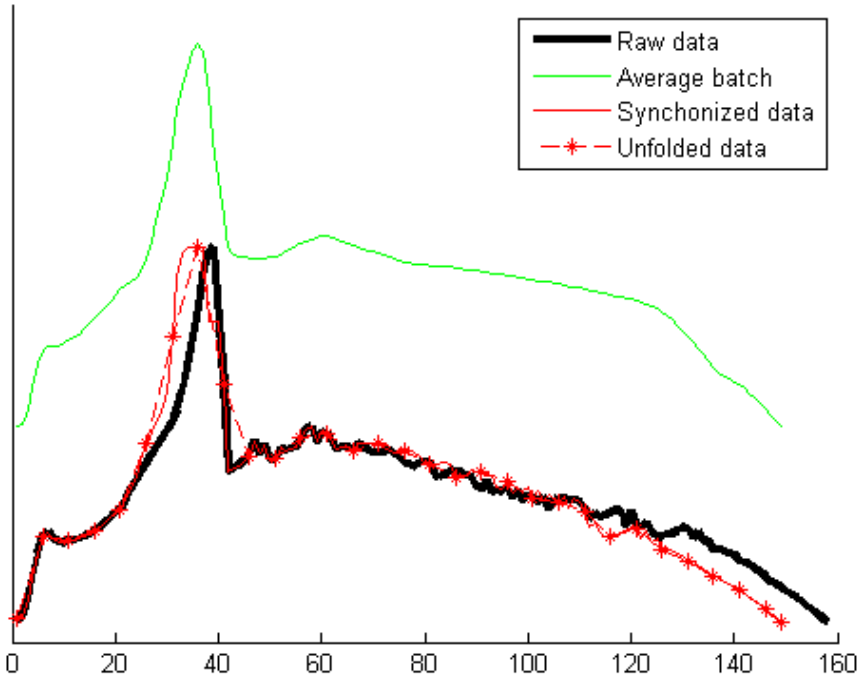

Figure 7.5: This shows the trajectories of reactor pressure. While this batch's pressure is offset, the general pattern of the batch is preserved.

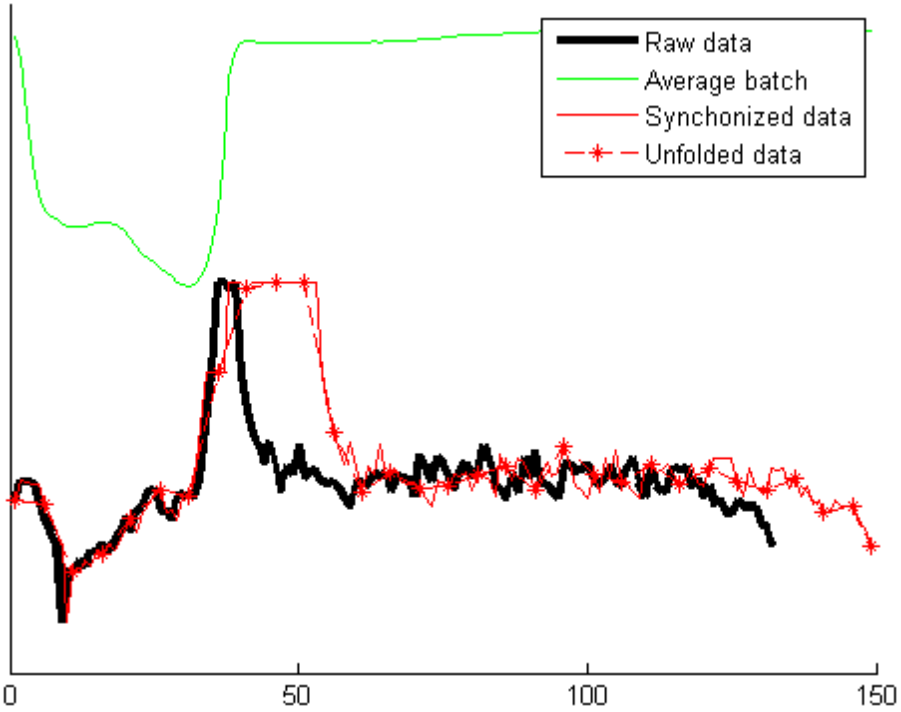

Figure 7.6: The synchronized PA flow from batch with a sticky valve still preserves the characteristic behavior of the fault while still synchronizing the batches relative to the average batch.

7.4 Fault Detection and Diagnosis on Batch Process

In this section, the methods of Chapter 4 are combined with DTW and multiway unfolding discussed in Chapter 2 to build FDI for time-varying batch processes and evaluate using cross-validation. Three different data based classifiers from Chapter 4 were tested against each other for the task of fault detection and diagnosis: PCA, 1-SOM, and MSOM. Results show the difference a more non-linear monitoring algorithm like SOM or MSOM could have on batch process monitoring.

We used the holdout method (or two-fold cross-validation) to separate training data from the testing dataset and measure the predictive performance of each statistical model. Table 7.1 shows the relative distribution of data between the different faults on the polymerization process. Typical of plant fault data sets, there is a large amount of data from normal operations, and relatively little from abnormal conditions. As in the separation tower study in Chapter 6, we used the SMOTE preprocessing technique from Chawla (2002) to balance the data sets for training classifiers. Data from the sticky valves were SMOTE at 400% while Normal and clogged filter data sets were reduced.

Table 7.1: Sizes of reactor fault data sets

Reactor Condition	Initial batch groups	Validation batches after cross-validation	Training batches after SMOTE
Normal	1611	806	50
Clogged Filter	124	62	50
Sticky Valve	20	10	50

The QE bound for MSOM fault detection was calculated in the same manner as discussed in Chapter 6. Figure 7.7 shows a histogram for one set of training data used in this study and shows that the training data are approximately exponentially distributed. We used a 95% threshold to

determine the location of the bounds of MSOM's normal region. Figure 7.8, a. and Figure 7.8, b. shows the SOM maps trained for the 1-SOM models. Both define a contiguous map region corresponding to clogged filter and sticky valve reactor conditions.

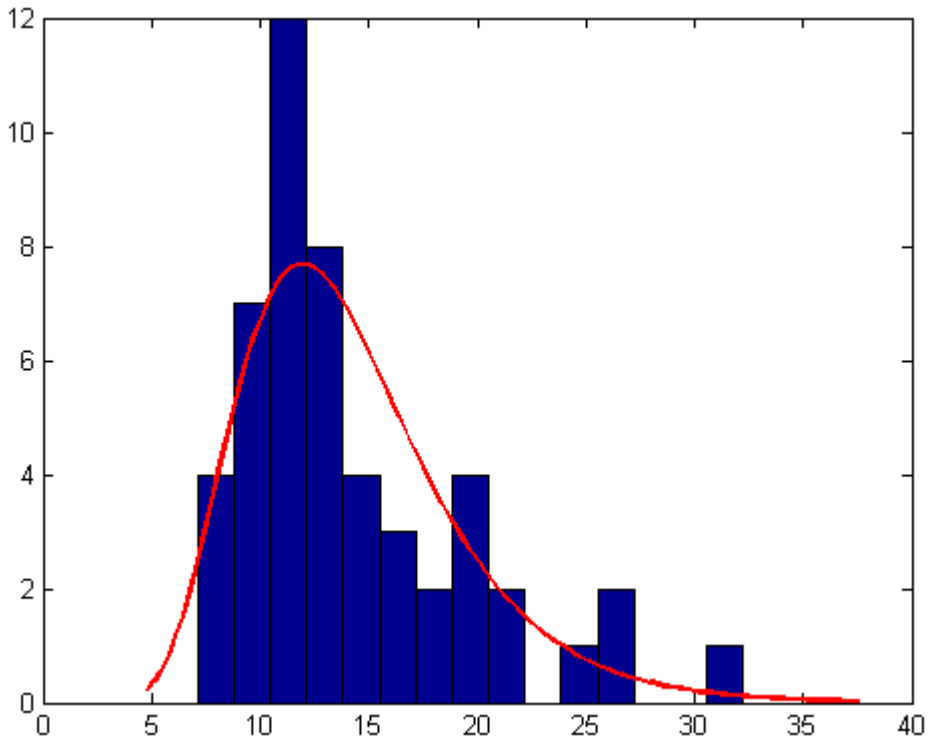

Figure 7.7: The QE of the training data relative to the map fit to normal operations for MSOM.

In each of the following two sections, PCA, 1-SOM, and MSOM fault detection strategies were used to detect batches affected by filter clogging or sticky valves with results in Tables 7.2 and 7.3. PCA and MSOM models were fit to data from the normal data set, while 1-SOM was trained to data from both normal data and fault classes according to 1-SOM monitoring defined in Section 4.4. False alarm rates were generated by testing whether each method would incorrectly register a fault on normal data. The false alarm results in Tables 7.2 and 7.3 are the same for PCA and MSOM, but because the 1SOM model differs in each case, it will report different false alarm rates.

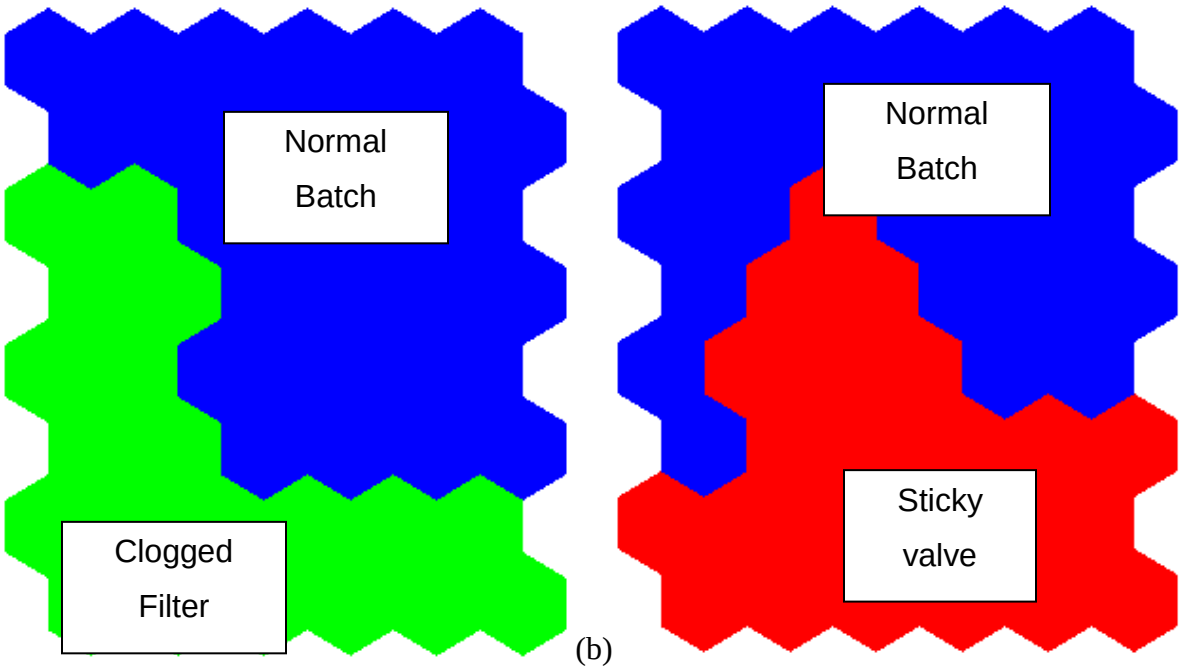

Figure 7.8: 1-SOM maps fit for fault detection of the clogged filter (a) and sticky valve (b) conditions.

7.4.1 Detection of filter clogging

Running both filter clogging testing data sets through the three fault detection models yielded the detection results in Table 7.2. Both PCA and MSOM successfully detected the filter clogging event, while SOM had a significantly lower detection rate. While PCA had the highest detection rate, it had a higher false alarm rate compared to the MSOM method. Consistent with results on the Tennessee Eastman Process, 1-SOM had a much higher false alarm rate compared to the other methods: more than a third of normal batches were incorrectly classified as faulty.

Table 7.2: Filter clog detection

	% Detected	% False Alarm
PCA	99.2%	17.3%
1-SOM	66.9%	34.5%
MSOM	94.4%	10.5%

7.4.2 Detection of valve sticking

Processing sticky valve batches with each monitoring yielded the results in Table 7.3. The sticky valve fault has a smaller effect on process measurements compared with the clogged filter fault, making it much more difficult to detect. MSOM produced the best detection and false alarm rate, but no method exceeded 50%.

Table 7.3: Valve sticking detection

	% Detected	% False Alarm
PCA	35.0%	17.3%
1-SOM	40.0%	15.5%
MSOM	45.0%	10.5%

7.5 Fault Detection Discussion

Hit diagrams of the 1-SOM maps used for the fault detection studies are given in Figure 7.9, a. and Figure 7.9, b. Both hit diagrams illustrate how a large amount of normal data is projected on to the faulty areas close to normal, leading to false alarms. Poor BMU matching may be due to the high dimensionality of the unfolded batch data. Consistent with the relatively poor results in detecting the sticky valve fault, the areas of the sticky valve region closest to in the map in Figure 7.9, b. contain the most incorrectly classified normal region, indicating that the nodes composing this region, and by extension the sticky valve training data used, are closer to normal than in the clogged filter case.

MSOM outperformed 1-SOM because each map vector in an MSOM map is trained only with data from its particular fault. Specialized MSOM maps contain fewer characteristics from other faults while 1-SOM regions with mixed characteristics can only have one class. This leads to misclassifications, particularly in transitional regions while a fault is in its early stages. MSOM

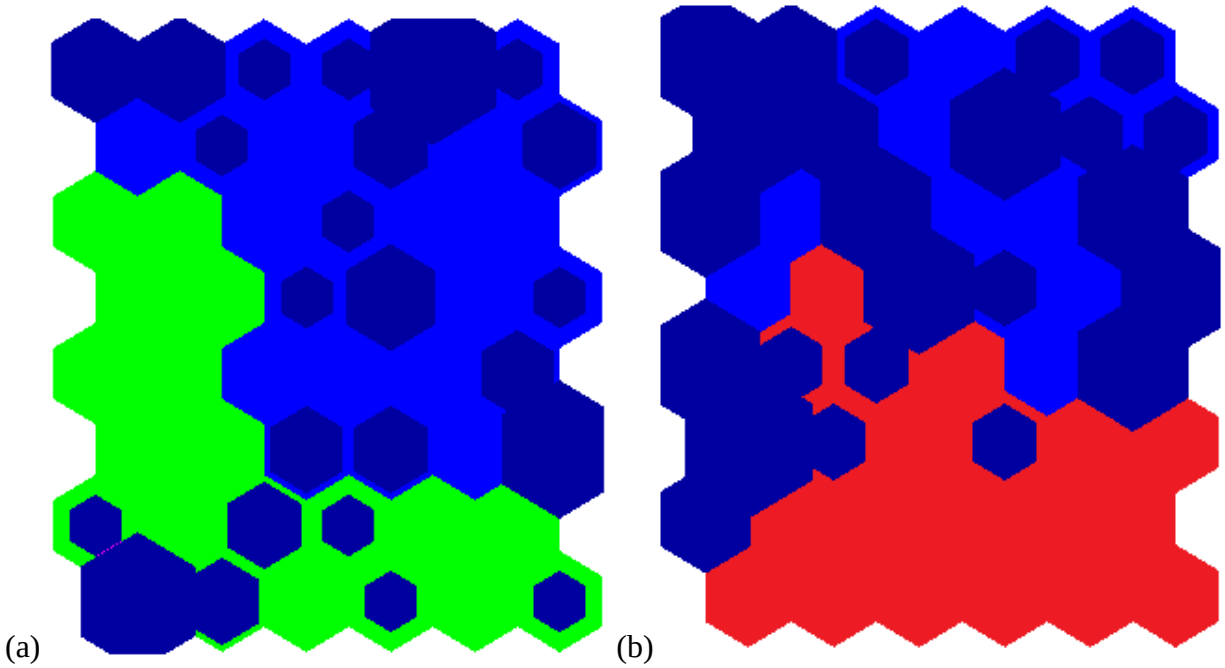

Figure 7.9: Hit diagrams of normal data on the maps shown in Figure 7.8. In both cases, a large amount of normal data is being projected on to the faulty side of the map, leading to misdiagnosis by the 1-SOM classifier.

would have different map nodes trained by different data sets, so map nodes in a mixed characteristic region move closer to their faulty trajectory and give a better classification of the transition regions.

Figures 7.10 and 7.11 show the fault detection statistics generated by the application of PCA and MSOM to a cross-validation fold of the data. The data have been organized such that the clogged filter points are at the beginning of the series, sticky valves are at the end of the data series, and all normal batches are in the middle. These figures show the larger number of false alarms by PCA and how much more strongly they are registered by the T^2 statistic compared to QE. Comparing the sticky valve points on the far right of the two graphs shows the slightly larger number of correctly detected sticky valves by MSOM compared to PCA.

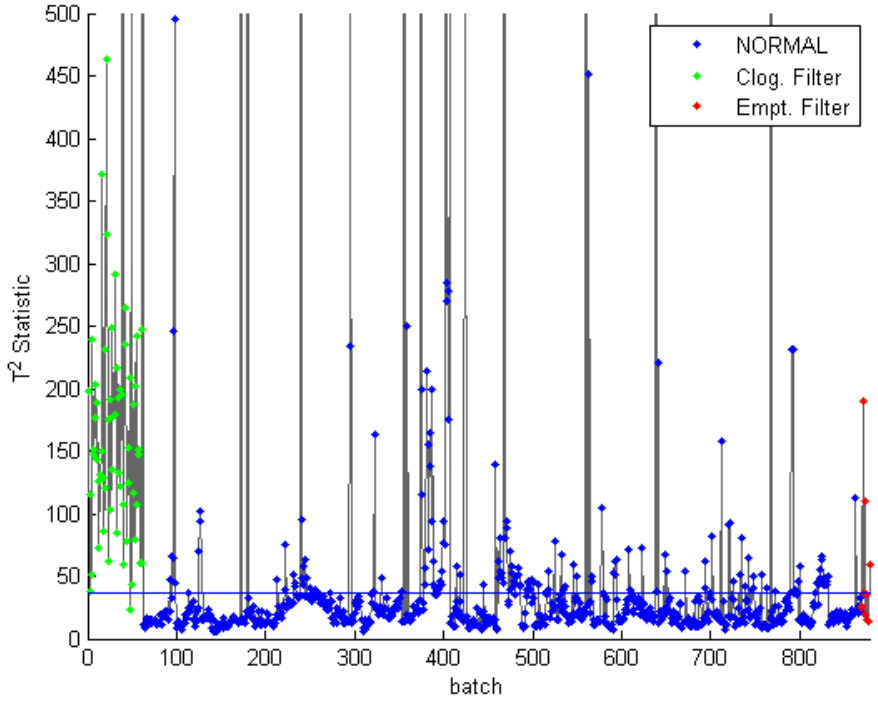

Figure 7.10: T squared statistic generated by MPCA.

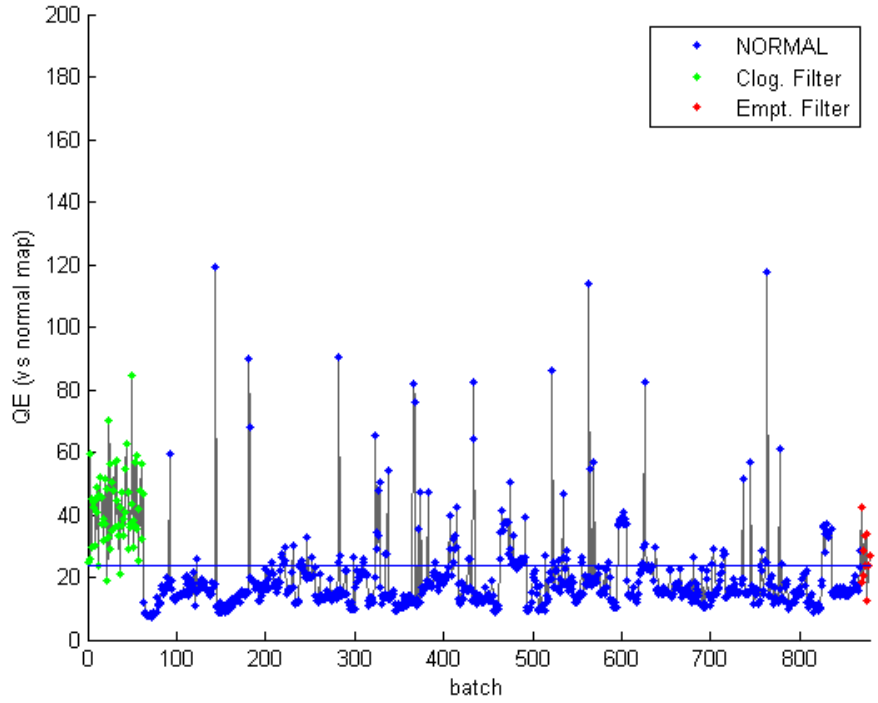

Figure 7.11: QE results from MSOM.

7.6 Diagnosis of Both Reactor Conditions

Lastly, the multiway adaptations of each technique were tested head-to-head on the fault diagnosis task. Table 7.4 presents the results. 1-SOM and MSOM perform approximately the same as it did for the fault diagnosis task, except 1SOM had a significantly higher false alarm rate due to additional fault classes affecting the map's characterization of normal operating conditions. The result that stands out the most is PCA's failure to diagnose any batch with a clogged filter. The reason for this can be seen in Figure 7.12, a. showing the fault diagnosis T^2 statistic generated by each fault PCA model at each time point checked. Likely due to issues with the small size of the training data used in creating the sticky valve model, it yields very low fault detection statistics for almost every type of batch, meaning MPCA consistently classified all fault batches with elevated T^2 statistics as sticky valves, even clogged filters batches. Figure 7.12, b. shows MSOM's improved diagnosis performance: the correct class has the lowest QE value most often, meaning the map corresponding to the correct class is the closest to that data point.

Table 7.4: Diagnosis of batch faults

	% Correct Diagnosis		
	MPCA	SOM	MSOM
Clogged Filter	0.0%	66.9%	91.9%
Sticky Valve	35.0%	45%	40.0%
1-SOM False alarm rate:		53.5%	

7.7 Conclusions

This study demonstrated the improved process monitoring abilities of the MSOM technique over PCA-based process monitoring on an industrial-scale batch process. We used data-based process monitoring techniques to model batches with clogged filters and sticky valves in the reactor pump-around system. These events affect the product quality and their detection can

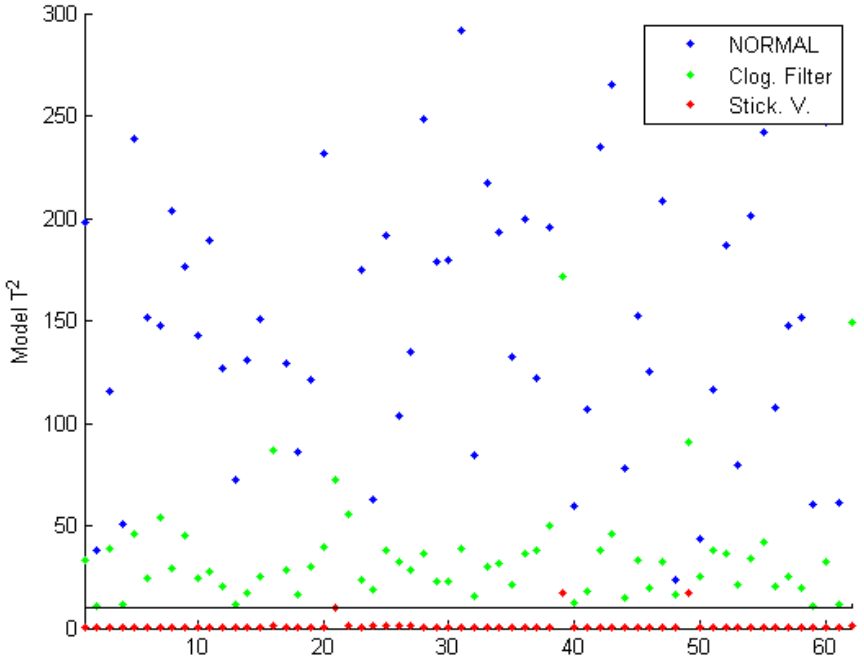

(a)

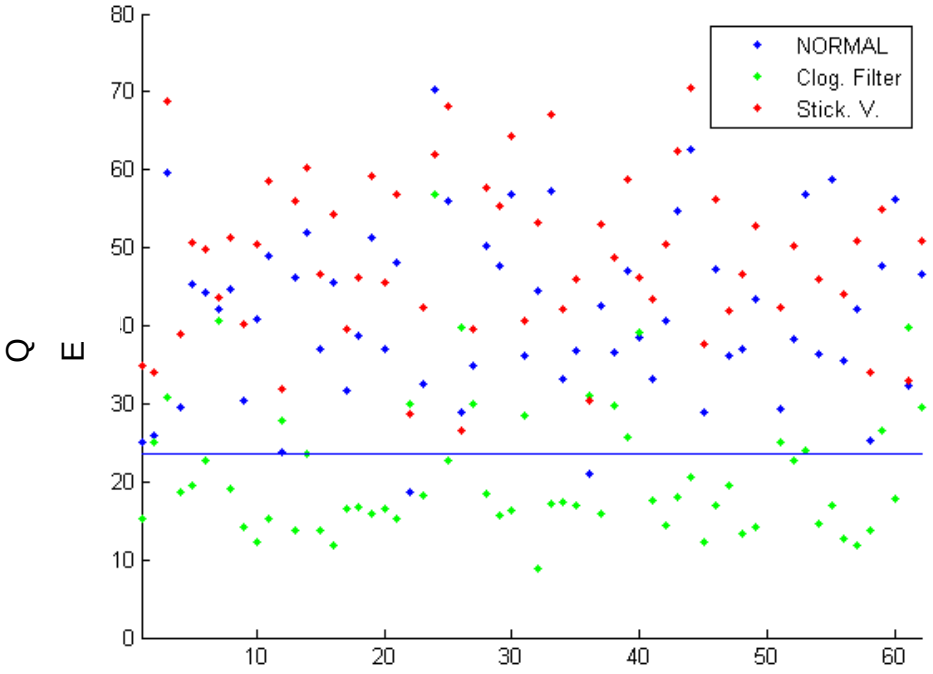

(b)

Figure 7.12: (a) From MPCA results, low T2 statistic from the sticky valve PCA model causes consistent misdiagnosis of clogged filter data. MSOM result plotted in (b) is more accurate. The horizontal blue line corresponds to each map's NOR threshold.

improve the consistency of the reactor product and lower separation costs at a product finishing plant.

The batch process monitoring schemes applied require advanced preprocessing techniques to account for process dynamics and to allow us to adapt steady-state process monitoring techniques. DTW was used to synchronize each batch into the same timeframe and enable the use of multiway unfolding to reduce complex batch data sets into a single matrix for analysis. Finally, the SMOTE procedure oversampled the smaller data set and undersampled the larger sets to ensure that each group of data had a balanced representation in the training set.

Three process monitoring strategies were used to monitor this process and detect faults: PCA, SOM, and MSOM. Batches with clogged filters were effectively detected by all the techniques considered, however the sticky valve was much more difficult to detect. The most effective technique at detecting the sticky valve, MSOM, only detected 45% of sticky valve faults. Similar difficulties were encountered in diagnosis. PCA consistently misclassified clogged filters as sticky valves due to the properties of the training data, while SOM had a very high false alarm rate. MSOM retained a similar performance as in the detection steps and achieved the best performance on challenging batch process.

7.8 References

Nomikos, P., & Macgregor, J. F. (1994). Monitoring batch processes using multiway principal component analysis. *American Institute of Chemical Engineers Journal, 40*(8), 1361-1375.

Yao, Y., & Gao, F. (2009). A survey of multistage/multiphase statistical modeling methods for batch processes. *Annual Reviews in Control, 33*, 172-183.

Chapter 8 - FastMan: A Software Tool for Data Mining Chemical Process Data

8.1 Introduction

The overall goal of this dissertation is to make data-driven process monitoring simpler to implement and maintain. Previous research on data clustering and dimensionality reduction evaluated a set of tools for mining chemical process historical databases and separating normal data from faulty data. We have studied a suite of tools to help lower the barrier for implementing supervised process monitoring algorithms in chemical plants, but without a software user interface, only engineers proficient in writing coding or other data mining tools could utilize the algorithms previously studied.

The final step is to bring all the tools previously researched into a single chemical process data mining software tool. Data mining is a relatively new field of study and is currently not a common part of a typical plant engineer's training. Few chemical process engineers have data mining skills, so a data mining software tool should be simple to use and insulate users from the intimate mathematical details of the data mining algorithms while at the same time assist them in conducting a valid analysis.

This computer program would be specialized for chemical process time series data mining. The key is to combine projections by dimensionality reduction techniques and data clustering results with a time series plot of the different measurements an engineer might be studying. After the engineer has used data clustering and dimensionality reduction to settle on new labels for the historical data, the output of this program can be saved and loaded into a tool with the relevant process monitoring algorithms for training or updating.

This chapter discusses FastMan (Fast Manual data classification), an assisted process data clustering tool developed as part of the research in this dissertation. The basic functionality of this

tool is demonstrated on a data set drawn from the industrial scale separation tower studied in Chapter 6.

8.2 Software Description and Demonstration

Figure 8.1 shows the initial user interface (UI) before any data has been loaded and important areas for its data mining functionality. The left of the UI will show a time series plot of

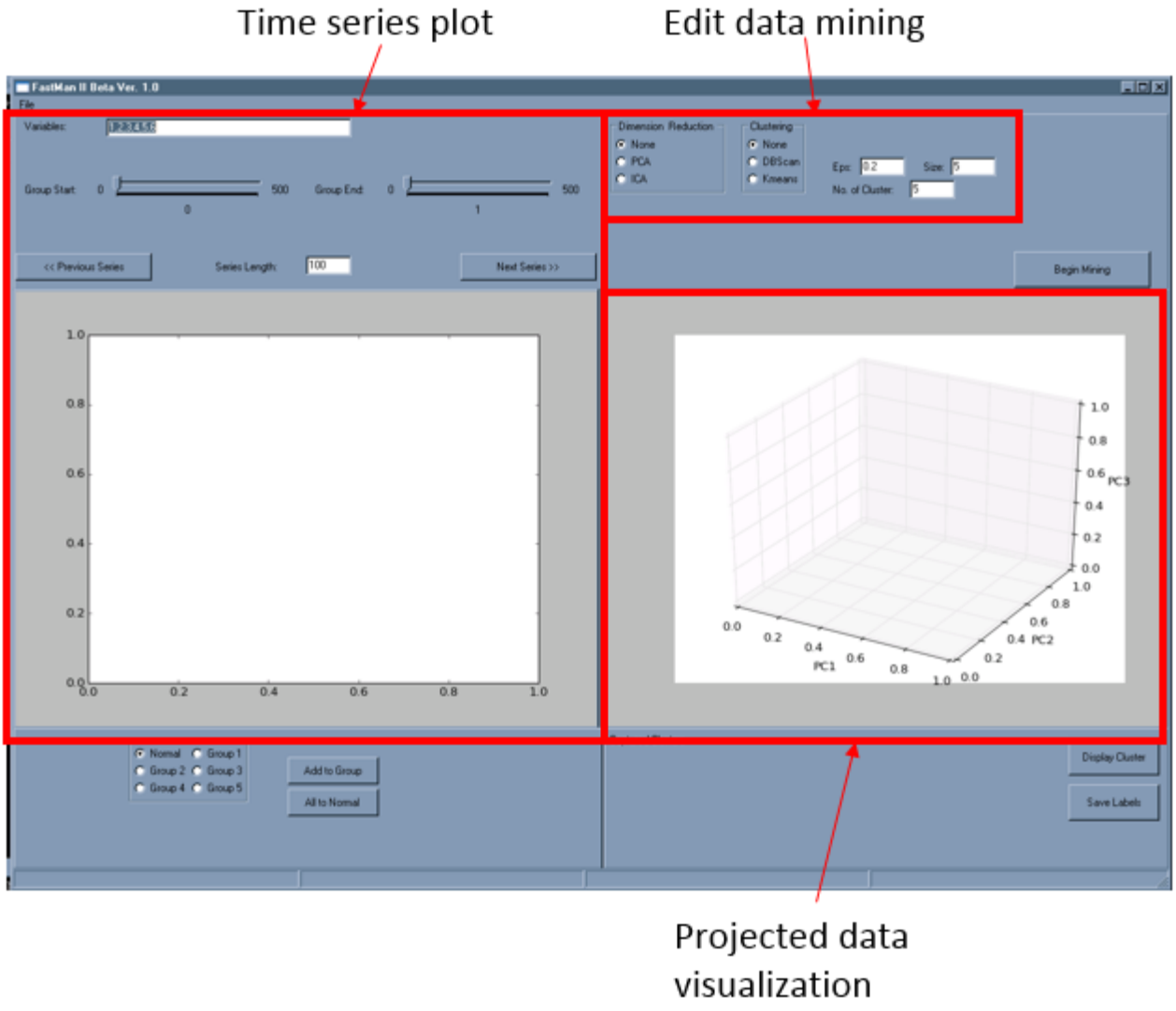

Figure 8.1: FastMan UI before data has been loaded. Clustering and projection figures are shown adjacent to each other to facilitate comparisons with time series data.

the data from the chemical process. The user has control over how much of the data to show and which sensors' data to plot. The slider bars are used to select data for group classification. The radio buttons at the bottom left are for the creation of user-specified data. The user must use the slider bars to select a series of data and click a radio button to add the specified label to the selected data.

The right side of the UI uses the data clustering and dimensionality reduction tools. The controls at the top can change the parameters of the data clustering algorithm used (k in K-means for example). The user can also select which dimensionality reduction technique to use to project the data with principal component analysis (PCA) functioning as the default. Arranging the two screens side by side in this manner is important because it highlights the connection between process behavior visible in the time series data and the movement of the state of the process in the DR projected data space on the right.

Figure 8.2 shows FastMan's UI with time series data from the industrial scale separation tower. The plot on the left shows a time series plot of all the data after normalization to unit mean and variance. By default, all sensor patterns are shown in the time series plot window. As no data clustering technique has been selected, the projected data to the right is shown in one color.

The screenshot in Figure 8.3 shows FastMan after DBSCAN clustering has been performed. Noise data is shown in black while the other clusters are plotted in different colors. Using controls in the bottom right of the UI, the user can select data from different clusters and give them custom labels. Selection of a cluster highlights its data in the time series plots to the left, allowing simpler evaluation of the data relative to the actual sensor behavior in the process. The light green cluster in the figure is from a single continuous series of data which corresponds to the fault condition the clustering research in Chapter 6 sought to locate.

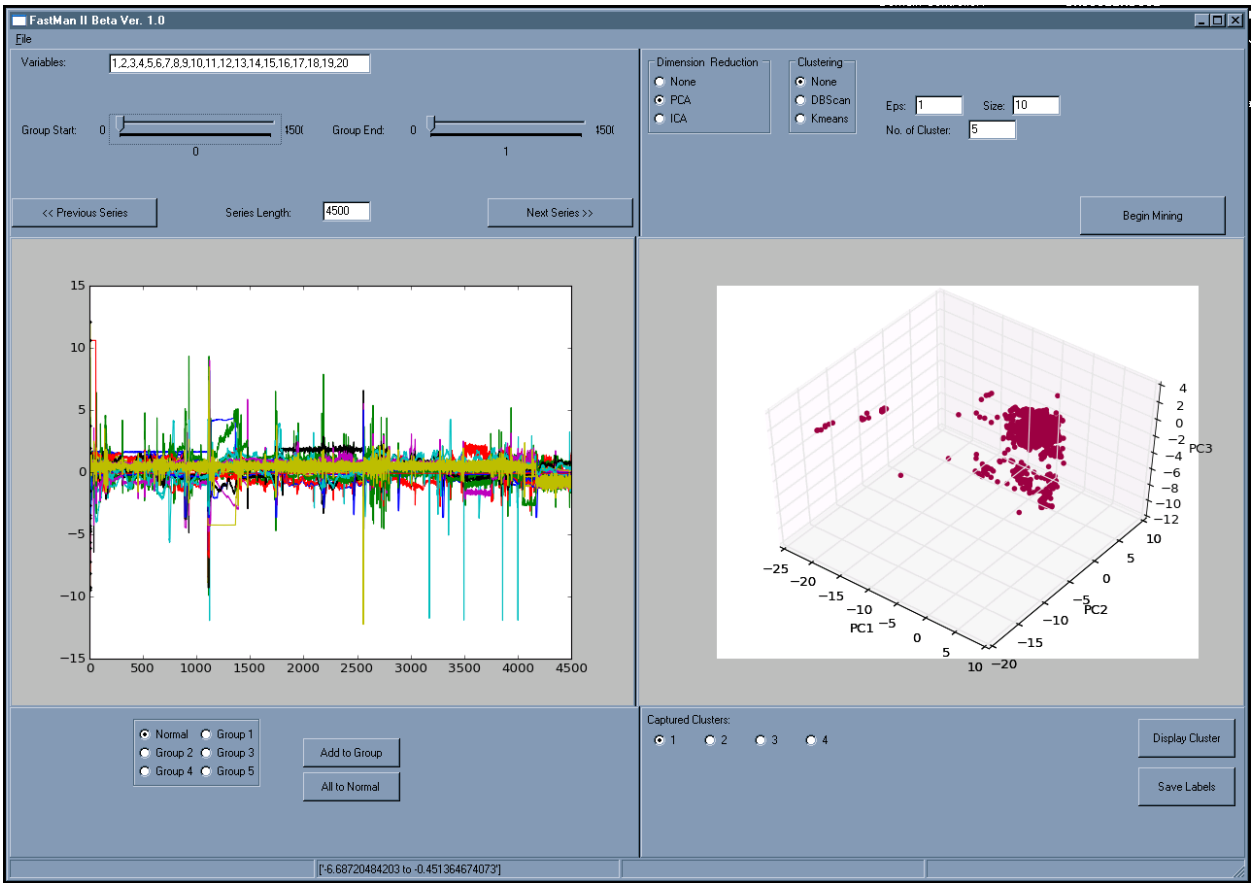

Figure 8.2: FastMan UI with data from the industrial separation tower.

8.3 Conclusions

This chapter demonstrated a software tool that could be used to assist in the creation of training data for supervised classification algorithms from raw chemical process data. The demonstration showed how projections of high dimensional process data can be clustered and data from process events of interest can be located in large amounts of chemical process data. Future work could further develop this tool and integrate the clustering functionality with a program to train, maintain, and use PCA, SOM, or other process monitoring algorithms.

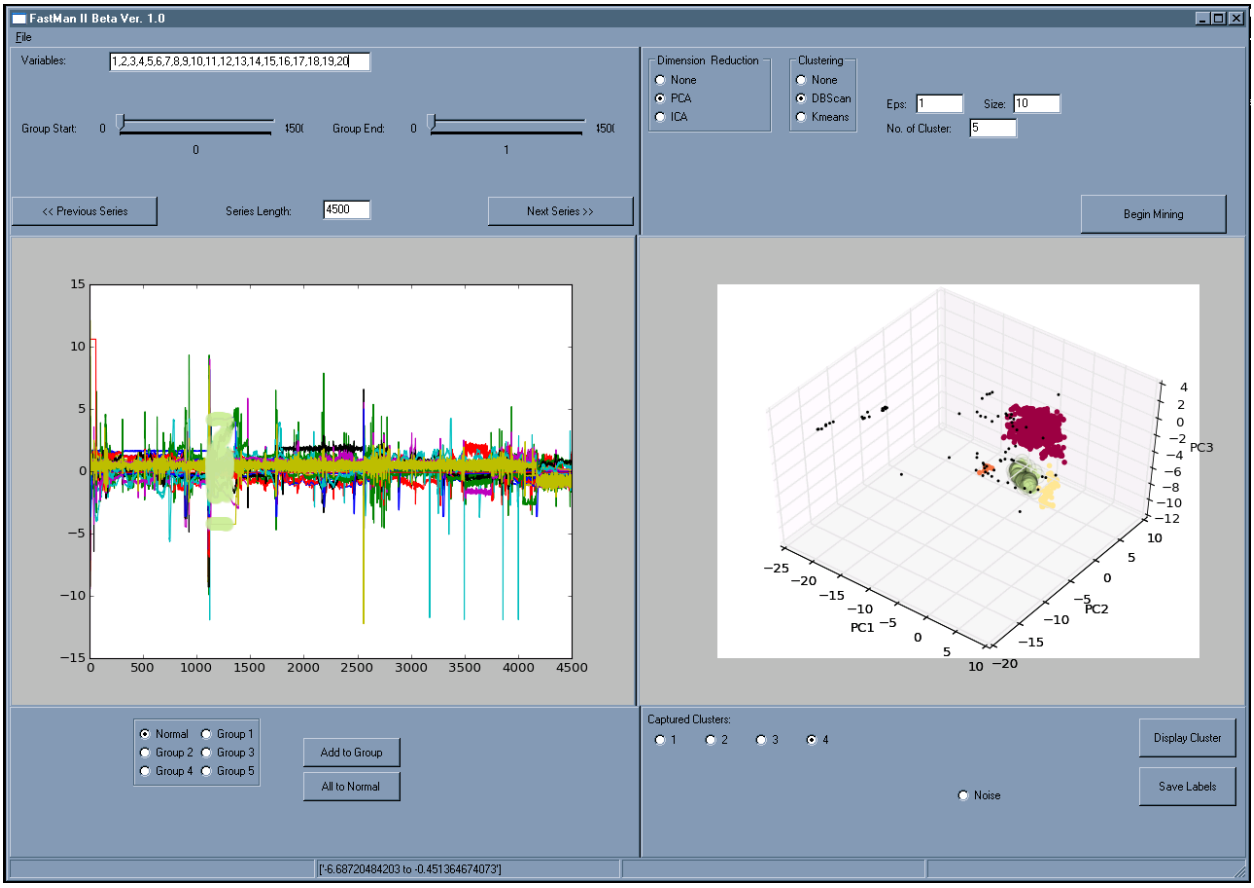

Figure 8.3: Projected data clustering results are displayed on the left. When the user selects a cluster its constituent data is highlighted in the time series on the right.

Chapter 9 - Conclusions

9.1 Summary of Results

The research in this dissertation has focused on improving the performance and construction of process monitoring algorithms. The contributions address challenges in finding training data in unlabeled chemical process databases, in process monitoring tasks, and in novelty detection. Each aspect of this research was demonstrated on a simulation and validated on real industrial processes. In summary, the findings of this dissertation are as follows:

- Improved process monitoring with multiple self-organizing maps (MSOM): we introduced a novel process monitoring strategy using multiple self-organizing maps to perform the complete suite of process monitoring tasks including fault detection, identification, and diagnosis. We demonstrate the advantages of MSOM by monitoring the benchmark Tennessee Eastman process and diagnosing a reduced set and the complete set of process faults. MSOM performed better than more standard techniques at detection and diagnosis while generating more accurate and informative contribution plots for identifying the section of the process responsible for a faulty status.
- Batch process monitoring with MSOM, dynamic time warping (DTW), and multiway unfolding: we adapted MSOM to batch process monitoring using multiway unfolding to process the batch data and DTW to synchronize each batch to a common time frame. The results of a batch monitoring study demonstrate MSOM's superior performance in detecting and diagnosing two faults in the batch.
- SOM applied for novelty detection on separation tower: we used SOM to model 3 different operating regimes of an industrial-scale separations tower. The SOM model we created diagnosed the process state more accurately than PCA models trained to the same set of

data. Furthermore, SOM contribution plots indicated the variables at the bottom of the tower that were responsible for the faulty status.

- Unsupervised classification of chemical process data: a data mining scheme based on dimensionality reduction and data clustering separated faulty process data from normal operations data in two case studies on the Tennessee Eastman process and the industrial-separation tower. Results between the different combinations of reduction and clustering techniques varied, but in general dimensionality reduction improved the accuracy of the clusters found relative to their true labels.
- FastMan - a process data mining software tool: we created a software tool designed to simplify the widespread application of supervised and unsupervised classification methods by engineering practitioners. FastMan connects projections of high dimensional data and data clustering results to time series plots of sensor data. The side-by-side visualization and plots of process data make data from abnormal operations easier to distinguish from normal operating data and simplifies the use of this data in fitting process monitoring methods.

9.2 Future Research Recommendations

The research in this dissertation opened new avenues of research in using data mining and machine learning for process monitoring. The following questions naturally follow from the results in this dissertation:

- Can data mining and machine learning predict equipment faults before they occur? Anticipating the failures in process equipment could offer substantial savings compared to fixed replacement maintenance schedules and avoid the costs of unexpected equipment failures in run-to-failure schemes.

- Given a set of labels from data clustering, what unsupervised clustering metrics are best for finding optimal clustering parameters for a given set of data? From the results of the Davies-Bouldin Index (DBI) in the complete clustering results of Appendix A, the most accurate clustering results do not always coincide with the best DBI value. Unsupervised clustering metrics are important tools to judge the suitability of clustering results, and better metrics could make cluster parameter selection easier.
- Given the discovery of several clusters in an industrial data set from different time periods, how can an engineer know the significance of the difference? It is possible that an engineer can observe two separate clusters that appear to be normal, but not be able to determine a clear reason for the difference. Further research on statistical or computational tools can address this data clustering issue and assist in interpreting clustering results.
- Many features could be added to FastMan to enhance its capabilities. There are certainly more dimensionality reduction and data clustering techniques than those implemented in Chapter 8, but additional features could make the software more interactive. Additional analysis tools to isolate the sensor measurements that differentiate clusters from each other are crucial for assisting engineers in extracting meaningful knowledge from clustering results. Also, the UI could be further modified to better suit chemical engineers. For example, chemical process databases contain many discrete variables that correspond to feed grades or changes in operations which could affect the clustering and monitoring of the process, and tools could be added to easily clean the loaded dataset using these variables.

Appendix A - Complete Clustering Results

In this dissertation, three data sets were studied using six dimensionality reduction techniques and four clustering techniques, while varying a parameter of each clustering technique between five different values. This approach gives rise to 120 different clustering runs, of which only the best of each DR and clustering combination are selected and presented with the results earlier. However, the remaining results are a important window into the challenges of data clustering and unsupervised classification. It is difficult to identify an effective parameter setting for some clustering techniques, and many of the results shown below vary dramatically depending on the precise setting of the key clustering parameter. For example, in Table 1 below, the best DBSCAN with no DR result was produced an ARI of 0.48, while other parameter setting over the same DR setting yielded ARIs of less than 0.1 (very inaccurate).

An important result reported in these results and not discussed is earlier is the V-measure and Davies-Bouldin Index (DBI). V-measure is the weighted average of the Completeness and Homogeneity of each clustering result and helps to judge those metrics in combination. The DBI of each clustering result is particularly important as DBI is an unsupervised cluster evaluation metric. In a real data clustering study where previous data labels are not known, DBI would be the only evaluation metric available to engineers. In many cases the DBI may not provide a good characterization of accuracy because its definition biases it towards spherical clusters.

Appendix Table 1: Tower data full clustering results from Chapter 6

DR tech	cluster tech	param	No. clust	ARI	Homog.	Complete.	Vmeas	DBI
No DR	DBSCAN	0.99	3	0.01	0.02	0.07	0.03	1.43
No DR	DBSCAN	0.95	8	0.48	0.67	0.32	0.43	1.29
No DR	DBSCAN	0.9	19	0.08	0.87	0.14	0.23	1.97
No DR	DBSCAN	0.8	24	0.06	0.87	0.13	0.22	2.33
No DR	DBSCAN	0.7	29	0.06	0.85	0.12	0.22	2.78
No DR	kmeans	2	2	0.08	0.07	0.03	0.05	2.17
No DR	kmeans	3	3	0.18	0.48	0.18	0.26	1.76
No DR	kmeans	4	4	0.19	0.57	0.21	0.31	1.18
No DR	kmeans	5	5	0.11	0.60	0.16	0.25	1.25
No DR	kmeans	6	6	0.07	0.65	0.14	0.23	1.26
No DR	Meanshift	1.8	4	-0.02	0.00	0.02	0.01	0.83
No DR	Meanshift	1.5	5	-0.02	0.00	0.01	0.00	0.53
No DR	Meanshift	1	10	0.58	0.47	0.44	0.45	1.11
No DR	Meanshift	0.5	11	0.08	0.83	0.14	0.25	1.91
No DR	Meanshift	0.2	37	0.01	0.19	0.05	0.08	1.34
No DR	BIRCH	1.8	3	-0.01	0.00	0.02	0.00	0.80
No DR	BIRCH	1.5	5	-0.01	0.00	0.01	0.00	0.59
No DR	BIRCH	1	8	0.07	0.10	0.04	0.06	0.72
No DR	BIRCH	0.5	62	0.03	0.80	0.10	0.17	0.71
No DR	BIRCH	0.2	474	0.00	0.90	0.06	0.11	0.70
PCA	DBSCAN	0.99	2	-0.02	0.00	0.02	0.01	1.23
PCA	DBSCAN	0.95	9	0.29	0.68	0.25	0.36	1.47
PCA	DBSCAN	0.9	16	0.09	0.84	0.14	0.24	1.90
PCA	DBSCAN	0.8	21	0.06	0.87	0.13	0.22	2.26
PCA	DBSCAN	0.7	28	0.06	0.85	0.13	0.22	2.77
PCA	kmeans	2	2	0.08	0.07	0.03	0.05	2.13
PCA	kmeans	3	3	0.19	0.56	0.21	0.31	1.55

PCA	kmeans	4	4	0.10	0.60	0.16	0.25	1.64
PCA	kmeans	5	5	0.18	0.60	0.18	0.28	1.09
PCA	kmeans	6	6	0.07	0.64	0.14	0.23	1.16
PCA	Meanshift	1.8	10	-0.03	0.01	0.02	0.01	0.59
PCA	Meanshift	1.5	7	-0.01	0.01	0.02	0.01	0.44
PCA	Meanshift	1	14	0.57	0.47	0.42	0.44	0.93
PCA	Meanshift	0.5	51	0.06	0.77	0.13	0.22	1.26
PCA	Meanshift	0.2	401	0.01	0.89	0.07	0.14	0.94
PCA	BIRCH	1.8	3	-0.01	0.00	0.02	0.00	0.78
PCA	BIRCH	1.5	3	-0.01	0.00	0.02	0.00	0.78
PCA	BIRCH	1	10	0.22	0.67	0.22	0.34	0.73
PCA	BIRCH	0.5	59	0.03	0.79	0.09	0.16	0.73
PCA	BIRCH	0.2	401	0.00	0.89	0.06	0.11	0.72
ICA	DBSCAN	0.99	2	-0.02	0.00	0.02	0.01	1.17
ICA	DBSCAN	0.95	8	0.59	0.46	0.44	0.45	1.70
ICA	DBSCAN	0.9	11	0.35	0.84	0.24	0.37	2.01
ICA	DBSCAN	0.8	20	0.07	0.87	0.14	0.24	2.44
ICA	DBSCAN	0.7	26	0.06	0.86	0.13	0.22	2.74
ICA	kmeans	2	2	-0.07	0.09	0.05	0.06	3.38
ICA	kmeans	3	3	0.57	0.44	0.48	0.46	1.52
ICA	kmeans	4	4	0.08	0.45	0.12	0.19	2.37
ICA	kmeans	5	5	0.24	0.45	0.20	0.27	1.52
ICA	kmeans	6	6	0.09	0.63	0.14	0.23	1.97
ICA	Meanshift	1.8	14	-0.02	0.01	0.02	0.01	1.15
ICA	Meanshift	1.5	14	-0.02	0.01	0.03	0.01	0.87
ICA	Meanshift	1	28	0.54	0.46	0.37	0.41	0.90
ICA	Meanshift	0.5	96	0.06	0.83	0.12	0.21	0.97
ICA	Meanshift	0.2	579	0.01	0.98	0.06	0.12	0.95
ICA	BIRCH	1.8	5	-0.01	0.00	0.01	0.00	0.68
ICA	BIRCH	1.5	5	-0.01	0.00	0.01	0.00	0.68

ICA	BIRCH	1	25	0.09	0.35	0.07	0.12	0.85
ICA	BIRCH	0.5	94	0.02	0.85	0.09	0.16	0.74
ICA	BIRCH	0.2	622	0.00	0.94	0.06	0.11	0.69
KPCA	DBSCAN	0.99	3	-0.10	0.04	0.03	0.04	0.90
KPCA	DBSCAN	0.95	8	0.02	0.31	0.09	0.14	1.75
KPCA	DBSCAN	0.9	17	0.03	0.57	0.11	0.18	2.52
KPCA	DBSCAN	0.8	27	0.06	0.84	0.13	0.22	2.49
KPCA	DBSCAN	0.7	25	0.08	0.89	0.15	0.25	2.16
KPCA	kmeans	2	2	0.07	0.25	0.12	0.16	1.75
KPCA	kmeans	3	3	-0.01	0.08	0.03	0.04	1.28
KPCA	kmeans	4	4	0.00	0.20	0.05	0.08	1.21
KPCA	kmeans	5	5	0.05	0.44	0.09	0.15	1.05
KPCA	kmeans	6	6	0.03	0.44	0.08	0.14	0.76
KPCA	Meanshift	1.8	1	0.00	0.00	1.00	0.00	inf
KPCA	Meanshift	1.5	1	0.00	0.00	1.00	0.00	Inf
KPCA	Meanshift	1	1	0.00	0.00	1.00	0.00	Inf
KPCA	Meanshift	0.5	8	0.05	0.61	0.11	0.18	2.96
KPCA	Meanshift	0.2	109	0.02	0.80	0.09	0.16	3.11
KPCA	BIRCH	1.8	1	0.00	0.00	1.00	0.00	Inf
KPCA	BIRCH	1.5	1	0.00	0.00	1.00	0.00	Inf
KPCA	BIRCH	1	1	0.00	0.00	1.00	0.00	Inf
KPCA	BIRCH	0.5	9	0.04	0.59	0.09	0.16	0.83
KPCA	BIRCH	0.2	105	0.01	0.82	0.07	0.13	1.05
Isomap	DBSCAN	0.99	4	0.58	0.47	0.46	0.46	1.82
Isomap	DBSCAN	0.95	17	0.08	0.88	0.14	0.24	1.77
Isomap	DBSCAN	0.9	23	0.05	0.88	0.12	0.21	2.52
Isomap	DBSCAN	0.8	34	0.04	0.87	0.11	0.20	2.74
Isomap	DBSCAN	0.7	35	0.05	0.97	0.13	0.23	2.43
Isomap	kmeans	2	2	0.62	0.39	0.52	0.44	0.51
Isomap	kmeans	3	3	0.22	0.40	0.16	0.23	0.80

Isomap	kmeans	4	4	0.08	0.50	0.13	0.21	1.17
Isomap	kmeans	5	5	0.06	0.44	0.10	0.16	1.02
Isomap	kmeans	6	6	0.10	0.74	0.15	0.25	1.09
Isomap	Meanshift	1.8	3	0.61	0.39	0.47	0.43	1.65
Isomap	Meanshift	1.5	5	0.60	0.47	0.48	0.47	1.16
Isomap	Meanshift	1	7	0.55	0.46	0.40	0.43	1.59
Isomap	Meanshift	0.5	27	0.07	0.86	0.13	0.22	1.74
Isomap	Meanshift	0.2	99	0.03	0.95	0.11	0.19	1.60
Isomap	BIRCH	1.8	1	0.00	0.00	1.00	0.00	Inf
Isomap	BIRCH	1.5	1	0.00	0.00	1.00	0.00	Inf
Isomap	BIRCH	1	9	0.20	0.42	0.15	0.22	0.89
Isomap	BIRCH	0.5	16	0.11	0.82	0.15	0.26	0.59
Isomap	BIRCH	0.2	98	0.02	0.87	0.08	0.15	0.60
SE	DBSCAN	0.99	11	0.09	0.25	0.08	0.12	1.51
SE	DBSCAN	0.95	28	0.08	0.96	0.14	0.24	4.75
SE	DBSCAN	0.9	27	0.08	0.96	0.14	0.24	4.97
SE	DBSCAN	0.8	30	0.06	0.97	0.11	0.19	7.40
SE	DBSCAN	0.7	21	0.05	0.96	0.09	0.17	6.23
SE	kmeans	2	2	-0.09	0.07	0.05	0.06	2.65
SE	kmeans	3	3	0.11	0.16	0.15	0.15	0.91
SE	kmeans	4	4	-0.11	0.08	0.04	0.05	1.33
SE	kmeans	5	5	0.10	0.26	0.10	0.14	1.02
SE	kmeans	6	6	0.20	0.64	0.19	0.30	0.63
SE	Meanshift	1.8	3	0.23	0.15	0.28	0.20	1.88
SE	Meanshift	1.5	5	0.16	0.17	0.15	0.16	1.64
SE	Meanshift	1	8	0.23	0.39	0.12	0.18	1.57
SE	Meanshift	0.5	15	0.07	0.87	0.13	0.22	2.02
SE	Meanshift	0.2	55	0.07	0.92	0.11	0.20	7.41
SE	BIRCH	1.8	1	0.00	0.00	1.00	0.00	Inf
SE	BIRCH	1.5	1	0.00	0.00	1.00	0.00	Inf

SE	BIRCH	1	5	0.71	0.78	0.43	0.55	0.59
SE	BIRCH	0.5	19	0.07	0.84	0.12	0.21	0.56
SE	BIRCH	0.2	64	0.03	0.90	0.09	0.16	0.54

Appendix Table 2: Clustering results on the reduced Tennessee Eastman Process data from Chapter 5

DR tech	cluster tech	param	No. clust	ARI	Homog.	Complete.	Vmeas	DBI
No DR	DBSCAN	0.99	3	0.10	0.21	0.96	0.34	0.58
No DR	DBSCAN	0.95	7	0.24	0.43	0.86	0.57	1.66
No DR	DBSCAN	0.9	5	0.25	0.43	0.83	0.57	1.67
No DR	DBSCAN	0.8	7	0.74	0.80	0.91	0.85	2.10
No DR	DBSCAN	0.7	10	0.81	0.86	0.86	0.86	8.12
No DR	kmeans	6	6	0.36	0.54	0.85	0.66	0.60
No DR	kmeans	7	7	0.40	0.58	0.82	0.68	0.82
No DR	kmeans	8	8	0.41	0.60	0.81	0.69	0.87
No DR	kmeans	9	9	0.59	0.72	0.79	0.75	0.87
No DR	kmeans	10	10	0.59	0.73	0.79	0.76	0.78
No DR	Meanshift	1.8	2	0.01	0.04	0.44	0.07	1.59
No DR	Meanshift	1.5	2	0.11	0.19	0.78	0.31	1.71
No DR	Meanshift	1	4	0.24	0.41	0.83	0.55	1.63
No DR	Meanshift	0.5	8	0.43	0.59	0.79	0.67	2.32
No DR	Meanshift	0.2	15	0.53	0.71	0.76	0.73	2.07
No DR	BIRCH	1.8	1	0.00	0.00	1.00	0.00	inf
No DR	BIRCH	1.5	1	0.00	0.00	1.00	0.00	inf
No DR	BIRCH	1	5	0.12	0.26	0.77	0.39	0.73
No DR	BIRCH	0.5	23	0.46	0.67	0.74	0.71	0.83
No DR	BIRCH	0.2	112	0.72	0.97	0.63	0.76	0.74
PCA	DBSCAN	0.99	3	0.10	0.21	0.96	0.34	0.63

PCA	DBSCAN	0.95	7	0.23	0.42	0.84	0.56	2.01
PCA	DBSCAN	0.9	5	0.24	0.42	0.83	0.56	1.54
PCA	DBSCAN	0.8	8	0.53	0.66	0.88	0.76	1.79
PCA	DBSCAN	0.7	6	0.49	0.61	0.84	0.71	1.68
PCA	kmeans	6	6	0.36	0.54	0.85	0.66	0.61
PCA	kmeans	7	7	0.40	0.58	0.82	0.68	0.70
PCA	kmeans	8	8	0.55	0.67	0.79	0.72	0.75
PCA	kmeans	9	9	0.59	0.72	0.79	0.75	0.75
PCA	kmeans	10	10	0.59	0.72	0.79	0.75	0.82
PCA	Meanshift	1.8	2	0.10	0.19	0.79	0.30	1.58
PCA	Meanshift	1.5	4	0.11	0.24	0.80	0.37	1.08
PCA	Meanshift	1	12	0.38	0.57	0.81	0.67	1.18
PCA	Meanshift	0.5	34	0.42	0.63	0.73	0.68	0.77
PCA	Meanshift	0.2	148	0.61	0.80	0.59	0.68	0.86
PCA	BIRCH	1.8	1	0.00	0.00	1.00	0.00	inf
PCA	BIRCH	1.5	1	0.00	0.00	1.00	0.00	inf
PCA	BIRCH	1	5	0.12	0.28	0.77	0.41	0.71
PCA	BIRCH	0.5	22	0.46	0.67	0.75	0.70	0.74
PCA	BIRCH	0.2	83	0.65	0.86	0.64	0.73	0.65
ICA	DBSCAN	0.99	4	0.10	0.21	0.91	0.34	0.89
ICA	DBSCAN	0.95	5	0.21	0.39	0.83	0.53	2.31
ICA	DBSCAN	0.9	5	0.24	0.43	0.83	0.56	2.56
ICA	DBSCAN	0.8	10	0.52	0.67	0.85	0.75	2.11
ICA	DBSCAN	0.7	10	0.52	0.66	0.77	0.71	2.37
ICA	kmeans	6	6	0.56	0.67	0.85	0.75	1.04
ICA	kmeans	7	7	0.55	0.67	0.84	0.74	0.82
ICA	kmeans	8	8	0.56	0.69	0.82	0.75	0.75
ICA	kmeans	9	9	0.56	0.69	0.81	0.75	0.66
ICA	kmeans	10	10	0.58	0.71	0.79	0.75	0.75
ICA	Meanshift	1.8	4	0.01	0.04	0.38	0.07	1.41

ICA	Meanshift	1.5	4	0.01	0.05	0.38	0.08	1.47
ICA	Meanshift	1	12	0.11	0.26	0.61	0.36	1.34
ICA	Meanshift	0.5	44	0.61	0.74	0.71	0.72	0.71
ICA	Meanshift	0.2	184	0.66	0.87	0.59	0.70	0.80
ICA	BIRCH	1.8	1	0.00	0.00	1.00	0.00	inf
ICA	BIRCH	1.5	1	0.00	0.00	1.00	0.00	inf
ICA	BIRCH	1	5	0.06	0.14	0.42	0.21	1.45
ICA	BIRCH	0.5	28	0.63	0.77	0.71	0.74	0.72
ICA	BIRCH	0.2	116	0.70	0.92	0.62	0.74	0.65
KPCA	DBSCAN	0.99	4	0.21	0.37	0.95	0.54	1.05
KPCA	DBSCAN	0.95	5	0.37	0.54	0.91	0.68	2.11
KPCA	DBSCAN	0.9	7	0.48	0.65	0.79	0.72	1.73
KPCA	DBSCAN	0.8	10	0.44	0.63	0.71	0.67	1.50
KPCA	DBSCAN	0.7	11	0.36	0.58	0.64	0.61	1.39
KPCA	kmeans	6	6	0.50	0.66	0.84	0.74	0.60
KPCA	kmeans	7	7	0.52	0.68	0.82	0.75	0.57
KPCA	kmeans	8	8	0.48	0.68	0.78	0.73	0.60
KPCA	kmeans	9	9	0.46	0.69	0.75	0.72	0.68
KPCA	kmeans	10	10	0.42	0.69	0.72	0.70	0.63
KPCA	Meanshift	1.8	2	0.00	0.02	0.12	0.03	5.22
KPCA	Meanshift	1.5	2	0.06	0.09	0.27	0.13	4.14
KPCA	Meanshift	1	8	0.47	0.66	0.75	0.70	1.60
KPCA	Meanshift	0.5	11	0.29	0.53	0.59	0.56	1.23
KPCA	Meanshift	0.2	115	0.20	0.59	0.40	0.48	1.12
KPCA	BIRCH	1.8	1	0.00	0.00	1.00	0.00	inf
KPCA	BIRCH	1.5	1	0.00	0.00	1.00	0.00	inf
KPCA	BIRCH	1	6	0.37	0.58	0.78	0.67	0.67
KPCA	BIRCH	0.5	14	0.34	0.69	0.64	0.66	0.75
KPCA	BIRCH	0.2	104	0.21	0.70	0.43	0.54	0.67
Isomap	DBSCAN	0.99	3	0.10	0.21	0.96	0.34	1.07

Isomap	DBSCAN	0.95	5	0.24	0.42	0.88	0.57	1.68
Isomap	DBSCAN	0.9	6	0.25	0.44	0.82	0.57	1.53
Isomap	DBSCAN	0.8	11	0.74	0.81	0.88	0.85	1.65
Isomap	DBSCAN	0.7	16	0.66	0.80	0.76	0.78	1.75
Isomap	kmeans	6	6	0.35	0.54	0.86	0.67	0.69
Isomap	kmeans	7	7	0.55	0.68	0.83	0.75	0.62
Isomap	kmeans	8	8	0.54	0.70	0.81	0.75	0.68
Isomap	kmeans	9	9	0.54	0.70	0.80	0.75	0.59
Isomap	kmeans	10	10	0.60	0.75	0.79	0.77	0.69
Isomap	Meanshift	1.8	3	0.19	0.29	0.90	0.44	0.98
Isomap	Meanshift	1.5	3	0.19	0.30	0.88	0.44	1.23
Isomap	Meanshift	1	6	0.28	0.46	0.77	0.57	1.26
Isomap	Meanshift	0.5	15	0.38	0.59	0.76	0.66	1.09
Isomap	Meanshift	0.2	56	0.62	0.81	0.67	0.74	1.04
Isomap	BIRCH	1.8	1	0.00	0.00	1.00	0.00	inf
Isomap	BIRCH	1.5	3	0.20	0.34	0.86	0.49	0.61
Isomap	BIRCH	1	5	0.32	0.50	0.87	0.63	0.40
Isomap	BIRCH	0.5	12	0.55	0.69	0.79	0.74	0.63
Isomap	BIRCH	0.2	35	0.70	0.88	0.71	0.78	0.60
SE	DBSCAN	0.99	3	0.01	0.05	0.75	0.09	1.71
SE	DBSCAN	0.95	9	0.56	0.73	0.87	0.79	2.18
SE	DBSCAN	0.9	13	0.55	0.71	0.82	0.76	1.59
SE	DBSCAN	0.8	15	0.67	0.78	0.78	0.78	1.68
SE	DBSCAN	0.7	22	0.55	0.71	0.69	0.70	1.74
SE	kmeans	6	6	0.69	0.76	0.90	0.83	1.27
SE	kmeans	7	7	0.64	0.75	0.89	0.81	1.00
SE	kmeans	8	8	0.68	0.78	0.82	0.80	1.05
SE	kmeans	9	9	0.70	0.83	0.84	0.83	0.75
SE	kmeans	10	10	0.79	0.87	0.83	0.85	0.72
SE	Meanshift	1.8	4	0.02	0.07	0.44	0.12	1.56

SE	Meanshift	1.5	5	0.02	0.08	0.39	0.14	1.23
SE	Meanshift	1	7	0.10	0.25	0.51	0.33	1.17
SE	Meanshift	0.5	19	0.44	0.62	0.65	0.64	1.08
SE	Meanshift	0.2	62	0.48	0.81	0.58	0.67	0.84
SE	BIRCH	1.8	1	0.00	0.00	1.00	0.00	inf
SE	BIRCH	1.5	1	0.00	0.00	1.00	0.00	inf
SE	BIRCH	1	7	0.26	0.48	0.76	0.59	0.81
SE	BIRCH	0.5	16	0.71	0.84	0.83	0.84	0.51
SE	BIRCH	0.2	58	0.52	0.93	0.60	0.72	0.45

Appendix Table 3: Clustering results on the full Tennessee Eastman Process data from Chapter 5

DR tech	cluster tech	param	No. clust	ARI	Homog.	Complete.	Vmeas	DBI
No DR	DBSCAN	0.99	4	0.01	0.07	0.89	0.13	1.66
No DR	DBSCAN	0.95	9	0.03	0.17	0.79	0.28	2.00
No DR	DBSCAN	0.9	14	0.04	0.20	0.78	0.31	2.18
No DR	DBSCAN	0.8	16	0.08	0.29	0.80	0.43	2.07
No DR	DBSCAN	0.7	19	0.13	0.37	0.80	0.51	2.69
No DR	kmeans	19	19	0.11	0.44	0.73	0.55	0.96
No DR	kmeans	20	20	0.10	0.42	0.73	0.53	0.89
No DR	kmeans	21	21	0.12	0.46	0.71	0.55	1.01
No DR	kmeans	22	22	0.11	0.46	0.73	0.56	0.91
No DR	kmeans	23	23	0.11	0.45	0.72	0.56	1.05
No DR	Meanshift	1.8	6	0.03	0.15	0.74	0.25	1.16
No DR	Meanshift	1.5	9	0.04	0.20	0.71	0.31	1.26
No DR	Meanshift	1	16	0.06	0.27	0.74	0.39	1.13
No DR	Meanshift	0.5	32	0.10	0.32	0.68	0.44	1.19
No DR	Meanshift	0.2	227	0.16	0.46	0.63	0.53	1.80

No DR	BIRCH	1.8	1	0.00	0.00	1.00	0.00	inf
No DR	BIRCH	1.5	10	0.02	0.16	0.66	0.25	1.16
No DR	BIRCH	1	22	0.05	0.30	0.73	0.42	0.92
No DR	BIRCH	0.5	133	0.09	0.48	0.62	0.54	0.83
No DR	BIRCH	0.2	633	0.20	0.71	0.55	0.62	0.74
PCA	DBSCAN	0.99	5	0.01	0.07	0.87	0.13	1.79
PCA	DBSCAN	0.95	10	0.03	0.16	0.78	0.27	1.88
PCA	DBSCAN	0.9	15	0.04	0.20	0.79	0.32	2.12
PCA	DBSCAN	0.8	16	0.08	0.30	0.79	0.43	2.12
PCA	DBSCAN	0.7	13	0.09	0.30	0.79	0.43	2.59
PCA	kmeans	19	19	0.12	0.44	0.71	0.54	0.94
PCA	kmeans	20	20	0.11	0.43	0.72	0.53	0.75
PCA	kmeans	21	21	0.12	0.45	0.71	0.55	0.87
PCA	kmeans	22	22	0.12	0.45	0.71	0.55	0.87
PCA	kmeans	23	23	0.13	0.46	0.71	0.56	0.93
PCA	Meanshift	1.8	10	0.03	0.18	0.72	0.29	1.09
PCA	Meanshift	1.5	15	0.04	0.21	0.71	0.33	0.83
PCA	Meanshift	1	41	0.06	0.29	0.70	0.41	0.88
PCA	Meanshift	0.5	179	0.10	0.39	0.62	0.48	0.74
PCA	Meanshift	0.2	654	0.16	0.57	0.54	0.55	1.19
PCA	BIRCH	1.8	3	0.00	0.02	0.59	0.04	0.55
PCA	BIRCH	1.5	11	0.02	0.16	0.67	0.26	0.99
PCA	BIRCH	1	20	0.05	0.29	0.72	0.41	0.85
PCA	BIRCH	0.5	126	0.09	0.46	0.62	0.53	0.79
PCA	BIRCH	0.2	459	0.18	0.63	0.54	0.58	0.61
ICA	DBSCAN	0.99	4	0.01	0.07	0.90	0.13	1.65
ICA	DBSCAN	0.95	10	0.03	0.16	0.79	0.27	1.92
ICA	DBSCAN	0.9	11	0.03	0.19	0.79	0.30	1.95
ICA	DBSCAN	0.8	12	0.08	0.29	0.83	0.43	1.66
ICA	DBSCAN	0.7	11	0.09	0.28	0.79	0.42	2.19

ICA	kmeans	19	19	0.11	0.43	0.71	0.53	0.88
ICA	kmeans	20	20	0.11	0.43	0.70	0.53	0.91
ICA	kmeans	21	21	0.11	0.43	0.69	0.53	1.01
ICA	kmeans	22	22	0.13	0.46	0.68	0.55	0.92
ICA	kmeans	23	23	0.12	0.46	0.70	0.55	0.94
ICA	Meanshift	1.8	10	0.04	0.21	0.73	0.32	1.22
ICA	Meanshift	1.5	19	0.05	0.25	0.72	0.37	1.13
ICA	Meanshift	1	50	0.08	0.32	0.68	0.44	0.90
ICA	Meanshift	0.5	224	0.13	0.46	0.61	0.53	0.85
ICA	Meanshift	0.2	789	0.16	0.56	0.53	0.54	0.88
ICA	BIRCH	1.8	1	0.00	0.00	1.00	0.00	inf
ICA	BIRCH	1.5	10	0.03	0.18	0.61	0.28	1.23
ICA	BIRCH	1	31	0.07	0.35	0.67	0.46	0.95
ICA	BIRCH	0.5	150	0.14	0.54	0.61	0.58	0.79
ICA	BIRCH	0.2	591	0.19	0.65	0.51	0.57	0.63
KPCA	DBSCAN	0.99	3	0.00	0.00	0.04	0.00	0.65
KPCA	DBSCAN	0.95	4	0.00	0.00	0.12	0.01	1.03
KPCA	DBSCAN	0.9	8	0.00	0.01	0.17	0.02	1.20
KPCA	DBSCAN	0.8	21	0.00	0.03	0.21	0.05	1.29
KPCA	DBSCAN	0.7	59	0.03	0.11	0.30	0.17	1.50
KPCA	kmeans	19	19	0.11	0.36	0.49	0.41	1.18
KPCA	kmeans	20	20	0.12	0.36	0.48	0.41	1.26
KPCA	kmeans	21	21	0.12	0.36	0.48	0.41	1.31
KPCA	kmeans	22	22	0.12	0.36	0.47	0.41	1.37
KPCA	kmeans	23	23	0.11	0.36	0.47	0.41	1.22
KPCA	Meanshift	1.8	2	0.01	0.05	0.30	0.09	2.39
KPCA	Meanshift	1.5	3	0.08	0.19	0.69	0.30	1.25
KPCA	Meanshift	1	9	0.13	0.34	0.69	0.46	1.56
KPCA	Meanshift	0.5	561	0.11	0.38	0.34	0.36	1.06
KPCA	Meanshift	0.2	1903	0.09	0.44	0.35	0.39	1.00

KPCA	BIRCH	1.8	1	0.00	0.00	1.00	0.00	inf
KPCA	BIRCH	1.5	5	0.10	0.28	0.72	0.40	1.23
KPCA	BIRCH	1	21	0.11	0.33	0.47	0.39	1.33
KPCA	BIRCH	0.5	493	0.12	0.42	0.36	0.39	0.97
KPCA	BIRCH	0.2	1956	0.10	0.54	0.37	0.44	0.39
Isomap	DBSCAN	0.99	5	0.01	0.07	0.88	0.13	1.38
Isomap	DBSCAN	0.95	14	0.03	0.18	0.80	0.30	1.65
Isomap	DBSCAN	0.9	14	0.04	0.20	0.81	0.32	1.40
Isomap	DBSCAN	0.8	32	0.09	0.34	0.77	0.47	2.25
Isomap	DBSCAN	0.7	38	0.13	0.39	0.73	0.50	3.56
Isomap	kmeans	19	19	0.13	0.46	0.74	0.57	0.77
Isomap	kmeans	20	20	0.12	0.44	0.72	0.55	0.72
Isomap	kmeans	21	21	0.12	0.45	0.73	0.55	0.66
Isomap	kmeans	22	22	0.13	0.48	0.73	0.58	0.75
Isomap	kmeans	23	23	0.15	0.48	0.71	0.58	0.79
Isomap	Meanshift	1.8	8	0.04	0.23	0.80	0.36	1.48
Isomap	Meanshift	1.5	10	0.04	0.24	0.78	0.36	1.39
Isomap	Meanshift	1	20	0.05	0.26	0.72	0.38	1.38
Isomap	Meanshift	0.5	68	0.07	0.33	0.65	0.44	0.95
Isomap	Meanshift	0.2	302	0.14	0.51	0.59	0.55	0.80
Isomap	BIRCH	1.8	3	0.02	0.11	0.90	0.19	0.44
Isomap	BIRCH	1.5	3	0.02	0.11	0.90	0.19	0.44
Isomap	BIRCH	1	16	0.05	0.27	0.77	0.40	0.73
Isomap	BIRCH	0.5	49	0.08	0.40	0.70	0.51	0.69
Isomap	BIRCH	0.2	201	0.13	0.55	0.61	0.58	0.62
SE	DBSCAN	0.99	5	0.01	0.09	0.86	0.16	1.91
SE	DBSCAN	0.95	13	0.02	0.15	0.74	0.25	1.41
SE	DBSCAN	0.9	13	0.06	0.27	0.81	0.40	1.53
SE	DBSCAN	0.8	31	0.08	0.33	0.70	0.45	1.95
SE	DBSCAN	0.7	60	0.08	0.35	0.58	0.44	1.95

SE	kmeans	19	19	0.13	0.46	0.68	0.55	0.68
SE	kmeans	20	20	0.18	0.51	0.71	0.60	0.68
SE	kmeans	21	21	0.19	0.54	0.72	0.62	0.71
SE	kmeans	22	22	0.19	0.54	0.71	0.61	0.68
SE	kmeans	23	23	0.20	0.54	0.69	0.60	0.67
SE	Meanshift	1.8	12	0.03	0.19	0.66	0.29	1.00
SE	Meanshift	1.5	13	0.04	0.19	0.64	0.30	0.95
SE	Meanshift	1	26	0.06	0.26	0.66	0.37	0.79
SE	Meanshift	0.5	70	0.08	0.34	0.59	0.43	0.78
SE	Meanshift	0.2	279	0.11	0.48	0.51	0.50	0.56
SE	BIRCH	1.8	4	0.02	0.10	0.86	0.19	0.67
SE	BIRCH	1.5	5	0.02	0.12	0.86	0.22	0.62
SE	BIRCH	1	28	0.12	0.44	0.73	0.55	0.56
SE	BIRCH	0.5	66	0.11	0.47	0.63	0.54	0.55
SE	BIRCH	0.2	236	0.17	0.62	0.54	0.58	0.49

Vita

Michael Thomas was born and raised in Baton Rouge, Louisiana and graduated from Catholic High School. He went on to attend Vanderbilt University where he studied simulations in the lab of Dr. Peter T. Cummings. In 2012, he graduated with a Bachelor of Engineering in chemical and biomolecular engineering. Later that year, he joined Jose Romagnoli's lab at LSU to begin his PhD and research process control and data mining. After the completion of his PhD studies, Michael hopes to start a career in applied research in industry.

Away from work, Michael enjoys many hobbies such as brewing beer, hiking, history, studying Chinese, and college football.